
**KTH Signals**
**Sensors and Systems**

# Novel RF MEMS Switch and Packaging Concepts

**Joachim Oberhammer**

MICROSYSTEM TECHNOLOGY
DEPARTMENT OF SIGNALS, SENSORS AND SYSTEMS
ROYAL INSTITUTE OF TECHNOLOGY

ISBN 91-7283-831-0
ISSN 0281-2878
TRITA-ILA-0401

*Submitted to the School of*
*Computer Science — Electrical Engineering — Engineering Physics (DEF),*
*Royal Institute of Technology (KTH), Stockholm, Sweden,*
*in partial fulfillment of the requirements for the degree of Doctor of Philosophy*
Stockholm 2004

*The front cover shows SEM-pictures of different top and bottom parts of MEMS switches fabricated by the author. The switches are designed to mechanically switch electrical signals in the frequency range from DC up to a few tens of GHz. The total dimensions of the parts shown in the pictures are about 1 mm. The size of the smallest features is 2 µm, and the layer thickness is from 40 nm up to 18.2 µm.*

*The pictures shown on pages xii, 4 and 78 are of minor scientific value and show motives from our world miniaturized in silicon by a circa 75 µm deep plasma etching process. The dimensions of the structures are indicated by the scaling bar in the lower parts of the pictures.*



Printed by Universitetsservice US AB, Stockholm 2004.

Thesis for the degree of Doctor of Philosophy at the Royal Institute of Technology, Stockholm, Sweden, 2004.

# Abstract

Radio-frequency microelectromechanical systems (RF MEMS) are highly miniaturized devices intended to switch, modulate, filter or tune electrical signals from DC to microwave frequencies. The micomachining techniques used to fabricate these components are based on the standard clean-room manufacturing processes for high-volume integrated semiconductor circuits. RF MEMS switches are characterized by their high isolation, low insertion loss, large bandwidth and by their unparalleled signal linearity. They are relatively simple to control, are very small and have almost zero power consumption. Despite these benefits, RF MEMS switches are not yet seen in commercial products because of reliability issues, limits in signal power handling and questions in packaging and integration. Also, the actuation voltages are typically too high for electronics applications and require additional drive circuitry.

This thesis presents a novel MEMS switch concept based on an S-shaped film actuator, which consists of a thin and flexible membrane rolling between a top and a bottom electrode. The special design makes it possible to have high RF isolation due to the large contact distance in the off-state, while maintaining low operation voltages due to the zipper-like movement of the electrostatic dual-actuator. The switch comprises two separately fabricated parts which allows simple integration even with RF circuits incompatible with certain MEMS fabrication processes. The two parts are assembled by chip or wafer bonding which results in an encapsulated, ready-to-dice package. The thesis discusses the concept of the switch and reports on the successful fabrication and evaluation of prototype devices.

Furthermore, this thesis presents research results in wafer-level packaging of (RF) MEMS devices by full-wafer bonding with an adhesive intermediate layer, which is structured before bonding to create defined cavities for housing MEMS devices. This technique has the advantage of simple, robust and low temperature fabrication, and is highly tolerant to surface non-uniformities and particles in the bonding interface. It allows cavities with a height of up to many tens of micrometers to be created directly in the bonding interface. In contrast to conventional wafer-level packaging methods with individual chip-capping, the encapsulation is done using a single wafer-bonding step. The thesis investigates the process parameters for patterned adhesive wafer bonding with benzocyclobutene, describes the fabrication of glass lid packages based on this technique, and introduces a method to create through-wafer electrical interconnections in glass substrates by a two-step etch technique, involving powder-blasting and chemical etching. Also, it discusses a technique of improving the hermetic properties of adhesive bonded structures by additional passivation layers. Finally, it presents a method to substantially improve the bond strength of patterned adhesive bonding by using the solid/liquid phase combination of a patterned polymer layer with a contact-printed thin adhesive film.

*Joachim Oberhammer*
*Microsystem Technology, Department of Signals, Sensors and Systems*
*Royal Institute of Technology, SE-100 44 Stockholm, Sweden*

*You are like a manuscript, not a completed book. A book has a beginning, a middle, and an end. It is printed by machines in a press and bound as a permanent unit. But you do not know from where you have come or where you will go. You are in search of the beginning and ending pages of life in order to make your manuscript complete.*

*Sri Swami Rama*
*1925–1996, Indian Sage*
*in "Path of Fire and Light: Vol. 2"*

***To D. F.***

*Your manuscript is both good and original, but the part that is good is not original and the part that is original is not good.*

*Samuel Johnson*
*1709–1784, British Author*

# Contents

*Freedom is not worth having if it does not include the freedom to make mistakes.*

*Mahatma Gandhi*
*1869–1948, Indian Politician*

# List of papers

The presented thesis is based on the following *international reviewed journal papers*:

1. *Selective Wafer-Level Adhesive Bonding with Benzocyclobutene for Fabrication of Cavities*
   **Joachim Oberhammer**, Frank Niklaus, and Göran Stemme
   *Sensors and Actuators A: Physical*, vol. 105, no. 3, pp. 297–304, July 2003.

2. *Sealing of Adhesive Bonded Devices on Wafer Level*
   **Joachim Oberhammer**, Frank Niklaus, and Göran Stemme
   *Sensors and Actuators A: Physical*, vol. 110, no. 1–3, pp. 407–412, Feb. 2004.

3. *Low-Voltage High-Isolation DC-to-RF MEMS Switch Based on an S-shaped Film Actuator*
   **Joachim Oberhammer** and Göran Stemme
   *IEEE Transactions on Electron Devices*, vol. 51, no. 1, pp. 149–155, Jan. 2004.

4. *Design and Fabrication Aspects of an S-shaped Film Actuator Based DC to RF MEMS Switch*
   **Joachim Oberhammer** and Göran Stemme
   *IEEE/ASME Journal of Microelectromechanical Systems*, vol. 13, no. 3, pp. 421–428, June 2004.

5. *Low-Cost Glass-Lid Packaging by Adhesive Full-Wafer Bonding with Two-Step Etched Electrical Feedthroughs*
   **Joachim Oberhammer** and Göran Stemme
   Submitted for journal publication.

6. *BCB Contact Printing for Patterned Adhesive Full-Wafer Bonded 0-Level Packages*
   **Joachim Oberhammer** and Göran Stemme
   *IEEE/ASME Journal of Microelectromechanical Systems*, accepted for publication, tentative print issue December 2004.

7. *A 2-bit Reconfigurable Meander Slot Antenna with High-Displacement Low-Voltage RF MEMS Switches*
   Marc Mowler, **Joachim Oberhammer**, Björn Lindmark, and Göran Stemme
   Manuscript for journal publication.

The *contribution of Joachim Oberhammer* to the different publications:

1 major part of design, all fabrication, all experiments, major part of writing
2 part of design, major part of fabrication, all experiments, all writing
3 major part of design, all fabrication, all experiments, major part of writing
4 major part of design, all fabrication, all experiments, major part of writing
5 major part of design, all fabrication, major part of experiments and writing
6 all design, all fabrication, major part of experiments, major part of writing
7 part of design, part of fabrication, part of writing

Also, the work has been presented at the following *international reviewed conferences*:

8. *Selective Wafer-Level Adhesive Bonding with Benzocyclobutene*
**Joachim Oberhammer**, Frank Niklaus, and Göran Stemme
*Proceedings Micromechanics Europe MME 2001*, Cork, Ireland, Sept. 16–18, 2001, pp. 54–57, *poster presentation.*

9. *Sealing of Adhesive Bonded Devices on Wafer Level*
**Joachim Oberhammer**, Frank Niklaus, and Göran Stemme
*Proceedings Eurosensors XVI*, Prague, Czech Republic, Sept. 15–18, 2002, pp. 298–299, *poster presentation.*

10. *Incrementally Etched Electrical Feedthroughs for Wafer-Level Transfer of Glass Lid Packages*
**Joachim Oberhammer** and Göran Stemme
*Proceedings of IEEE Transducers 2003*, Boston, MA, USA, June 8–12, 2003, pp. 1832–1835, *oral presentation.*

11. *RF Characterization of Low-Voltage High-Isolation MEMS Series Switch Based on a S-shaped Film Actuator*
**Joachim Oberhammer** and Göran Stemme
*SBMO/IEEE MTT-S International Microwave and Optoelectronics Conference IMOC 2003*, Foz de Iguazú, Brazil, Sept. 20–23, 2003, pp. 537–540, *oral presentation.*

12. *Contact Printing for Improved Bond-Strength of Patterned Adhesive Full-Wafer Bonded 0-Level Packaging*
**Joachim Oberhammer** and Göran Stemme
*IEEE Micro Electro Mechanical Systems 2004*, Maastricht, The Netherlands, Jan. 25–29, 2004, pp. 713–716, *poster presentation.*

13. *S-shaped Film Actuator for Low-Voltage High-Isolation MEMS Metal Contact Switches*
**Joachim Oberhammer** and Göran Stemme
*IEEE Micro Electro Mechanical Systems 2004*, Maastricht, The Netherlands, Jan. 25–29, 2004, pp. 637–640, *oral presentation.*

It has also been presented at the following *international workshops*:

14. *Adhesive Wafer Bonding for Packaging Applications*
    Frank Niklaus, **Joachim Oberhammer**, and Göran Stemme
    *Workshop on MEMS Sensor Packaging 2003*, Copenhagen, Denmark, Mar. 20–21, 2003, *oral presentation by Frank Niklaus.*

15. *A 2-bit Reconfigurable Meander Slot Antenna with High-Displacement Low-Voltage RF MEMS Switches*
    Marc Mowler, **Joachim Oberhammer**, Björn Lindmark, and Göran Stemme
    *MEMSWave — Workshop on MEMS for Millimeterwave Communication 2004*, Uppsala, Sweden, June 30–July 2, 2004, pp. D20–D24, *oral presentation by Marc Mowler.*

The RF MEMS switch the journal papers 3 and 4 are based on was also brought closer to the public by the full-page article *Nytt koncept för RF–switchar* (*New concept for RF–switches*) published in the weekly Scandinavian electronics magazine *Elektronik i Norden*, no. 19, November 28, 2003, p. 46, written by Jonas Karlsson.

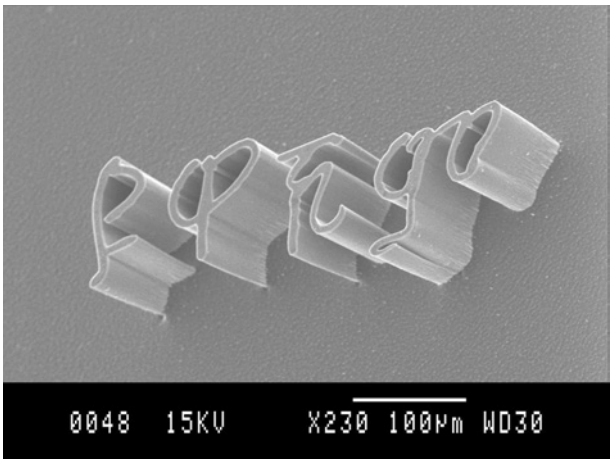


The first name of the author in Tigrinia (JU WA CHI M), one of the three official languages of Eritrea. The letters are etched about 75 $\mu$m deep into a silicon wafer by an inductive coupled plasma tool. The line width is between 3 and 10 $\mu$m, and the structures have a height to width aspect ratio of up to 25:1.

*I would have written a shorter letter but*
*I didn't have the time.*

*Blaise Pascal*
*1623–1662, French Scientist*

# 1 Introduction

## 1.1 General introduction

Besides the need for computational circuits in our information age, the success of microelectronics is based on its ability for miniaturization, integration and high volume production, leading to very low chip prices which allows them to be used in the low end mass produced devices surrounding us in everyday life.

Microelectromechanical systems (MEMS), are integrated microdevices combining electrical components with active and passive interface functions to the physical surroundings, interacting with motion, sound, light, radio waves, gases, liquids, the chemical environment, thermic radiation, etc. Thus, if the traditional microelectronic chip is the "brain" or the information processing unit, the MEMS part adds the "senses" to the microsystem. The variety of new functionalities opens a new world for microdevices, whose impact on society is predicted to become similar to the impact of microelectronics up to today. The high potential of the enabling technology MEMS lies — similar to microelectronics, since MEMS fabrication is based on traditional, highly developed and optimized semiconductor manufacturing processes, infrastructure and logistics — in the possibilities of miniaturization with advantageous scaling properties for improved device or system performance, a high level of circuit integration to improve performance or to reduce barriers to incorporation into larger systems, and batch fabrication for very large volume production. The latter results in unbeatable product uniformity and low prices per unit. The complexity of the mechanical parts and interfaces of a MEMS device, reliability issues and the non-standardized packaging procedure, as well as the fact that the production volume and the degree of miniaturization are decisive for the price of the final device and thus for its market potential, have so far only led to a few successful commercialized high-volume MEMS products. Examples are accelerometers, pressure sensors and recently also gyros in automotive applications[1], inkjet print heads and actuators for hard disk read/write heads, as illustrated in Table 1. However, there are niche-markets where the required device performance dominates over the cost of a low-volume product. Typical examples for such MEMS devices are pressure sensors for minimal invasive diagnostics and surgery, besides high-end military and space applications. In recent years, semiconductor equipment manufacturers have been putting increasing efforts into machines dedicated for MEMS production. Due to this tendency, in line with fabrication and material costs pushed down by the advancing IC industry[2], we hopefully soon will

[1] Already in 2000 a BMW 740i had over 70 MEMS devices aboard [1].

[2] With the IC industries moving to 8 and 12 inch production lines, 4 and 6 inch factories and equipment are available cost-effectively for MEMS. To give another example: the costs of SOI wafers, a favorable substrate for MEMS sensor applications, are expected to sink drastically to about 3 times of the costs of conventional silicon wafers, since SOI wafers are predicted to account for half of CMOS sub-180 nm production on 300 mm wafers in about 5 years [2].

**Table 1.** Commercialization of selected MEMS devices (based on [3], 2000).

| Product | Discovery | Evolution | Cost reduction, application expansion | Full commercialization |
|---|---|---|---|---|
| pressure sensors[a] | 1954–1960 | 1960–1975 | 1975–1990 | 1990–present |
| accelerometers[b] | 1974–1985 | 1985–1990 | 1990–1998 | 1998 |
| gas sensors | 1986–1994 | 1994–1998 | 1998–2005 | 2005 |
| valves | 1980–1988 | 1988–1996 | 1996–2002 | 2002 |
| nozzles | 1972–1984 | 1984–1990 | 1990–1998 | 1998 |
| photonics/displays | 1980–1986 | 1986–1998 | 1998–2004 | 2004 |
| bio/chem. sensors | 1980–1994 | 1994–1999 | 1999–2004 | 2004 |
| rotation sensors[c] | 1982–1990 | 1990–1996 | 1996–2002 | 2002 |
| RF switches | 1994–1998 | 1998–2001 | 2001–2005 | 2005 |
| micro relays | 1977–1982 | 1993–1998 | 1998–2006 | 2006 |

[a]Silicon strain gauges have been commercially available since 1958 [1], and in 2003, SensoNor, Norway, now an Infineon Technologies company, fabricated about 20 million tire pressure sensors.
[b]The first commercial accelerometer was brought on the market by Analog Devices in 1990 [1] and the total sales of accelerometers fabricated by Analog Devices in the year 2003 was over 50 million [4].
[c]Robert Bosch GmbH, Germany, fabricated over 4 million gyros in 2003 [4].

see more MEMS volume products also in less exclusive market segments.

RF MEMS are micromachined devices interacting with electrical signals up to the radio frequency range. The components of main interest are micromachined switches, mechanically tunable capacitors and three-dimensional inductors, which offer superior performance compared to their electronic counterparts. Of all of the emerging subfields of MEMS with ongoing research and development activities, RF MEMS is believed to have the largest market potential since the high volume consumer market of personal communication devices already exists and literally cries out for new technologies expanding its possibilities. Technology reliability, integrability, the demanded short development times and the risk of taking a completely new type of component into a high volume product on a very competitive market have so far inhibited the leap from research labs to commercial production lines. High-end applications such as automated measurement and test equipment, automotive safety and communication systems, military and space applications are believed to be the initial application fields of RF MEMS components.

This thesis focuses on two topics of RF MEMS switches: firstly, it presents a new electrostatically actuated microswitch design which, due to its concept, addresses and offers solutions in many critical aspects such as low voltage design, large traveling distance of the switching contacts which is important for achieving high isolation, the device packaging and in the integration with RF circuits. Secondly, this thesis presents new ideas in the field of near-hermetic wafer-level packaging by full-wafer bonding with a patterned adhesive layer. Issues such as in-plane and vertical interconnections are discussed, and solutions are provided to improve the hermeticity of polymer packaging and the bond strength of patterned adhesive bonded wafers.

## 1.2 Objectives and methodology of this thesis

A thesis, following a statement by Christopher Clack, University College London, UK, is the *acquisition and dissemination of new knowledge*. I would like to add that writing a thesis is also a most welcome possibility to reflect over the knowledge acquired during the preceding years, and that it is a learning process about how to prepare this knowledge for distributing and presenting it to the interested community. It also makes it possible to give a personal accent to the research topics, thus letting the people participate on the experiences accumulated by being exposed to all the little problems a researcher encounters during his daily work.

From a MEMS device perspective, the presented thesis adds knowledge in the fields of RF MEMS switches and MEMS wafer-level packaging by showing new concepts and ideas which are proved by successful fabrication, experiments and evaluation.

From a micromachining point of view, the thesis provides new knowledge mainly in the field of adhesive bonding and in the fabrication of thin-film microactuators.

From a scientific perspective, finally, the value of this thesis in terms of novelty and relevance for the field is attested by the acceptance of the appended international journal papers and the referred international conference proceedings through an established scientific reviewing process.

## 1.3 Structure of this thesis

According to the procedures at the Royal Institute of Technology, this thesis consists of a brief introductory part and of a part with the appended journal papers.

The intention of the introductory part is not to recite the known knowledge in the field, but rather to give an overview of the motivation and the activities in the field, and to provide references for further study of the related topics (Section 2). However, a few selected topics are discussed in a more extensive way in Section 2.2. The references, collected at the end of the introductory part, are chosen by the preference of the author in terms of their relevance according to the intention stated above, and are not intended to give a complete overview of the research activities in the field.

Furthermore, the introductory part of this thesis presents the research topics of the scientific work this thesis is based on, discussing their concepts and relevance and comparing them to related existing work (Sections 3, 4). Finally, the introductory part closes with a detailed summary of the appended papers (Section 5), drawing conclusions (Section 6) and giving a brief outlook over the possible continuation of the work described in this thesis (Section 7).

The second part consists of the reprints of the journal papers this thesis is based on. The conference proceedings listed on pages x and xi are not included in this thesis but their content is also discussed in the introductory part.

Finally, I kindly ask for tolerance of the many footnotes spread all over the book. I know about the arguments against footnotes but I still think the way they are used in this book is a good compromise between providing interesting detailed information and not distracting the reader from the main flow of reading, which I have tried to keep on a less detailed level.

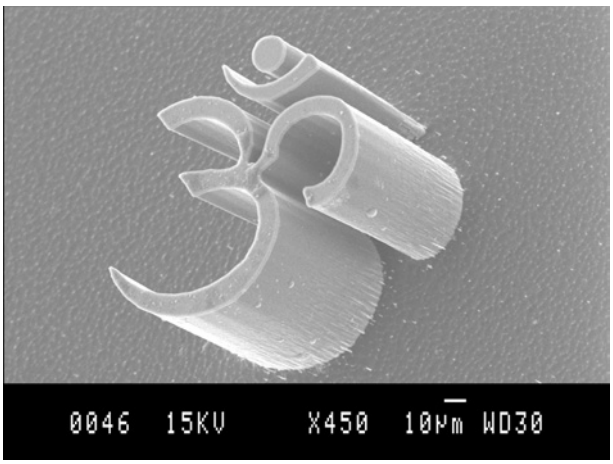


*All men dream: but not equally.*
*Those who dream by night in the dusty recesses*
*of their minds*
*wake in the day to find that all was vanity:*
*but the dreamers of the day are dangerous men,*
*for they may act their dream with open eyes,*
*to make it possible.*

*Thomas Edward Lawrence*
*1888-1935, British Soldier, Writer,*
*in "The Seven Pillars of Wisdom"*

*You can't really be strong until you can see a funny side to things.*

*Ken Kesey*
*1935–2001, American Writer,*
*in "One flow over the cuckoo's nest"*

# 2 Background

## 2.1 RF MEMS switches

### 2.1.1 RF MEMS

The first MEMS switch was fabricated already in 1979 by K. E. Petersen [5], showing the possibilities of the emerging micromachining technology. In 1991, L. E. Larson presented a MEMS switch dedicated to switching RF signals up to a few tens of GHz [6]. Despite the immaturity of the device, its electrical signal characteristics were so remarkable that it brought many research institutes and universities on the track of RF MEMS [7–14]. In the middle of the nineties of the last century, one publication followed another on new RF MEMS device concepts, and by the end of the nineties the research included more and more device reliability issues, indicating the increasing matureness of the technology. The device of main interest, due to its excellent performance, was and still is the micromachined switch. Other RF MEMS components are mechanical [15–19], dielectric [20] and cavity [21, 22] resonators for frequency-selecting applications, tunable capacitors [23–33], three-dimensional inductors [34–39], as well as micromachined antennas [40–42] and transmission lines [43–46]. RF circuits based on MEMS components are wide-band phase-shifters realized with MEMS switches [47–50] or micromachined tunable capacitors [51, 52], reconfigurable antennas [53–56], voltage controlled oscillators (VCO, [8, 57, 58]) and impedance tuning circuits [59, 60], just to give a few examples.

In a total, all these devices are characterized by their outstanding performance — low insertion loss and high signal linearity for the switches; high frequency selectivity and very small chip size of filters based on mechanical resonators; high Q-value and high self resonance frequency (SRF) of micromachined inductors; high tuning range, low series resistance and high linearity of mechanically tunable capacitors [7, 10] — but on the other hand also by their fabrication complexity, reliability issues [61–64], the difficulty of integrating them with traditional electronic circuits, by their special packaging requirements [9, 11, 65–67], and by device specific problems, such as the high impedance of micromechanical resonators and the relatively low power handling ability of MEMS switches.

Wireless MEMS is a term often used synonymously to RF MEMS and indicates the market potential of MEMS components in consumer products with telecommunication functionality, demanding low size, low weight, low power consumption, reconfigurability and good signal properties to fulfill new telecommunication standards [8, 10, 14, 68, 69]. These requirements make RF MEMS devices very suitable for replacing bulky passive off-chip components, which currently inhibit further miniaturization of wireless equipment since they consume most of the circuit board size and, in contrast to RF MEMS devices, cannot be integrated on-chip without sacrific-

ing performance [11]. Wireless applications are a low cost and high volume market where introducing devices of a new mechanical type with uncertain reliability entails high risk. Especially in this field it will be very difficult for MEMS switches to compete with semiconductor switches, which are available in high volumes for 0.3–0.6 USD/circuit [70]. Also, the down-turn of the telecommunication sector since 2001 with an investment stop in emerging technologies was a barrier in the ascension of RF MEMS. Many companies specialized in RF MEMS development crashed because their cash reserve was not sufficient to support cash outlay operations until volume orders could be delivered and paid[3].

Microwave acoustic devices [71] such as film bulk acoustic resonators (FBAR, [72]), solidly mounted resonators (SMR, [73]) and often also surface acoustic wave (SAW) devices [74] are considered RF MEMS components since they involve micromachining processes in their fabrication. In contrast to the other RF MEMS components mentioned above, these acoustic signal processing devices are already in production in high volumes. SAW filters have been used in consumer products since the 1970s and their world-wide production, according to an estimation published in March 2002, is in the region of 3 billion devices per year, mainly used in mobile radio systems [71]. Also FBAR based devices have been on the market in high volumes for a couple of years, and by July 2002, Agilent Technologies alone was shipping more than 1 million FBAR duplexers per month. The success of these microwave acoustic devices anticipates the market potential and the market's need of RF MEMS devices to even further push technological limits and fulfill customer demands.

> *The beauty of MEMS switches is their near-ideal behavior and the relative ease of their circuit designs.*
>
> *Gabriel M. Rebeiz [70]*

### 2.1.2 Why miniaturized *mechanical* switches?

By experience, the most vulnerable and the life-time determining components of an electrical device are its mechanical parts. Also, the reliability and the performance of electrical/electronical components has been increasing during the last decades at an incredible pace. Especially electronic switches have been the object of extensive research and development activities since they are the very basic components of our information age characteristic computational devices. Why then would one seriously think about using a miniaturized *mechanical* component for switching electrical signals in technological high-end applications?

The development of digital switches (transistors) in logic devices has proceeded at an incredible speed over the last decades in terms of components per chip, cost per function, clock rates, power consumption, compactness and functionality [86, 87]. However, the limits of digitally controllable analog signal switches have not been advancing that fast, and electronic switches based on PIN diodes and field

[3] A recent example is PHS MEMS located in Grenoble, France, probably the until now largest European MEMS company specialized in RF MEMS, founded in 1998 and declared to be in liquidation in February 2004, with 95 dismissed employees.

**Table 2.** Performance comparison of switches based on PIN-diode, FET, MEMS or conventional electromechanical relay (EMR) technology, designed for switching RF signals.

| Parameter | Unit | PIN diode switch [7,70,75–80] | FET switch [7,70,75, 81–83] | EMR[a] [84,85] | MEMS switch [7,70,75] |
|---|---|---|---|---|---|
| actuation voltage | V | ±3–5 | 3–5 | 3–24 | 20–80 |
| actuation current | mA | 3–20 | 0 | 150–15 | 0 |
| power consumption | mW | 5–100 | 0.05–0.1 | <400 | 0.05–0.1[b] |
| switching time | $\mu$s | 0.01–0.1 | 0.001–0.1 | >1000 | 1–300 |
| off-state capacitance | fF | 18–80 | 70–140 | – | 1–6 |
| series resistance | Ω | 2–4 | 4–6 | <0.1 | 0.5–2 |
| cutoff frequency | THz | 1–4 | 0.5–2 | 0.005 | 20–80 |
| RF isolation (1–10 GHz) | dB | >35 | 15–25 | >40 | >40 |
| RF isolation (>10 GHz) | dB | 20–35 | <20 | – | 25–40 |
| insertion loss (1–10 GHz) | dB | 0.3–0.7 | 0.4–2 | <0.3 | 0.05–0.2 |
| insertion loss (>10 GHz) | dB | 0.7–2 | >2 | – | 0.1–0.2 |
| isolation voltage | – | medium | low | high | low |
| power handling (1 GHz) | $W_{CW}$ | <10 | <5 | 10 | <0.5 |
| signal linearity (IP3) | dBm | 27–45 | 27–53 | >60 | 66–80 |
| size | – | small | very small | large | small |
| cost — SPDT type [84] | USD | 0.9–8 | 0.5–4.5 | 0.85–12 | 8–20 |
| life cycles [84] | – | $>10^9$ | $>10^9$ | $0.5–5\times10^6$ | $>10^8$ |

[a]PCB mounted relays for high-frequency switching applications, such as the OMRON G6 series
[b]includes drive circuitry

**Table 3.** Advantages and disadvantages of MEMS switches.

| Advantages | Disadvantages |
|---|---|
| very high DC and RF isolation | high actuation voltages needed[a] |
| very low insertion loss | low switching speed |
| high signal linearity | limited power handling |
| almost zero power consumption[a] | lifetime uncertain |
| very large bandwidth[b] | problematic integration with RF circuits |
| miniaturization | special packaging necessary |
| simple control circuits | reliability uncertain |
| high volume production possible | price uncertain |
| very resistant to external influences[c] | |

[a]for electrostatically actuated switches
[b]without sacrificing performance
[c]temperature, radiation, mechanical shock

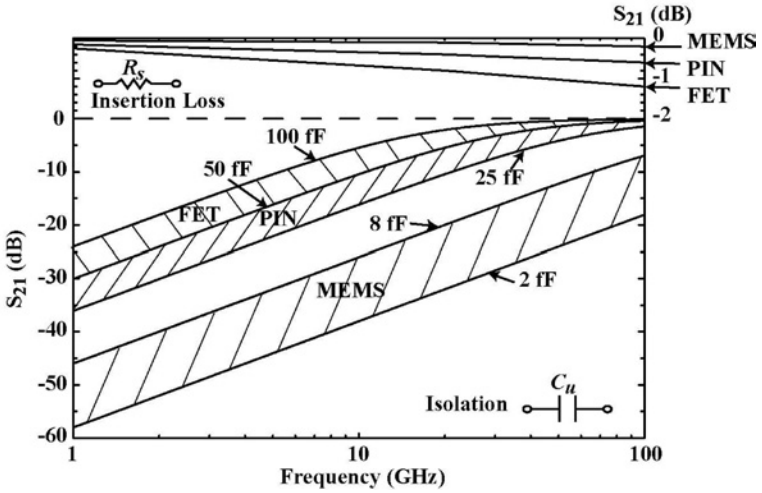


**Figure 1.** Typical RF performance of MEMS metal-contact switches compared to PIN-diode and FET based switches, extracted from a simplified equivalent circuit model [88].

effect transistors (FET) can hardly meet the performance requirements of today's communication systems, especially concerning the isolation, the insertion loss (on resistance) and the signal linearity. Even though also semiconductor-based switches have been improving over the last decade [76–78, 81–83], their RF signal performance still decreases drastically with frequency above 1 GHz where they are limited either in power handling or they show a very large insertion loss, poor isolation and high signal distortion [7]. However, MEMS switches perform very well over an extremely large bandwidth with very uniform characteristics, even above 100 GHz [75]. That is the advantage of having a purely mechanical element opening and closing or short-circuiting an almost unimpaired transmission line. Table 2 compares the performance of PIN-diode and FET based electronic switches and high-frequency electromechanical relays (EMR) with RF MEMS switches. The superior RF signal handling properties of MEMS metal contact switches are also demonstrated in Figure 1.

Unfortunately, MEMS switches also have some obvious disadvantages, which are compared to their advantages in Table 3. This problematic has inhibited the leap from the lab to the fab, since so far no system and component manufacturer has dared to take the risk of embedding a device uncertain in its reliability and lifetime into a volume product.

It is very interesting to observe that miniaturized mechanical relays, as small as 0.3 $cm^3$ in last generation telecom applications [89], still out-perform their electronic counterparts, solid-state relays (SSR), especially in isolation, on-resistance and even in price. This drives a significant commercial need for a device which bridges the technical and economical gaps between electromechanical "macro-relays" and solid-state devices, in particular to address the need for extreme miniaturization while preserving the benefits of metal contact switching. MEMS fabrication technology offers the benefits of economies of scale, precision, and device matching capabilities that are un-

**Table 4.** Categorizing of MEMS devices in terms of their mechanical complexity[a].

| | Category 1 | Category 2 | Category 3 | Category 4 |
|---|---|---|---|---|
| moving parts | – | × | × | × |
| touching surfaces | – | – | × | × |
| impacting surfaces[b] | – | – | – | × |
| examples | inkjet heads, microneedles | accelerometers, gyros | valves | metal contact switches |
| complexity | low | → | | high |
| reliability | less critical | → | | highly critical |

[a]Based on information from an oral presentation by G. M. Rebeiz at the Transducers 2003 conference, Boston, USA, June 8–12, 2003.

[b]The physical impact — force or rubbing — between the two surfaces determines the functionality of the device.

paralleled in conventional assembly-based manufacturing. Therefore, micromachining seems to be a very attractive technology for fabricating extremely miniaturized, high-volume, low-cost micromechanical relays [90].

Even from a MEMS perspective, a micromachined switch — especially a DC metal contact switch — is mechanically a rather problematic and complicated device compared to other typical MEMS devices, as illustrated in Table 4. However, because of their market potential, MEMS switches are attracting a lot of attention from universities, research institutes and industries. The need of better signal switching properties in more sophisticated telecommunication standards and in high-end applications might compensate for the technological skepticism [7, 10, 14, 91].

At the end of this introducing section I would like to acknowledge the so far most exhaustive source on RF MEMS switches and the probably best book ever written on this sub-topic of MEMS: Gabriel M. Rebeiz's "RF MEMS: Theory, Design, and Technology" [75], discussing the status of the field by September 2002. This book is so rich in detail that it seems to address all conceivable aspects of the matter. It completely meets the requirement stated as the first sentence in its preface: "All I wanted to do is to write a *deep book*" (italics as in the original). Many thanks to the author and his co-writers for sharing their knowledge and preparing it in such an extraordinary way!

### 2.1.3 MEMS switch types

A MEMS switch is a bistable mechanical device fabricated by micromachining techniques, allowing the free propagation of an electrical signal from an input to an output in one state and blocking the signal in the other state. Stability in one or both of the states is achieved with or without applying an external energy source, and the transition between the two states is controlled by imposing or releasing the external

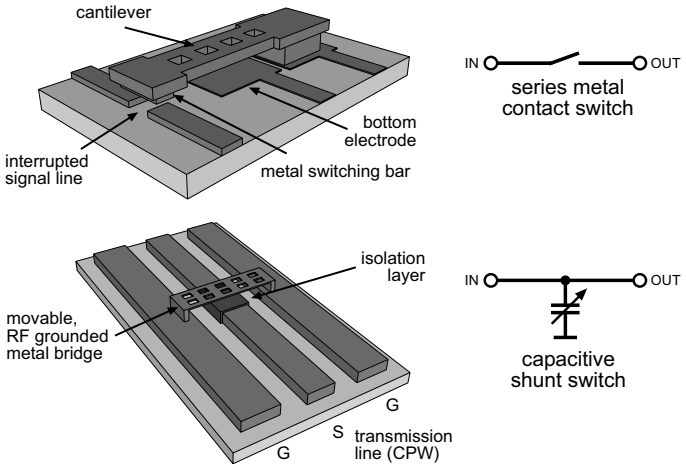


**Figure 2.** The two most common electrostatically actuated MEMS switch types.

effort.

RF MEMS switches can, among others, be classified by their actuation principle, by the circuit configuration, the fabrication technology or by the intended application. Table 5 illustrates some possibilities to categorize MEMS switches.

About 80% of the switches presented so far belong to the two most common switch types, schematically illustrated in Figure 2:

- **Electrostatically actuated series switches with metal contacts:** A cantilever or membrane with a switching metal contact bar vertically opens or closes the signal line. Switches of this category are normally off, and the incoming RF wave is reflected by the interrupted signal line in the off-state. In the on-state, the signal can propagate over the metal contact bar short-circuiting the gap between the input and the output line. This switch type is capable of switching DC to RF signals and is both in its fabrication and in its reliability more complicated than the next type, mainly because of its metal contacts.

- **Electrostatically actuated capacitive shunt switches:** Consist of a metal bridge or membrane connected to RF ground and moving vertically above the isolated signal line. The switch is normally on, and in the down position, the bridge capacitively short-circuits the signal line to the RF ground. Thus, in the down-state (off-state), the signal propagates via the bridge to the ground and the isolation mainly depends on the parasitic inductance of the whole ground path[6]. This switch type is basically not suitable for low frequency signals. It is relatively simple in its fabrication, very fast with a switching time of only a few microseconds, and very small compared to the metal contact switches which need a stronger actuator to obtain the necessary contact and opening forces.

[6]The parasitic inductance is often used as a design feature, since it creates, together with the bridge capacitance, a series resonant circuit providing increased isolation around the resonance frequency [70, 93].

**Table 5.** Possible categories of MEMS switches.

| Classified by | Categories | Comments |
|---|---|---|
| circuit type | ◦ series switch | metal contact or capacitive |
| | ◦ shunt switch | metal contact or capacitive |
| switching contact | ◦ metal contact | DC to a few tens of GHz |
| | ◦ capacitive | RF >2 GHz[a] |
| I/O configuration | ◦ SPST | single pole, single through |
| | ◦ SPDT, etc. | single pole, double through |
| actuation mechanism[b] | ◦ electrostatic | fast, low power, simple, high voltage |
| | ◦ electrothermal | slow, high power[c], low voltage |
| | ◦ magnetostatic | high force, high power[c], complex fabrication, large distances |
| | ◦ mercury-droplet | very limited applications |
| | ◦ piezoelectric | complicated fabrication |
| | ◦ combined mechanisms | complicated fabrication, good performance |
| movement | ◦ lateral | large size, difficult contact fabrication |
| | ◦ vertical | most common and most suitable for surface-micromachining |
| | ◦ torsional | low voltage, push-pull concept, simple, large contact distance |
| | ◦ rotary, in-plane | complicated, uncommon |
| moving structure | ◦ membrane | large actuation electrodes, low voltage |
| | ◦ bridge | low RF intrusion |
| | ◦ cantilever | single side clamped bridge |
| fabrication technology | ◦ on top of RF circuits | SOC integration, only CMOS/GaAs compatible processes |
| | ◦ CMOS technology | using the standard CMOS back-end process chain, very restricted, very low cost |
| | ◦ transfer bonded | SOC integration, complicated, very flexible designs |
| | ◦ unrestricted | SOP integration or single package |
| | ◦ non-standard substrates | fabrication on low-cost laminates, restricted clean-room compatibility |
| switching application | ◦ microrelay | to switch currents >10 mA |
| | ◦ DC..RF signal | for automated test equipment (ATE) e.g. |
| | ◦ RF signal | low power, low current (<1 mA) RF signals |
| | ◦ RF power | RF signal switching >10 dBm |

[a] the so-called floating metal-layer capacitive switch has good performance down to ≈300 MHz [92]
[b] for a comparison see also Section 2.2.1
[c] unless using a bistable latching mechanism

From an application point of view, a third type should be added, even though it is not a "true" RF MEMS switch, and, in its basic concept, is just a variation of the first switch type:

- **Microrelays**[7]**:** Highly miniaturized metal-contact relays fabricated by micromachining techniques. The most common actuation mechanisms are electrostatic, magnetostatic or electrothermal, and the relays are designed with larger contact and restoring forces from a few to a few tens of milliNewtons to be able to handle currents over 10 mA. The contact resistance is rather small and in the range of a few hundred milliOhms or lower. The contact distance in the off-state has to be at least 10–20 $\mu$m to provide sufficient DC isolation up to about 400 V in air. Reliability is a big issue for this type of switch, since the relatively weak MEMS actuator has to open metal contacts carrying larger currents. A longer switching time in the millisecond region is tolerated by most of the target applications[8].

### 2.1.4 Some selected MEMS switches

A variety of switch concepts with interesting design features have been published over the last decade. The following paragraphs give an overview of some MEMS switches, commenting on their special characteristics and performance. The selection criteria for the listed switches are: novelty at the time they were introduced, relevance in functionality, outstanding performance, special design features, fabrication processes or special choice of structural materials. The items are sorted chronologically by the date of the first publication, even if a later published journal paper with more extensive information than a first published conference paper is given as the reference.

It is very interesting to observe that research institutes, companies and universities are similarly engaged in switch development and also in publishing results in scientific journals and at conferences. However, it is clearly visible that companies put their efforts in metal contact switches with, if possible, good microwave performance, whereas the field of capacitive microwave shunt switches is still dominated by universities and research institutes. The latter switch type is of great interest for military applications, which could be one reason why companies might not be so eager to disclose their activities to the community.

A survey of MEMS switches should not be limited to scientific publications, especially since this field is of so much commercial interest. Patents are a rich source of information on switch designs and reveal many clever, otherwise unpublished ideas. Also, the activities of many companies such as Intel, Northrop Grumman, NEC, Nokia or Ericsson, publishing rarely or not at all on MEMS switches in scientific papers, can

[7]The term "microrelay" is often used for all types of MEMS switches whose switched signal path is electrically isolated from the actuation circuit, i.e. not a so-called "in-line" switch. In this book however, the term "microrelay" is used for highly miniaturized, micromachined electromechanical relays to switch larger DC to low frequency currents, in contrast to a mere signal switch for currents below 1 mA.

[8]Basically, one must distinguish between the actuator response time and the actual switching time: for most applications, a very slow actuator is not crucial, but the actual movement of the contacts should not be longer than a few milliseconds to avoid degradation of the contacts due to sparking and discharging in close approximation.

be tracked down. Patents are not as suitable as good review papers for newcomers to study, but they are a better source for a person already having some knowledge in the field, since they often provide more extensive information and consist of much more details than scientific publications. It is also interesting to note that patent applications anticipate chronologically the development of MEMS switches. Just to give one example: The switch research and development published in 1997 by Zavracky/Majumder at Northeastern University, MA, USA, in cooperation with Analog Devices and now continued at Radant MEMS, goes back to basic ideas which were filed as patents by Zavracky already in 1984, long before Larson published his historical RF MEMS switch paper in 1991. Table 6 lists a few interesting, granted US patents on electrostatically actuated series switches with metal contacts, from the mid 80s of the last century up to 2004.

**Table 6.** Interesting US patents on electrostatically actuated MEMS series switches, granted by April 28, 2004. Sorted by the date of filing of the patent, with references to scientific publications if directly corresponding to the patented designs.

| Patent no. | filed on | Inventor (assignee) | Description |
|---|---|---|---|
| 4543457 | 25.01.1984 | Petersen et al. (Transensory Devices) | pressure, acceleration, force digitizing switch |
| 4674180 | 01.05.1984 | Zavracky, Morrison (Foxbro) | historical cantilever switch patent |
| 5121089 | 01.11.1990 | Larson (Hughes) | rotating RF MEMS switch [6] |
| 5619061 | 31.10.1994 | Goldsmith et al. (Texas Instr., now Raytheon) | many switch variations (in-line, torsional, ..) |
| 5578976 | 22.06.1995 | Yao (Rockwell) | Rockwell cantilever switch [94] |
| 5673785 | 03.10.1995 | Schlaak, Schimkat (Siemens) | curled membrane switch [95] |
| 5638946 | 11.01.1996 | Zavracky (Northeastern Univ.) | series switch, base for a later Analog Devices (now Radant) switch [96] |
| 6162657 | 06.11.1997 | Schiele, Kozlowski (Fraunhofer Ges.) | curled cantilever switch [97] |
| 6046659 | 15.05.1998 | Loo, Hyman, et al. (Hughes, now HRL) | classical cantilever-spring design with sandwich structure [98] |
| 6100477 | 17.07.1998 | Randall, Kao (Texas Instruments) | recessed membrane switch |
| 6143997 | 04.06.1999 | Feng and Shen (Univ. of Illinois) | guided, free-standing membrane switch |
| 6229683 | 30.06.1999 | Goodwin-Johansson (MCNC) | curled cantilever; electrodes surrounding the contacts; buried electrodes |
| 6307452 | 16.09.1999 | Sun (Motorola) | folded spring membrane switch with distance bumps |
| 6307169 | 01.02.2000 | Sun et al. (Motorola) | single anchored, membrane-type switch [99] |

**Table 6.** continued.

| Patent no. | filed on | Inventor (assignee) | Description |
|---|---|---|---|
| 6373007 | 19.04.2000 | Calcatera et al. (US Air force) | 3-metal-layer, vertically stacked shunt/series switch |
| 6469603 | 19.06.2000 | Ruan, Shen (Arizona State Univ.) | latching micro-magnetic relay [100], later at MICROLAB Inc. |
| 6655011 | 02.10.2000 | Kornrumpf et al. (General Electric) | mechanically bistable, vertically moving switch |
| 6483395 | 16.03.2001 | Kasai et al. (NEC) | membrane type with distributed stiffness; transfer-bonded switch |
| 6646215 | 29.06.2001 | Nelson (Teravicin Techologies) | cantilever switch with pull-mechanism to separate the contacts |
| 6529093 | 06.07.2001 | Ma (Intel) | stepped actuation electrodes switch |
| 6531668 | 30.08.2001 | Ma (Intel) | hollow-shaped in-line switch |
| 6535091 | 06.11.2001 | Bechtle et al. (Sarnoff) | torsional switch |
| 6720851 | 01.04.2002 | Hallbjörner et al. (Ericsson) | switch with mechanically tunable membrane stiffness |
| 6628183 | 10.05.2002 | Kang, Cho (Samsung) | center-anchored minimal invasive, ultra-miniaturized series switch |
| 6657525 | 31.05.2002 | Dickens et al. (Northrop Grumman) | stiff membrane; folded, thin springs; distance keepers |
| 6624720 | 15.08.2002 | Allison, Lee (Raytheon) | 4-pole switching device based on four cantilever switches |
| 6639494 | 18.12.2002 | Bluzer (Northrop Grumman) | bridge switch with three symmetric arms |

### Series switches

The ancestor of all RF MEMS switches was published in 1991 by Hughes Research Laboratories, CA, USA. The rotating microwave transmission line switch initiated world-wide RF MEMS activities since it proved to have excellent RF signal performance. Its insertion loss $S_{21,ON}$[9] was less than 0.5 dB and its isolation $S_{21,OFF}$ was greater than 35 dB from DC to 45 GHz. However, the required actuation voltages were above 100 V, and the switch had difficulties in establishing proper contact between the rotor and the switch contacts [6].

In 1994, the University of Neuchâtel presented a switch fabricated with traditional LPCVD surface micromachining processes. The switch could be operated at 50–75 V and was integrated with MOSFETs on the same substrate. However, the contact resistance of the doped polysilicon structure was in the order of 10 kΩ [101].

In 1995, people at Texas Instruments, USA, presented an electrostatically actuated switch based on a modified micromechanical membrane structure initially developed

[9]In accordance with common practice, all data of logarithmic $S$-parameters is given in absolute (positive) values throughout this thesis. Mathematically it would be more correct to set a negative sign, since all of the $S$-parameters of a passive network can only be within the area of the unit-circle, i.e. $|S_{xx,lin}| \leq 1$.

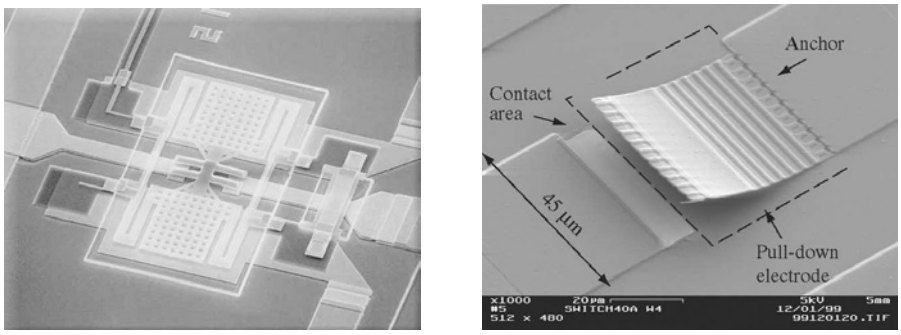


(a) (b)

**Figure 3.** (a) Rockwell Science Center membrane based metal contact switch (size about 250×250 $\mu$m [104]), and (b) MIT Lincoln Labs in-line switch [105].

for an optical mirror array[10]. The membrane could be actuated at voltages between 30 and 50 V. The switch was intended for a 4-bit time delay phase shifter [103].

Also in 1995, the Rockwell Science Center, CA, USA showed a $SiO_2$ cantilever switch with gold contacts, electrostatically actuated at 28 V and fabricated on a polyimide sacrificial layer. With a 3 $\mu$m contact distance in the off-state, the switch had quite good DC and RF characteristics ($S_{21,ON}$ <0.12 dB, $S_{21,OFF}$ >50 dB up to 4 GHz [94]). Another series switch recently developed at the center is shown in Figure 3(a).

In 1997, the Northeastern University, Boston, MA, USA, in cooperation with Analog Devices, published an electrostatically actuated (30–400 V) switch consisting of an electroplated nickel cantilever on top of a copper sacrificial layer, illustrated in Figure 4(a) [96]. Based on this design but later electroplated in gold, in 1999 they presented an extremely small in-line switch with a size of only 30×75 $\mu$m$^2$, shown in Figure 4(b). The off-state gap of the two parallel contacts with an area of only 5 $\mu$m$^2$ each was only about 0.6 $\mu$m and the actuation voltage of the very stiff structure was above 60 V. Despite the extremely small contact distance, the isolation was quite good (40 dB at 4 GHz) and the contact resistance was 1–1.5 $\Omega$ with two parallel contacts, resulting in an insertion loss of about 0.15 dB [106]. The technology was licensed to Radant MEMS Inc., founded in May 2000, where the research and development work is being continued [107]. In 2002, a device very similar to the first design was demonstrated by NMRC, Cork, Ireland, most probably also in cooperation with the local MEMS devision of Analog Devices in Limerick, Ireland, using sputtered titanium as the structural material and polyimide as the sacrificial layer [108].

In 1999, OMRON, Japan, one of the world's largest manufacturers of mechanical relays, introduced an electrostatically actuated (19.2 V) mono-crystalline silicon membrane switch, whose structural elements were etched in a SOI-wafer and transferred to a silicon target substrate by anodic bonding. The switch, probably still

[10]The digital micromirror array, developed by Texas Instruments since about 1983 and finally brought on the market in 1996, is a small success story of a highly complex MEMS volume product. By the end of April 2004, Texas Instruments announced the shipment of its three millionth digital light processing (DLP) device [102].

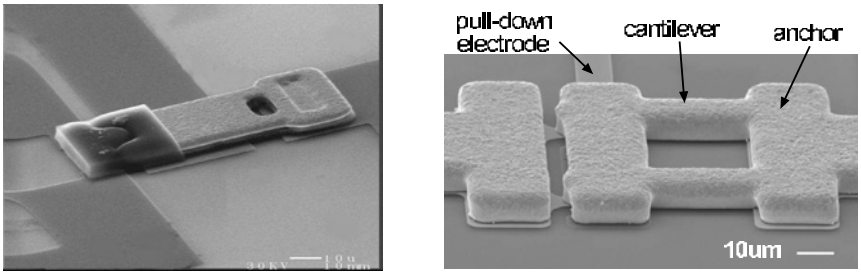


(a) (b)

**Figure 4.** (a) 4-terminal microswitch by Analog Devices (now Radant MEMS [96]), and (b) in-line series switch by the same company [106].

one of the most maturely developed devices of its kind, was presented in a glass-frit package and had good performance from DC up to a few GHz [109].

Switch integration by wafer-scale transfer-bonding was also used for an electrostatically actuated switch at the University of California, Berkeley, USA, in 2000. A polysilicon/silicon nitride membrane, fabricated on a silicon dioxide sacrificial layer on the donor wafer, was transferred to the target wafer by gold to gold thermocompression bonding. The contact distance could not be controlled accurately and varied from 1.5 to 10 $\mu$m, resulting in actuation voltages of 25–120 V [110].

In 2000, the Korea Advanced Institute of Science and Technology (KAIST), presented an interesting switch concept for very low actuation voltage without sacrificing device performance. The switch consisted of a SiN leverage beam fixated by torsional springs and was endowed with a push-pull concept allowing active opening and closing. Actuation voltages as low as 5 V were reported, and the leverage effect of the beam resulted in a relatively large contact distance despite an electrode distance of only 1 $\mu$m, providing fair RF performance ($S_{21,ON}$ ≈1 dB, $S_{21,OFF}$ ≈40 dB at 1 GHz and 30 dB at 4 GHz). Without the pull mechanism, the same switch achieved an isolation of only 17 dB at 4 GHz [111]. Independent of the proposed design at KAIST, the push-pull concept with torsional springs was adapted for switches at the University of Hawaii, Manoa, USA, published in 1999 [112], and at the University of California, Berkeley, USA, in 2000, for a design variation of the switch mentioned in the previous paragraph [110]. Also Infineon Technologies, Germany, picked up the idea in 2001 for a double switch operating at voltages below 10 V and fabricated in a BiCMOS compatible process [113]. Without being published otherwise, a patent on a torsional hinged SPDT switch was filed by people at TRW Inc., CA, USA, in 1999 [114], and inventors at Sarnoff Corp., NJ, USA, filed a patent on a relatively complex torsional switch structure in 2001 [115].

In 2000, the MIT Lincoln Labs in Lexington, MA, USA, presented a very compact and simple in-line switch design based on a curled electrostatic actuator operating at 35–80 V. The cantilever, shown in Figure 3(b), was composed of a $SiO_2$/Al/$SiO_2$ sandwich structure with a controlled out-of-plane bending resulting in a 10–15 $\mu$m contact distance between the platinum contacts [105]. The switch was also realized in a capacitive series switch configuration with an on-off capacitance ratio of over

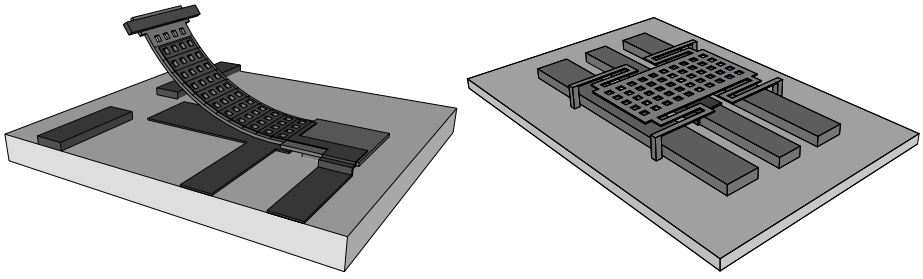

(a) (b)

**Figure 5.** (a) Curled cantilever switch with a large contact distance and relatively low actuation voltage due to the small effective electrode distance resulting in a zipper-like movement of the structure when closing; (b) typical membrane switch. The large electrode area and the soft-spring suspension lead to a low actuation voltage, but poor RF performance and decreased reliability.

300 and was intended to be used in arrays for reconfigurable distributed microwave components [116].

In 2001, Samsung's internal research institute, SAIT, Korea, published an electrostatically actuated switch of very low actuation voltage. Its SiN membrane was fabricated on a photoresist sacrificial layer and the switch achieved very high RF isolation despite actuation voltages of only 3–5 V ($S_{21,ON}$ =0.9 dB, $S_{21,OFF}$=46 dB at 2 GHz). However, no data was presented on the restoring force of the relatively weak structure and stiction problems might be expected[11] [117].

A sytem-on-a-package (SOP) integrated solution was presented by Motorola, AZ, USA, in 2002. The electrostatically actuated cantilever switch (30–60 V) with very good RF performance ($S_{21,ON}$ =0.3 dB, $S_{21,OFF}$=50 dB at 2 GHz) was integrated together with a separate charge pump electronic chip into one hermetic package. The total power consumption of this "true" microsystem was 200 $\mu$W at an actuation voltage of 3 V, thus meeting the low voltage requirements for wireless equipment. The Motorola approach is very interesting since it shows that the company's RF MEMS experts believe in a "high voltage" switch concept with better reliability due to a larger restoring force, even for targeting low voltage applications, made possible by an integrated electronic "high voltage" drive circuitry [99].

One of the other giants in the semiconductor industry, ST Microelectronics, France/ Italy, is following a completely different track both in cracking the low-voltage problem and in the switch integration. In 2003, STMicroelectronics disclosed information on a combined electrothermally and electrostatically actuated SiN membrane switch jointly developed with their long-term research partner CEA-LETI, Grenoble, France. The switching contacts are closed by the thermal actuator (2 V, 20 mA, for 200 $\mu$s), and clamped by an electrostatic actuator with 10–15 V. With an off-state contact distance of 3 $\mu$m, the switch achieved a remarkable RF performance at 2 GHz ($S_{21,ON}$ =0.18 dB, $S_{21,OFF}$=57 dB). The switch is integrated on chip-level (SOC) with electronics, since it is fabricated directly on top of CMOS circuits [118].

[11] For an estimation of the restoring force, see Section 2.2.1.

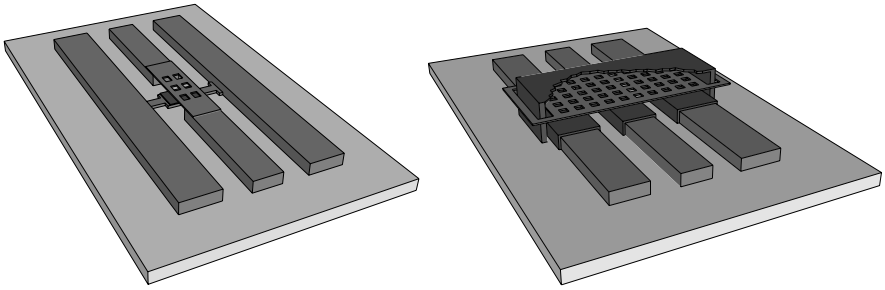

(a) (b)

**Figure 6.** (a) Longitudinal capacitive shunt switch [93]; (b) hinged switch with completely unsupported membrane moving between the top and the bottom electrodes, with potentially very low actuation voltages (the top electrode is partially removed in the drawing to reveal the membrane).

### Shunt switches

In 1998, the University of Michigan, Ann Arbor, USA, published on an electrostatically actuated (14–16 V) switch. The 2 $\mu$m thick, electroplated gold membrane of this switch was embedded between bottom and top electrodes, the latter providing additional forces to open the switch. Aluminum was used as sacrificial layer material, and 50 nm of parylene was coated on the metal structure for isolation and anti-stiction purpose. The RF performance of the switch was quite good ($S_{21,ON}$[12]=0.2 dB at 20 GHz, $S_{21,OFF}$ >30 dB for frequencies <40 GHz [119]). A low spring-constant switch recently developed by the RF MEMS team at the university is shown in Figure 7(a). In this switch, the inductance of the signal path in the down state is determined by the special geometry of the beams supporting the membrane, providing improved isolation because of resonance behavior in the target frequency range.

Also in 1998, at Raytheon, Dallas, USA, people formerly working on MEMS switches at Texas Instruments presented a capacitive shunt switch based on a 0.4 $\mu$m thick aluminum membrane supported by 4 $\mu$m tall, sputtered aluminum posts embedded in a polyimide sacrificial layer. Using silicon nitride as the dielectric material for the isolation layer, the switch achieved an on-off capacitance ratio of 80–110, which resulted in an insertion loss of 0.25 dB and an isolation of 35 dB at 35 GHz. The actuation voltage of the switch shown in Figure 7(b) was between 30 and 50 V [120]. Their first paper was followed by a series of publications addressing dielectric charging problems and lifetime characterization [121].

Researchers at the University of Illinois, USA, came up with a very interesting idea to lower the actuation voltage of a metal contact shunt switch. Their switch,

[12]The terms "on" and "off" are not used consistently for capacitive shunt switches in literature. In this book, they are used from a system point of view and refer to the signal propagation in the "black box MEMS-switch" and not to the mechanical actuation. Thus, "on" means that the signal can freely propagate from the input to the output and that the switch is not actuated (membrane up), and "off" means that the input signal is disconnected from the output whereas the switch is actuated (membrane down). MEMS as a technology is the slave of its application: the switch is "on" when the actuator is "off" and vice versa.

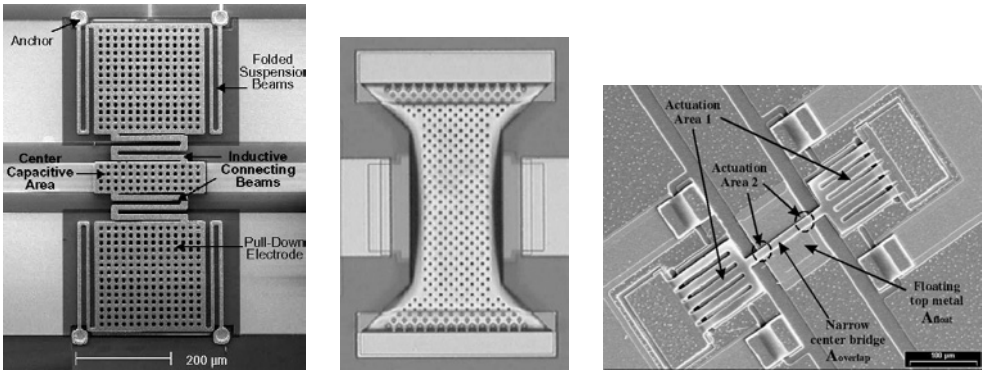


(a) (b) (c)

**Figure 7.** (a) Low spring-constant capacitive shunt switch by the University of Michigan [70]; (b) the classical Raytheon capacitive shunt switch (size about 280×120 $\mu$m$^2$ [120]); (c) floating metal layer capacitive shunt switch by IMEC [125].

presented in 2000, consisted of a 1 $\mu$m thick evaporated, unsupported gold membrane, fabricated between 2 polyimide sacrificial layers, and kept in place by hinges allowing free movement between the bottom and the top electrodes. Since no restoring spring elements are needed for this concept, actuation voltages as low as 9 V could be achieved. The DC to RF performance was also remarkable ($S_{21,ON}$ <0.1 dB up to 40 GHz, $S_{21,OFF}$=50 dB at 1 GHz and 25 dB at 40 GHz [122]).

In 2000, the University of Michigan, Ann Arbor, USA, very active in the field of RF MEMS switching circuits, presented a cross-configuration of 4 electrostatically actuated capacitive shunt switches tuned for the Ka-band. This special arrangement, despite a small off-state contact distance of 1.5–2.5 $\mu$m and actuation voltages as low as 15–25 V to move the 2–2.5 $\mu$m thick gold bridge, resulted in reduced RF reflections and in high isolation over a wide frequency range ($S_{21,ON}$=0.3–0.6 dB, $S_{21,OFF}$=45–50 dB at 22–38 GHz [123]).

Also in 2000, the LG corporate Institute of Technology, Seoul, Korea, presented a capacitive switch using a 190 nm thick strontium titanate oxide ($SrTiO_3$) isolation layer with very high relative permeability, resulting in an on-off capacitance ratio of 600. The gold or copper switch membrane was electroplated on top of a polyimide or photoresist sacrificial layer. The overall RF performance of the switch was very impressive ($S_{21,ON}$=0.08 dB at 10 GHz, $S_{21,OFF}$=42 dB at 5 GHz [124]).

An interesting design variation was introduced in 2001 by Robert Bosch GmbH, Germany. The membrane of their longitudinal capacitive shunt switch is part of the signal line and, when lowered by applying approximately 25 V, is capacitively short-circuited by a ground potential connection between the two ground lines of the coplanar waveguide, as illustrated in Figure 6(a). The inductance of the signal path of that connection, together with the off-state capacitance, builds a series resonance circuit which is optimized in different designs for 24 or 77 GHz ($S_{21,ON}$ <0.3 dB, $S_{21,OFF}$ >33 dB). These frequencies suggest that the target application is automotive radar [93].

In 2002, the University of Michigan, Ann Arbor, USA, published an electrostatically actuated metal contact shunt switch using the classical membrane design of capacitive shunt switches. A 0.8 $\mu$m thick gold membrane, fabricated on a $SiO_2$ sacrificial layer, short-circuits the signal line when actuated at about 50 V [126].

Also in 2002, IMEC, Belgium, Europe's largest independent microelectronics research center, presented a very clever switch design. It has a 100 nm thick aluminum layer deposited on top of a 200 nm thick tantalum pentoxide ($Ta_2O_5$) isolation layer, as shown in Figure 7(c). The additional metal plane acts as an electrically floating layer, which, when touched by a very narrow aluminum bridge, takes on RF ground potential and thus capacitively short-circuits the signal line. This concept has the advantages that 1) the area of the moving bridge does not determine the short-circuiting capacitance and can therefore be very narrow, with very little influence on the RF signal propagation in the on-state, and 2) since it is deposited and not mechanically movable, the floating metal layer is in very intimate contact with the isolation layer, resulting in an optimal, very high off-state capacitance as compared to the classical design where the capacitance is decreased by the surface-roughness between the touching layers and due to local bending of the membrane. The achieved on-off capacitance ratio of this switch design exceeds 600, which is remarkable for its small size and the materials involved [92]. The concept also eliminates the stiction problem caused by charge trapping in the thin dielectric layer, which is one of the major failure mechanism of capacitive shunt switches [75, Section 7.1].

Stiction caused by charge trapping does not occur in so-called all-metal switches, which do not involve any isolation layer. In 2003, the University of Illinois, USA, presented a metal-contact shunt switch using minute separation posts underneath the metal membrane as illustrated in Figures 8(a) and (b), increasing the overall switch reliability [127].

### Vertically actuated microrelays

As stated above, these devices are basically just design variations of metal contact series switches. Instead of targeting DC to RF signal switching applications, they

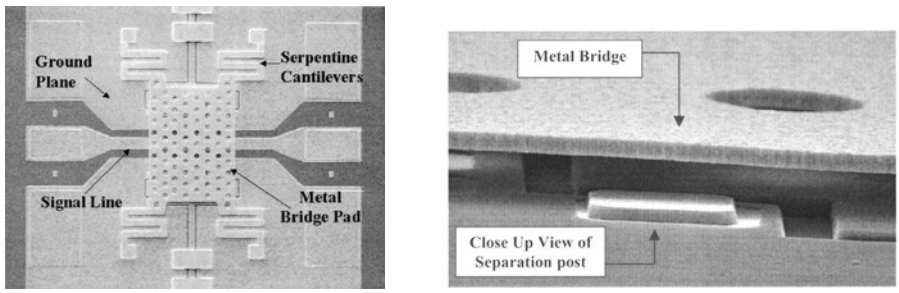


(a) (b)

**Figure 8.** All-metal shunt switch by the University of Illinois: (a) overview of the membrane switch (size about 250×150 $\mu m^2$), and (b) close-up SEM image of a separation post (dimensions not available [127]).

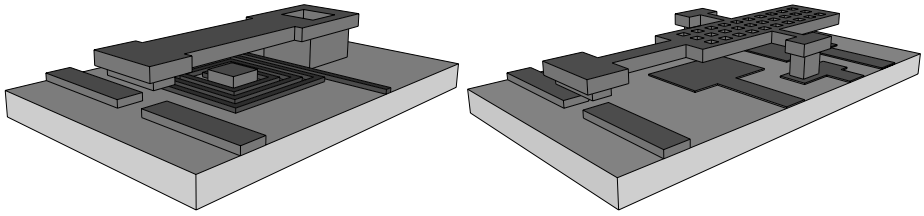

(a) (b)

**Figure 9.** (a) Typical magnetostatic microrelay with a ferromagnetic armature closed by the magnetic field of a coil; (b) switch with leverage beam mounted on torsion springs: push-pull functionality, large contact distance and low actuation voltage.

are designed for larger signal currents from DC to low frequencies. Therefore, they are more susceptible to contact welding which, in addition to a larger contact distance required for better DC isolation and a larger contact force for low resistance, necessitates a stronger actuator design leading to a larger and slower device.

In 1997, the Fraunhofer Institute, Munich, Germany, presented an electrostatically actuated (20–90 V) $SiO_2/Au/SiO_2$ cantilever microrelay fabricated onto a 4 $\mu$m thick polyimide sacrificial layer. The residual stress in the sandwich structure made the beam curle out of plane and thus provided a sufficient restoring force and a large distance of 10–60 $\mu$m between the gold switching contacts [97].

In 1998, Siemens Berlin, Germany, presented an electrostatic curled actuator named the "moving-wedge" actuator, which was expected to lower the actuation voltage. The switch could be operated at 24 V and was also tested successfully to survive over $10^6$ switching cycles carrying a remarkable load of 100 mA between the AuNi5 contacts mounted on an interesting contact spring construction [95].

In 1998, CSEM, Neuchâtel, Switzerland, in cooperation with CP Clare N. V., Belgium, published on a magnetostatically actuated microrelay fabricated on a ferromagnetic FeSi substrate. The actuator consisted of a NiFe electroplated armature processed on a top wafer which was transfer-bonded to the substrate containing a two-layer copper coil with 127 turns. The power consumption of that device was 16 mW at an actuation voltage of 1.9 V, creating a contact force of 1 mN [128]. With a size of approximately $5.3\times4.1$ mm$^2$, the relay was hermetically packaged by a solder-bonding transfer process, had an off-state contact distance of 22 $\mu$m, and was successfully tested up to $10^5$ switching cycles when carrying a 10 mA load [129].

An electrothermally actuated cantilever switch was developed at Tohoku University, Sendai, Japan, and published in 2001. Its actuation mechanism consumed 20–80 mW at an operation voltage of 5 V. A special feature of this switch is spring metal contacts increasing the effective contact area at low contact forces. Also, the switch was fully packaged in a very sophisticated way, including electrical interconnections through a covering glass wafer [130].

In 2002, the Delphi Research Labs, MI, USA, presented an electrostatically actuated microrelay based on a copper electroplated blade closing a 3 $\mu$m contact distance when a voltage of 25 V was applied. Furthermore, the switch was provided with an electronic arc suppression circuit to enhance its lifetime. $1.7\times10^6$ cycles were achieved

at a 50 mA load, and even 5100 cycles when switching a 350 mA current [131].

**Laterally actuated metal-contact series switches and microrelays**

Lateral switches have also been the object of research activities. The major advantage of lateral actuation is that the actuator, the conductor pads, the support structures and often even the contacts can be fabricated in a single lithographic step. Also, an additional counter-actuator to actively open the switch does not necessarily impose increased fabrication complexity, and a large displacement is much simpler to design for lateral actuators than for vertically moving structures. Lateral switches with electrothermal V-shaped actuators are quite strong and an output force of up to 8 mN was reported at an actuation power of 180 mW [132]. These features make them perfectly suitable for microrelay applications. However, lateral switches are more area consuming than their vertically moving counterparts, and the deposition of the contact material on a vertical wall is much more difficult [75, 133, 134].

In 1998, the MEMS Technology Application Center (now Cronos Integrated Microsystems), NA, USA, presented an electrothermally actuated, nickel electroplated relay with a size of about 1 $mm^2$. An actuation power of up to 300 mW created a contact force of 1–10 mN, resulting in contact resistances of 100–200 m$\Omega$ for 2 $\mu$m thick gold contacts, and 500–700 m$\Omega$ for rhodium contacts. Switching a current of 10 mA over 1 million cycles was performed successfully [90]. In 2001, the company presented a VHF bandpass filter tunable by 6 electrothermally actuated microrelays with a current handling capability of 1 A each. The relay was found to survive 53 million cold-switched operating cycles carrying an RF power of 25 W between each switching transition [135].

An electrostatically actuated lateral switch was presented by the Fraunhofer Institute, Munich, Germany, in 1999. The switch was etched by an ICP tool into the 30 $\mu$m thick device layer of an SOI wafer. The actuator bends a cantilever beam with the switching contact along a curved electrode at actuation voltages of 50–260 V [133].

In 2002, the Berkeley Sensor and Actuator Center at the University of California at Davis, CA, USA, published an electrothermally driven relay, consisting of LPCVD

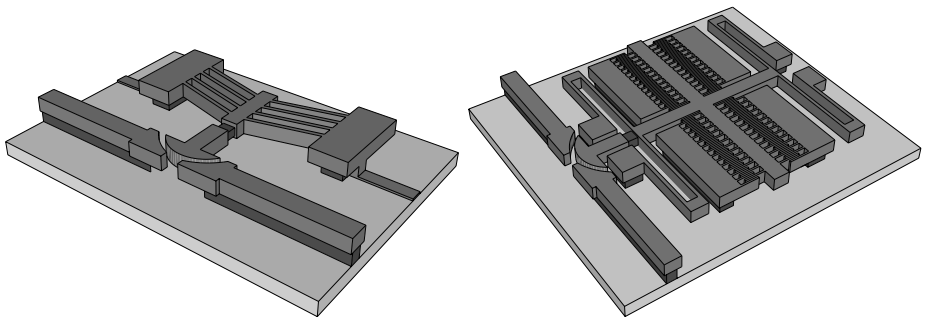

(a) (b)

**Figure 10.** Lateral microrelays: (a) electrothermal actuator; (b) electrostatic comb-drive actuators for both opening and closing.

polysilicon as the structural material for the actuator, the gold coated signal lines and for the contact head. The latter was thermally and electrically isolated from the actuator by a SiN plug. The thermal actuator was cascaded in an optimized way to create a total displacement of up to 9.2 $\mu$m at a power consumption of 20–40 mW [136].

In 2003, the Massachusetts Institute of Technology, Cambridge, MA, USA, presented a lateral microrelay with a very interesting bistable electrothermal actuation mechanism. Being about 8 mm wide, the actuator was quite area consuming, and was designed to have a nominal contact force of 4 mN at a displacement of 137 $\mu$m. Initial tests resulted in a contact resistance of 60 m$\Omega$ with 2.5 $\mu$m thick electroplated copper contacts, making it able to carry a static load of 3 A [137].

**Switches using special fabrication technology**

The switches discussed in this paragraph are probably not so maturely developed and might not have very outstanding performance, but they show new and interesting methods in fabrication technology especially suitable for switch integration and for merging MEMS and integrated circuits.

Almost all MEMS switches listed in this section are CMOS-compatible. Thus, they could be post-processed on a substrate already containing RF circuits since their highest process temperature does not exceed about 350 °C[13]. In a different approach, further integrating and lowering the costs, the switches are even fabricated by standard CMOS back-end technology. In 2001, the Oriental Institute of Technology, in cooperation with the National Taiwan University, both in Taipei, Taiwan, presented a lateral moving switch fabricated in a conventional 0.6 $\mu$m single polysilicon three metal layer CMOS process. Only a single additional, mask-less free-etch process step had to be carried out to release the structures [138]. A similar approach was investigated by the IBM Watson Research Center, NY, USA, and presented in 2004. Here, vertically moving metal contact switches and mechanical resonators were fabricated by base copper damascene processes from IC interconnect technology. The switches could be activated at voltages of about 40 V and showed acceptable performance up to 2 GHz [139].

MEMS devices — and thus RF MEMS switches — are traditionally fabricated on wafers, the standardized substrate of the semiconductor industry. The substrate and fabrication costs are usually distributed over several thousands of chips, leading to very low costs per device despite the expensive clean-room technology. However, certain applications such as antennas in the lower GHz range cannot be miniaturized and require space in the order of many square-centimeters. On the other hand, their rather large process tolerances do not require semiconductor manufacturing precision. Thus, it would be too expensive to waste a semiconductor substrate with a yield of only a few devices per wafer, especially, since the antenna structures could be fabricated very cheaply using conventional printed circuit board (PCB) technology. Whenever MEMS switches are intended to reconfigure such antennas, they should not be fabricated together with the antennas on the same substrate for these economical

[13]The absolutely highest temperature allowed in CMOS post-processing is 480 °C. However, also the exposure time of the circuits to these temperatures is an influencing factor. As a rule of thumb, all post-fabrication steps above 400 °C are problematic.

reasons. Therefore, the idea to fabricate the MEMS switches on a large-area substrate is close at hand. In 2003, the University of California at Irvine, USA, published on a fabrication process for directly constructing RF MEMS capacitive switches on a laminated microwave PCB. Traditional semiconductor/MEMS fabrication processes cannot be used on these substrates, and special processes such as wet metal etching, compressive molding planarization, and a low temperature, high-density, inductively coupled plasma chemical vapor deposition (HDICP-CVD[14]) were used to fabricate the aluminum-membrane switches on a standard, low-cost FR4 substrate. The switches could be actuated at 35 V and had acceptable RF performance in the frequency range from 5 to 30 GHz [140].

In 2001, the University of Colorado, USA, published on flexible circuit based RF MEMS switches, fabricated by using the typical flexible circuit processes and materials. The switch membranes consisted of low-cost Kapton-E polyimide with copper cladding, bonded at 130 °C to a patterned benzocyclobutene (BCB) spacer layer on RT/Duroid 6002 substrate with a copper transmission line. With a chip size of about 1 $cm^2$ and a contact distance of 40–50 $\mu$m, the switches could be actuated at about 70–90 V [141].

**Other interesting switch types**

Acceleration switches are devices closing a contact by a mass moving due to external acceleration. These switches are not typical RF MEMS switches, but research and development in this area has been going on for more than a decade and the engineering solutions of these devices, especially in integration and packaging, are very mature. Compared to conventional piezoresistor or capacitive read-out accelerometers, these switches have the advantages of high immunity to electromagnetic influence (EMI), simple signal preconditioning, and very simple fabrication and integration with ICs. All these advantages make them perfectly suitable for their high-volume target market, even though the price of analog electronics and analog-to-digital converters (ADC) has been dropping rapidly over the last decade. In 1996, KAIST, Korea, presented a pre-stressed bimorph beam switch with a 7 $\mu$g proof mass. The switch was tunable in its acceleration sensitivity by a voltage of 0–76 V [142]. Siemens AG, later Infineon Technologies, Germany, has also been quite active in this field since the middle of the 1990s. They have been working on laterally moving, CMOS compatible, electroplated structures which can be fabricated directly on top of integrated circuits [143]. Furthermore, they presented an array of acceleration switches with different acceleration thresholds, thus a "quasi-analog" accelerometer [144]. In 2002, the Tohoku University, Sendai, Japan, in cooperation with Sensor company, Hanyu, Japan, presented a bulk micromachined acceleration switch whose on-state duration, determined by the mass, squeeze-film damping and by a clever mechanism to extend the hold time, is designed to convert the acceleration magnitude [145].

The next paragraphs introduce a few switches with interesting and certainly inspiring actuation mechanisms. The different designs show the possibilities of the creative and unlimited MEMS world when solving engineering problems.

[14] for deposition of silicon nitride below 100 °C

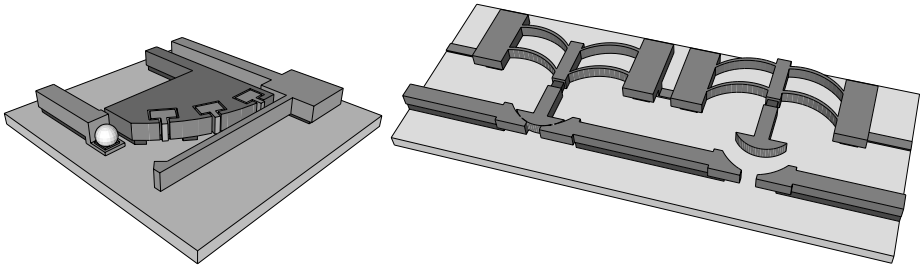

(a) (b)

**Figure 11.** Interesting switch concepts: (a) mercury drop switch with cantilever beam bending along a curved electrostatic electrode [146]; (b) mechanical bistable lateral switch shown in the on and in the off-state [134].

Mercury-wetted macro-relays have been used since 1940 to solve the reliability and life-time problems of solid-solid contact relays [147]. At the University of California, Los Angeles, CA, USA, this idea was adapted for a micromachined relay based on mercury microdrop contacts in 1996. A suspended microheater in a deionized water reservoir grows a vapor bubble whose pressure induces the movement of a mercury droplet short-circuiting two metal contacts [148]. In another embodiment, a mercury drop evaporated on a gold pad is contacted by a laterally moving, electrostatically actuated polysilicon cantilever, as illustrated in Figure 11(a). However, the contact resistance of the mercury contact relays was unsatisfactory and above 1 kΩ [146].

Mechanical stability in both the on and the off-state is a highly ranked design feature especially for electrothermally actuated switches. One attempt to achieve this goal was presented by the New Jersey Institute of Technology, Newark, NJ, USA, in 1998. Their switch consists of a two-segment multimorph cantilever. The bistable relay could be operated with thermal power pulses of 10–12 mW for 0.5 ms and the lateral displacement of the contacts was about 30 $\mu$m [149].

In 2002, Ford, MI, USA, in cooperation with the Brigham Young University, Provo, UT, USA, published an electrothermally actuated micromachined relay with a size of 1.92 mm$^2$. The switch, schematically drawn in Figure 11(b), is based on an interesting bistable snapping mechanism with a very large contact displacement of 88 $\mu$m. Even though optimized for the chosen geometry, only a relatively low contact force of less than 25 $\mu$N could be reported [134].

In 2001, the company MICROLAB Inc., Chandler, AZ, USA, proposed an interesting zero-power magnetostatic switch concept based on a micro magnetic latching mechanism. Only a short positive or negative current pulse (80–120 mA at 5–6 V for 0.4 s) is needed to reverse the magnetic polarity of a permalloy cantilever suspended by torsional springs in an external magnetic field. Depending on the magnetic polarization in the cantilever, a positive or negative torque is created, bringing the switch into two stable positions. The contact forces achieved with this design were relatively small (40 $\mu$N) and the main disadvantage of the whole concept is the need of a permanent magnet mounted under the substrate [100].

### 2.1.5 Applications of MEMS switches

MEMS switches are intended to switch the propagation path of an analog signal with a very high signal purity. This function might be used to connect/disconnect an electrical potential, or to select signals, for instance the incoming and the outgoing signal of an antenna, or to reconfigure a sub-system. Typical applications of the latter type are switching of filter banks, tuning of filters by switching capacitors or inductors [135], switching of delay lines in phase-shifters [47–50], impedance matching by switching stub-lines [59] or capacitors [60], and configuration of antenna patterns or frequencies by switching antennas or parts of an antenna [53–56].

Depending on the frequency specifications, either capacitive or metal contact switches are preferred for certain applications.

To switch DC to RF signals, typically required in high-quality test and measurement equipment, the most demanded properties are an extremely large bandwidth from DC to a few tens of GHz with very good signal properties over the whole bandwidth. The switching speed and the power consumption are less important. Metal contact switches are good candidates for these applications.

Microrelays are intended for applications where DC to low frequency currents have to be switched. Here it is important to galvanically decouple the input from the output in the off-state, and to have a small series resistance for a low voltage drop and low power dissipation in the on-state.

Capacitive shunt switches are usually designed for frequencies above 1 GHz and

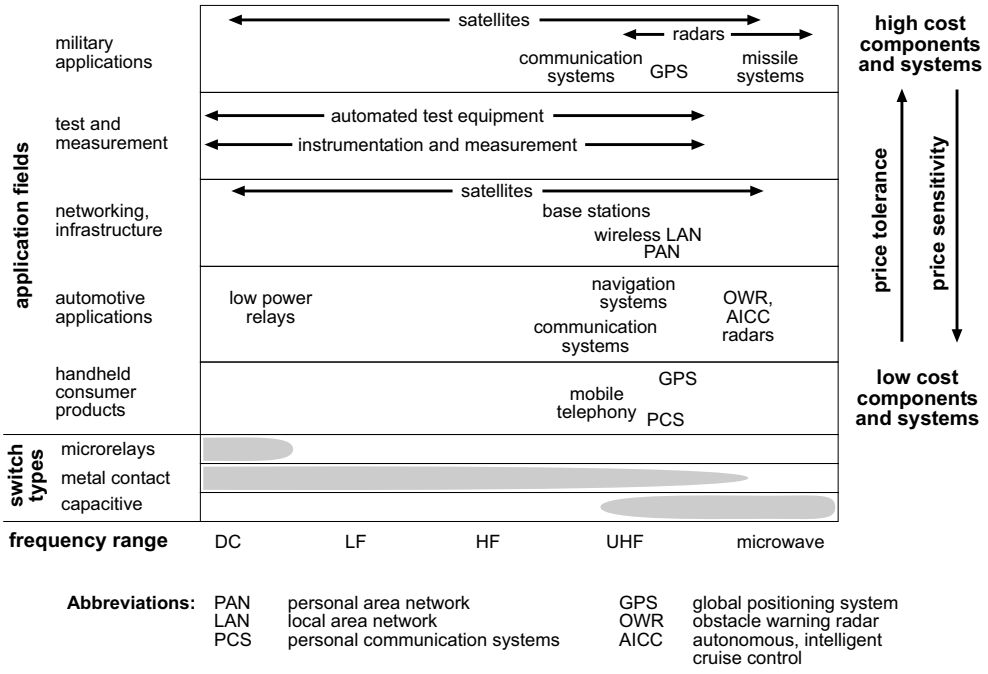


**Figure 12.** Main application fields of MEMS switches.

small bandwidths. Especially when targeting wireless equipment, low power consumption and small size are required.

Military and space applications also favor MEMS components because of their robustness against external influences such as radiation, temperatures and strong electromagnetic fields, and because of their high shock resistance.

Switch reliability and a large number of switching cycles of the order of tens of billions are equally important for most applications.

The diagram in Figure 12 gives an overview of different MEMS switch applications, displayed over the signal frequency. The diagram also gives information on the price sensitivity of the specific applications. It can be expected that MEMS switches are first going to be introduced in less cost critical areas before they might be considered for low-cost, high volume markets.

*It is better merely to live one's life,*
*realizing one's potential,*
*rather than wishing*
*for sanctification.*

*He who lives in filial piety and love*
*has no need of ethical teaching.*

*When cunning and profit are renounced,*
*stealing and fraud will disappear.*
*But ethics and kindness, and even wisdom,*
*are insufficient in themselves.*

*Better by far to see the simplicity*
*of raw silk's beauty*
*and the uncarved block;*
*to be one with onself,*
*and with one's brother.*

*It is better by far*
*to be one with the Tao,*
*developing selflessness,*
*tempering desire,*
*removing the wish,*
*but being compassionate.*

*Lao Tzu*
*Tao Te Ching, Chapter 19*
*(translation by Stan Rosenthal)*

*"I refuse to prove that I exist," says God, "for proof denies faith, and without faith, I am nothing."*

*Douglas Noel Adams*
*1952–2001, British Science Fiction Writer,*
*in "The Hitch Hiker's Guide to the Galaxy"*

## 2.2 Design considerations of electrostatically actuated metal-contact switches

A quick search in the INSPEC database of scientific publications in April 2004, using the search terms "MEMS switch" ∨ "microswitch" ∨ "microrelay", results in approximately 1600 records. Most publications report on new switch designs with characterization results, discussing their general advantages and talking about their applications. Details are often not disclosed to protect intellectual property and to stay ahead of competitors. Only a few sources specifically address design related issues, discuss the influence of the variety of design parameters, and compare different concepts with each other [75, 89, 123, 150–153].

This section addresses some selected, typical and in my opinion important design problems of electrostatically actuated metal-contact switches. It reports on the influences of various design parameters on each other and tries to provide a feeling for designing a MEMS switch. It also covers the dominant reliability problems of contact switches.

The high art of managing complex MEMS devices is still their fabrication and the knowledge about the mechanical behavior of multi-layer structures. Material issues such as the properties of low-stress free-standing films are not of minor importance but are not discussed in this section whose focus is on a device and system level, and I would like to refer to the fabrication chapters of standard (RF) MEMS sourcebooks [75, 154, 155]. However, material related issues of electrical contacts under low mechanical forces are a crucial point for microrelays and metal-contact microswitches, and are therefore briefly addressed in Section 2.2.3.

The packaging and the integration of RF MEMS switches, two of the major obstacles on their way to commercialization, are discussed in Section 2.3.5.

### 2.2.1 Actuation voltage, displacement, contact and restoring forces

These four switch parameters are tightly coupled to each other, which makes good switch design very difficult. Figure 13(a) is a schematic drawing of a simple electrostatically actuated cantilever switch, and Figure 13(b) shows a simplified quasi-static electromechanical equivalent circuit model of such a cantilever-spring or membrane-spring based switch. These are the most common MEMS series switch types and are discussed in this section. The active forces, when establishing the contact and when opening it, are illustrated in Figure 13(c). The overall goal of any switch design is to balance these forces to achieve the desired contact performance, expressed in the contact resistance and in the contact reliability.

Figure 14 shows how the design parameters actuation electrode area $A$, distance between the electrodes $d$ (not to be confused with the switching contact distance),

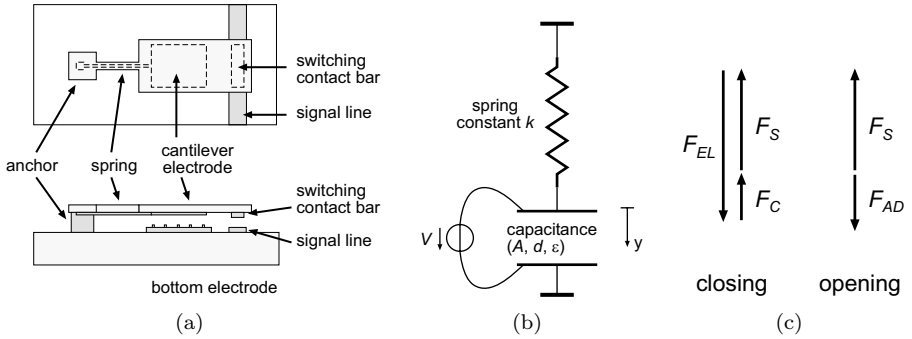


**Figure 13.** (a) Top and side view of a cantilever based switch; (b) simplified mechanical equivalent circuit model; (c) active forces when establishing and when opening the contact (forces as defined in the text and in Figure 14).

actuation voltage $V$ and spring constant $k$ control the active forces and the contact performance of the switch model. The choice of contact material has also an important influence, which will be discussed in Section 2.2.3. The distance between the electrodes is closely connected to the contact displacement, which determines the DC and RF isolation of the switch, see Section 2.2.2. The isolation is not directly considered in the discussion of this section, but it should be kept in mind that certain very low electrode distances practically do not make sense for the discussed model, because the switch would not provide acceptable isolation.

Basically, a high contact force $F_c$ results in a low contact resistance, and a high restoring force is desired to prevent contact stiction caused by microwelding. A high restoring spring force $F_s$ can be achieved by a relatively stiff structure and a large displacement, both requiring an increased electrostatic force $F_{el}$ to pull down the structure. Also, increasing the restoring force demands an even stronger electrostatic actuator to maintain the desired contact force (see Figure 13(c)). The electrostatic force can only be increased by the actuation voltage or by a larger actuation electrode area, resulting in a larger switch size. To complicate it even more, the effective restoring force is the spring force minus the adhesion force $F_{ad}$. The adhesion force is very difficult to predict or to control, since the contact physics in microswitches is still not very well understood [153, 156].

The actuation voltages of current electrostatic switch designs are between 15 and 80 V to achieve sufficient switching performance [70, 75]. These voltages are by far not compatible with the voltage levels used in electronic products. Thermal and magnetostatic actuators can be designed in a way resulting in actuation voltages below 5 V, but their high power consumption, unless using a bistable latching mechanism, is even less acceptable especially when targeting wireless applications. Also, switches based on electrostatic actuation are the most promising designs in terms of reliability and wafer-scale manufacturing possibilities [70]. Another strong advantage of electrostatic actuation mechanisms is the fact that the maximum force is created in the end position with touching contacts. The last paragraph of this section lists the advantages and disadvantages of common actuation mechanisms for MEMS switches with almost-zero power consumption in both the on and the off-states.

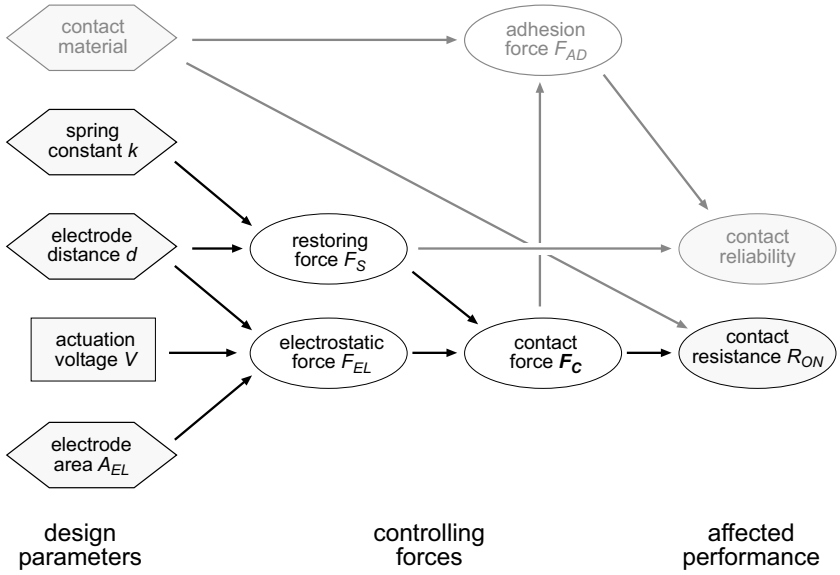


**Figure 14.** Illustration of the connection between the design parameters and the active forces in the switch model and how they affect its performance in terms of contact resistance and reliability.

The pull-down voltage required by a switch as illustrated in Figure 13(a) can be calculated approximately with the simplified mechanical model shown in Figure 13(b). The electrostatic force and the restoring spring force are given by [7]

$$F_{el} = \frac{1}{2}\epsilon_0\epsilon_r \frac{A}{(d-y)^2}V^2 \tag{1}$$

$$F_s = -ky \tag{2}$$

with $\epsilon_r$ the effective relative permeability, $A$ the electrode area, $d$ the initial distance between the electrodes, $V$ the actuation voltage, $k$ the spring constant reflecting the mechanical stiffness, and $y$ the idealized parallel deflection of the beam. The upper electrode snaps against the lower one if the electrostatic force is larger than the spring force. That is the case for when the distance between the electrodes falls below a critical distance, and can be explained by the positive feedback mechanism in the electrostatic actuation. The attracting electrostatic force grows with the square of $\frac{1}{d}$, whereas the restoring spring force only grows linearly with the distance. The critical distance is $y = \frac{1}{3}d$ and is independent of the design geometry[15] [75, Section 2.6].

[15]This fact also limits the theoretical maximum tuning range of a simple, parallel-plate based MEMS tunable capacitor to $(C_{max} - C_{min})/C_{min} = 50\%$ [7]. There are, however, active control methods to extend the stable operation range even for the simple parallel-plate tunable capacitor [157].

**Table 7.** Actuator geometry and performance comparison of a few switches where the model of Figure 13 is applicable (all data, unless calculated, from the given literature references and [75, Chapter 5]).

| Company, institute | Spring constant $k$ in N·m$^{-1}$ | Estimated electrode distance[a] $d$ in $\mu$m | Electrode size $A$ in $\mu$m$^2$ | Actuation voltage $V$ in V | Contact force $F_c$ in $\mu$N | Estimated restoring force[b] $F_s$ in $\mu$N |
|---|---|---|---|---|---|---|
| Rockwell [104] | 15 | 3.8 | 2×75×75 | 50–60 | –[c] | 38 |
| Motorola [99] | 35–40 | 2.6 | 100×80 | 40–60 | –[c] | 64 |
| HRL [98] | 4–8 | 3.9 | 100×100 | 30–40 | 400 | 16 |
| Analog Devices [106] | 100 | 0.8 | 15×25 | 60–80 | 100 | 53 |
| OMRON [158] | 400 | 3.5 | 2×800×1600 | 13–20 | 5000 | 933[d] |
| Univ. of Michigan [159] | 20–50 | 2.2 | 2×50×100 | 30–40 | –[c] | 51 |
| Samsung [117] | 1 | 4.0 | 2×300×150 | 3–5 | –[c] | 2.7 |

[a]calculated from $A$, $k$, and $V$: $d = \frac{3}{2}\sqrt[3]{\frac{\epsilon A V^2}{k}}$
[b]calculated by $F_s = ky$, approximating $y = \frac{2}{3}d$
[c]not published; an approximated calculation is not applicable
[d]the value reported in the literature is 1000 $\mu$N

Thus, the pull-down voltage of the cantilever switch can be estimated by

$$V_{min} \geq \sqrt{\left(\frac{2}{3}\right)^3 \frac{kd^3}{\epsilon_0 \epsilon_r A}} \tag{3}$$

It can be seen that the minimum required actuation voltage is proportional to $d^{\frac{3}{2}}$ and indirectly proportional to $\sqrt{A}$.

Table 7 gives an overview of the actuator geometries, the actuation voltage and the contact and restoring forces of a few selected switches where the discussed model is applicable. These examples show that a stiff structure results in a larger restoring force, but requires either larger electrode areas or a higher actuation voltage unless the electrode distance is very small (which basically decreases the signal isolation because the contact distance is then also smaller for the discussed model).

Let us participate at a little game between the forces $F_{el}$, $F_s$ and $F_c$ on the four-dimensional board of $A$, $d$, $V$, $k$.

Figure 15, upper part, shows a contour plot of the pull-down voltage $V_{min}$ depending on the initial electrode distance $d$ and on the side length of the actuation electrodes $\sqrt{A}$, for a spring constant of 30 N·m$^{-1}$, representing a typical MEMS switch. Most vertical switch designs have a spring constant of 15–40 N·m$^{-1}$, resulting in a restoring spring force of 30–120 $\mu$N for a typical electrode distance of 3 $\mu$m [75, Section 2.9]. The lower graph in Figure 15 shows the corresponding electrostatic force, the restoring spring force and the contact force in the down-state, assuming a to-

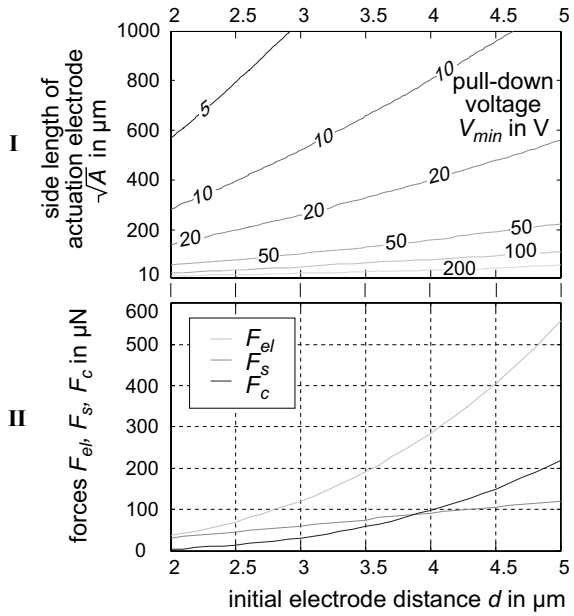


**Figure 15.** Simulation resuls of the slightly corrected (see text) switch equivalent model from Figure 13(b), for a spring constant of 30 $\mathrm{N{\cdot}m^{-1}}$. Upper graph: dependence of the pull-down voltage on the initial electrode distance and on the side length of the actuation electrode area; lower graph: electrostatic, spring and contact forces depending on the initial electrode distance (see text). The two diagrams are connected by the common X-axis.

tal deflection down to a remaining electrode distance $d_{cont}$ of 1 $\mu$m. The resulting contact force is calculated by $F_c = (F_{el} - F_s) \cdot 50\%$, whereas the weighting factor of 50% reflects the fact that the contact force is only about 40–90% of the pull-down force, with the remainder part contributing to beam flexture or being lost by touching electrodes [75, Section 2.9]. The two graphs have the initial electrode distance $d$ as the common axis, which allows to find the acting forces of each point in the pull-down voltage plot. This does not mean that the electrostatic force is area-independent but dependent on the initial electrode distance, as might be simulated by the lower graph, since the product $A \times V^2$ is constant in the upper graph along any vertical line with $d$=constant. In other words, a larger electrode area allows a lower actuation voltage to create the same forces, which is reflected in the graphs.

In Figure 16, the voltage is kept constant and the active forces are displayed depending on the electrode size and on the initial gap distance (quadrant II). Quadrant I shows the related restoring spring force and quadrant III the electrostatic force. Also here, the graphs of the different quadrants are connected by their common axes. The textured area in the second quadrant shows the "forbidden" design area: switches with a geometry chosen out of this area do not snap down for the given actuation voltage. Sub-figure (a) represents a weaker switch design with a spring constant of 30 $\mathrm{N{\cdot}m^{-1}}$ and an actuation voltage of 25 V, and Sub-figure (b) displays a stronger switch design with a spring constant of 150 $\mathrm{N{\cdot}m^{-1}}$ and an actuation voltage of 60 V. For both

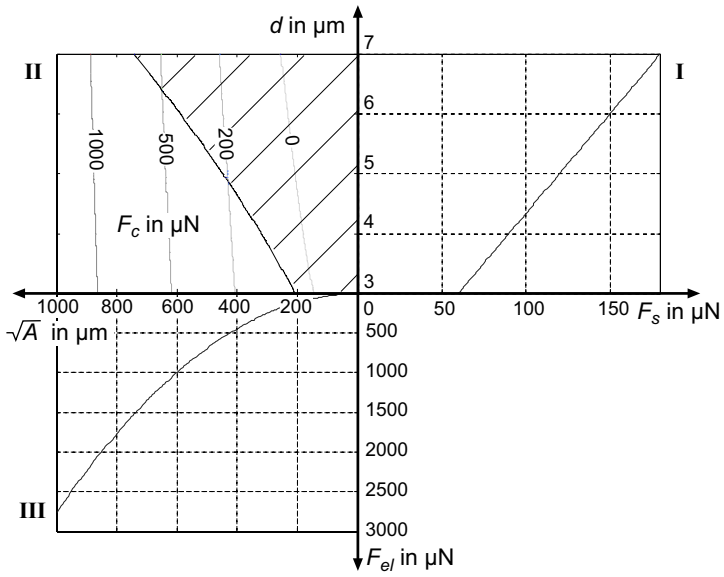


(a)

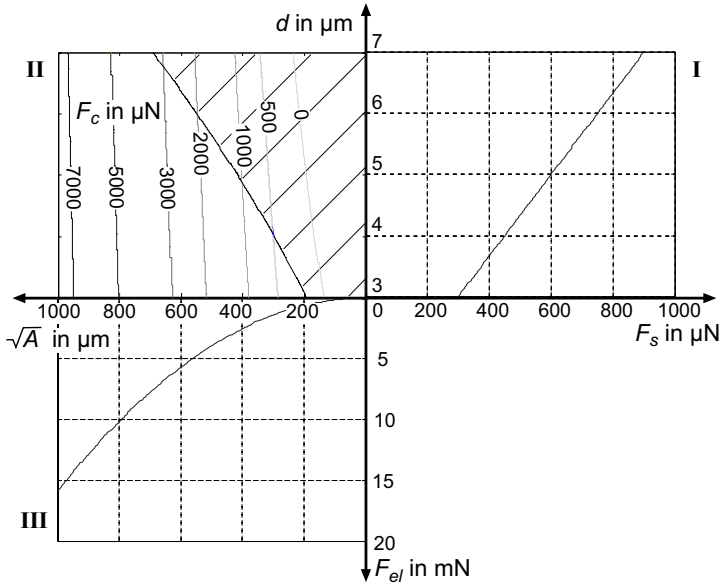


(b)

**Figure 16.** Active forces depending on design geometry: (a) weak switch design with a spring constant of $k$=30 N·m$^{-1}$, an actuation voltage of $V$=25 V, and a down-state electrode distance of $d_{cont}$=1 $\mu$m; (b) stronger design with $V$=60 V, $k$=150 N·m$^{-1}$, and $d_{cont}$=1 $\mu$m.

designs the remaining electrode distance in the down state is assumed to 1 $\mu$m. The "stronger" design provides quite large contact and restoring forces suitable for switching currents with high reliability, especially when using a large electrode area. An example of this type of switch is the OMRON switch [109, 158, 160]. A contrasting design philosophy was realized in the Samsung metal contact switch, actuated at very low voltages with average sized actuation electrodes. This is achieved by an extremely low spring constant at the price of a very small restoring force and therefore probably also low contact reliability [117]. For a direct comparison see also Table 7.

The discussed model does not take into account any isolation layer between the two electrodes. Such an isolation layer does not substantially decrease the necessary pull-down voltage, since most of the electrostatic energy is stored in the free space and not in the dielectric layer, but would increase the contact force. This is only relevant for very weak switch designs (to switch low power signals), which require a low on-resistance but tolerate a relatively low restoring force. For more reliable switch designs, the electrostatic actuator has to be quite strong to overcome the required stiffness of the structure. A strong actuator already results in a large contact force and does not necessarily have to be increased by an additional dielectric layer (see Figure 16(b)). Not to give a wrong impression: the main function of a dielectric layer is still the electrical isolation between the electrodes. In general, isolation layers should be avoided by using a so-called all-metal switch design because of the tendency to electrostatic stiction, as discussed in Section 2.2.4.

All these reflections and calculations on the model show that it is not so easy to create an effective switch design with low actuation voltages (for electronic compatibility), small electrode areas (for small chip size and low cost per switch) and large contact distance (for high isolation), by maintaining a reasonable restoring force (for contact reliability) and contact force (for low resistance). The RF MEMS community is aware of this problem and many different electrostatically actuated switch concepts seeking clever design solutions have been published over the last decade:

- **Curled cantilever/membrane:**
  Out of plane bending structure due to a residual stress gradient or a stress difference in a multi-layer structure, providing low effective electrode distance ("zipper-like" or so-called touch-mode actuation [161]) on the fixed side but with large deflection on the freestanding (contact) side [95, 97, 105], see Figures 3(b) and 5(a) on pages 15 and 17, respectively.

  **Advantages:** low actuation voltage and large contact distance

  **Disadvantages:** stress level difficult to control; increased susceptibility to electrode stiction because of large areas in very close contact

- **Curved or stepped electrodes:**
  The "zipper" effect mentioned above is achieved by a curve-shaped undeformable counter-electrode; typically used in lateral actuators because of their simple fabrication [133, 146]; possibility for vertical actuators: stepped electrodes [162].

  **Advantages:** low actuation voltage, increased contact distance

  **Disadvantage:** in the case of a vertical actuator increased fabrication complexity

- **Push-pull concepts to provide an active restoring force:**
  - **Push-pull mechanism with additional top electrode:** Membrane or cantilever with electrode moving between the two fixed top and bottom electrodes [119].

    **Advantages:** active opening and closing, allows flexible structure with low actuation voltage

    **Disadvantages:** increased fabrication complexity, not necessarily larger contact distance since the electrostatic forces of the basic parallel-plate configurations are very small over a larger distance
  - **Torsional suspended actuators with leverage effect:** Push-pull electrodes on both sides of the rotational axes of a plane suspended on one of its symmetry axes, tilting the plane when actuated to one side or to the other. The switching contact is mounted on the far outside edge or on a leverage beam to further extend the displacement [110–113], see Figure 9(b) on page 21.

    **Advantages:** active closing and active opening, very low actuation voltage, large contact distance

    **Disadvantages:** design of the suspension stiff enough against vertical movement but with very low rotational spring constant
  - **Pull-mechanisms to separate the contacts:** Fulcrum contact structure providing a rotational axis in the down-state to open the contacts together with a part of the pull-down electrode [163].

    **Advantages:** active restoring force with very little additional fabrication complexity, low actuation voltage

    **Disadvantages:** does not improve the open contact distance

- **Free-moving membrane actuator:**
  Completely freestanding membrane moving vertically along hinges between a top and a bottom electrode [122], see Figure 6(b).

  **Advantages:** theoretically no restoring spring energy → very low actuation voltage

  **Disadvantages:** wedging membrane on the hinges (friction and stiction problems), complicated fabrication, low opening force at a reasonable contact distance

Despite all of these possibilities, the cantilever-spring or membrane-spring concept as discussed in this section still seems to be the most favored one, mainly because of its robustness in fabrication, its simplicity in usage and because of its predictability. The probably most mature switch designs, the OMRON, the Motorola, the Analog Devices/Radant, the Rockwell Science Center and the HRL switches, are based on this concept. The first three of them have solved the problems of the membrane-spring concept in different ways that are interesting to compare (see also Table 7 on page 32):

**OMRON switch:** very stiff spring for high restoring force; very large electrode areas for relatively low actuation voltage

**Motorola switch:** stiff spring for high restoring force; small electrode areas requiring large actuation voltage, accomplished by a more complex electronic drive circuitry

**Analog Devices switch:** very stiff spring for high restoring force; very small contact gap and small overlapping contact areas, resulting in relatively low actuation voltages and requiring only small electrode areas

It is also very interesting to observe that one of the Analog Devices/Radant switch designs, the Motorola, the HRL and a recently presented high-power switch from the University of Michigan [164] show a bewildering likeness in their design. This tendency seems to anticipate a "natural selection process" in MEMS metal contact switches, which hopefully does not mean that there will not be any further substantial improvements in the performance of MEMS switches.

The switch presented in this thesis is a combination of the push-pull concept with top electrode and a double-curled actuator using the low-voltage "zipper"-effect both with the bottom and the top electrodes (see Section 3).

For completeness, the following list gives an overview of the actuation voltages, displacements and active forces in electrostatically actuated switches compared to alternative actuation mechanisms with zero power consumption in both the on and the off-state:

- **Electrostatic actuators:**

  **Advantages:** simple in fabrication and operation, very well investigated, maximum force in the contact position, strong contact force for small chip sizes, pull-in hysteresis[16]

  **Disadvantages:** requires relatively high actuation voltages, the displacement is basically limited to a few micrometers

- **Electrothermal, lateral moving actuators with mechanical latching mechanisms** [134, 137]:

  **Advantages:** large displacement, low actuation voltage, fabrication relatively simple

  **Disadvantages:** very large size, maximum force during the transition and not in the end positions, mechanical latching provides relatively small contact forces

- **Electrothermal with electrostatic clamping** [118]:

  **Advantages:** low voltage, large displacement, maximum force in the contact position, large contact force, small size

[16] Especially for microrelays, a very important feature of electrostatic actuators: the hold-voltage is lower than the actuation voltage, which defines the switching state very well even at unstable control voltages.

**Disadvantages:** complex fabrication

- **Magnetostatic, latching by switching magnetic polarization** [100]:

  **Advantages:** low actuation voltage, restoring force to a certain extend controllable by the actuation current

  **Disadvantages:** low displacement, low contact force, low restoring force, complex fabrication involving the mounting of a permanent magnet

- **Other, less commonly used actuation mechanisms:**

  - **Electrothermal, vertically moving, with mechanical latching mechanism** [149]: low actuation voltage, large vertical and lateral, but uncontrollable displacement, low contact force
  - **Piezoelectric:** so far only used for a tunable capacitor based on a PZT layer [31], requires rather thick piezoelectric layers for a displacement of a couple of micrometers with an acceptable contact force, difficult fabrication and process incompatibility[17]

Other possible combinations of these actuation and latching mechanisms are not considered here, since, to the knowledge of the author, they have so far not been reported in the literature.

### 2.2.2 Contact distance vs. isolation

#### DC isolation

The DC voltage isolation of a switch is given by the maximum voltage which can be applied in the off-state between the input and the output without having a breakdown between the separated contacts. By experience, such a breakdown occurs when a certain field strength is reached in the isolation gas (for dry air, atmospheric pressure, room-temperature, about 3 kV·cm$^{-1}$ $\cong$ 30 V·$\mu$m$^{-1}$). Therefore, the isolation or so-called stand-off voltage basically depends on the atmosphere inside the switch package and on the contact distance.

For dimensions of the order of a few tens of micrometer the breakdown mechanisms are different. In large scale systems, electrical breakdown arises due to electrons accelerated in the electric field colliding successively with molecules which are ionized and thus result in more electrons which are subsequently accelerated by the field and cause further collisions (Townsend or avalanche effect [165]). For dimensions of the same order as the mean free electron path to collision or for very low pressures with decreased probability of collision, ionizing breakdown cannot occur. For very small pressure-distance products, the breakdown voltage theoretically even increases after having passed a theoretical minimum, as illustrated in Figure 17(a). In dry air, the minimum voltage at which a breakdown is possible is 327 V, corresponding to a field strength of 66 V·$\mu$m$^{-1}$ at atmospheric pressure. This minimum was confirmed

[17] It is assumed that some companies are currently working on PZT-based switches [75, Section 5.22].

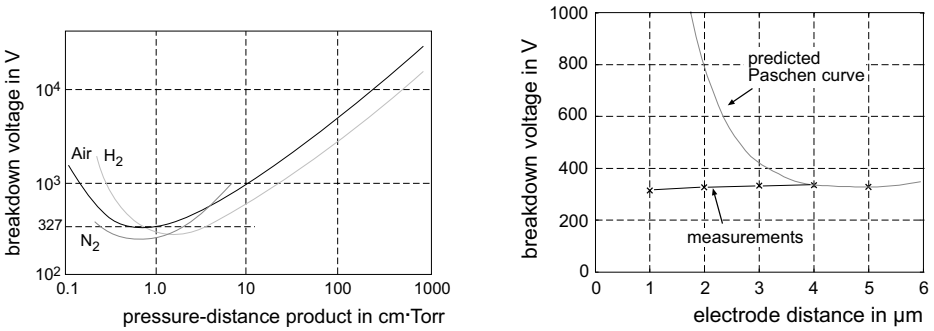


**Figure 17.** The Paschen curve: (a) theoretical breakdown voltage for dry air, nitrogen and hydrogen against the pressure-distance product [165]; (b) measured breakdown voltage on the left side of the Paschen minimum in dry air [75, 166].

by measurements reporting on a breakdown voltage of 64 V·$\mu$m$^{-1}$ [167]. In further experiments, the predicted theoretical increase of the breakdown voltage for lower pressures/dimensions on the left side of the minimum could not be verified, as shown in Figure 17(b). This can be explained by extremely high local field strengths due to surface roughness which plays an increasing role for very low gap distances [166]. Thus, the breakdown occurs by field emission depending on the surface properties. Irregular and unstable discharging phenomena can also occur at larger distances if the field strength exceeds 28 V·$\mu$m$^{-1}$, without leading to a breakdown [167]. Discharging does not destroy the electrodes but, in the long term, a stable glow discharge degrades them and should be avoided in normal operation modes.

From a practical point of view, a MEMS in-line switch with deposited metal contacts provides reliable isolation for 300 V at gap distances of 10–20 $\mu$m and about 150 V for contact distances of 2–4 $\mu$m.

### RF isolation

The RF isolation of an electrical switch is defined by the ratio of the output voltage to the input voltage in the off-state, which basically is the so-called $S_{21}$-parameter for a passive two-port network[18]. Since this ratio can vary over many orders of magnitude, a logarithmic scale is commonly used.

One might assume that the isolation in the microwave band is mainly determined by the coupling capacitance between the overlapping switching contact areas. When comparing the measured isolation with the calculated value from the capacitance between the contacts, it can be seen that the effective coupling capacitance must be much larger. Table 8 compares the calculated contact capacitances to the effective coupling capacitances reported in the literature for a few selected switches. For "standard" membrane and cantilever switch designs, the measured coupling capacitance by far even exceeds the single contact capacitance. The reason for this discrepancy is

[18] For a reversable network, the $S$-parameter matrix is symmetric and $S_{21}$ is equal to $S_{12}$.

**Table 8.** Comparison of the overlapping contact area, contact distance, off-state capacitance and RF isolation of different metal-contact series switches (all data, unless calculated, from the given literature references and [75, Chapter 5]).

| Company, institute | *Reported in the literature* | | | | *Calculated* | |
|---|---|---|---|---|---|---|
| | Overlapping contact area $A$ $\mu m^2$ | Contact distance $d$ $\mu m$ | Total off-capacitance $C_{off}$ fF | Isolation (4 GHz) $S_{21}$ dB | Parallel plate capacitance[a] $C_A$ fF | Ratio $\frac{C_{off}}{C_A}$ |
| Rockwell [104] | 150 | 2–2.5 | 1.75–2 | 50 | 0.5–0.7 | ≈3 |
| Motorola [99] | 300 | 2–3 | 2 | 44 | 0.9–1.3 | ≈1.8 |
| HRL [98] | 400 | 1.5–2 | 3 | 45 | 1.8–2.4 | ≈1.5 |
| Analog Devices[b] [106] | 10 | 0.6–1 | 4 | 40 | 0.1–0.2 | ≈25 |
| MIT-Lincoln Labs[b] [105] | 360 | 2–15 | 4–6 | 40 | 0.2–1.6 | 4–20 |
| OMRON [158] | 500[c] | 3 | 5 | 35 | 1.5 | 3.3 |
| Univ. of Michigan [159] | 1200[c] | 1.5–2 | 6–8 | 35 | 5–7 | ≈1.2 |
| KTH[d] | 3500 | 14.2 | 4.2 | 40 | 2.2 | 1.9 |

[a]for one contact only; calculated from $A$ and $d$; fringe capacitances not taken into account; no dielectric layer

[b]a so-called in-line switch with a single interruption in the signal line; thus, the total off-state capacitance consists of $C_A + C_f + C_p$

[c]estimation from pictures

[d]the switch presented in this thesis

that the total coupling capacitance is composed of

$$C_{off} = \frac{1}{2}\left(C_A + C_f\right) + C_p \tag{4}$$

with $C_A$ the parallel-plate capacitance of the open contacts, $C_f$ their fringe-field capacitance, and $C_p$ the parasitic capacitance between the open ends of the transmission line, as shown in Figure 18(a). The fringe capacitance is proportional to the ratio of the contact distance to the overlapping contact length, and can even exceed the parallel-plate capacitance itself. The coupling capacitance between the open ends of the transmission line mainly depends on the gap between the two signal lines and on the signal line width. For a typical switch design on silicon, this coupling capacitance is 2–4 fF, and it is about 50% lower for GaAs-substrate based switches [75, Section 4.9]. The contour plot in Figure 18(b) is an attempt to estimate the anticipated isolation from the overlapping contact area and the off-state contact distance at 4 GHz. The isolation, calculated for a 50 Ω system, is based on the approximation $C_{off} \approx \frac{1}{2} C_A \left(1 + f_{fringe}\right) + C_p$, assuming a fringe-factor $f_{fringe}$ of 100% and a transmission line capacitance of 3 pF. These parameters were derived by finding the best matching parameters based on the design and measurement data of the Rockwell, Motorola, OMRON, HRL, University of Michigan and KTH switches from

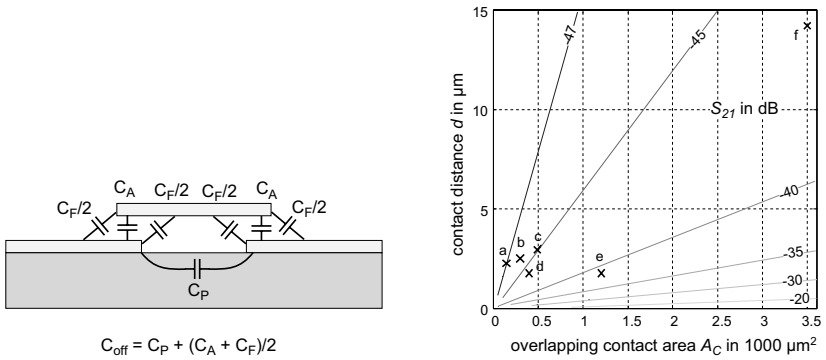


**Figure 18.** (a) Simplified off-state model of a series switch with contact area capacitance $C_A$, fringe capacitance $C_f$, and parasitic substrate coupling capacitance $C_p$; (b) contour plot of the approximate RF isolation at 4 GHz, depending on the contact distance and on the overlapping contact area, calculated as described in the text, with marks corresponding to some of the switches from Table 8: a) Rockwell, b) Motorola, c) OMRON, d) HRL, e) Univ. of Michigan, and f) KTH switch.

Table 8. The Analog Devices switch was not considered for the curve-fitting, since it deviates from the other switch designs by its small contact area and contact distance, resulting in extremely high parasitic capacitances compared to the mere contact capacitance, as calculated in the table. The Lincoln Labs switch was not taken into account either, due to the reported large variation of the contact distance.

The simulation data presented in Figure 19 tries to verify the estimated parasitic coupling capacitance for the transmission line. The effective capacitance between the two ends of the signal line is extracted from simulation results of the RF isolation, depending on the line width and the gap between the open ends[19]. One is tempted to assume that different design geometries could simply be characterized by the ratio of the gap distance to the signal line width, which is not the case, as shown in Figure 19(b). The simulation was done with the high-frequency planar solver Sonnet 9.51, and the estimated capacitances are slightly lower than the results of comparable simulations reported earlier in [75, Section 4.9]. The thickness of the metal lines is not taken into account in this discussion since it plays only a minor role because it is much smaller than the lateral dimensions of the transmission line.

[19]The parasitic coupling capacitance is extracted from $S_{21}$ by using the following correlation:

$$Z_p = 2 \cdot Z_0 \cdot \frac{1 - \hat{S}_{21}}{\hat{S}_{21}} \qquad \text{and} \qquad C_p = -\frac{1}{\omega \cdot \mathrm{Im}\,(Z_p)}$$

$\hat{S}_{21}$ is the insertion loss of the interrupted line normalized by the insertion loss $S_{21}$ of the through line, $Z_0$ the characteristic impedance of the transmission line, and $\omega$ the angular frequency. Even though the insertion loss of the through line is very small compared to the open line, the normalization is necessary to eliminate the phase shift. The extraction of the coupling capacitive makes sense only if the complex coupling impedance is dominated by a capacitive component, i.e. $\mathrm{Im}(Z_p) < 0$ and $|\,\mathrm{Im}(Z_p)| \gg \mathrm{Re}\,(Z_p)$, and, if the calculated $C_p$ is nearly constant over the investigated frequency band. Otherwise this simple equivalent circuit model would not be appropriate.

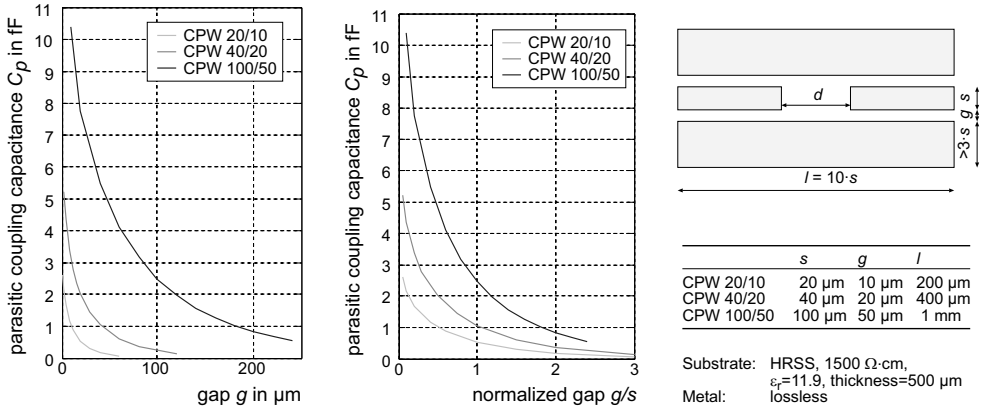


**Figure 19.** Simulated parasitic coupling capacitance against line separation for different interrupted CPW geometries on a high resistivity silicon substrate: (a) $C_p$ against gap $g$; (b) $C_p$ against normalized gap $g/s$; (c) geometry of the simulation model.

### 2.2.3 Metal contacts and their reliability

The metal contacts are the most crucial part of a MEMS switch since they determine the on-state resistance and the current handling capability, and are the source of the most dominant failure mechanisms in the type of switches under discussion. Besides literature addressing metal contact issues in conventional relays [168–176], a variety of publications report on the contact physics, contact forces and contact reliability in MEMS switches and relays [89, 156, 167, 177–182]. The main issues determining contact performance in microswitches are discussed in the following paragraphs.

#### Contact force, resistance, materials, and effective contact area

The contact force of typical MEMS switches is between 10 $\mu$N and 10 mN, compared to conventional relays with forces from 100 mN upward [89]. The dependence of the contact resistance on the contact pressure has been thoroughly investigated for different contact materials [89,156,167,177–183]. According to the literature, a stable contact resistance of 80–200 m$\Omega$ can be achieved at about 100 $\mu$N for gold, which is the most common contact material, dropping to 10–20 m$\Omega$ at 1 mN [177]. For AuNi5, a force of at least 300 $\mu$N is necessary for a stable contact resistance below 100 m$\Omega$ [156]. Rhodium, another but less common choice, gives a stable contact resistance of about 1 $\Omega$ at a minimum force of 600 $\mu$N, as displayed in Figure 20 [179]. Other well-suited materials are sputtered or plated rhenium and gold-palladium alloys with a contact resistance of 0.5–3 $\Omega$ for 0.2–2 mN contact force [75, Section 7.3], or hard-gold AuCuCd with a stable contact resistance of 50–80 m$\Omega$ at a contact force of 200 $\mu$N [178]. Platinum was also used for contact material alloys in a MEMS switch design, but it was not commented on the composition and performance [105]. The contact resistance of gold is about 10 times lower than that of AuNi alloys,

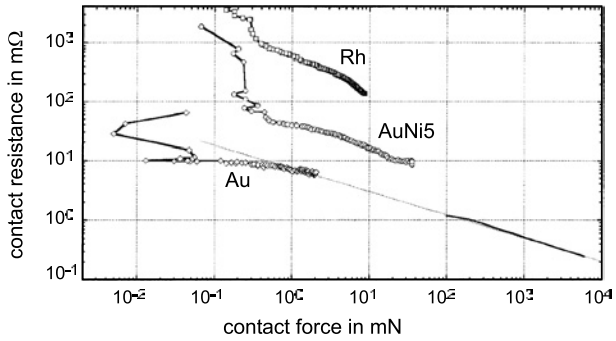


**Figure 20.** Contact resistance versus contact force for gold, rhodium and 5% alloyed nickel in gold [179].

which again is lower than that of rhodium by a factor of 10. Besides the different resistivities, this can be explained by the hardness of the materials, resulting in a larger effective contact area for a low hardness at a given contact force, due to elastic deformation of the metal. The effective contact area is then one of the main factors influencing the contact resistance. A larger contact area results in a smaller resistance, as expected. Smaller areas are also characterized by non-linear behavior, i.e. the resistance increases with increasing current, which can be explained by local annealing effects caused by increased localized heating due to the smaller thermal conductivity of smaller contact areas. In general, the better heat dissipation of larger effective contact areas is *the* critical design criterion to maintain low contact resistance, high power handling capability, and a minimum of surface adhesion wear [177].

Materials with a native oxide such as aluminum, copper, nickel or silicon, are not the first choice since they require a substantial contact force for an acceptable contact resistance. Due to its hardness, silicon, even though very suitable since it often is already used as the structural material of the device, results in very high contact resistances of the order of 20 kΩ [101].

In all, gold and gold alloys in a hermetic atmosphere (nitride or air at atmospheric pressure) are still the contact materials of first choice for microrelays because of their low hardness and low resistivity, both resulting in a low contact resistance, their relatively high melting temperature for a soft material, and their resistance to absorption of surface contaminants [75, 181]. However, the final choice of the contact material also depends on the specific application.

### Contact contamination

Clean contacts are extremely important for microrelays compared to conventional relays since the very low contact forces are not able to break absorbed contaminant films. Sample preparation with tetrachloroethylene followed by alcohol and deionized water was found to be a sufficient cleaning method [177]. Another successful tested procedure is cleaning in isopropanol with 40 subsequent switching cycles at 40 mA,

called "Schaltreinigung" [156]. In both cases, the samples were afterward kept and tested in a nitrogen atmosphere. Besides residues left over from fabrication steps with organic materials, surface contamination can also occur by absorption or condensation of gases, either during the packaging procedure or during operation, if the device is not sealed hermetically. From a material point of view, gold is very suitable since it strongly resists surface layer formation [75, Section 7.4].

### Metal deposition process

The deposition processes of the contact material affects its contact performance. Sputtered gold is much harder than electroplated gold and therefore less susceptible to surface damage. Also, higher gold deposition temperatures (hot sputtering at 200 °C, for example) result in a dense and compact grain size and show less surface change due to material transfer and annealing at higher currents than gold deposited at lower temperatures [177].

### Adhesion force and microwelding

The estimation of the adhesion force is very important to design the necessary restoring force of the switch actuator. The adhesion force is the least understood parameter of metal contacts in microrelays, and strongly deviating values were reported for different switch designs. Besides the contact material, the switching history influences the remaining adhesion force after releasing the actuation mechanism. The adhesion force depends on the hardness of the contact material, and was reported to be between 0.3 and 2.7 mN for Au and between 0 and 0.3 mN for AuNi5 in an experimental setup [156]. For a practical switch design (the Motorola switch discussed in the Sections 2.1.4, 2.2.1 and 2.2.2) the stiction force was found to be about 130 $\mu$N. The reader might find it interesting to compare these values to the relatively low estimated restoring forces of some MEMS switches listed in Table 7 on page 32.

Heat dissipation in the contacts is a very important parameter since increased contact temperature softens the material, resulting in a larger effective contact area with larger adhesion. At even higher temperatures caused by local current densities, a soft material with low melting point deforms plastically under the contact pressure, and static microwelding might occur, which can be assumed to be the major failure mechanism at larger switching currents [181]. The very sudden decrease in life time with the switched current is demonstrated in Table 9.

The probability of failure due to contact adhesion depends also on the switching history, which is not only characterized by the switching conditions and the number of cycles, but also by the dwell time of the closed contacts. It is well known for relays in the macro-world that contacts have an increasing tendency to stick to each other if the closed contact is maintained for a very long time, especially when applying an electrical load. Unfortunately, no reliability data has been published for MEMS switches about this type of aging with closed contacts.

**Table 9.** Selection of life-time studies of metal contact switches.

| Institute, company | Contact description | Life-time test conditions and results |
|---|---|---|
| Analog Devices [96] | gold, $R_{ON}$=50 m$\Omega$ | hot switching, in air: $10^5$–$10^7$ cycles up to 1 mA, a few hundred cycles at 10 mA; in nitrogen: $10^9$ cycles cold switched, $2\times10^8$ cycles hot switched at 10 mA (criterion for failure: $R_{ON}$ >100 $\Omega$) |
| Delphi Labs [131] | copper, $R_{ON}$=40–60 m$\Omega$ | with arc-suppressing circuit: $1.7\times10^6$ cycles at 50 mA, >2000 cycles at 350 mA; without arc-suppressing circuit: 20 cycles at 350 mA |
| CP Clare [129] | gold | $3\times10^7$ cycles at 5 mA, $10^5$ cycles at 10 mA, >1000 cycles at 200 mA |
| Siemens [95] | AuNi5, contact spring | hot-switched: $6\times10^6$ cycles at 100 mA |

### Other contact degrading mechanisms

Besides less harmful discharging phenomena between contacts in close approximation (see Section 2.2.2), sparking is a major contact degrading mechanism in macro-world metal contact relays. Arcs during the switch transition are a discharging problem caused by parasitic inductances which can create a relatively high voltage over the just opened contacts, trying to continue the current flow in the line, according to $V_L = L\frac{di}{dt}$, with $L$ the total parasitic inductance and $\frac{di}{dt}$ the time dependent change of the current due to the contact separation. The parasitic inductances in microswitches (especially in microswitch measurement setups) as well as the switched currents are usually quite low and probably play a minor roll in the overall contact degradation, also because of the very fast switch transition times. An exception is the switching of inductive loads with MEMS switches [131]. However, sparking was also identified as a failure mechanism in low current MEMS switches, but the underlying mechanisms are not yet definitely identified [181].

Due to the failure mechanisms mentioned above, a metal contact microswitch dies in a short-circuit, to use the language of semiconductor electronics. This fact is a major drawback from an application point of view. Table 9 lists the results of life-time tests of a few MEMS switches, without discussing the actuation mechanisms and the restoring forces. More life-time test results can be found in [75, Section 7.5]. In general, the life-time is given by the number of switching cycles before the device fails due to mechanical (actuator) or electrical problems (contact stiction or a drastic increase of the contact resistance). Unfortunately, the tests are often not carried out under comparable conditions, which sometimes are not even specified:

- **Cold-switching:** Only a small measurement current (100 $\mu$A e.g.) is switched. The main failure mechanisms (microwelding, stiction due to softening) do not occur and very high cycle-numbers can be achieved.

- **Switching without signal current during the switch transition:** The switch is exposed to a current load in the on-state of the switch. Before opening the contacts, however, the load is removed. The switching contacts are more susceptible to stiction and to static microwelding at very large currents. Relatively high cycle-numbers are reported.

- **Hot-switching with load during switch transition:** The whole palette of other failure-mechanisms due to contact degradation can occur. The number of switching cycles is relatively low and depends on the switch design, drastically decreasing at signal currents above 10–20 mA.

A variation of hot-switching is the use of an external electronic switch in parallel to the MEMS switch, opening the line after the MEMS switch has opened, and closing it before the MEMS switch [131]. This technique results in a very low on-resistance (the MEMS switch resistance dominates) and provides substantially improved reliability since no real hot-switching is carried out, but the isolation and other performance parameters are determined by the electronic switch.

### 2.2.4 Adhesion between actuation electrodes

Besides contact stiction as the main failure mechanism of metal-contact switches, as discussed in the previous section, unwanted adhesion can also occur between touching electrodes during operation, which is also a very important failure mechanism of MEMS switches. This type of failure might have different causes in electrostatic actuators, listed in the order of their importance for MEMS switches:

1. **Electrostatic stiction:** Caused by charge injection and charge trapping in dielectric layers, mainly dependent on the field strength, if above 2 $MV \cdot cm^{-1}$ [184], and on the dwelling time in the active state [63].

2. **Hydrogen bridging:** Hydrophilic surfaces such as the native oxides of all silicon based dielectrics (nitrides and oxides) are highly hydrophilic and contain absorbed water layers. When two of these surfaces are brought into close contact, hydrogen bonds may form and result in quite high adhesion energy [161, 185].

3. **Capillary condensation between contacting surfaces:** Liquid condensate can drastically increase the effective contact area of otherwise rough surfaces and can cause stiction [185].

4. **Van der Waals forces between solid bodies:** Caused by mutual electric interaction of the induced dipoles in two touching bodies, strongly dependent on surface roughness [185].

Stiction occuring during processing is not discussed since that causes a yield and not a reliability problem.

Possible means of preventing the mentioned effects are:

- **Hermetic packaging:** Drastically reduces causes 2 and 3, since they depend on the relative humidity of the working environment [161].

- **Increased surface roughness:** Reduces mainly effect 4, which is a main concern only for surface roughnesses below a few nanometers typical of traditional LPCVD based surface micromachining [185, 186].
- **Anti-stiction coating:** Hydrophobic self assembled monolayer (SAM) coatings prevent the formation of hydrated layers and thus effects 2 and 3 [161, 185, 186]. However, anti-stiction coating of the total structure is not possible for metal-contact switches.
- **Distance keepers:** Small separation posts drastically reduce the contact area and thus the probability of stiction for all of the effects described above. As a further significant advantage, isolation layers between electrodes are unnecessary, leading to a so-called all-metal switch. Separation posts are the most efficient method against effect 1 [127, 185]. The slightly more complex fabrication is compensated by the various advantages: no electrostatic stiction, no adhesion problems between dielectric and metal layers, and less stress in the structure (see also Figure 8 on page 20).
- **Conscious choice of materials:**
  - Silicon dioxide has a much lower trap density than silicon nitride and is therefore less susceptible to electrostatic stiction [187], reducing effect 1. However, dioxide takes up more moisture than nitride [188] and might be worse overall if the stiction causes 2 and 3 are not eliminated by other methods such as hermetic packaging. Another rule: LPCVD layers have a lower trap density than PECVD layers [75, Section 7.2].
  - Noble metals without native oxides should preferably be used instead of aluminum or silicon to prevent problem 2.
- **Low electrostatic actuation voltage design:** Charge injection is exponential with voltage and a reduction in the actuation voltage by 6 V results in a 10-fold increase in the lifetime of a capacitive MEMS switch [121], thus, reducing effect 1.
- **Bipolar actuation voltage:** The polarity of the voltage does not affect the electrostatic force. Negative voltage pulses when releasing the actuation voltage reduce trapped charges and result in a vast improvement in the switch reliability [75, Section 7.2]. Charge trapping is also avoided by using AC actuation voltage [161]. Both methods reduce problem 1 at the cost of increased complexity of the electronic drive circuitry.

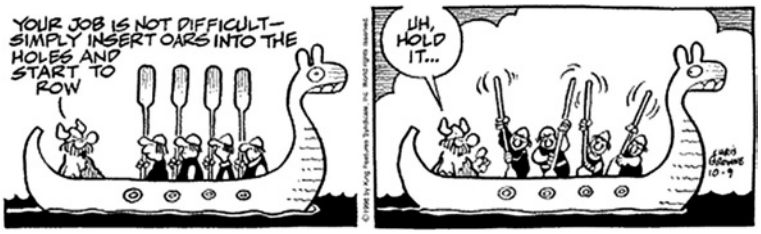

**Der Panther**
*Im Jardin des Plantes, Paris*

Sein Blick ist vom Vorübergehn der Stäbe
so müd geworden, daß er nichts mehr hält.
Ihm ist, als ob es tausend Stäbe gäbe
und hinter tausend Stäben keine Welt.

Der weiche Gang geschmeidig starker Schritte,
der sich im allerkleinsten Kreise dreht,
ist wie ein Tanz von Kraft um eine Mitte,
in der betäubt ein großer Wille steht.

Nur manchmal schiebt der Vorhang der Pupille
sich lautlos auf—. Dann geht ein Bild hinein,
geht durch der Glieder angespannte Stille—
und hört im Herzen auf zu sein.

*Rainer Maria Rilke,*
*aus "Neue Gedichte", 1902*

**The Panther**
*In the Jardin des Plantes, Paris*

His gaze is from the passing of bars
so exhausted, that it doesn't hold a thing anymore.
For him, it's as if there were thousands of bars
and behind the thousands of bars no world.

The sure stride of lithe, powerful steps,
that around the smallest of circles turns,
is like a dance of pure energy about a center,
in which a great will stands numbed.

Only occasionally, without a sound, do the covers
of the eyes slide open—. An image rushes in,
goes through the tensed silence of the frame—
only to vanish, forever, in the heart.

*Rainer Maria Rilke,*
*in "New Poems", 1902*
*(translation by Cliff Crego)*

*Once we are destined to live out our lives in the prison of our mind, our duty is to furnish it well.*

*Peter Ustinov*
*1921–2004, British Actor,*
*Writer, Director*

## 2.3 MEMS wafer-level packaging

### 2.3.1 MEMS packaging

The main functions of a microsystem package are the following:

- environmental protection: chemicals, temperature, electrical and magnetic fields
- routing of electrical interconnections
- interfacing of sensor and actuator elements with their environment
- hermetic sealing (if required)
- heat dissipation
- mechanical support and mechanical protection
- mechanical stress relaxation
- integration of multi chips into one single package
- standardized package for automated device handling on a system assembly level
- providing test interfaces
- handling during tests after different fabrication steps

Except a few points mentioned above, these requirements are not much different from conventional electronic packaging. However, the packaging is regarded as a very critical block in the successful commercialization of microsystems. The packaging costs contribute with a major factor to the total device fabrication costs, varying from 20% for a simple plastic encapsulated pressure sensor to 95% for special pressure sensors designed to withstand an extremely harsh environment [189, Chapter 1.4]. The main reasons for these high costs, as compared to microelectronics packaging, are the following:

- Microsystems consist of more complex three-dimensional structures.
- Moving mechanical parts often require an encapsulated cavity with a controlled atmosphere (hermetic package).
- Each MEMS design is unique and, compared to electronic devices where the packaging is less dependent on the chip functionality, the package has to be individually developed for each microsystem.

- Standard packaging procedures and processes are often not suitable for MEMS devices.
- Microsystems typically interact with their environment. Thus, the chips are more directly exposed to harsher conditions with higher demands on the overall packaging, and the working media has to be interfaced by the microsytem.
- Especially the fabrication of three-dimensional structures with high aspect ratios results in larger geometrical variations than the typical fabrication of semiconductors. Thus, the package design has to be more tolerant to large product non-uniformity.
- The uniqueness of MEMS devices also requires unique test methods after different fabrication and packaging steps. Special test interfaces have to be provided by the package.
- The reliability of electronic packages is very well investigated and also much better understood because the failure mechanisms are less dependent on the circuit function. In contrast, each type of MEMS device has its own particular failure mechanisms which makes it difficult to provide a suitable and reliable package.
- Up to now, many (low volume) MEMS components are packaged manually with inappropriate tools in an expensive and time consuming process.
- For economical reasons, a MEMS package should be compatible with low-cost printed circuit board (PCB) assembly technology designed for semiconductor chips. However, the complex device functions of many microsystems do not allow a standard package.

The whole packaging procedure of a MEMS device typically consists of different steps. For instance, the automotive sensors shown in Figure 21 are packaged by the following procedure:

1. Encapsulation of the mechanical structure (here: by wafer bonding).
2. Mounting of the MEMS device, together with an integrated circuit chip, on a leadframe flag with standardized size and contact pads for DIP or SOP packages.
3. Wire bonding of the chips to the frame, and between the chips.
4. Passivation of the chips and the bonding wires by a layer of silicone gel.
5. Molding of the frame with the mounted chips in an epoxy compound, giving the final shape of the plastic package.

MEMS packaging, especially for low volume products, is often done completely on chip level. Thus, the wafer for the device fabrication is diced before the packaging procedure, which is carried out individually on each chip. Wafer-level packaging or so-called zero-level packaging are terms used when some parts of the packaging, typically including the sealing, are done before the wafer dicing. These packaging steps

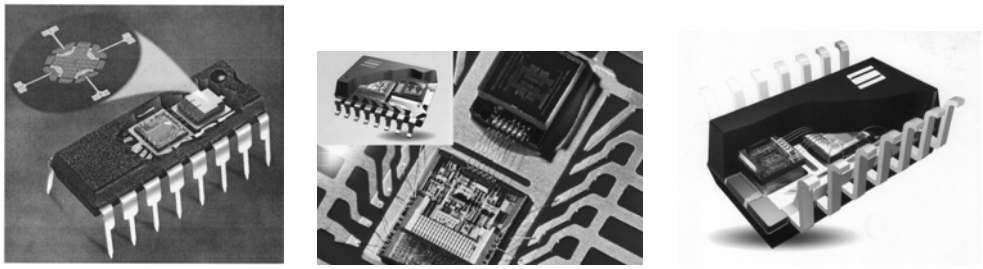

(a) (b) (c)

**Figure 21.** Examples of packaged automotive sensors: (a) accelerometer by Motorola in DIP package [193]; (b) gyro sensor by SensoNor in SOP package; (c) tire pressure sensor by SensoNor in SOP package [194].

are carried out on all devices at the same time. In connection with the higher packaging densities enabled by wafer-level packaging techniques, the highly parallel process steps lower the overall packaging costs. Furthermore, the devices are already packaged before the critical dicing step which involves a high risk of contamination and requires the full protection of mechanically moving parts. Typical wafer-level packaging techniques are thin and thick film deposition processes for device sealing [189,190] and wafer bonding [191,192].

Figure 21(a) shows an accelerometer by Motorola [193] put into an industry standard 16-pin dual-in-line package (DIP), together with an electronics chip. This approach of integrating the MEMS device with the electronics circuitry in the package and not on a chip-level is called system-on-a-package (SOP). The MEMS-chip is encapsulated hermetically by full-wafer glass-frit bonding, which is, besides anodic bonding, the most common hermetic sealing method by wafer bonding (see Section 2.3.2).

Figure 21(b) shows a gyro sensor fabricated by SensoNor, Horten, Norway, also following the system-in-a-package idea, for a small-outline-package (SOP[20]). The MEMS chip is hermetically sealed by anodic wafer bonding. A very similar fabrication and packaging procedure is utilized for a tire pressure sensor by the same company, shown in Figure 21(c). Besides the pressure sensor, this device also includes a radial acceleration sensor, a temperature sensor and a battery voltage monitoring function [194].

### 2.3.2 Wafer bonding techniques

Wafer bonding is the joining of one substrate to another substrate. Typically, wafers made of the same material or wafers of different materials can be bonded together. The origins of wafer bonding are back in the 1980s and the main commercial application is still in the area of creating silicon-on-insulator (SOI) substrates for RF electronics [192].

However, wafer bonding attracted attention as a sealing and packaging method for bulk-etched cavities containing micromechanical sensor elements. It actually can

[20] Unfortunately, the abbreviation SOP is commonly used both for system-on-a-package and for small-outline-package.

**Table 10.** An overview of the most common wafer bonding techniques.

| Bonding method | Temperature °C | Hermeticity | Reliability | Bond strength MPa | Comments |
|---|---|---|---|---|---|
| | | *Surface bonding* | | | |
| anodic bonding | medium, 200–500 | yes | good | >30 | requires flat surface, high voltages |
| fusion bonding | very high, 700–1400 | yes | good | >20 | requires surface preparation, flat surface |
| surface activated bonding | very low, RT[a]–200 | yes | not certain | >10 | requires flat surface, surface preparation |
| | | *Metallic interlayer* | | | |
| eutectic bonding | medium, 180–400 | yes | not certain | 20 | particle insensitive |
| thermo-compression bonding | medium, 350–500 | not certain | not certain | 10 | very high pressure required |
| solder bonding | low, 180–300 | yes | not certain | | particle insensitive |
| | | *Insulating interlayer* | | | |
| adhesive bonding | low, RT–300 | no | not certain | 10–25 | very particle insensitive, very versatile |
| glass-frit bonding | med./high, >400 | yes | good | | particle insensitive, versatile |

[a]room temperature

be regarded as *the* enabling technique for many high-volume, low-cost MEMS sensors such as the ones shown in Figure 21.

The main applications of wafer bonding in MEMS, besides functional or protective sealing [195–198], are vertical stacking of devices, which is also interesting in semiconductor fabrication for stacking memory chips [199], and combining structures fabricated on two different substrates, if the fabrication of the structures is not compatible or too complex for one single substrate. This technique of merging two wafers with subsequent removal of one of the two substrates is called transfer-bonding [200].

The most common wafer materials used in (RF) MEMS fabrication are silicon with different doping levels and crystal orientations as well as pyrex and quartz glass. Silicon carbide and gallium arsenide are getting increased attention. Ceramic substrates such as aluminum nitride (AlN) and alumina ($Al_2O_3$) are the most commonly used substrates in MEMS chip packaging, but are rarely used directly as a fabrication substrate. On a system level (multichip modules), typical electronic substrates such as low temperature co-fired ceramics (LTCC) are also used in MEMS packaging. Ceramic substrates allow hermetic MEMS packages [201].

Table 10 and the following list give an overview of the wafer bonding techniques used in MEMS fabrication.

*Anodic bonding* [195, 202, 203] provides reliable sealing and is suitable for high vacuum packaging down to a few milliTorr. This technique can be used for different substrate material combinations: glass-to-glass, glass-to-silicon, glass-to-metal, silicon-to-silicon. Accelerometers fabricated in very high volumes are typically sealed by anodic bonding of a pyrex glass to a silicon wafer. Anodic bonding is carried out at relatively low temperatures of 200–400 °C, but involves high voltages of 200–1700 V, which might damage microelectronic circuits. Another threat to electronics is sodium ion diffusion from pyrex glass into the silicon wafer. Anodic bonding is very particle-sensitive, and a surface roughness of less than a few nanometers is required [204]. Another problem of anodic bonding, as well as of the other "surface" bonding techniques, is the difficulty of creating in-plane electrical interconnections through the seal. However, a few methods of creating feedthroughs were reported in the literature:

- Very thin electrical feedthroughs with a thickness in the order of 50 to 100 nm can be manufactured with a special layout design without decreasing the hermeticity of the package [205].
- Interconnection lines with a thickness of up to 500 nm were demonstrated by etching recesses in the glass wafer, which were subsequently filled by metal evaporation. The metal overlaps the corners of the recesses to achieve a seal even on the slopes of the etched glass [206].
- Anodic bonding is possible with polished surfaces. Thus, in-plane interconnection lines can be covered by a polysilicon layer which is polished afterward [207].
- Interconnections can be created by doping resistors which are buried in the substrate and covered with an epitaxially deposited silicon layer, as done for the high volume automotive sensors fabricated by SensoNor, Norway.

*Fusion or direct bonding* [208–210] is also a widely used technique for hermetic packaging. The bonding surfaces have to be extremely flat and clean, and the bonding is primarily accomplished by the induced chemical forces between the surfaces which have to be activated by hydration or by a hydrophilic process. The bonding occurs "spontaneously" at oxidising ambient, and has to be followed by an annealing step [189, Chapter 2.6]. For the annealing, very high temperatures of 700–1400 °C are necessary to yield a durable bond. Direct bonding without annealing step can also be done with polymer materials, typically with PMMA or PDMS, involving a surface treatment in a plasma cleaner but yielding in a less strong bond [211].

*Surface activated bonding (SAB)* [212,213] is basically also a direct bonding technique requiring very flat surfaces and special surface preparation. Here, the bonding energy originates from a very strong adhesive force acting between two atomically clean solid surfaces under contact [214], while in most of the other bonding techniques the bonding energy is provided by the processing temperature in combination with the imposed bonding pressure. The cleaning procedure typically consists of a dry etching process such as ion beam bombardment or radical irradiation, carried out in ultrahigh vacuum. Bonding by the SAB method is completed even at room

temperature and can be applied to a variety of different materials (Al, Cu, Ag, Au, Sn, Ti, Ni, SiC, $Si_3N_4$, $Al_2O_3$, AlN, diamond and silicon [213]).

*Eutectic bonding* [215, 216] is diffusion based joining of two metals. The bonding occurs at the so-called eutectic point, which is the lowest fusion temperature of an alloy with a melting point lower than that of any other combination of the same components, and much lower than the melting points of the involved metals. At temperatures above this eutectic point, rapid diffusion of one material into the other occurs, which results in the formation of an eutectic alloy. Eutectic bonding is assisted by pressurizing the surfaces. Typical material combinations are Au 97%-Si 2.83% with an eutectic temperature of 363 °C (the melting temperatures of silicon and gold are 1410 °C and 1064.4 °C, respectively), or solder forming of Sn 62% with Pb 38% at 183 °C (melting temperatures: Sn: 231.9 °C, Pb: 327.4 °C). Silicon and gold are the preferred materials in MEMS because of processing simplicity and compatibiliy, but it is difficult to obtain high-quality sealing at temperatures below 400 °C [213].

*Glass-frit bonding* [217], also called low-temperature melting glass bonding, is an adhesive bonding method with an inorganic intermediate bonding layer. The glass-frit is deposited on one or both of the wafers. Then the wafers are brought into intimate contact and heated. The glass-frit reflows and forms a rather strong bond, suitable for hermetic packaging. Typical glass curing temperatures are between 400 and 1100 °C. This method is very insensitive to particles and can be applied on various wafer materials. It results in a hermetic bond but is not suitable for sealing high-vacuum cavities, because the glass-frit releases trapped gases.

*Solder bonding* [218, 219] is similar to eutectic bonding. Here, the metal solder is applied as a compound material to the bonding surfaces. The surfaces are brought into contact and heated to the melting temperature of the solder. The solder reflows which causes intimate contact between the two parts, leading to a permanent and hermetic bond. Fluxes in the solder, used to remove oxides from the metal surfaces, should be avoided because they evaporate during the heating and might condense on critical mechanical parts inside the package. Similar to eutectic bonding, solder bonding is less sensitive to particles than anodic or fusion bonding. To create higher temperatures of up to 800 °C in the bonding interface without harming the structures to be packaged, localized heating by embedded resistors was found to be suitable for MEMS sealing, both for solder and for eutectic bonding [220].

*Thermocompression bonding* [221–223], often referred to as solid-state welding, is a bonding method involving a very high pressure between the two surfaces to be bonded. The pressure causes plastic deformation, which results in intimate contact between the opposing surfaces. This process is often assisted by heat, either by "global" heating [221], ultrasonic energy [224], or localized microwave heating [225]. Common material combinations are gold-to-gold, aluminum-to-gold, aluminum-to-aluminum and aluminum-to-glass. Typical bonding pressures are about 300 MPa, and temperatures of 350–500 °C are necessary to achieve an acceptable result.

In general, data in the literature about the bonding pressure has to be read very carefully whenever structured wafers are bonded. For practical reasons, the bonding pressure is typically referred to as the applied pressure between the two chucks in the bonding tool. However, the effective pressure $p_{eff}$ between the touching structures, which determines the conditions for forming the bond, depends not only on the chuck pressure $p_{chuck}$ but also on the ratio of the total chuck area $A_C$ to the effective contact area $A_{eff}$:

$$p_{eff} = p_{chuck} \frac{A_C}{A_{eff}} \tag{5}$$

Keeping this in mind explains the different values mentioned in the literature, varying by a few orders of magnitude. For instance, the necessary bonding pressure for gold thermocompression bonding is stated to be about 300 MPa in [222], but a chuck pressure of only 4 MPa achieved very good results for the same process in [223]. The ratio of about 100 between these values can be explained by the mask layout used in [223], consisting of ring-shaped structures intended to hermetically seal cavities for MEMS devices.

### 2.3.3 Polymer adhesive wafer bonding

Wafer bonding with a polymer intermediate bonding layer [222, 226–228] is increasingly attracting attention because of its many interesting advantages:

- low bonding temperature from room temperature up to 300 °C
- simple, low-cost processing (spin-on polymers)
- high bond strength
- highly tolerant to particles and surface non-uniformities of several $\mu$m due to the good planarization and wetting properties of most adhesives, which even enable thick electrical interconnection lines to be embedded in the adhesive layer
- many different substrate materials can be joined
- compatibility of many polymers with standard clean-room processing
- the bonding layer acts as a stress buffer between the two substrates due to the elastic properties of polymers
- the possibility of patterning the adhesive layer before the bonding procedure, to create three-dimensional structures and to get cavities for housing MEMS devices directly in the bonding layer
- RF interconnection lines in or through the adhesive layer have very low signal attenuation and low reflections since adhesives with low loss tangent and low dielectric constants are available
- many polymers with different properties (thermo-set, thermo-plastic, curing temperature, viscosity, etc.) are available on the market, making this technology very versatile and suitable for various applications

The main disadvantages of polymer bonding for MEMS packaging should also be revealed:

- Polymers are permeable to gases to a much higher degree than metals or ceramics [190, Chapter 14].
- The long-term stability of polymers is uncertain.
- Most polymers have limited temperature stability.
- Polymers, especially when not pre-cured, are very soft which results in larger post-bonding alignment inaccuracies because of unavoidable sheer forces between the bond chucks. For adhesive bonding, the alignment uncertainty is of the order of tens of micrometers [222], as compared to anodic bonding with a post-bonding alignment accuracy of less than 2 $\mu$m.

Typical materials used for adhesive bonding in MEMS are epoxy-based polymers such as benzocyclobutene (BCB [229,230]) and SU-8 [231,232], epoxy-based photoresists [229], polyimides [233] and B-stage epoxies [234].

Epoxy-based polymers, such as BCB, and the so-called liquid crystal polymers (LCP) provide a certain gas-tightness, and packages involving such polymers are often classified as "near-hermetic" packages. BCB for bonding is discussed in Section 4 and in papers 1, 2, 5 and 6, and LCP, a relatively new material in MEMS which might play a larger role in adhesive bonding in the future, is discussed in the following paragraph.

LCP are thermoplastic polymers made of aligned molecule chains with crystal-like spatial regularity, exhibiting unique electrical, physical and chemical properties [235]. Table 11 compares the properties of LCP with kapton and BCB. For oxygen, carbon dioxide, nitrogen, argon, hydrogen and helium, LCP have above-average barrier performance and the permeation of gases through LCP is not affected by humidity, not even at elevated temperatures. Also, for being a polymer, LCP films have an extremely low moisture uptake and show excellent chemical resistance [236]. From a mechanical point of view, it is remarkable that the coefficient of thermal expansion (CTE) can be controlled in a predictable way during the processing, even reaching very low values [237]. LCP can be etched almost isotropically in oxygen plasma without additional reactive ions, with an etch rate of about 0.25 $\mu$m·min$^{-1}$ at a power of 350 W [235]. To the knowledge of the author, LCP are currently only available as sheet material and not in liquid form and are therefore not suitable for spin-coating, since they get liquid only above the melting temperature of about 280 °C.

### 2.3.4 Hermetic sealing on wafer-level

MEMS hermetic packaging on wafer-level can be classified into two categories: 1) surface-micromachined micro-shells and 2) bonding methods, either chip to wafer or wafer to wafer. Full-wafer bonding techniques, still the most common hermetic packaging techniques in high-volume MEMS production, were already discussed in Section 2.3.2. For chip to wafer capping, the same bonding physics is used as for full-wafer bonding, but each device is encapsulated individually by flip-chip-like pick-and-place techniques. Eutectic bonding and solder reflow sealing [238] are the most commonly used

**Table 11.** Comparison of the properties of a typical liquid crystal polymer (LCP) with kapton and BCB [235].

| Property | Unit | LCP | Kapton | BCB |
|---|---|---|---|---|
| manufacturer | | Celanese/Ticona | DuPont | Dow Chemical |
| product specification | | Vectra A-950 | HN200 | Cyclotene 3022 |
| melting temperature | °C | 280 | 400 | N/A[a] |
| dielectric constant | – | 2.8 | 3.5 | 2.65 |
| loss factor, tan $\delta$ | – | ≈0.004 | 0.002 | 0.0008–0.002 |
| moisture absorption | – | <0.02% | 2.8% | <0.12% |
| coef. of therm. expan. | ppm $K^{-1}$ | 0–30[b] | 20 | 52 |
| tensile strength | MPa | 200 | 234 | 85 |
| Young's modulus | GPa | 9 | 2.5 | 2.0 |
| specific gravity | kg·$dm^{-3}$ | 1.4 | 1.42 | 1.05 |

[a] since a thermoset, and not a thermoplastic material
[b] can be determined during the fabrication process

chip sealing techniques. Typically, hermetic packaging by full-wafer bonding as well as chip-to-wafer bonding is quite space-consuming since the sealing rings require a width of a few hundred micrometers to create an effective gas barrier. Also, the total package height is of the order of the thickness of two wafers. However, atmosphere control is better for anodic and fusion bonding than for the surface-micromachining techniques discussed in the following paragraph.

Surface-micromachining leads to very compact and thin micro-shells requiring just a bit more space than the actual devices to be packaged. The traditional sealing procedure by LPCVD processes is illustrated in Figure 22. An additional sacrificial layer (typically $SiO_2$) is deposited onto the MEMS structures and then covered by the encapsulating shell with narrow etch holes. Both the functional and the package sacrificial layer are removed in one step (typically HF wet or vapor etching) and the release holes are closed afterward by depositing a sealing layer which penetrates into the etch holes and etch channels, but not into the encapsulated cavity [239–241]. Instead of release holes, a HF permeable polysilicon layer can be used, which afterward is covered by the sealing layer [242, 243]. The disadvantage of LPCVD surface micromachining is the high deposition temperatures, typically above 700 °C, making this sealing technique basically not suitable for pre-fabricated electronic circuitry. However, it was shown that it is possible to combine this sealing technique with a BiCMOS process, when the CMOS structures are fabricated first without metal interconnections, then the MEMS devices including the sealing procedure, and finally the CMOS back-end metal layers [244]. Besides LPCVD, metal evaporation [245] and reflow of solder in vacuum [246] were successfully used to seal LPCVD fabricated micro-shells. Also, an approach using only process steps with temperatures below 250 °C for both the micro-shell and the sealing fabrication was presented recently. Here, the encapsulation is formed by electroplating nickel onto a photoresist sacrificial layer which is etched afterward by a KOH-based photoresist remover. The etch

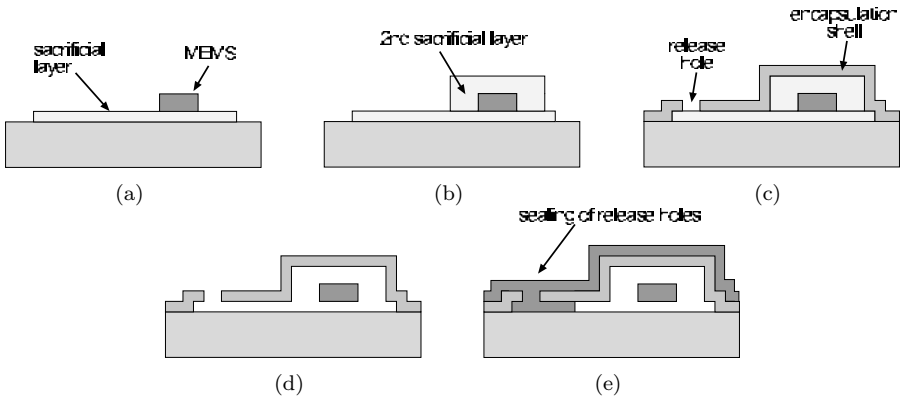


**Figure 22.** Schematic process flow of fabrication integrated encapsulation by surface micromachining techniques.

channels are finally sealed by reflowing lead-free and fluxless solder bumps, printed onto the chips, in vacuum [247].

An alternative to hermetic packaging on wafer-level is hermetic ceramic or metal packaging on chip level. Drawbacks of this approach are the high cost of ceramic and metal can packages and the problematic of exposing fragile micromechanical parts to contamination during the wafer dicing, the cleaning and the chip handling [248]. Thus, wafer-level encapsulation is probably the only feasible approach for a high-volume low-cost MEMS product.

If the package should keep very low pressures, the use of so-called getter materials might be considered, which absorb free gases inside the package. Such gases come from outgasing of the involved materials (especially glass), mainly if the bonding is done at elevated temperatures. Pre-heating of the components before the sealing is a very effective method to minimize material outgasing, but it is nevertheless insufficient for cavity pressures below 10 $\mu$bar. Typical getter materials consist of metal alloys containing Ba, Ti, Fe or Al [249, 250]. Pressures lower than $10^{-8}$ bar were reported using so-called non-evaporable getters [251]. However, using a getter implies delicate processing steps in the fabrication. Thus, getter materials are seldom used in MEMS [252]. Getter materials are more frequently used in GaAs semiconductor circuits to absorb hydrogen and moisture, preventing so-called hydrogen poisoning. Here, typical getters consist of an active oxide and and desiccant in a flexible silicon polymer matrix. The active oxide reacts with hydrogen, converting it to $H_2O$, and the desiccant absorbs the moisture, thus permanently removing the harmful gases [253].

### 2.3.5 Wafer-level packaging of RF MEMS switches

Packaging problems are thought to be one of the main reasons why RF MEMS switches are still not available on a commercial basis [7, 53]. Besides the general MEMS packaging problems, as discussed in Section 2.3.1, the packaging of RF MEMS switches is additionally confronted with the following difficulties:

- Electrical interconnection lines, penetrating through the (hermetic) package, should have low signal attenuation and low reflections. Thus, metal sealing (eutectic or solder bonding) with isolated signal lines through or underneath the sealing ring, might not be appropriate.

- Hermetic packaging is required for reliability and performance stability, especially for metal contact switches, to avoid surface absorption of contaminants and moisture uptake in isolation layers, causing stiction.

- Especially when targeting wireless applications, the chip size is very important. Thus, wafer bonding as used for many high-volume hermetic MEMS packages might not be possible without additional thinning of at least one of the substrates.

- All involved materials, including substrates, passivation layers and mounting frames, should have good RF properties.

The following paragraphs give a few examples of RF MEMS switch packages, with a special focus on RF interconnection solutions.

The typical chip-level hermetic packaging method by soldering and wire-bonding a MEMS device into a low temperature co-fired ceramic package (LTCC) and subsequent sealing with a soldered metal lid can be adapted for a RF MEMS device when optimizing the RF signal paths. Flip-chip bonding of the MEMS device to the ceramic carrier, in combination with a pin grid array (PGA) package has proved minimized signal attenuation [254].

In 2001, researchers at IMEC, Leuven, Belgium, reported on a wafer-level package for RF MEMS consisting of a glass sealing cap which is flip-chip bonded by indent solder reflow sealing onto the RF substrate containing the MEMS switches. RF feedthroughs, embedded in a BCB polymer layer below the metal sealing ring, were characterized in their RF performance up to 50 GHz [66]. The BCB layer has also the advantage that it can be used as an additional thick-film isolation layer to the substrate which decreases the substrate losses if the RF transmission lines are mainly placed on top of it. This packaging concept is shown in Figure 23(a). Also, hermeticity tests were carried out and the package was found to pass the helium leak

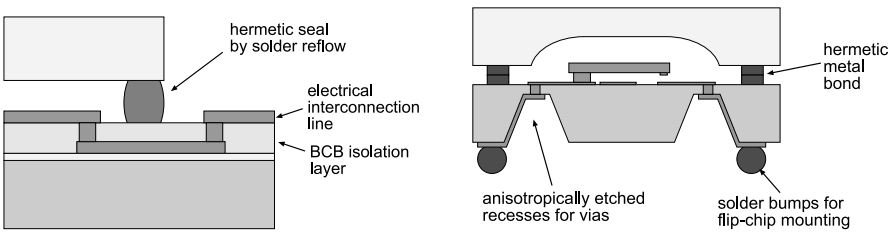


(a) (b)

**Figure 23.** Hermetic packaging concepts with metal sealing rings: (a) transmission lines embedded in a thick-film isolation layer [66]; (b) RF transmission lines penetrate the wafer and not the metal seal to avoid signal attenuation [67].

test specifications by the MIL-STD 883E procedure. As the authors state in the paper and investigate in a subsequent publication [255], the leak test results have to be interpreted carefully since the packaged cavities were very small and the packaging method cannot be considered as hermetic, since it involves polymers (compare Section 4.5). However, a ceramic isolation material such as $SiO_2$ or SiN could be used instead of BCB to improve the hermeticity, but then planarization problems have to be faced.

Metal sealing rings can be used even for RF applications if the RF interconnection lines do not penetrate through the sealing ring, but vertically through the wafer. Such a technique, combining a back-side anisotropic wet-etch in KOH or TMAH with metal deposition and patterning of the electrical interconnection lines by electroplated photoresist, was presented by the University of Michigan, Ann Arbor, USA, in 2001, and the RF attenuation was found to be very low [67]. Figure 23(b) shows the principle of the packaging concept. This approach, with modified fabrication sequences, was used in some following publications [256], and the idea of deposited metal lines on sloped, isotropically etched side-walls was also picked up to propose a general multilevel interconnection and packaging concept [257].

In silicon substrates, through-wafer vias allowing metal seals can also be fabricated by other techniques, such as

- photo-assisted electro-chemical etching of the deep holes in silicon and filling with Au-20wt%Sn solder by the so-called molten metal suctioned method [258]
- deep reactive ion etching (DRIE) of silicon using the Bosch process with subsequent oxidation of the walls for isolation purpose, deposition of doped polysilicon as the conducting material, and filling of the holes with low temperature oxide (LTO) and another polysilicon layer [259]
- DRIE of silicon, with a silicon nitride barrier and electroplated copper vias [260]. This technique was also used by the same authors to create a Faraday cage suppressing crosstalk [261]. A probably similar fabrication procedure with additional solder bumps was developed for a RF MEMS package [262]. DRIE in combination with electroplated copper on the sidewalls was already shown by researchers at Standford University, CA, USA, in 1999, but without sealing the holes [263]. Electroplating of gold in DRIE vias with subsequent plating of solder bumps was used for a RF MEMS packaging procedure on ulra-thin silicon substrates of 50 $\mu$m thickness. Here, the package was hermetically sealed by Au/Sn-Au metal bonding [264].

A very interesting device-scale micropackage was demonstrated by the National Taiwan University, Taipei, Taiwan, in 2003. A microshell is formed by electroplating nickel on an aluminum sacrificial layer in etched recesses in a glass wafer. After eching the sacrificial layer, the microcap is freed and suspended only through long tethers attached to the carrier glass, which are broken after the individual flip-chip transfer by solder bonding of the caps to a substrate wafer. This microshell fabrication and transfer technique was demonstrated to package a tunable capacitor successfully, where the electrically conducting microcap also acted as the top electrode for the three-plate tunable capacitor structure [265].

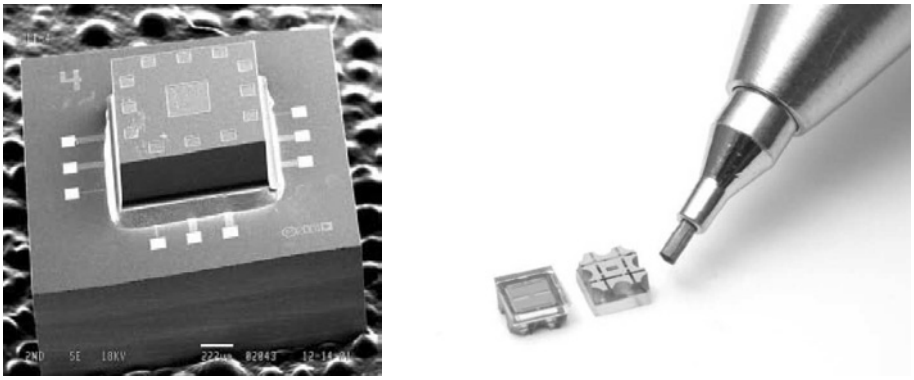

(a) (b)

**Figure 24.** Wafer-level packaging concepts of RF MEMS switches proposed by companies: (a) Radant MEMS switch packaged with full-wafer glass-frit bonding; (b) OMRON RF switch also using glass-frit wafer bonding, with metalized through-wafer vias.

A glass-frit wafer bonding process was used by Radant MEMS to hermetically package their RF MEMS switches. Figure 24(a) shows a single packaged Radant MEMS switch [266]. Also OMRON packaged their RF MEMS switch by glass-frit wafer bonding, and interconnections to the back-side of the wafer were created by metalization of through-wafer holes, as shown in Figure 24(b). The total package is only $1.8\times1.8\times1.0$ mm$^3$ in size, and the cavity of the device is sealed with inert nitrogen gas [158].

The electrothermally actuated microrelay by Tohoku University, Sendai, Japan, is hermetically packaged by anodic bonding of a pyrex glass wafer to a SOI substrate. The electrical feedthroughs are created by DRIE of vias through the pyrex wafer, which are filled by plated nickel. Furthermore, the electrical contacts between the top and the bottom wafer are established during the bonding procedure [130].

Sand-blasted holes, subsequently filled with electroplated gold plugs, were used by the Korean Institute of Science and Technology, Seoul, Korea, in 2002, to create through-wafer vias in a 300 $\mu$m thick pyrex glass substrate. The glass wafer containing etched cavities was bonded to a quartz substrate with B-stage epoxy to create near-hermetic packages for RF MEMS devices [234].

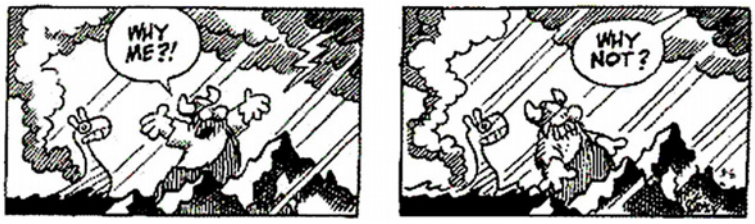

*Man is the only animal for whom his own existence is a problem which he has to solve.*

*Erich Fromm*
*1900–1980, German Social Psychologist*

*The earth teaches us more about ourselves than all the books in the world, because it is resistant to us. Self-discovery comes when man measures himself against an obstacle.*

*Antoine de Saint-Exupéry*
*1900–1944, French Aviator, Writer,*
*in "Wind, Sand and Stars"*

*The only journey is the one within.*

*Rainer Maria Rilke*
*1875–1926, Austrian Poet*

*The human mind is like a drunken monkey; it wants to jump from one place to another, seeking externally the solace and peace that are already within.*

*Sri Swami Rama*
*1925–1996, Indian Sage*

*Only in quiet waters things mirror themselves undistorted. Only in a quiet mind is adequate perception of the world.*

*Hans Margolius*
*1902–1984, German Writer*

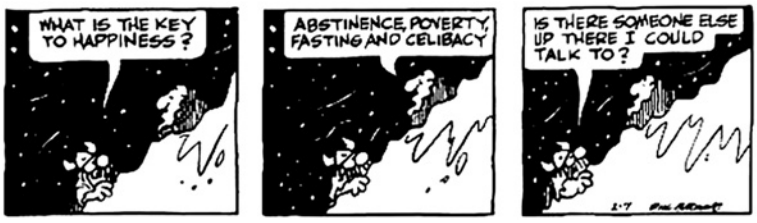

*Creativity requires the courage to let go of certainties.*

*Erich Fromm*
*1900–1980, Social Psychologist*

# 3 The S-shaped film actuator based switch

This section is intended to introduce the S-shaped film actuator based switch and to discuss the advantages and disadvantages of the novel concept. It also presents the prototype design and the characterization results of the first fabricated devices. More detailed information about the switch, its fabrication and the measurements can be found in the journal papers 3 and 4.

## 3.1 The switch concept

The conventional and so far most common concept of an electrostatically actuated switch is based on a cantilever-spring system, as shown in Figure 25. This concept evolves a few problems, as already raised in Section 2.2.1:

- A large contact distance in the off-state involves also a large distance between the actuation electrodes, which requires a high actuation voltage.
- The restoring force to open the switching contacts is supplied by the spring energy stored in the deformed cantilever. A large restoring force needed to overcome the adhesion force between the contacts requires a rather stiff structure which increases the actuation voltage.
- The contact force determining the contact resistance (see Section 2.2.3) is the difference between the electrostatic force and the restoring force. Thus, a large restoring force requires an even stronger electrostatic actuator, which demands an increased electrode area or a higher actuation voltage.
- A small electrode distance in the off-state, keeping the actuation voltage and the electrode size at an acceptable level, also results in a small contact distance. That leads to a large coupling capacitance between the open contacts, resulting in poor RF isolation, especially for large overlapping contact areas.

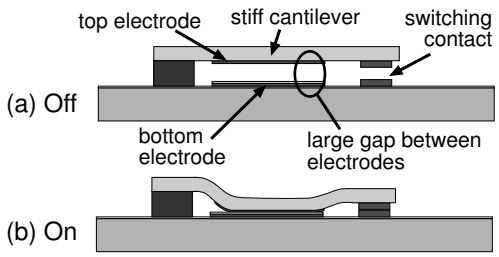


**Figure 25.** Illustration of the conventional concept of an electrostatically actuated switch.

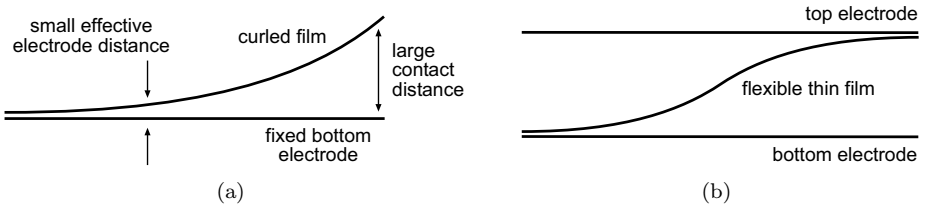


(a) (b)

**Figure 26.** Evolution from the curled actuator (a) to the S-shaped film actuator (b), endowed with an additional counter-actuator.

A curled actuator as illustrated in Figure 26(a), a so-called touch-mode actuator [161] moving in a zipper-like matter, improves the conventional design. It offers the possibility to have a large deflection of the cantilever tip by maintaining a small effective electrode distance for low voltage isolation. For a switch, this actuation concept allows the contact distance to exceed the sacrificial layer thickness by factors of over 10. However, the actuation voltages typically reported are not as low as expected [95, 97, 105]. This can be explained by the fact that the stress gradient in the film needed for the characteristic out-of-plane bending has to be overcome by the electrostatic force in order to close the switch. A thinner, less stiff film would also result in a curled beam and would require less energy to be actuated. Unfortunately, a thinner film also decreases the restoring force making the switch more susceptible to failure caused by contact stiction. A possible solution to this problem is a counter-actuator providing active opening capability. This can be achieved by using a second low-voltage curled actuator flipped upside down. Figure 26(b) shows the combined actuator with the characteristic S-shape of the film moving between the bottom and top electrodes. Due to the two combined zipper actuators working on a very thin and flexible membrane, the vertical movement of successive parts of the membrane anticipates a characteristic rolling rather than a pure up-and-down movement.

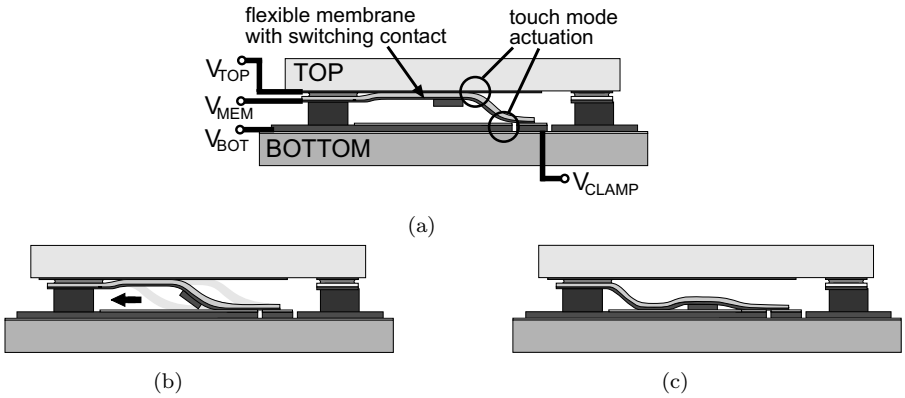


(a)

(b) (c)

**Figure 27.** The S-shaped film actuator based switch in the off-state (a), during the transition (b) and in its on-state (c).

This S-shaped actuator was used for a gas valve with dimensions in the millimeter range in 1997 [267]. The novel switch, proposed in this thesis, is based on this concept and shown in Figure 27 in its on and off-states and during the transition between its two stable states. The switch is fabricated in two different parts which are assembled after the release-etch of the membrane, as illustrated in Figure 28. Figure 29 shows SEM pictures of the two parts of the switch and Figure 30 shows the two parts of an until now unpublished, smaller switch variant. A three-dimensional view of the top and the bottom part of the switch can be seen on page 76 and on page 77, respectively, as stereo images for parallel-eye viewing.

The characteristic S-shape of the film is created when assembling the two parts, which brings the tip of the free-etched membrane in contact with the bottom electrodes. To ensure the low-voltage zipper-like movement in both directions, the membrane tip must always be in contact with the opposite (bottom) part. For this purpose, the bottom part is endowed with additional clamping electrodes which electrostatically pull the membrane tip down to the bottom electrodes. The clamping electrodes are not necessary to establish the initial contact of the membrane tip with the bottom part, but are intended to improve the overall switch reliability, since stiction between

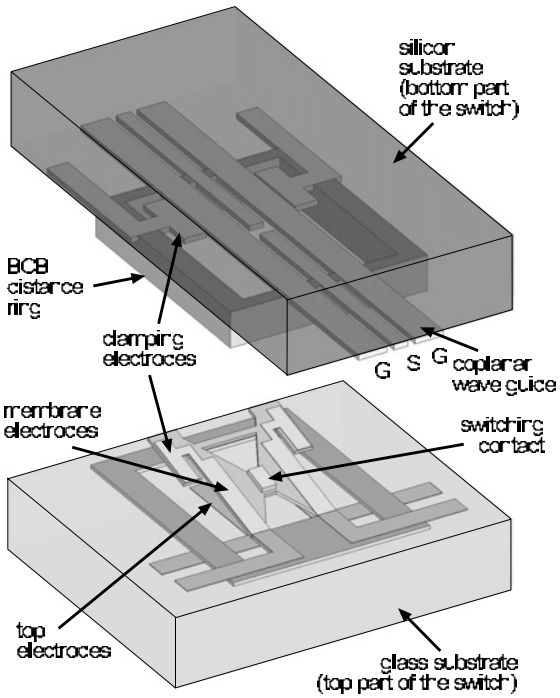


**Figure 28.** Schematic illustration of the film actuator switch with the switch shown upside-down. The silicon substrate contains the coplanar waveguide, the clamping electrodes and the BCB distance ring. The glass substrate contains the top electrodes, the silicon nitride film with the membrane electrodes and the switching contact. Details such as isolation layers and etch holes are not shown in the drawing.

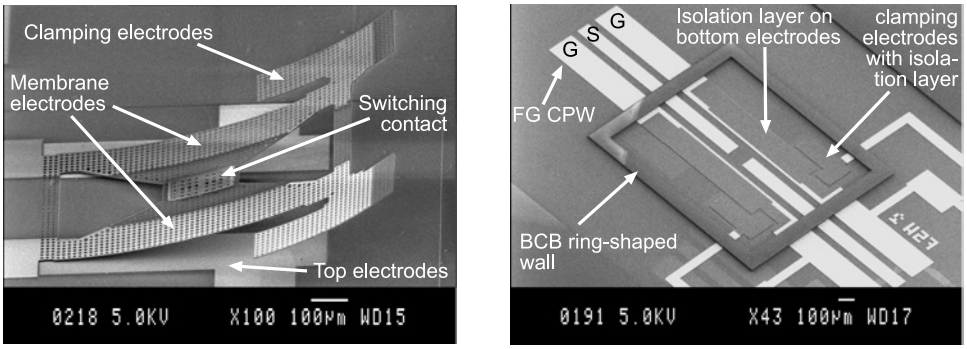


(a) (b)

**Figure 29.** SEM-pictures of the two parts of the switch before the final assembly: (a) top part with free-etched membrane; (b) bottom part with coplanar waveguide and polymer sealing ring defining the distance between the two parts.

the membrane and the top electrodes could prevent the membrane from curling down after opening the switch, which might prohibit an intended closing of the switch. Also, the clamping electrodes do not require any additional photolithography or etching step, and, since the clamping parts on the membrane are electrically connected to the membrane electrodes, not even additional interconnections or contact pads on the top part are needed.

It should be noted that the stress gradient in the membrane, which puts the tip of the membrane in contact with the bottom part of the switch, does not significantly increase the actuation voltage as in the case of a single curled actuator, since the membrane is very thin and flexible with very little stored spring energy.

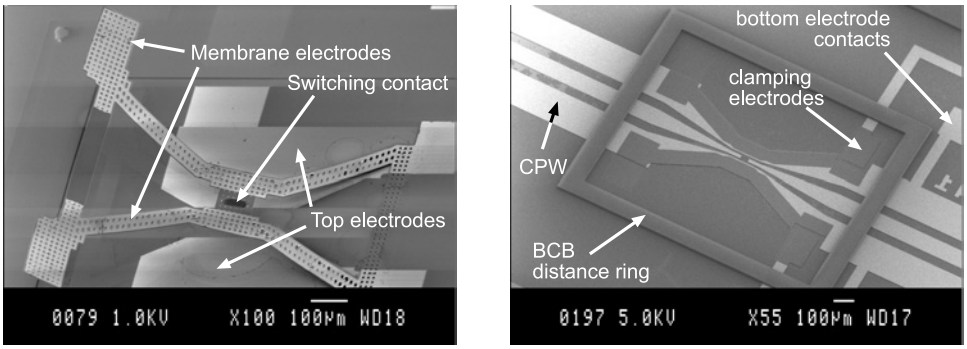


(a) (b)

**Figure 30.** SEM-pictures of the top (a) and the bottom (b) parts of a smaller, until now unpublished switch variant.

## 3.2 Discussion of the concept

The concept of the S-shaped film actuator based switch has the following advantages:

- The touch-mode actuators require very low actuation voltage to open and close the switch.
- The contact distance can basically be designed independent of the actuation voltage.
- The upper touch-mode actuator provides an active opening capability, which, to a certain extend, gives external control over the opening force and increases the overall switch reliability.
- The vertical electrostatic actuation principle provides almost-zero power consumption.
- The vertically moving actuator is fabricated by standard surface micromachining process steps.
- Due to the active opening capability, no passive restoring spring force is required, which allows a design with a very thin and flexible membrane, further lowering the actuation voltage.
- The large contact distance allows very large overlapping contact areas without compromising the RF isolation. Large nominal (or overlapping) contact areas do not directly lower the contact resistance if the contact force is not increased. However, they provide a better heat distribution from the effective contact spots heated by the dissipated power of the signal current flowing over the contact interface. Avoiding local overheating is one of the main measures increasing contact reliability for switching larger currents (see Section 2.2.3).
- The film rolls longitudinally in the direction of the signal transmission line. Thus, the ground lines of the coplanar waveguide are used as the bottom electrodes, and the membrane electrodes are placed directly above them, congruent with the bottom electrodes. Such a design results in minimum distortions of the wave propagation in the on-state, and in an almost perfect open line in the off-state.
- The contact pressure on the switching bar is created symmetrically both laterally and longitudinally in the direction of the transmission line.
- The fabrication of the part with the moving structure (top part) is carried out on a different substrate than the part with the signal line to be switched (bottom part). That means that basically there are only very few restrictions in fabrication compatibility, and the top part with the membrane can be transferred to any type of substrate containing RF circuits[21]. In paper 7, the upper

[21] The bonding process is the only restricting fabrication step, since mis-matched coefficients of thermal expansion (CTE) of the two substrates might evolve problems if the bonding process requires a temperature typically above 100 °C.

part of a capacitive version of the switch is intended to be placed directly onto a substrate with a meander-shaped reconfigurable antenna.

- The assembly can be done either by flip-chip-like pick-and-place techniques (flexible, space efficient on the top wafer, higher yield), or by full wafer bonding if the switch density is high enough for economical reasons. Both methods result in an integrated and protected "ready-to-dice" package.
- The final vertical distance between the two parts can be controlled very accurately by the thickness of the polymer distance ring, as opposed to other switch transfer concepts reported in the literature, for instance thermal compression bonding [110].
- The actuation mechanism is suitable both for shunt and series switch configuration.

Furthermore, it should be noted that this concept can also be realized in a true single-pole-double-through (SPDT) configuration using only one single switch: The input line, electrically connected to the membrane as in the case of a so-called in-line switch, can be switched via the membrane either to a top or bottom contact on the top and bottom parts of the switch, respectively.

Besides the promising advantages of the switch concept, it also has some disadvantages:

- Switch control is more complicated since the concept requires a total of four electrodes, compared to two electrodes in a conventional switch design. However, only the potential of the membrane electrodes has to be altered to switch from one state to the other, as illustrated in Table 12. Also, the clamping electrodes were found not to be necessary for operating the prototype devices, and might be left out if not considered for reliability reasons. Thus, the switch can be operated by three control potentials which are necessary for any concept with active opening (push-pull) capability.
- The vertically stacked, three actuation electrode structure increases the fabrication complexity and the production costs.
- The two parts of the switch have to be electrically interconnected which is not trivial, depending on the overall packaging concept.
- The very thin membrane undergoes complex mechanical deformations compared to a cantilever in a conventional switch design, which might be a reliability issue,

**Table 12.** Driving potentials of the actuation electrodes during operation of the switch, as referred to Figure 27(a).

| Switch state | $V_{TOP}$ | $V_{MEM}$ | $V_{BOT}$=GND | $V_{CLAMP}$ |
|---|---|---|---|---|
| On | + | + | 0 | + |
| Off | + | 0 | 0 | + |

even though, by experience, MEMS contact switches rather die due to electrical contact problems than due to failure of their mechanical actuators.

- An "all-metal switch" design without electrical isolation layers between the actuation electrodes to avoid electrostatic charging problems is either more complex (metal-isolator-metal sandwich of the membrane) or mechanically more vulnerable (pure metal membrane with an isolating plug supporting the metal contact bar). In both cases, the stress imposed by the rolling movement of the film might involve mechanical reliability problems.
- Due to the flexibility of the thin membrane, the contact force is rather small if the electrodes cannot be placed very close to the contact bar (which is often not possible for DC isolation or for RF design reasons). A solution to this problem is a higher local stiffness of the membrane, just around the contacts. However, that complicates the fabrication, decreases the reliability (mechanical stress at the transition of the thin to the thicker membrane part), and results in a larger structure consisting of a conventional, stiff platform with two thin-membrane touch-mode actuators.
- The transfer-bonded switch concept involves typical problems such as alignment accuracy between the two parts/wafers.
- The contact bar "rolls" with the membrane which means that always the same end of the bar closes the signal line last and opens it first. Thus, contact degradation due to discharging and sparking always occurs on the same end.

## 3.3 The first prototypes

The fabrication of the switch prototypes is done on two different substrates, as illustrated in the process flow in Figure 31. A detailed process description is given in paper 4. For easier access to the electrical contacts of the top and the bottom parts which are facing each other, the two parts were assembled manually in a cross shape, as shown in Figure 32. The overall device is quite large because of the many large contact pads, but the encapsulated cavity with the switch has a size of about 1 $mm^2$ and is just a small fraction of the total construct, as outlined in Figure 32(a). However, also the switch itself is quite large compared to other MEMS switches, even when considering that it is already encapsulated. In the current design, the ratio of the vertical membrane displacement to the membrane length is about 1:65, imposing very little mechanical stress on the membrane. Therefore, it is assumed that the lateral dimensions of the switch can be downscaled without compromising either the actuation voltage or the contact distance, and hopefully not the reliability either.

Some of the advantages of this switch concept, as discussed in Section 3.2, are related to the possibility of having a very large contact distance and very large overlapping contact areas without sacrificing either the RF performance or the low actuation voltage. The prototypes have an off-state contact distance of 14.2 $\mu$m, which is about 5 to 7 times larger than in conventional designs (compare Table 8 on page 40), and with 3500 $\mu m^2$ for each contact, the overlapping contact area is about 10 times larger than in conventional designs.

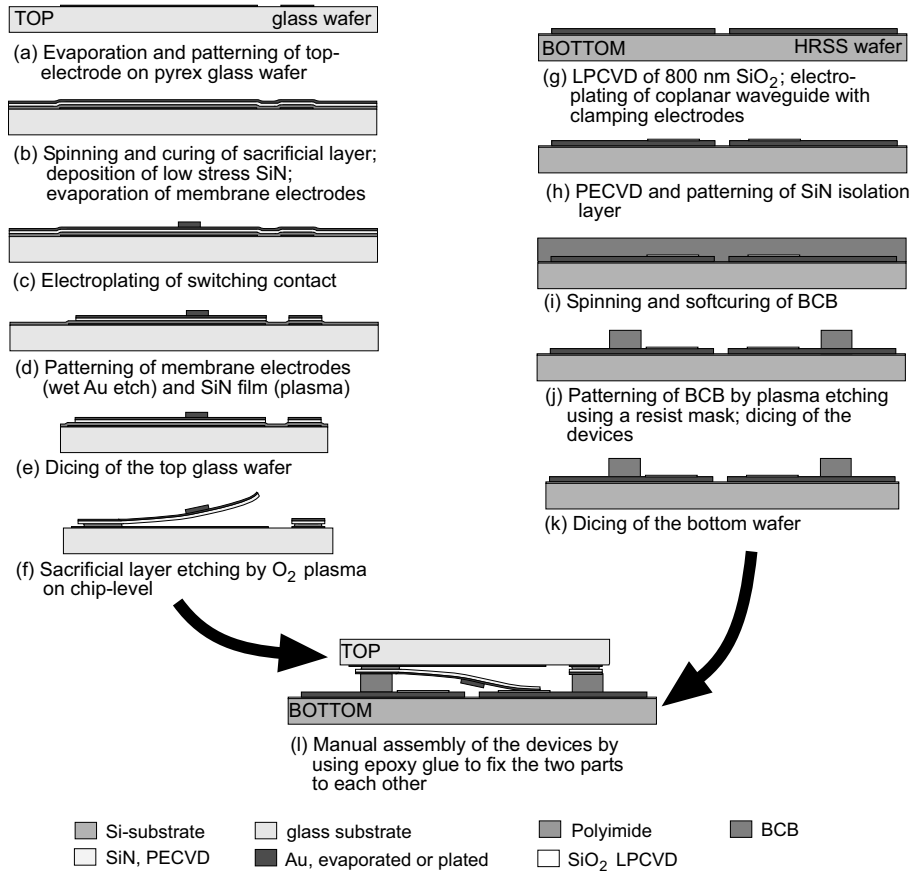


**Figure 31.** Process flow of the prototype fabrication of the S-shaped film actuator based switch.

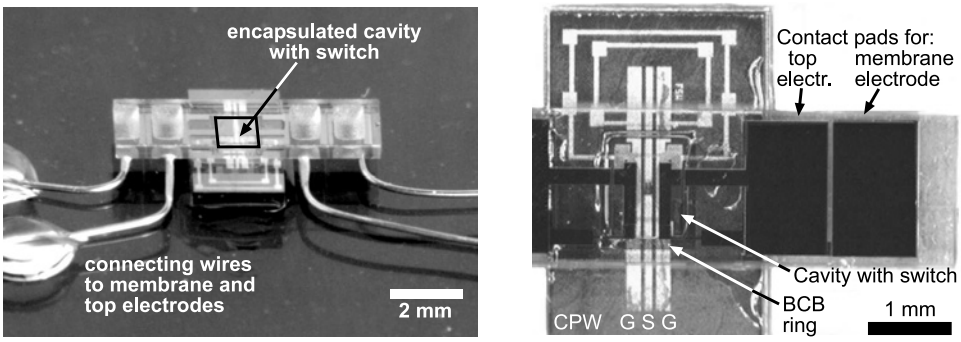


(a) (b)

**Figure 32.** Photographs with full view (a) and close-up view (b) of one of the manually assembled prototype switches.

**Table 13.** Comparison of the film actuator switch prototype with the OMRON RF MEMS switch [109].

| | OMRON switch | Prototype of film actuator based switch |
|---|---|---|
| switch type | series metal contact | series metal contact |
| operation principle | vertically moving membrane | S-shaped rolling film actuator |
| actuation for closing | electrostatic forces | electrostatic forces |
| actuation for opening | spring forces | electrostatic forces |
| structural material | monocrystalline silicon | PECVD silicon nitride |
| signal line and contact | 1.0–1.6 $\mu$m sputtered gold [160] | 2.0 $\mu$m electroplated gold |
| packaged chip size | 3.0×2.0×1.0 mm$^3$ [a] | 1.7×1.4×1.0 mm$^3$ [b] |
| membrane size | 1400×1700 $\mu$m$^2$ | 950×900 $\mu$m$^2$ |
| membrane thickness | 18–24 $\mu$m [75] | 1 $\mu$m SiN + 0.190 $\mu$m Au/Cr |
| total electrode size | 2×1 000 000 $\mu$m$^2$ | 2×82 500 $\mu$m$^2$ |
| switching contact area | unknown to the authors | 2×3500 $\mu$m$^2$ |
| open contact distance | 3 $\mu$m | 14.2 $\mu$m |
| actuation voltage | 19.2 V to close | 12 V to open, 15.8 V to close |
| contact force | 5 mN at 24 V, calculated | 102 $\mu$N at 15 V, simulated |
| contact resistance | <50 m$\Omega$ | 0.65 $\Omega$ |
| RF isolation | 40–30 dB (2–10 GHz) | 45–30 dB (2–15 GHz) |
| insertion loss | <0.5 dB | 2.5 dB at 10 GHz |
| open-state capacitance | 5 fF [75] | 4.2 fF |
| switch transfer by | anodic bonding (>350 °C) [c] | patterned adhesive bonding (BCB, 280 °C) [d] |
| packaging | CSP on wafer level by glass-frit bonding (450 °C) | together with switch transfer, "ready-to-dice" package |
| sealing ring | 250 $\mu$m wide, 10 $\mu$m high, glass-frit | 200 $\mu$m wide, 18.2 $\mu$m high, BCB |
| package gas tightness | hermetic package | near-hermetic package |

[a] a smaller device with a chip-scale-package (CSP) of 1.8×1.8×1.0 mm$^3$ was recently presented [158]

[b] size of the packaged prototype switch, excluding contact pad areas for manual probing

[c] thermo-compression bonding in [158]

[d] design target: to be done by patterned adhesive full-wafer bonding with BCB; the prototypes are assembled manually and fixed by epoxy drops

Table 13 compares characteristic design and measurement data of the switch to data of the OMRON RF MEMS switch, which is of similar dimensions and was already discussed in Sections 2.1.4, 2.2.1 and 2.2.2. The OMRON switch is currently one of the most mature MEMS switches in device performance and in its overall concept including the packaging, developed since about 1996 by the world's largest manufacturer of mechanical relays.

### 3.3.1 Prototype packaging

The switch is designed to be housed by the cavity between the two substrates, which is defined by the distance ring fabricated on the bottom wafer. Benzocyclobutene (BCB), an epoxy-based polymer from the Dow Chemical Company, is used to form the ring. The patterned polymer is hard-cured during the final assembly of the switch, leading to a relatively strong bond between the two parts. More information about adhesive bonding and patterned BCB-bonding can be found in Section 4. BCB, as all polymers, is permeable to gases and this type of packaging can therefore not be considered hermetic. Packaging with BCB is often referred to as "near-hermetic" packaging because, among polymers, BCB is one of the least permeable materials. However, it is a sufficient barrier against liquids and at least protects the switch from water during the dicing process and from dust during other post-processes outside clean-room facilities. Some advantages of BCB are its low dielectric constant and its low losses at high frequencies, making it ideally suitable as a sealing ring material to encapsulate RF devices. Also, the good planarization ability of the polymer allows the use of thick electrical interconnection lines penetrating through the wall (see Section 4). The BCB thickness is 18.2 $\mu$m for all of the fabricated prototypes, and the width of the wall is 100 $\mu$m.

The assembly of the switch can be done either individually on chip level (chip to chip) or on wafer level, and in the latter case either by individual pick-and-place techniques (chip to wafer) or by full wafer bonding (wafer to wafer). The sequential order of the dicing and the free-etching of the switch membrane is different for the chip-to-chip (or chip-to-wafer) assembly than for the wafer-to-wafer assembly:

**Chip-to-chip or chip-to-wafer:** 1) dicing of the top wafer; 2) sacrificial layer etching of the individual chips; 3) mounting of the chips to their counterparts, either on chip-level or on wafer-level

**Wafer-to-wafer:** 1) sacrificial layer etching on wafer-level; 2) assembly of the two parts by full-wafer bonding; 3) dicing of the chips (see also Section 4.2)

The design target is assembly by wafer-to-wafer bonding, packaging all of the switches on the wafer in one single process step. However, the prototype devices were assembled on chip level as shown in Figure 32. Also, the two parts were additionally fixed by epoxy. The electrodes on the top part, which are upside down, are accessed by electrical wires glued with conducting epoxy to the contact pads, and the electrodes on the bottom part are accessed by semiconductor measurement probes.

### 3.3.2 Prototype evaluation

Detailed information about the prototype characterization is provided in papers 3 and 4. Table 14 summarizes the most important results and the following paragraphs comment on some of them, especially on the insertion loss and on the contact force, which were both found not to be as good as expected.

The actuation voltages to open and close the switch are well below 20 V, which is remarkable for first prototype devices.

The measured insertion loss of the prototypes is far higher than expected and completely unsatisfactory for a micromechanical switch. The insertion loss cannot be

**Table 14.** Summary of the most important results of the prototype evaluation.

| Investigated parameter | Measurement value | Comments |
|---|---|---|
| actuation voltage (open) | 12.0 V | |
| actuation voltage (close) | 15.8 V | |
| clamping voltage | 19.2 V | to fully tie down the clamping electrodes |
| total DC resistance | 650 mΩ | including a 3.3 mm long signal line |
| contact resistance | 275 Ω | per contact |
| contact force | 102 $\mu$N | per contact, simulated with ANSYS at an actuation voltage of 15 V |
| RF isolation | 45 dB (<2 GHz), 30 dB (15 GHz) | contact distance of 14.2 $\mu$m, overlapping contact area of 3500 $\mu$m$^2$ per contact |
| series capacitance | 4.2 fF | simulated with FEMLAB |
| insertion loss | 2.5 dB at 10 GHz | see comments in the text |

explained by the reflections, which are not so high and the waveguide is relatively well matched (47.4 Ω measured, 50 Ω design target). Radiation losses can also be excluded due to the small electrical dimensions of the device, especially for frequencies in the lower GHz range. Therefore, the measured too high insertion loss is assumed mainly to be caused by the following:

- The calibration was not carried out with an on-wafer calibration set, but with a calibration kit on a low-loss ceramic substrate.
- The coplanar waveguide itself has quite a high loss. This can be concluded from the measurement data of the waveguide without switch, included in Figure 33(b). The simulated insertion loss of the waveguide is also shown in the figure, and there is quite a large discrepancy between the simulated and the measured data, as in the case of the waveguide with the switch. The substrate resistivity is 1500 Ω·cm and probably too low for the waveguide which is separated from the substrate only by a 800 nm thick silicon dioxide layer.

However, even considering the high losses of the waveguide, the measurements show a remaining insertion loss of about 1.5 dB. The reason for this is not fully understood since the measured total DC resistance only creates an estimated insertion loss of about 0.06 dB (calculated value for a 50 Ω system).

The contact force was estimated by simulations with ANSYS to be 102 $\mu$N per contact. This value is relatively low and corresponds to about the minimum value necessary for a stable contact resistance in the sub-Ω range, as described in the literature (see Section 2.2.3). The measured contact resistance of 275 mΩ per contact is comparable to the values reported in the literature for the simulated contact force, which confirms the simulation model. Compared to the size of the actuator, however, the contact force is relatively low. The total size of the overlapping area of the bottom and membrane electrodes is about 150 000 $\mu$m$^2$, which potentially could create an over 300 times larger force of about 30 $\mu$N. Since the membrane is very flexible, which is

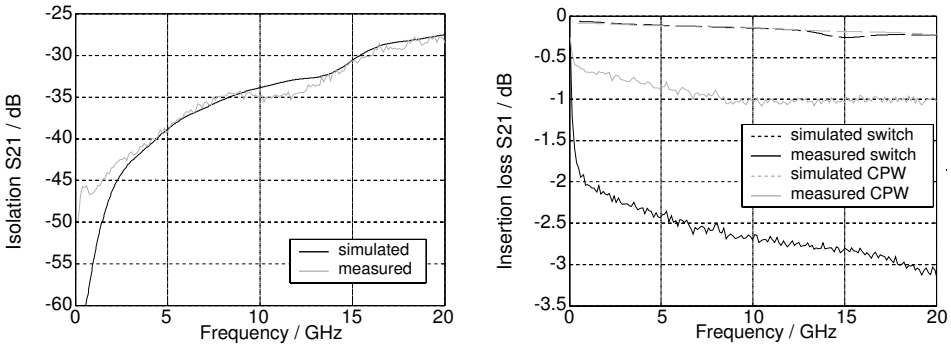


(a) (b)

**Figure 33.** RF measurements of one of the prototype switches: (a) isolation; (b) insertion loss.

a design criterion, most of the force is lost due to touching electrodes. The contact force could be increased by

- A stiffer membrane around the contacts, which can be achieved by using a different material for that part of the membrane or by depositing a thicker membrane layer around the contacts. Both methods increase the fabrication complexity.

- Closer positioning of the actuation electrodes to the contacts, which can be achieved by changing the overall RF design with a shorter distance between the ground lines and the signal line (the current design has a relatively large gap of 50 $\mu$m).

- Thicker metal contacts on the membrane: creates a larger effective area of the electrostatic actuator since the touching point between the membrane electrodes and the bottom electrodes is moved farther away from the contacts.

- An isolation layer with a larger dielectric constant basically also increases the contact force. However, the isolation layer only affects the contact force if its thickness is a substantial part of the total distance between the actuation electrodes and only the electrode area not touching the isolation layer contributes to the contact force. Also, the current design uses silicon nitride with a relative dielectric constant of approximately 7.5; materials with larger permeability are more difficult to process and have an increased susceptibility to electrostatic stiction (see Section 2.2.4).

The reliability of the switch has so far not been investigated extensively. Also the process parameters, in particular those of the silicon nitride deposition, should be optimized before investigating and publishing on the reliability of the concept, and the switches should be evaluated in an inert atmosphere to be able to compare the results to other MEMS switches. However, the author made some observations during

the evaluation of the prototype switches, which was carried out in air at atmospheric pressure and room temperature:

- Electrostatic stiction could not be observed. This can be explained by the relatively low actuation voltages (see Section 2.2.4) and the active opening capability of the switch. However, the actuator was not kept actively in one state for longer periods of time (hours or days) to investigate this phenomenon.
- The membrane is mechanically extremely strong. All 34 membranes on all of the processed wafers could be released successfully and the membranes can be pushed with probe tips without being damaged. During the individual assembly of the two parts of the switch, some membranes were destroyed when the tip of the out-of-plane bending membrane latched behind the thick BCB structures of the bottom wafer (thus, if the pre-alignment is done incautiously).
- The clamping electrodes were found not to be necessary since the membrane curls sufficiently out-of-plane and touches the bottom electrodes already after the assembly of the switch and each time after releasing the actuation voltage between the membrane and the top electrodes. Also, stiction between these electrodes was not found to be a problem during the prototype evaluation. However, depending on the design it might make sense to include clamping electrodes for reliability reasons (see Section 3.1).
- The membrane bilayer consisting of silicon nitride and a thin gold layer withstands thermal induced stress when exposed to temperatures of up to 280 °C needed for the proposed assembly process by full-wafer bonding.
- Once the switch is assembled it is mechanically very robust and shock-resistant.
- Irreversible breakdown occurs at about 90 to 100 V between the membrane and the bottom electrodes.
- The main reliability problem of the prototypes is the metal contacts. It was observed that either ohmic contact could not be established when closing the switch or the contacts got stuck easily. The reason for the former failure mechanism is most probably a combination of the relatively low contact forces and of surface contaminants, since the prototype switches were not assembled in clean-room environment and since the contacts can not be cleaned after releasing the membrane. The stiction problems are assumed to be caused by the soft electroplated gold and by the very large contact areas.

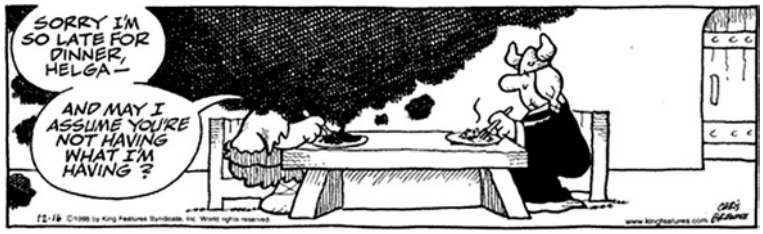

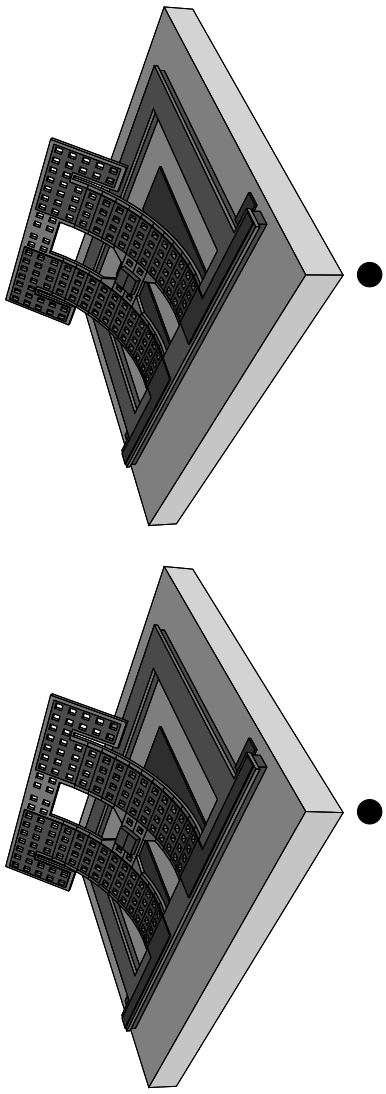

Stereo images of the top part (this page) and the bottom part (next page) of the switch.

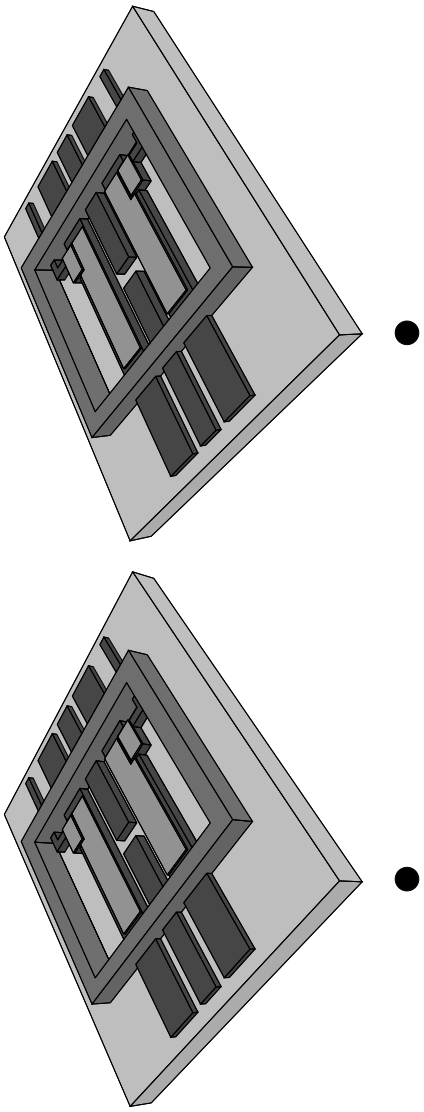

To view the stereo images, rotate the book so that the two black filled circles are on a horizontal line about 30 cm in front of you. Relax your eye muscles bringing your eyes in parallel view, until the two circles are on top of each other. If a crossed-eye view is more convenient, do not hesitate to cut out the drawings and put them beside each other in the opposite way.

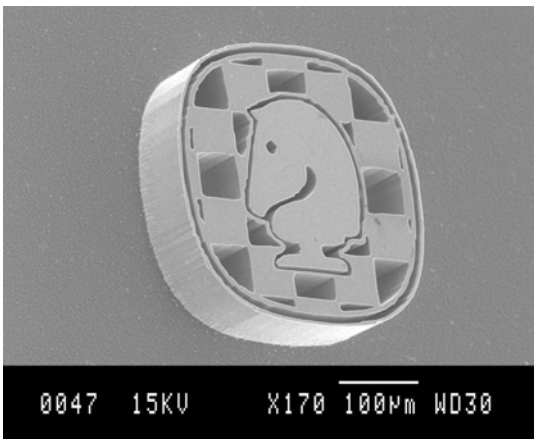


*Chess teaches the humility of defeat.*

*Source Unknown*

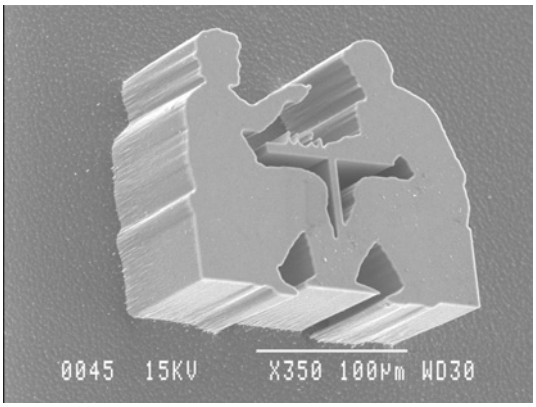


*Chess is ruthless: you've got to be prepared to kill people.*

*Nigel Short*
*1965– , British Chess Grand Master*

*A pile of rocks ceases to be a rock when somebody contemplates it with the idea of a cathedral in mind.*

*Antoine de Saint-Exupéry*
*1900–1944, French Aviator, Writer,*
*in "Flight to Arras"*

# 4 Packaging by patterned adhesive full-wafer bonding

## 4.1 Patterned adhesive full-wafer bonding

Some polymers used for adhesive bonding can be patterned before the bonding process, as mentioned in Section 2.3.3. Thus, the structures in the polymer create cavities directly in the bonding layer, which can be used to house MEMS devices or as channels or chambers in microfluidic applications.

The requirements for a polymer suitable for patterned adhesive bonding are the following:

- The polymer must be suitable for adhesive wafer bonding (low or no outgasing avoiding delamination in the bonding layer, sufficient physical strength in shear and tension, low viscosity).
- The polymer has to be suitable for patterning either by etching techniques, through photosensitive components of the polymer chain or by local deposition processes such as screen or contact printing.
- The patterning of the polymer should not require a fully cross-linked polymer, i.e. the polymer should still be adhesive enough after the patterning procedure to result in a strong bond.

In the work presented in this thesis, divinylsiloxane bisbenzocyclobutene (BCB) from the Dow Chemical Company is used. BCB is an epoxy-based thermo-set polymer which has been used in electronics production for dielectric layers, as underfill material, for stress-distribution layers and for opto-electronic applications since about 1993 [268–277]. The material has a low dielectric permittivity which makes it very suitable for RF applications and for high clock-rate digital circuits [278]. Some of the characteristic properties of BCB are listed in Table 15. It is available in a version which can be patterned by dry-etching [279, 280] and in a negative photosensitive version [281]. Both types are suitable for bonding, since the polymer fulfills the requirements listed above. Outgasing during the curing process is not detectable since its polymerization does not involve catalysts [229]. It can be spin-coated in a single layer with a thickness up to 40 $\mu$m and multi-layer coating is also possible.

BCB was used as an adhesive material for full-wafer bonding to fabricate flow channels [282] and to transfer structures or films from one wafer to another [200]. In these applications the material was unpatterned and uncured before the bonding procedure. The fabrication of three-dimensional structures by bonding with photosensitive BCB was investigated by another research group [230] almost in parallel to

**Table 15.** Characteristic properties of the polymer benzocyclobutene.

| Property | Unit | Value |
|---|---|---|
| hard curing temperature | °C | 250–300 |
| soft curing temperature | °C | 190–210 |
| glass transition temperature | °C | >350 |
| polymerization level, precursor | – | 40% (dry etch), 50% (photosensitive) |
| Young's modulus | GPa | 2.0 ± 0.2 |
| tensile strength | MPa | 85 ± 9 |
| coefficient of thermal expansion | ppm $K^{-1}$ | 52 (20 °C), 36–61 (-50..175 °C) |
| elongation | – | 6 ± 2.5 % |
| density | kg·$dm^{-3}$ | 1.05 |
| moisture uptake (weight) | | <0.12% (81% r.h.) |
| shrinkage during curing | – | <5% |
| planarization degree[a] | – | >90% |
| relative permittivity | – | 2.65 (1–10 GHz) |
| power dissipation factor | – | 0.0008–0.002 (1 MHz–10 GHz) |
| breakdown voltage | kV·$cm^{-1}$ | 3000 |

[a]the degree of planarization is defined as $\left(1-\frac{t_s}{t}\right)\cdot 100\%$, where $t$ is the thickness of the structures to be covered, and $t_s$ is the resulting bump on the top surface of the polymer when spun onto the structures with a thickness of $2{\cdot}t$

the work reported in paper 1, and the bonding of patterned to unpatterned polyimide structures was published in [283].

The dry-etch BCB has to be cured before its patterning procedure in order to be chemically and physically resistant enough for the plasma etching. If fully cross-linked, the material is no longer "sticky" enough for the subsequent bonding. Thus, the BCB should be partly cross-linked in a so-called "soft-cure" process step to about 50% of

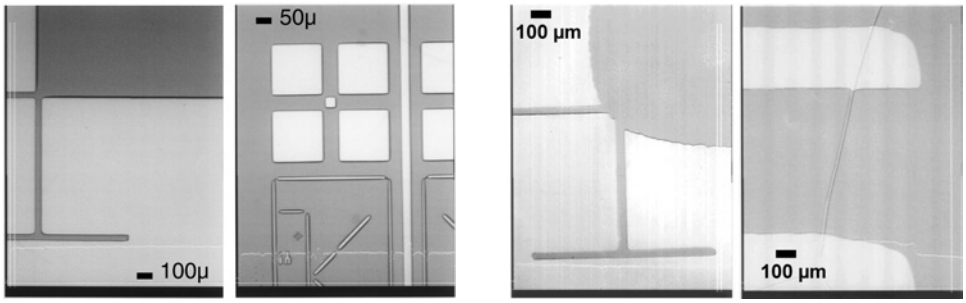


(a) (b)

**Figure 34.** Shape retention of bonded dry-etch BCB patterns depending on the soft-curing parameters: (a) well bonded pattern, soft-cured at 200 °C; (b) shape reflow due to an insufficient soft-curing temperature of 160 °C.

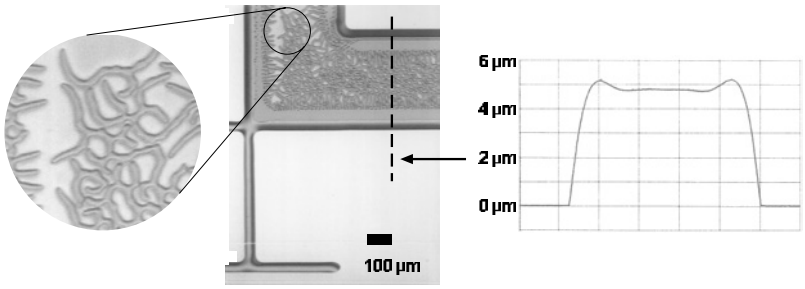


**Figure 35.** Incomplete bond due to surface non-uniformity of the patterned structures, soft-cured at 190 °C, bonded at a pressure of 2.5 bar.

polymerization, to ensure both sufficient consistancy and chemical resistance for the patterning processes and enough adhesion for the bonding. Paper 1 investigates the optimal processing parameters for the soft-curing and the bonding of dry-etch and photosensitive BCB. For dry-etch BCB, the most suitable soft-curing temperature range was found to be 190–210 °C for 40 minutes. The optimal bonding pressure depends on the mask pattern. However, a pressure of 2.0–2.5 bar on a 4 inch chuck was found to be a suitable start value for masks with a remaining BCB area of 40–70%. The BCB is fully cross-linked during the bonding when the bond chucks are heated above 250 °C for about 1 hour. The bonding temperature can be raised to decrease the bonding time, but BCB becomes thermally unstable above 300 °C and the bond strength decreases drastically [277]. Figure 34(a) shows a well bonded BCB pattern and Figure 34(b) illustrates the effect of insufficient soft-curing of the dry-etch BCB before the bonding procedure. The same mask was used in both experiments and the BCB thickness was about 5 $\mu$m. The bonding pressure was in both cases 2.5 bar applied for 1 hour at a temperature of 250 °C.

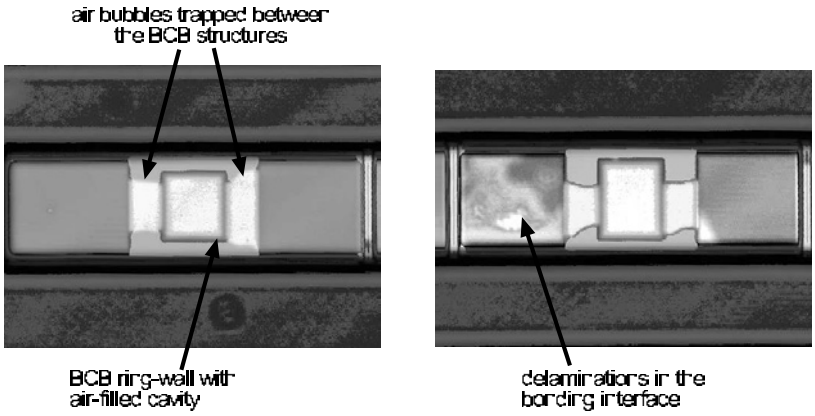


**Figure 36.** Scanning acoustic microscope (SAM) pictures of (a) a homogeneous bond and (b) delamination in the bond interface, using a transducer with a frequency of 50 MHz.

Since the BCB is relatively rigid after the soft-curing, the bond quality depends strongly on the surface uniformity of the BCB pattern. For a BCB thickness of about 5 $\mu$m the material is no longer soft enough to compensate for non-uniformities of about 0.1–0.2 $\mu$m, as shown in Figure 35.

Delamination in the bonding interface can be detected visually by looking through a microscope when using a transparent top wafer, as shown in Figures 34 and 35, or by scanning acoustic microscopy (SAM), as illustrated in Figure 36.

## 4.2 Glass lid encapsulation by patterned adhesive wafer bonding

The conventional wafer-level encapsulation procedure by transferring individual sealing caps to the substrate wafer using flip-chip-like pick-and-place techniques is illustrated in Figure 37. Solder-bonding of thin silicon microcaps was investigated for this purpose [284] and B-stage epoxy was used as bonding material in [234]. As suggested in the previos section, patterned BCB is a very interesting material to encapsulate cavities in this way. Photo-sensitive BCB rings on the target wafer were found to be suitable for individual glass lid packaging [255].

Paper 5 introduces a further parallelization of this wafer-level packaging technique, where the encapsulation procedure is done by full-wafer process steps (so-called wafer-scale packaging): a covering glass wafer is bonded to the substrate wafer containing the BCB patterns, and the glass caps are separated after the bonding by dicing only the top glass wafer, as illustrated in Figure 38. The dicing of the top wafer without harming the bottom substrate allows access to electrical contact pads on the bottom substrate. This was not possible in a reported packaging procedure using AuSn eutectic bonding, where the capping wafer and the substrate wafer were diced together [285]. The selective dicing is possible if the BCB pattern is taller than the vertical accuracy of the die saw, which might not be the case for many practical applications. Therefore, paper 5 also presents a technique to solve this problem. The outlines of the final glass lids are sliced in the front-side of the glass wafer before the bonding, which allows a larger vertical accuracy of the dicing process after the bonding, as shown in the fabrication sketch in Figure 39.

It is also possible to separate the encapsulation lids by etching the top wafer

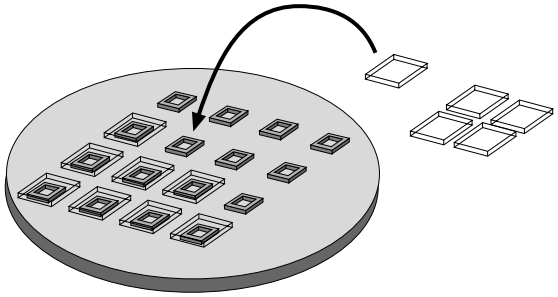

**Figure 37.** Glass lid encapsulation on wafer-level by pick-and-place bonding of individual caps.

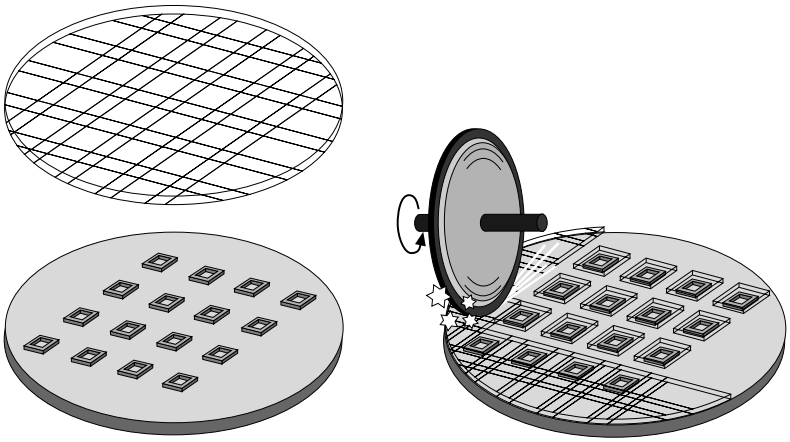

(a) (b)

**Figure 38.** Glass lid encapsulation by (a) full-wafer bonding with a patterned adhesive layer, and (b) dicing of the glass caps after the bonding procedure.

instead of dicing it. This technique, creating sealing caps from a full wafer by etching trenches in the top wafer after the adhesive bonding procedure, was proposed recently to package surface acoustic wave (SAW) filters [286]. The choice of the right method depends on the application and on the substrate material. However, the dicing method proposed in papers 5 and 6 has the following advantages:

- very low cost, since done outside clean-room facilities with a very simple machine, especially compared to a through-wafer plasma etch process
- mask-less process
- very simple and robust

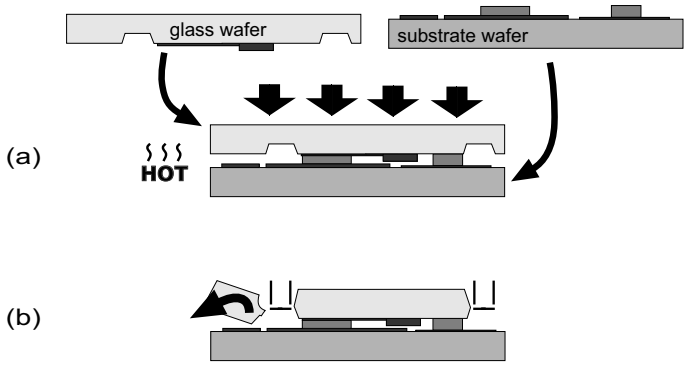


**Figure 39.** Illustration of the glass lid encapsulation process with pre-dicing of the front-side of the glass wafer, as described in the text. As shown in the drawing, the top glass wafer may also contain microsystem structures.

- no substrate material restrictions
- no special requirements on etch-stop layers

The main disadvantage of the dicing technique compared to the etching technique is that the dicing pattern is restricted to complete lines over the full wafer.

Figure 40(a) shows an array of glass lids created by this technique after dicing the top glass wafer only, and Figure 40(b) is a photograph of a single encapsulated chip.

## 4.3 Vertical and in-plane interconnections

Through-wafer vias are often needed in packaging, when electrical components on the front-side of a chip have to be accessed from the back-side. Such vias are fabricated by etching holes through the substrate and filling them or by coating their sidewalls with an electrically conducting material.

The etching techniques for such vias in glass wafers presented so far are deep reactive ion etching (DRIE), adapted for pyrex glass [287], and electrochemical discharge drilling [288]. Almost in parallel to the work presented in this thesis, researchers at the Korea Institute of Science and Technology, in cooperation with the Samsung Advanced Institute of Technology (SAIT), published on sandblasted holes in pyrex glass wafers for through-wafer vias filled by gold, electroplated onto a Cr/Au seed layer on the sidewalls of the vias [234].

Paper 5 introduces a new technique to create through-wafer vias in glass substrates. The technique consists of two etch steps, where the first one is carried out from the backside "almost-through" the wafer and the second etch step finally completes the holes. Powder-blasting [289] is used as the first etch step, and the second etch step consists of a short wet etch in concentrated hydrofluoric acid (HF) to further etch the recesses down to the contact pads, as illustrated in Figure 41.

Splitting up the whole etch process into two steps has the following advantages:

- The main etch step from the back-side (here accomplished by powder-blasting) is carried out before any other process step on the glass wafer and can therefore be done outside clean-room facilities, lowering the fabrication costs.

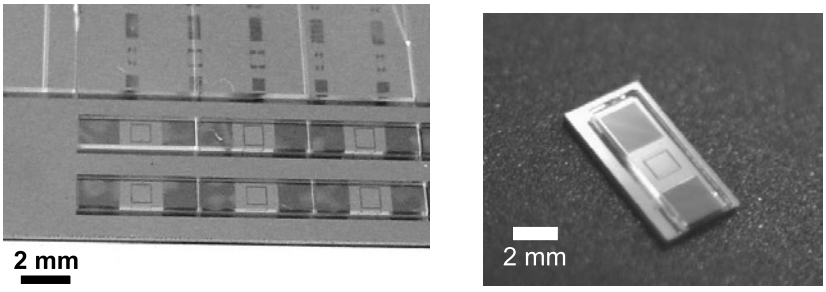


(a) (b)

**Figure 40.** Photographs of glass lids created by patterned adhesive full-wafer bonding, (a) after dicing the top wafer and (b) a single chip after also dicing the substrate wafer.

- Powder-blasting is a rather inexpensive process for relatively controlled deep etching in glass.
- The surface of the front-side is completely intact after etching the deep recesses by the first etching step; thus surface micromachining is basically unrestricted on the front-side.
- The metal contact pads to be accessed from the back-side act also as an etch-stop layer for the HF etch-step.
- Both etch processes are applicable on different types of glass wafers, even though Pyrex 7740 and Hoya SD-2 glass are the preferred substrates due to their high and uniform etch-rates in HF.
- The final wet-etch step is carried out after the bonding; thus, the structures on the front-side of the glass wafer are protected from the etching chemical.

Whenever adhesive bonding is used for the bonding, the polymer might not provide sufficient resistance against the chemical etch. In this case, the bond interface should not be exposed to the etch solution, which can be achieved by using a wafer holder with single side protection.

The two-step etch technique can basically also be applied on other substrates than glass using a different physical, chemical or plasma-etch combination. The main disadvantage of powder-blasting is the large feature size. It is difficult to achieve a height to width aspect ratio of over 2:1 and the sidewall slope is typically about

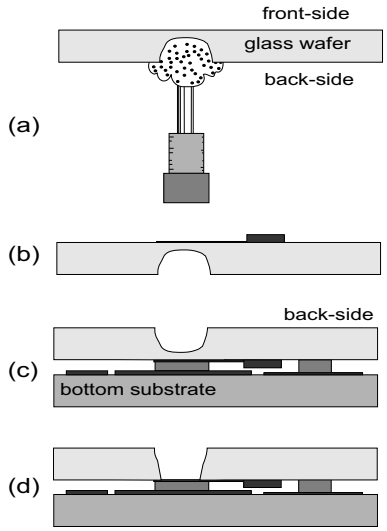


**Figure 41.** Overview of the fabrication procedure of through-wafer electrical interconnections in glass wafers, used as a packaging method together with patterned adhesive bonding: (a) powder-blasting of deep recesses in the back-side of the glass wafer; (b) surface-micromachining of structures and contact pads on the front side; (c) bonding; (d) short wet etch to complete the vias.

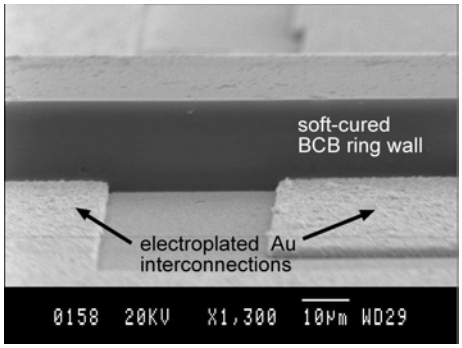


**Figure 42.** In-plane electrical interconnections of electroplated gold with a thickness of 2 $\mu$m penetrating through a 18.2 $\mu$m thick BCB wall.

70° [289–291]. Thus, the minimum hole dimensions to etch about 90% deep into the wafer have to be of the order of the thickness of the wafer. Besides accessing the contact pads by wire bonding, as described in paper 5, the slope of the sidewalls offers the possibility to deposit a metal on the walls to electrically connect the contact pad to the back-side of the wafer (such a technique is used for the packaging of the OMRON switch [158]).

In-plane interconnections penetrating through the BCB wall can be made because of the excellent planarization properties of BCB [271], providing a sufficiently flat surface for the adhesive bonding. Even thick interconnection lines of 2 $\mu$m are very smoothly covered by a BCB film of a thickness of 18.2 $\mu$m, as illustrated in Figure 42.

## 4.4 Bond strength improvement by bonding with a solid/liquid BCB pattern

The bond strength of a patterned BCB layer is lower than the bond strength of an unpatterned layer since the polymer has to be cross-linked to a certain degree before the bonding in order to be sufficiently chemically and physically resistant for the patterning procedure. Also, the soft-cured BCB is less elastic than an uncured and basically liquid BCB layer, which decreases the bonding yield in case of surface non-uniformities, as discussed in Section 4.1.

Paper 6 presents a simple method which combines the advantages of a patterned adhesive layer with the advantages of a liquid polymer phase before the bonding. The pattern in the adhesive layer is "inked" by pressing the substrate containing the pattern (bottom wafer) toward an auxiliary wafer with a thin and still uncured polymer layer. After removing the auxiliary wafer, a thin film is locally transferred to the pattern of the bottom wafer, which is finally bonded to the second wafer (top wafer). The procedure to fabricate glass lid encapsulations with this special bonding technique is illustrated in Figure 43. The fabrication is very robust and the BCB pattern on the bottom wafer can even be fully cured before the transfer of the film, which makes the final bonding result independent of crucial soft-cure parameters. Also, the pattern can basically be made with any other material, and other adhesives

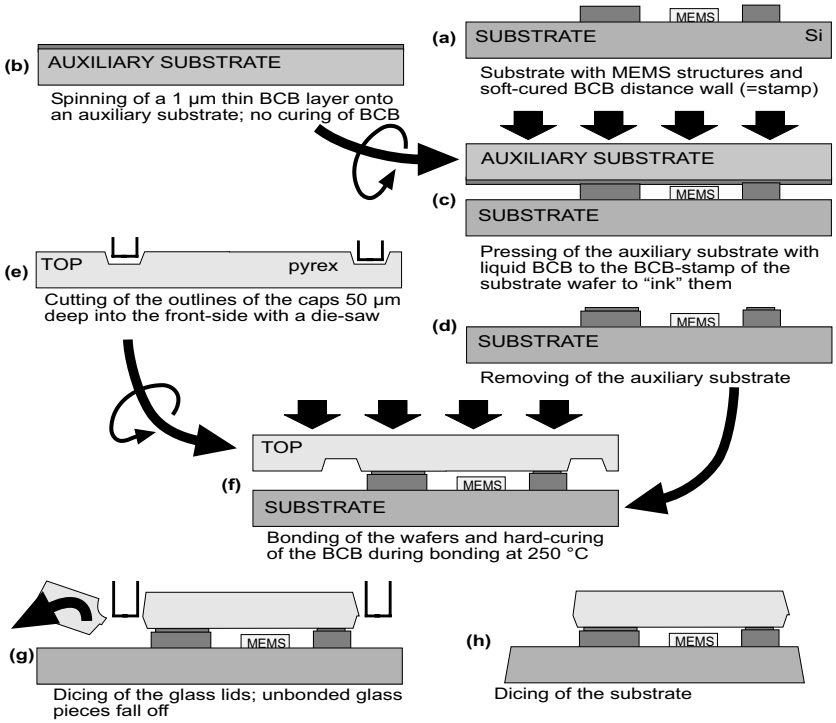


**Figure 43.** Fabrication steps to create glass lid encapsulations by full-wafer bonding, using the bonding technique with solid/liquid BCB pattern for improved bond strength.

than BCB might be used to ink the structures.

Using BCB, features with a size as small as 10 $\mu$m could successfully be inked and bonded. The bond strength improvement of this BCB contact printing technique compared to the conventional patterned BCB bonding, as described in Section 4.1, is illustrated in the diagram in Figure 44. The influence of adhesion promoter, the shape flow of the viscous BCB, the distortion of the negative imprint pattern in the BCB layer on the auxiliary wafer, and the failure mechanisms occurring during the tensile strength tests are discussed in detail in paper 6.

## 4.5 Hermeticity evaluation

The main disadvantage of polymers in packaging is that these organic materials are highly permeable to gases and moisture compared to ceramics and metals, as shown in Figure 45. Thus, adhesive bonding is in principle not suitable for hermetic packaging.

The hermeticity properties of BCB used in MEMS packaging were investigated in [255] and in papers 1 and 2 by helium leak tests following the procedure described in MIL-STD-833E, Method 1014.9 [292]. This method comprises a test procedure involving a gross and a fine leak test. For the gross leak test, the samples are put into a heated perfluorocarbon solution with low surface tension and a high boiling temperature of 140–200 °C, and defects in the sealing layer can be detected as gas

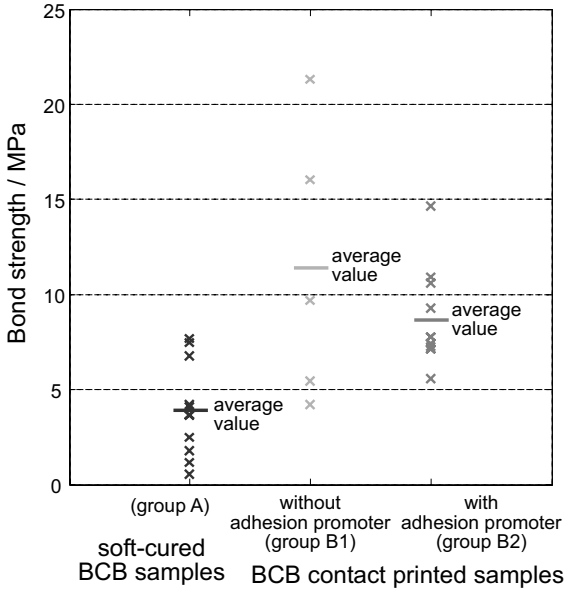


**Figure 44.** Tensile strength measurements of samples bonded with the BCB contact printing technique compared to the conventional soft-cured patterned BCB bonding technique.

bubbles coming out of the holes, since the gas trapped in the encapsulated cavity expands when heated by the solution. Small holes causing a leak rate of less than $10^{-4}$ mbar·l·s$^{-1}$ cannot be found with the gross leak test because the vapor pressure can not overcome the surface tension of the liquid. The fine leak test consists of device exposure to helium with a pressure of 5.2 bar for 2 hours. During that dwell time, helium penetrates into the sealed cavity and the leak rate can be measured directly after the exposure with a helium leak detector with a typical sensitivity as low as $10^{-11}$ mbar·l·s$^{-1}$ for an ALCATEL ASM 142 measurement device.

This test procedure was not found to be very suitable for encapsulated volumes below 1 mm$^3$ because the helium escapes too fast from a small cavity even for relatively small leaks. Only extremely small leaks can keep a stable helium flow for a few minutes after the exposure. Thus, the upper detection limit of the fine leak tests is lower for small cavities, and leaks of a certain size can neither be detected by the fine leak test nor by the gross leak test [255].

Therefore, relatively large samples were used for all of the tests presented in the papers 1 and 2, and the conclusions in paper 2 were drawn by comparing the measured leak rates rather than from the absolute measurement values. Furthermore, the influence of the time interval between the helium bombardment and each single measurement was investigated and considered, since the leak rate drops rapidly especially when measuring small devices. The specifications of the MIL standard only require the measurements to be taken within 60 minutes after the helium exposure. This inexact definition of the measurement step is only appropriate when the leak rate does not change rapidly over time, which is not the case for small test devices,

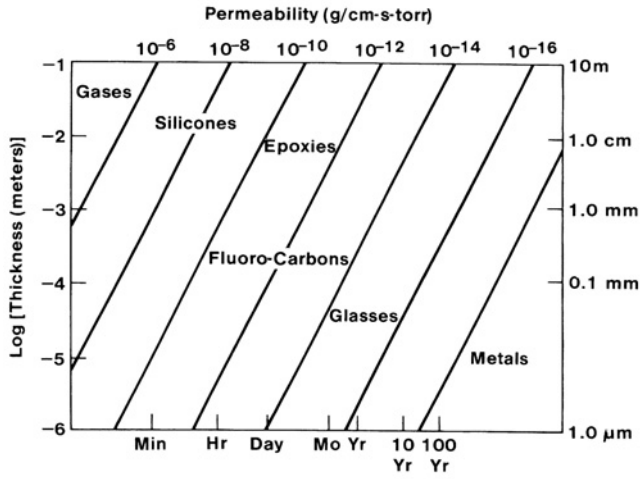


**Figure 45.** Effectiveness of sealant materials measured by the time for moisture to permeate various sealant materials in one defined geometry [190, Section 14.4.1].

where the leak rate changes drastically and is undetectable after only a few minutes.

As a conclusion, helium leak tests are still very informative about the hermeticity of a MEMS package since the measurement devices are very sensitive. However, the test limits defined in the MIL standard are not applicable and the measurement results have to be interpreted carefully.

## 4.6 Sealing by additional cladding layers

Paper 2 presents a mask-less hermetic encapsulation technique based on adhesive full-wafer bonding by cladding the adhesive with an additional diffusion barrier. Both PECVD silicon nitride and evaporated gold were investigated for that purpose. Silicon nitride is already widely used as a passivation and protective diffusion barrier in

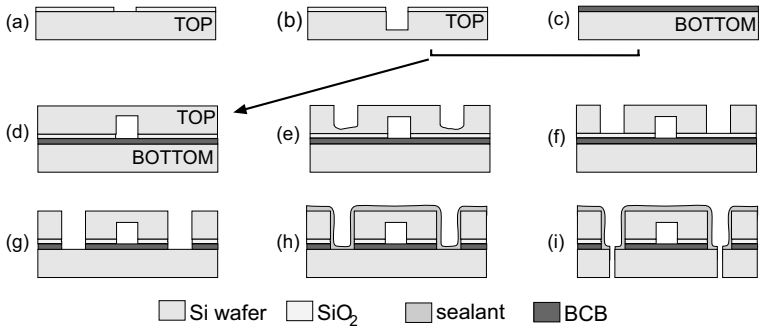


**Figure 46.** Fabrication procedure of the adhesive bonded test structures covered with the additional diffusion barrier.

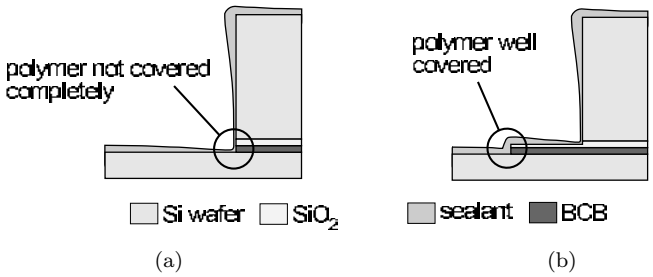


**Figure 47.** Step coverage of the polymer by the deposited diffusion barrier for (a) the fabrication technique as shown in Figure 46, and (b) the improved fabrication procedure as described in paper 2 and in the text.

IC processing to inhibit electro-oxidation (corrosion) and metal migration [293, 294], which are attributed to the presence of moisture in the package [190].

Figure 46 shows the basic idea of the test device fabrication with the sealing on wafer-level: A top wafer containing the etched cavities to be encapsulated (a)–(b) is bonded to a bottom wafer with a spin-coated, 5 $\mu$m thick layer of BCB (c)–(d). Then, grooves separating the samples are diced in the top wafer with a relatively thick saw blade (e). The grooves are etched further down to the bottom substrate by plasma-etching (f)–(g), and the devices are finally sealed by depositing the diffusion barrier (h). The devices are separated by a second dicing step with a thin saw blade (i).

This procedure is relatively simple but unfortunately did not work as intended. The deposited cladding material does not fully cover the concave corner directly underneath the 500 $\mu$m thick top wafer as illustrated in Figure 47(a). The sealing method was improved by creating a step in the base of the device consisting of the polymer

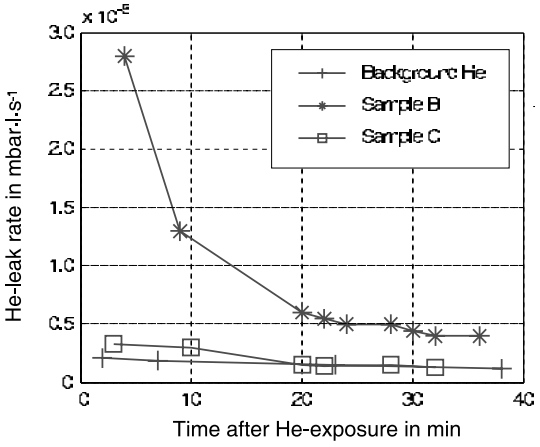


**Figure 48.** Helium leak rates over time for two samples fabricated with the straight-down etch technique (sample B) and with the improved cladding technique (sample C), compared to the background helium rate.

layer and covered by the silicon dioxide layer left from the hard mask which defined the cavity in the top wafer. This step is created by an additional plasma etch step widening the trenches by etching the sidewalls of the top wafer. The step in the basis of the device leads to full coverage of the unprotected polymer areas, as illustrated in Figure 47(b). The total fabrication procedure, slightly more complex than illustrated in Figure 46, is still mask-less since it does not involve any photolithography process, and is described in detail in paper 2.

Hermeticity tests carried out on samples using the straight-down etching technique and on samples using the modified fabrication procedure show definitively an improvement of the hermeticity of the sealed cavities, as illustrated in Figure 48.

***about some minor and major mistakes happening in the clean-room by doing the work for this thesis ...***

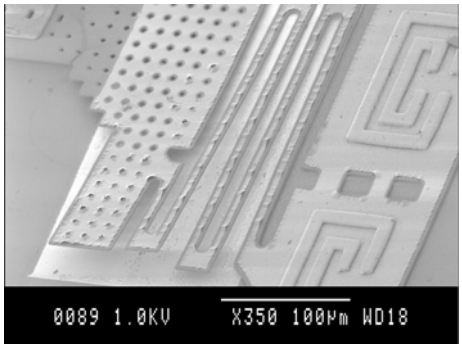


*Science must have originated in the feeling that something was wrong.*

*Thomas Carlyle*
*1795–1881, Scottish Philosopher*

*Sometimes the best gain is to lose.*

*George Herbert*
*1593–1632, British Metaphysical Poet*

*Nothing is more intolerable than to have to admit to yourself your own errors.*

*Ludwig van Beethoven*
*1770–1827, German Composer*

*There is a crack in everything, that's how the light gets in.*

*Leonard Cohen*
*1934– , Canadian Singer*


*Our greatest glory is not in never falling, but in rising every time we fall.*

*Confucius*
*BC 551–479, Chinese Ethical Teacher*

*Man needs difficulties; they are necessary for health.*

*Carl Gustav Jung*
*1875–1961, Swiss Psychiatrist*

*A clever man commits no minor blunders.*

*Johann Wolfgang von Goethe*
*1749–1832, German Poet*

*I hear — I forget. I see — I remember. I do — I understand.*

*Confucius*
*BC 551–479, Chinese Ethical Teacher*

*Success is not the key to happiness. Happiness is the key to success. If you love what you are doing, you will be successful.*

*Albert Schweitzer*
*1875–1965, Medical Missionary, Theologian*

# 5 Summary of appended papers

## Quick summary

**Paper 1** investigates the process parameters for adhesive bonding with patterned dry-etch BCB layers as well as photosensitive BCB layers.

**Paper 2** reports on a method of improving the hermeticity of adhesive bonded cavities by using an additional passivation layer as diffusion barrier.

**Paper 3** introduces the S-shaped film actuator based switch with characterization results of the first prototypes.

**Paper 4** discusses design details and fabrication aspects of the switch.

**Paper 5** shows a method to create glass lid packages by full-wafer bonding with a patterned BCB layer, including thick in-plane interconnections and vertical through-wafer vias in glass substrates by a novel two-step etch technique.

**Paper 6** reports on a method to significantly improve the bond strength of patterned adhesive bonded wafers by combining a pre-cured patterned BCB layer with an uncured contact printed BCB film.

**Paper 7** discusses the design and initial measurement results of a 2-bit meander slot antenna intended to be reconfigurable by the film actuator based switch.

## Detailed summary

**Paper 1:** *Selective Wafer-Level Adhesive Bonding with Benzocyclobutene for Fabrication of Cavities*

This paper describes an adhesive wafer-bonding technique in which the adhesive material is structured prior to bonding. This technique can be used to create encapsulated cavities of different heights and sizes directly in the bonding layer. Benzocyclobutene (BCB) was used as the adhesive bonding material. The structuring of the BCB was done either by dry etching or by using photosensitive BCB. The process parameters needed to achieve a high bond quality while retaining the shapes of the structures in the bonding layer were investigated. Furthermore, helium leak tests were performed to investigate the suitability of selective adhesive bonding for applications requiring quasi-hermetic seals.

**Keywords:** adhesive bonding, BCB, helium leak tests, selective bonding, wafer level packaging.

**Paper 2:** *Sealing of Adhesive Bonded Devices on Wafer Level*

This paper presents a low temperature wafer-level encapsulation technique to hermetically seal adhesive bonded microsystem structures by cladding the adhesive with an additional diffusion barrier. Two wafers containing cavities for MEMS devices were bonded using benzocyclobutene (BCB). The devices were sealed by a combined dicing and self-aligning etching technique and by finally coating the structures with evaporated gold or PECVD silicon nitride. The sealing layer was inspected visually by SEM and helium leak tests were carried out. For the larger test devices, the helium leak test method was found to be suitable for comparative measurements, and the passivation of the devices with silicon nitride showed an improvement of the package hermeticity.

**Keywords:** adhesive bonding, BCB, hermetic sealing, wafer level packaging.

**Paper 3:** *Low-Voltage High-Isolation DC-to-RF MEMS Switch Based on an S-shaped Film Actuator*

This paper describes a novel electrostatically actuated microelectromechanical series switch for switching DC to RF signals. The device is based on a flexible S-shaped film moving between a top and a bottom electrode in touch-mode actuation. This concept, in contrast to most other MEMS switches, allows a design with a low actuation voltage independent of the off-state contact distance. Larger nominal switching contact areas are possible while maintaining high isolation in the off-state. Prototype switches were successfully fabricated and evaluated.

**Keywords:** electrostatic actuator, film actuator, MEMS switches, microwave switches, RF MEMS.

**Paper 4:** *Design and Fabrication Aspects of an S-shaped Film Actuator Based DC to RF MEMS Switch*

This paper reports on design and fabrication aspects of a new microelectromechanical series switch for switching DC to RF signals. The switch consists of a flexible S-shaped film with the switching contact, rolling between a top and a bottom electrode in electrostatic touch-mode actuation. This concept enables a low actuation voltage design independent of the contact distance in the off-state. The RF transmission line and the MEMS part of the switch are fabricated on separate wafers, allowing implementation of the switch with different RF substrates. The final assembly is done on device level for the first prototypes, even though the design provides the possibility of an assembly by full wafer bonding leading to a "ready-to-dice", near-hermetic packaged switch.

**Keywords:** film actuator, MEMS switches, RF MEMS, touch-mode actuation.

**Paper 5:** *Low-Cost Glass-Lid Packaging by Adhesive Full-Wafer Bonding with Two-Step Etched Electrical Feedthroughs*

This paper reports on a low-cost fabrication technique to create glass lid encapsulations for 0-level near-hermetic packaging of microsystem devices using adhesive full-wafer bonding with a previously patterned polymer layer of benzocyclobutene (BCB). Furthermore, a new two-step technique to create low-density feedthroughs in glass substrates for electrical interconnections through the wafer is introduced. The vias are fabricated by combining a mechanical etch step by powder-blasting and a subsequent short hydrofluoric acid wet etch step. Both techniques were successfully combined to fabricate glass lid encapsulations by adhesive full-wafer bonding with thick electrical interconnections penetrating through the patterned adhesive layer, and with vertical vias through the glass wafer to electrically access structures on the glass lids.

**Keywords:** adhesive bonding, glass lid encapsulation, powder blasting, through-wafer vias, wafer-level packaging.

**Paper 6:** *BCB Contact Printing for Patterned Adhesive Full-Wafer Bonded 0-Level Packages*

An adhesive bonding method with benzocyclobutene is presented which combines the advantages of patterned adhesive bonding with the advantages of bonding with an uncured polymer layer. The pre-cured pattern in the adhesive layer is "inked" with uncured polymer by pressing the substrate toward an auxiliary wafer with a thin liquid polymer layer. The substrate with the inked pattern is finally bonded to a glass wafer to create glass lid packages by full-wafer bonding. The bond interface was investigated by scanning acoustic microscopy and the failure mechanisms occurring during pull-tests were investigated. Tensile strength tests revealed a significantly improved bond strength compared to soft-cured patterned BCB bonding.

**Keywords:** adhesive bonding, BCB, bond strength, contact printing, MEMS packaging, wafer-level packaging.

**Paper 7:** *A 2-bit Reconfigurable Meander Slot Antenna with High-displacement Low-voltage RF MEMS Switches (manuscript)*

This paper presents a novel meander slot antenna which is intended to be reconfigured by two RF MEMS switches of the S-shaped film actuator switch type. The active reconfiguration of the antenna allows four different operating frequencies with high frequency selectivity and good impedance matching. The upper part of the micromachined switch is intended to be placed directly on the antenna substrate by flip-chip-like mounting. The manuscript presents simulation and initial measurement results of the antenna without mounted switches and discusses the special implementation concept of the switches onto the antenna substrate.

**Keywords:** meander slot antenna, reconfigurable antenna, RF MEMS switch, switch integration.

## *about decisions ...*

*Decide promptly, but never give any reasons. Your decisions may be right, but your reasons are sure to be wrong.*

*Lord Mansfield*
*1867–1915, British Artist, Author*

*Our lives are a sum total of the choices we have made.*

*Wayne Dyer*
*1940– , American Psychotherapist*

*It is only in our decisions that we are important.*

*Jean-Paul Sartre*
*1905–1980, French Writer*

*A weak man has doubts before a decision, a strong man has them afterwards.*

*Karl Kraus*
*1874–1936, Austrian Satirist*

*We will either find a way, or make one.*

*Hannibal*
*BC 247–182, Carthaginian General*

*Indecision is the seedling of fear.*

*Napoleon Hill*
*1883–1970, American Speaker*

*The quality of decision is like the well-timed swoop of a falcon which enables it to strike and destroy its victim.*

*Sun Tzu*
*BC 400–430, Chinese Statesman, in "The Art of War"*

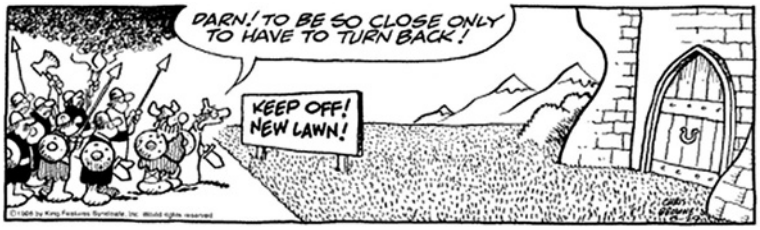

*Satisfaction lies in the effort, not in the attainment, full effort is full victory.*

*Mahatma Gandhi*
*1869–1948, Indian Political*

# 6 Conclusions

This thesis presents a novel RF MEMS switch based on an S-shaped film actuator. The switch consists of a thin silicon nitride membrane rolling between a top and a bottom electrode. This design provides the following main advantages:

- large contact distance for high signal isolation and large overlapping contact areas
- low actuation voltage independent of the contact distance
- active opening capability
- metal contacts for large bandwidth DC to RF signal switching
- electrostatic actuation for almost-zero power consumption
- minimum distortions of the RF signal with the film rolling longitudinal to the transmission line
- two-part assembly for integration with substrates and circuits incompatible with MEMS fabrication
- wafer-level assembly by individual flip-chip bonding or by full-wafer bonding, both providing a near-hermetic, ready-to-dice package

The thesis

- introduces and discusses the concept, comparing its advantages and disadvantages,
- provides information on the design and on the fabrication of the devices,
- presents the characterization results of the actuator, and
- reports on the measured and simulated RF performance of the fabricated prototypes.

The first devices of the switch were successfully fabricated and characterized, confirming the concept with most of the expected advantages, despite a few design-related problems of the prototypes. The S-shaped film actuator was found to be suitable for RF MEMS switching devices with demands on high signal isolation, low actuation voltage and almost-zero power consumption.

Furthermore, this thesis introduces novel ideas on packaging of (RF) MEMS devices by adhesive full-wafer bonding:

- The process parameters of patterned adhesive bonding were investigated, and this technique was successfully applied to create cavities for MEMS devices by full-wafer bonding.
- Hermeticity tests were carried out on such encapsulated cavities, and it was shown that the gas-tightness of the packages can be improved by additional passivation layers.
- Wafer-scale glass lid encapsulation by patterned adhesive full-wafer bonding with subsequent dicing of the glass wafer without harming structures on the substrate wafer was successfully demonstrated.
- The fabrication of electrical in-plane interconnections penetrating through the polymer sealing rings was investigated and a method to create vertical through-wafer interconnects in glass substrates, by using a novel two-step etch technique based on powder-blasting and wet-etching, was applied to the glass-lid encapsulation technique.
- The bond strength of patterned adhesive wafer bonding was substantially improved by a contact printing method, inking the pattern with a liquid polymer film, which combines the advantages of patterned adhesive bonding with the higher bond strength of uncured polymer bonding.
- The bond interfaces were qualitatively and quantitatively investigated by tensile strength measurements, visual inspection with optical microscopes, razor-blade tests, and scanning acoustic microscopy.

Patterned adhesive full-wafer bonding was found to be a simple, robust and highly parallel near-hermetic wafer-level packaging technique for MEMS devices.


HAGAR, WERE YOU ALWAYS SO SUSPICIOUS OF PEOPLE ?
NO, THERE WAS A TIME WHEN I TRUSTED EVERYONE I MET...
THEN I LEARNED HOW TO WALK AND TALK

## *some inspiration from a very nice place in the south ...*

*I really lack the words to compliment myself today.*

*Alberto Tomba*
*1966– , Italian Alpine Ski Star*

*Nebulat, ergo cogito.*

*Umberto Eco*
*1932– , Italian Semiologist, Novelist*

*When the danger is past God is cheated.*

*Italian Proverb of Unknown Origin*

*On the piazza, the sun is shining for everyone.*

*Italian Proverb of Unknown Origin*

*It may be you fear more to deliver judgment upon me than I fear judgment.*

*Giordano Bruno*
*1548–1600, Italian Scientist*

*Power tires those alone who don't have it.*

*Giulio Andreotti*
*1919– , Former Italian Prime Minister*

*He who knows little knows enough if he knows how to hold is tongue.*

*Italian Proverb of Unknown Origin*

*I'm a pessimist because of intelligence, but an optimist because of will.*

*Antonio Gramsci*
*1891–1937, Italian Political Theorist*

*Anyone who has obeyed nature by transmitting a piece of gossip experiences the explosive relief that accompanies the satisfying of a primary need.*

*Primo Levi*
*1919–1987, Italian Author*

*He who is not impatient is not in love.*

*Italian Proverb of Unknown Origin*

*Adversity reveals genius, prosperity conceals it.*

*Horace*
*BC 65–8, Italian Poet*

*See everything, overlook a great deal, correct a little.*

*Pope John XXIII*
*1881–1963, Italian Head of Roman Catholic Order*

*One does not kill oneself for love of a woman, but because love — any love — reveals us in our nakedness, our misery, our vulnerability, our nothingness.*

*Cesare Pavese*
*1908–1950, Italian Novelist*

*A little man often cast a long shadow.*

*Italian Proverb of Unknown Origin*

*Myth is nourished by silence as well as by words.*

*Italo Calvino*
*1923–1985, Italian Novelist*

*When men speak of the future, the Gods laugh.*

*Chinese Proverb*

# 7 Outlook

The presented RF MEMS switch is a quite complex device and I am glad that I was able to fabricate and to characterize the first prototypes. However, the device evaluation has revealed some problems and a second generation design should address the following topics, as discussed in Section 3.3.2:

- improved RF design of the coplanar waveguide
- larger contact force for lower contact resistance
- surface contamination and stiction problems of the metal contacts
- miniaturization of the total device size by reducing the lateral dimensions, while maintaining the large contact distance
- batch assembly by full-wafer bonding in clean-room environment
- access of the electrodes on the top part of the switch from the bottom wafer by integrated vertical interconnections

The reliability of the switch, encapsulated in an inert atmosphere, should be fully investigated, in connection to the processing parameters of the silicon nitride film and variations of the actuator size, the contact distance and the contact area. It would also be interesting to evaluate the RF benefits of a capacitive shunt version of the switch.

It is a pleasure for me to see that the work on MEMS switches based on this concept will continue in our microsystem group in two different application fields. Capacitive shunt switches from the first design are going to be used for reconfigurable antennas in a joint project at our department, as reported in the manuscript in the appendix. The other application uses the combination of high signal isolation and electrostatic actuation of the film actuator for switching telecommunication networks.

Patterned adhesive full-wafer bonding is a valuable packaging tool which is already used in commercial applications. The ideas presented in this thesis, especially the contact-printing method to improve the bond strength, are hopefully valuable for the future development in the field. The main problem of packages fabricated by adhesive bonding is the insufficient hermeticity of the polymer bonding materials. Sealing by additional passivation layers, as presented in this thesis, might be an option for certain applications, but adhesives with improved hermeticity, probably non-organic materials such as the already widely used but difficult to pattern glass-frit, are necessary for a wider use of adhesive bonding in near-hermetic and hermetic packaging. The technology is already quite mature on a device and system level and seems just to be waiting for new impulses from the material science world. The MEMS engineer however is still challenged with design problems such as the vertical electrical interconnections between the adhesive bonded wafers, an issue which might attract increased attention of the research community in this field.

*So your work is to analyze this incomplete manuscript of life and to explore what happened to the manuscript here and there. It is not necessary for you to understand everything about your past. You should not torment yourself in trying to learn it. If you do not understand your past, you are not ignorant, you are merely innocent. You are here at a certain point in this present life. By understanding your present situation you can understand the future and the past. The manuscript of your life has been written by you.*

*Sri Swami Rama*
*1925–1996, Indian Sage*
*in "Path of Fire and Light: Vol. 2"*

*No duty is more urgent than that of returning thanks.*

*Saint Ambrose*
*339–397, Bishop of Milan*

# Acknowledgments

Finally, the acknowledgments. For those of you who thought this to be the first page to read: you are right in the sense that these are definitively the most important pages of the book!

The work presented in this thesis was carried out at the Microsystem Technology division of the Department of Signals, Sensors and Systems at the Royal Institute of Technology, Stockholm, Sweden. Partial financial support for this research was provided by the SUMMIT microRF competence center of Vinnova, the Swedish Agency for Innovation Systems, and by Vetenskapsrådet, the Swedish Research Council.

This work would not have been possible without the assistance and the help of many people I would like to express my sincere gratitude to.

First of all, I would like to thank my supervisor Prof. Göran Stemme for his guidance, for being so patient with the demanding and sometimes a bit egoistic temper from the south, for giving me much freedom in many decisions but bringing me back to the right track whenever I got stuck in less relevant questions.

I am also very grateful to my present colleagues and friends in the Microsystem Technology group: to Kjell for his skillful mechanics for measurement setups and other more or less scientific projects, to Ulla for helping with so many little problems which seem to be unsolvable for a foreigner, to Frank for introducing me to the clean-room and for funny observations and comments on new countries and their people, to Sjoerd for his uncountable hints and tips in microsystem fabrication and evaluation, for his encouraging enthusiasm and for the funny and friendly atmosphere following him step by step, to Björn for sharing so many thoughts, to Thomas for being so patient with all my Macintosh related computer problems (and there are only Macintosh related computer problems, per definition), to Jessica for helping me with all my English language-related doubts despite some of my often politically incorrect comments, to Wouter for his inspiring mind and his positive attitude, to Stefan for showing interest in continuing my work, to Hans for sharing all his knowledge and experience and for taking care of so many official documents and meetings in the SUMMIT project, to Niclas for always having an open ear for technical questions, to Calle for never letting me forget the coffee break and the Wednesday-"bulle", and, last but not least, to Aman, my Eritrean office-neighbor, for all the joyful moments and for making me lose so many senseless sport bets on Italian football.

Many thanks to my former colleagues, Helene, Niklas, Patrick, Patrik, Peter and Thorbjörn, for teaching me so many things on microsystems and on how to deal with the unavoidable problems in our research group. I am also very pleased and thankful for the enthusiasm and the very fruitful work Sebastian has carried out during his master thesis under my supervision.

Special thanks to Cecilia for giving me a hand whenever I was desperately lost in the clean-room and for answering all my questions on complicated machines which

explode when you press the wrong button ... without your help, Cecilia, the switch had never been possible!

Some parts of this work were carried out in cooperation with companies, research institutes and universities. I would like to acknowledge the efforts of Katarina Boustedt and Kåre Gustafsson, Ericsson AB, for managing our SUMMIT microRF subproject during the first years and for establishing many contacts, to Göran Palmskog and Björn Hygrell from the former optoelectronics department of Ericsson AB, for giving me access to their hermeticity measurement devices, to Leena Korhonen, Ericsson Mobile Communications AB, for her friendly assistance with the scanning acoustic microscope, to Anders Thorsén and Anna-Sara Hedman, Acreo AB, to Andreas Billström, Saab Ericsson Space, and to Jan Ulander and Sture Roos, Network Automation, for the fruitful cooperation in the SUMMIT project. Furthermore, I am very thankful to Mo Zhimin and Johan Liu, Division of Electronics Production, Chalmers University of Technology, Gothenburg, for carrying out the tensile strength tests on my BCB bonded samples. Many thanks to Björn Lindmark from the antenna group at our department, who explained me the behavior of the electromagnetic waves riding on my switch and assisted me with the complicated RF measurements. Thanks to all of you for your support!

Also, I would like to take the opportunity to express my gratitude to Boo Soon Kang and his Oriental Sushi team around the corner where we have been eating our lunch uncountable times, for defending the good and well-educated taste in this country, and to Arvo Pärt for expressing my feelings toward the long Scandinavian winter.

I am very grateful to all the people helping me with the housing problem in Stockholm, especially Dirk, Damaris, Eva and Wouter. Many many thanks to Bodil with Fredrik and Josefin, and to Hélène with Lilly for welcoming me in your homes. I am sure I will always remember the many funny moments together with you!

To all my friends in Stockholm I have been having a great time with, especially to Sebastian, Mónika, Matthieu, Buster, Kevin, Yves, Julia, and Lisa. I am very grateful to Alexander for being a close friend during all this time in Stockholm, and to Albert and Katja with Sara and Iaco, currently living somewhere on the other side of the equator, for your efforts to making me feel home in Sweden and for introducing me to many interesting leisure time activities in the amazingly beautiful Swedish nature.

It is not easy to live abroad for such a long time and I am very glad to be able to keep or to re-discover contact with so many people from former places I was living in or I was visiting: to Alex P. with Monika in Graz, Austria, Alex R. in Vienna, Austria, Hubert in Verona, Italy, Martin in Stuttgart, Germany, Reno with Caroline in Zurich, Switzerland, Erich in Sand, Italy, Philipp in Bozen, Italy, to Bernd, Washington, DC. To Ralf in Graz, Austria, for our unbelievable deep and unrestricted e-mail communication, to Thomas and Egmont especially for your administrative help in Graz, to Christa in Winterthur, Switzerland, for intensive conversations and for distracting me so nicely from my work on this book, and, finally, to Gerold in Sand, Italy, for our entertaining Thursday-evening almost-wireless two-dimensional distance Blitz-chess tournaments.

To my mother, my father, my sister, my brother and our lazy old cat: thank you very very much for being so patient during my long stays abroad, for your support and for the good thoughts you have been sending me throughout all these years I have been living so far away from home.

Stockholm, in the summer 2004, Joachim Oberhammer

## A Small Dictionary of Useful Research Phrases

| Research Phrase | Translation |
|---|---|
| It has long been known... | I didn't look up the original reference. |
| A definite trend is evident... | These data are practically meaningless. |
| Of great theoretical and practical importance... | Interesting to me. |
| While it has not been possible to provide definite answers to these questions... | An unsuccessful experiment, but I still hope to get it published. |
| Three of the samples were chosen for detailed study... | The results of the others didn't make any sense. |
| Typical results are shown... | The best results are shown. |
| These results will be shown in a subsequent report... | I might get around to this sometime if I'm pushed. |
| The most reliable results are those obtained by Jones... | He was my graduate assistant. |
| It is believed that... | I think. |
| It is generally believed that... | A couple of other people think so too. |
| It is clear that much additional work will be required before a complete understanding of the phenomenon occurs... | I don't understand it. |
| Correct within an order of magnitude... | Wrong. |
| It is hoped that this study will stimulate further investigation in this field... | This is a lousy paper, but so are all the others on this miserable topic. |
| Thanks are due to Joe Blotz for assistance with the experiment and to George Frink for valuable discussions... | Blotz did the work and Frink explained to me what it meant. |
| A careful analysis of obtainable data... | Three pages of notes were obliterated when I knocked over a glass of beer. |

***... and now please read this thesis again!***

*A civilization is built on what is required of men, not on that which is provided for them.*

*Antoine de Saint-Exupéry*
*1900–1944, French Aviator, Writer*

# References

[1] "An introduction to MEMS (micro-electromechanical systems)," Prime Faraday Technology Watch, available at http://www.primetechnologywatch.org.uk, Tech. Rep., Jan. 2002.

[2] Statement of Martin Reid, chairman, president and CEO of Ibis Technology, MA, USA, in "SOI: new products, lower prices, big promise", in *Semiconductor Manufacturing*, vol. 4, no. 12, pp. 18–30, Dec. 2003.

[3] P. Rai-Choudhury, *MEMS and MOEMS Technology and Applications*. Bellingham, WA, USA: SPIE–The International Society for Optical Engineering, Dec. 2000, vol. SPIE PRESS Monograph PM85.

[4] K. E. Petersen, Cepheid, Invited Talk at the Micro Structure Workshop MSW 2004, Ystad, Sweden, Mar. 30–31, 2004.

[5] ——, "Micromechanical membrane switches on silicon," *IBM Journal of Research and Development*, vol. 23, no. 4, pp. 376–385, July 1979.

[6] L. E. Larson, R. H. Hackett, and R. F. Lohr, "Microactuators for GaAs-based microwave integrated circuits," in *Proc. Transducers 1991*, San Franzisco, USA, June 24–27, 1991, pp. 743–746.

[7] J. Yao, "RF MEMS from a device perspective," *Journal of Micromechanics and Microengineering*, vol. 10, pp. R9–R38, 2000.

[8] C. T.-C. Nguyen, L. P. B. Katehi, and G. M. Rebeiz, "Micromachined devices for wireless communications," *Proceedings of the IEEE*, vol. 86, no. 8, pp. 1756–1768, Aug. 1998.

[9] L. Katehi, J. Harvey, and E. Brown, "MEMS and Si micromachined circuits for high-frequency applications," *IEEE Transactions on Microwave Theory and Techniques*, vol. 50, no. 3, pp. 858–866, Mar. 2002.

[10] H. A. C. Tilmans, "MEMS components for wireless communications (invited paper)," in *Proc. Eurosensors XVI*, Prague, Czech Republic, Sept. 15–18, 2002, pp. 1–34.

[11] H. A. C. Tilmans, W. De Raedt, and E. Beyne, "MEMS for wireless communications: 'from RF-MEMS components to RF-MEMS-SiP'," *Journal of Micromechanics and Microengineering*, vol. 13, no. 4, pp. S139–S163, July 2003.

[12] R. Richards and H. De Los Santos, "MEMS for RF/microwave wireless applications: the next wave," *Microwave Journal*, vol. 44, no. 3, pp. 20, 24, 28, 32, 34, 38, 41, March 2001.

[13] H. De Los Santos and R. Richards, "MEMS for RF/microwave wireless applications: the next wave — Part II," *Microwave Journal*, vol. 44, no. 7, pp. 142–144, 146, 148, 150, 152, July 2001.

[14] K. Grenier, L. Rabbia, A. Tackacs, P. Pons, T. Parra, P. Caudriller, O. Pascal, H. Aubert, J. Graffeuil, and R. Plana, "MEMS technology as a contender for the future wireless applications," in *Proc. IEEE Semiconductor Conference CAS 2001*, Sinaia, Romania, Oct. 9–13, 2001, pp. 101–110.

[15] C. T.-C. Nguyen and R. T. Howe, "An integrated CMOS micromechanical resonator high-Q oscillator," *IEEE Journal of Solid-State Circuits*, vol. 34, no. 4, pp. 440–455, Apr. 1999.

[16] C. T.-C. Nguyen, "Transceiver front-end architectures using vibrating micromechanical signal processors," in *Proc. of the IEEE Meeting on Silicon Monolithic Integrated Circuits in RF Systems 2001*, Ann Arbor, Mi, USA, Sept. 12–14, 2001, pp. 23–32.

[17] D. Galayko, A. Kaiser, L. Buchaillot, D. Collard, and C. Combi, "Microelectromechanical variable-bandwidth IF frequency filters with tunable electrostatical coupling spring," in *Proc. IEEE Micro Electro Mechanical Systems 2003*, Kyoto, Japan, Jan. 19–23, 2003, pp. 153–156.

[18] J. Wang, J. E. Butler, T. Feygelson, and C. T.-C. Nguyen, "1.51-GHz nanocrystalline diamond micromechanical disk resonator with material-mismatches isolating support," in *Proc. IEEE Micro Electro Mechanical Systems 2004*, Maastricht, The Netherlands, Jan. 25–29, 2004, pp. 641–644.

[19] S.-S. Li, Y.-W. Lin, Y. Xie, Z. Ren, and C. T.-C. Nguyen, "Micromechanical "hollow-disk" ring resonators," in *Proc. IEEE Micro Electro Mechanical Systems 2004*, Maastricht, The Netherlands, Jan. 25–29, 2004, pp. 821–824.

[20] B. Guillon, D. Cros, P. Pons, K. Grenier, T. Parra, J. Cazaux, J. Lalaurie, J. Graffeuil, and R. Plana, "Design and realization of high Q millimeter-wave structures through micromachining techniques," in *IEEE MTT-S Microwave Symposium Digest 1999*, vol. 4, Anaheim, CA, USA, June 13–19, 1999, pp. 1519–1522.

[21] C. Tavernier, R. Henderson, and J. Papapolymerou, "A reduced-size silicon micromachined high-Q resonator at 5.7 GHz," *IEEE Trans. on Microwave Theory and Techniques*, vol. 50, no. 10, pp. 2305–2314, Oct. 2002.

[22] L. Harle and L. Katehi, "A vertically integrated micromachined filter," *IEEE Trans. on Microwave Theory and Techniques*, vol. 50, no. 9, pp. 2063–2068, Sept. 2002.

[23] A. Dec and K. Suyama, "Micromachined electro-mechanically tunable capacitors and their applications to RF IC's," *IEEE Trans. on Microwave Theory and Techniques*, vol. 46, no. 12, pp. 2587–2596, Dec. 1998.

[24] H. Nieminen, V. Ermolov, K. Nybergh, S. Silanto, and T. Ryhänen, "Micro-electromechanical capacitors for RF applications," *Journal of Micromechanics and Microengineering*, vol. 12, no. 2, pp. 177–186, Mar. 2002.

[25] Z. Feng, W. Zhang, B. Su, K. Harsh, K. Gupta, V. Bright, and Y. Lee, "Design and modeling of rf mems tunable capacitors using electro-thermal actuators," in *IEEE MTT-S Microwave Symposium Digest 1999*, Anaheim, CA, USA, June 13–19, 1999, pp. 1507–1510.

[26] J.-B. Yoon and C.-C. Nguyen, "A high-q tunable micromechanical capacitor with movable dielectric for RF applications," in *Proc. IEEE Electron Devices Meeting 2000*, San Francisco, CA, USA, Dec. 10–13, 2000, pp. 489–492.

[27] J. J. Yao, S. T. Park, and J. DeNatale, "High tuning-ratio MEMS-based tunable capacitors for RF communications applications," in *Solid-State Sensor and Actuator Workshop*, Hilton Head, SC, USA, June 8–11, 1998, pp. 124–127.

[28] K. F. Harsh, B. Su, W. Zhang, V. M. Bright, and Y. C. Lee, "The realization and design considerations of a flip-chip integrated MEMS tunable capacitor," *Sensors and Actuators A: Physical*, vol. 80, no. 2, pp. 108–118, Mar. 2000.

[29] J. Wilson, R. Bashirullah, D. Nackashi, D. Winick, B. Duewer, and P. D. Franzon, "Design of rotating MEMS tunable capacitors for use at RF and microwave frequencies," in *Proc. SPIE Design Characterization, and Packaging for MEMS and Microelectronics II*, vol. 4593, Adelaide, Australia, Dec. 17–19, 2001, pp. 186–197.

[30] J. Zou, C. Liu, and J. E. Schutt-Ainé, "Development of a wide-tuning-range two-parallel-plate tunable capacitor for integrated wireless communication systems," *Int. Journal of RF and Microwave Computer-Aided Engineering*, vol. 11, no. 5, pp. 322–329, Aug. 2001.

[31] J. Park, Y. Yee, H. Nam, and J. Bu, "Micromachined RF MEMS tunable capacitors using piezoelectric actuators," in *Proc. IEEE MTT-S Int. Microwave Symposium Digest 2001*, vol. 3, Phoenix, AZ, USA, May 20–25, 2001, pp. 2111–2114.

[32] E. Hung and S. Senturia, "Tunable capacitors with programmable capacitance-voltage characteristic," in *Solid-State Sensor and Actuator Workshop 1998*, Hilton Head Island, SC, USA, June 8–11, 1998, pp. 292–295.

[33] H. D. Nguyen, D. Hah, P. R. Patterson, R. Chao, W. Piyawattanametha, E. K. Lau, and M. C. Wu, "Angular vertical comb-driven tunable capacitor with high-tuning capabilities," *IEEE Journal of Microelectromechanical Systems*, vol. 13, no. 3, pp. 406–413, June 2004.

[34] J.-B. Yoon, C.-H. Han, E. Yoon, and C.-K. Kim, "High-performance three-dimensional on-chip inductors fabricated by novel micromachining technology for RF MMIC," in *IEEE MTT-S Microwave Symposium Digest 1999*, Anaheim, Ca, USA, June 13–19, 1999, pp. 1523–1526.

[35] P. Albert, J. Costello, and L. Salomon, "MEMS in CMOS — 21st century RF and microwave applications," *RF Design*, vol. 23, no. 7, pp. 32–26, July 2000.

[36] P. Pieters, K. Vaesen, W. Diels, G. Carchon, S. Brebels, W. De Raedt, E. Beyne, and R. Mertens, "High-Q integrated spiral inductors for high performance wireless front-end systems," in *IEEE Radio and Wireless Conference RAWCON 2000*, Denver, CO, USA, Sept. 10–13, 2000, pp. 251–254.

[37] Y.-S. Choi, J.-B. Yoon, B.-I. Kim, and E. Yoon, "A high-performance MEMS transformer for silicon RF ICs," in *Proc. IEEE Micro Electro Mechanical Systems 2002*, Las Vegas, NV, USA, Jan. 20–24, 2002, pp. 653–656.

[38] H. Jiang, Y. Wang, J.-L. Yeh, and N. Tien, "On-chip spiral inductors suspended over deep copper-lined cavities," *IEEE Trans. on Microwave Theory and Techniques*, vol. 48, no. 12, pp. 2415–2423, Dec. 2000.

[39] H. De Los Santos, "On the ultimate limits of IC inductors — an RF MEMS perspective," in *Proc. IEEE Electronic Components and Technology Conference ECTC 2002*, San Diego, CA, USA, May 28–31, 2002, pp. 1027–1031.

[40] G. P. Gauthier, A. Courtay, and G. M. Rebeiz, "Microstrip antennas on synthesized low dielectric-constant substrates," *IEEE Transactions on Antennas and Propagation*, vol. 45, no. 8, pp. 1310–1314, Aug. 1997.

[41] J.-C. Chiao, Y. Fu, I. M. Chio, M. DeLisio, and L.-Y. Lin, "Mems reconfigurable vee antenna," in *IEEE MTT-S Microwave Symposium Digest 1999*, Anaheim, CA, USA, June 13–19, 1999, pp. 1515–1518.

[42] J. Digby, C. Collins, B. Towlson, L. Karatzas, G. Parkhurst, J. Chamberlain, J. Bowen, R. Pollard, R. Miles, D. Steenson, D. Brown, and N. Cronin, "Integrated micro-machined antenna for 200 GHz operation," in *IEEE MTT-S Microwave Symposium Digest 1997*, Denver, CO, USA, June 8–13, 1997, pp. 561–564.

[43] K. Herrick, T. Schwarz, and L. Katehi, "Si-micromachined coplanar waveguides for use in high-frequency circuits," *IEEE Trans. on Microwave Theory and Techniques*, vol. 46, no. 6, pp. 762–768, 1998.

[44] E.-C. Park, Y.-S. Choi, B.-I. Kim, J.-B. Yoon, and E. Yoon, "A low loss MEMS transmission line with shielded ground," in *Proc. IEEE Micro Electro Mechanical Systems 2003*, Kyoto, Japan, Jan. 19–23, 2003, pp. 136–139.

[45] Y. Yoshida, T. Nishino, J. Jiao, S.-S. Lee, Y. Suehiro, K. Miyaguchi, T. Fukami, M. Kimata, and O. Ishida, "A novel grounded coplanar waveguide with cavity structure," in *Proc. IEEE Micro Electro Mechanical Systems 2003*, Kyoto, Japan, Jan. 19–23, 2003, pp. 140–143.

[46] H.-T. Kim, S. Jung, J.-H. Park, C.-W. Baek, Y.-K. Kim, and Y. Kwon, "A new micromachined overlap CPW structure with low attenuation over wide impedance ranges," in *IEEE MTT-S Microwave Symposium Digest 2000*, Boston, MA, USA, June 11–16, 2000, pp. 299–302.

[47] B. Norvell, R. Hancock, J. Smith, M. Pugh, S. Theis, and J. Kriatkofsky, "Micro electro mechanical switch (MEMS) technology applied to electronically scanned arrays for space based radar," in *Proc. IEEE Aerospace Conference 1999*, Aspen, CO, USA, Mar. 6–13, 1999, pp. 239–247.

[48] G. M. Rebeiz, G.-L. Tan, and J. S. Hayden, "RF MEMS phase shifters: design and applications," *IEEE Microwave Magazine*, vol. 3, no. 2, pp. 72–81, June 2002.

[49] J. Teti and F. Darreff, "MEMS 2-bit phase-shifter failure mode and reliability considerations for large $X$-band arrays," *IEEE Trans. on Microwave Theory and Techniques*, vol. 52, no. 2, pp. 693–701, Feb. 2004.

[50] J. Y. Ko, Y. J. amd Park, H. T. Kim, and J. U. Bu, "Integrated five-bit RF MEMS phase shifter for satellite broadcasting/communication systems," in *Proc. IEEE Micro Electro Mechanical Systems 2003*, Kyoto, Japan, Jan. 19–23, 2003, pp. 144–148.

[51] H. Zhang, A. Laws, K. C. Gupta, Y. C. Lee, and V. M. Bright, "MEMS variable-capacitor phase shifters part I: Loaded-line phase shifter," *Int. Journal of RF and Microwave Computer-Aided Engineering*, vol. 13, no. 4, pp. 321–337, July 2003.

[52] N. Barker and G. Rebeiz, "Optimization of distributed MEMS transmission-line phase shifters-U-band and W-band designs," *IEEE Trans. on Microwave Theory and Techniques*, vol. 48, no. 11, pp. 1957–1966, Nov. 2000.

[53] E. R. Brown, "RF-MEMS switches for reconfigurable integrated circuits (invited paper)," *IEEE Trans. on Microwave Theory and Techniques*, vol. 46, no. 11, pp. 1868–1880, Nov. 1998.

[54] B. Cetiner, J. Qian, H. Chang, M. Bachman, G. Li, and F. De Flaviis, "Monolithic integration of RF MEMS switches with a diversity antenna on PCB substrate," *IEEE Trans. on Microwave Theory and Techniques*, vol. 51, no. 1, pp. 332–335, Jan. 2003.

[55] M. Ulm, J. Schobel, M. Reimann, T. Buck, J. Dechow, R. Muller-Fiedler, H.-P. Trah, and E. Kasper, "Millimeter-wave microelectromechanical (MEMS) switches for automotive surround sensing systems," in *Proc. IEEE Topical Meeting on Silicon Monolithic Integrated Circuits in RF Systems 2003*, Apr. 9–11, 2003, pp. 142–149.

[56] J.-C. Chiao, S.-Y. Cheng, J. J. L. Chang, I. M. Chio, Y. Kang, and J. Hayasaka, "MEMS reconfigurable antennas," *Int. Journal of RF and Microwave Computer-Aided Engineering*, vol. 11, no. 5, pp. 301–309, Sept. 2001.

[57] A. Dec and K. Suyama, "Microwave MEMS-based voltage-controlled oscillators," *IEEE Transactions on Microwave Theory and Techniques*, vol. 48, no. 11, pp. 1943–1949, 2000.

[58] E.-C. Park, Y.-S. Choi, J.-B. Yoon, S. Hong, and E. Yoon, "Fully integrated low phase-noise VCOs with on-chip MEMS inductors," *IEEE Transactions on Microwave Theory and Techniques*, vol. 51, no. 1, pp. 289–296, Jan. 2003.

[59] J. Papapolymerou, K. Lange, C. Goldsmith, A. Malczewski, and J. Kleber, "Reconfigurable double-stub tuners using MEMS switches for intelligent RF front-ends," *IEEE Trans. on Microwave Theory and Techniques*, vol. 51, no. 1, pp. 271–278, Jan. 2003.

[60] H.-T. Kim, S. Jung, K. Kang, J.-H. Park, Y.-K. Kim, and Y. Kwon, "Low-loss analog and digital micromachined impedance tuners at the Ka-band," *IEEE Trans. on Microwave Theory and Techniques*, vol. 49, no. 1, pp. 2394–2400, Dec. 2001.

[61] I. De Wolf and W. M. van Spengen, "Techniques to study the reliability of metal RF MEMS capacitive switches," *Microelectronics Reliability*, vol. 42, no. 9–11, pp. 1789–1794, Sept.-Nov. 2002.

[62] S. Melle, F. Flourens, D. Dubuc, K. Grenier, P. Pons, F. Pressecq, J. Kuchenbecker, U. Muraro, L. Bary, and R. Plana, "Reliability behavior of RF MEMS," in *Proc. IEEE Semiconductor Conference CAS 2003*, Sinaia, Romania, Sept. 28–Oct. 2, 2003, pp. 21–26.

[63] W. van Spengen, R. Puers, R. Mertens, and I. De Wolf, "Experimental characterization of stiction due to charging in RF MEMS," in *Proc. IEEE Int. Electron Devices Meeting IEDM 2002*, San Francisco, CA, USA, Dec. 8–11, 2002, pp. 901–904.

[64] J. DeNatale and R. Mihailovich, "RF MEMS reliability," in *Proc. Transducers 2003*, Boston, MA, USA, June 8–12, 2003, pp. 943–946.

[65] M. Cohn, R. Roehnelt, J.-H. Xu, A. Shteinberg, and S. Cheung, "MEMS packaging on a budget (fiscal and thermal)," in *Proc. IEEE Int. Conference on Electronics, Circuits and Systems 2002*, Dubrovnik, Croatia, Sept. 15–18, 2002, pp. 287–290.

[66] A. Jourdain, S. Brebels, W. De Raedt, and H. A. C. Tilmans, "Influence of 0-level packaging on the microwave performance of RF-MEMS devices," in *Proc. European Microwave Conference 2001*, London, UK, Sept. 24–28, 2001, pp. 403–406.

[67] A. Margomenos, D. Peroulis, J. Becker, and L. Katehi, "Silicon micromachined interconnects for on-wafer packaging of MEMS devices," in *Proc. IEEE Silicon Monolithic Integrated Circuits in RF Systems 2001*, Ann Arbor, MI, USA, Sept. 12–14, 2001, pp. 33–36.

[68] S. Cass, "Large jobs for little devices," *IEEE Spectrum*, vol. 38, no. 1, pp. 72–73, Jan. 2001.

[69] G. Fischer, W. Eckl, and G. Kaminski, "RF-MEMS and SiC/GaN as enabling technologies for a reconfigurable multi-band/multi-standard radio," *Bell Labs Technical Journal*, vol. 7, no. 3, pp. 169–189, Mar. 2003.

[70] G. M. Rebeiz and J. B. Muldavin, "RF MEMS switches and switch circuits," *IEEE Microwave Magazine*, vol. 2, no. 4, pp. 59–71, Dec. 2001.

[71] R. Weigel, D. Morgan, J. Owens, A. Ballato, K. Lakin, K. Hashimoto, and C. Ruppel, "Microwave acoustic materials, devices, and applications," *IEEE Transactions on Microwave Theory and Techniques*, vol. 50, no. 3, pp. 738–749, Mar. 2002.

[72] A. Aigner, "MEMS in RF filter applications: Thin-film bulk acoustic wave technology," *Sensors Update*, vol. 12, no. 1, pp. 175–210, Feb. 2003.

[73] K. Lakin, "Thin film resonators and filters," in *Proc. IEEE Ultrasonics Symposium 1999*, vol. 2, Caesars Tahoe, NV, USA, Oct. 17–20, 1999, pp. 895–906.

[74] C. K. Campbell, *Surface Acoustic Wave Devices for Mobile and Wireless Communications*. Boston: Academic Press, 1998.

[75] G. M. Rebeiz, *RF MEMS Theory, Design and Technology*, 1st ed. Hoboken, New Jersey: Wiley, 2003.

[76] S.-W. Paek, H.-I. Kang, K.-I. Jeon, M.-D. Jeong, D.-W. Kim, C.-R. Lim, J.-H. Lee, W.-S. Lee, J.-E. Oh, and K.-W. Chung, "1–26 GHz high power p-i-n diode switch," in *IEEE MTT-S Int. Microwave Symposium Digest 2000*, vol. 1, Boston, MA, USA, June 11–16, 2000, pp. 505–508.

[77] T. Shimura, Y. Mimino, K. Nakamura, Y. Aoki, and S. Kuroda, "High isolation V-band SPDT switch MMIC for high power use [HEMTs application]," in *IEEE MTT-S Int. Microwave Symposium Digest 2001*, vol. 1, Phoenix, AZ, USA, May 20–25, 2001, pp. 245–248.

[78] T. Shigematsu, N. Suematsu, N. Takeuchi, Y. Iyama, and A. Mizobuchi, "A 6-18 GHz 20 W SPDT switch using shunt discrete PIN diodes," in *IEEE MTT-S Int. Microwave Symposium Digest 1997*, vol. 2, Denver, CO, USA, June 8–13, 1997, pp. 527–530.

[79] *The PIN Diode Circuit Designers' Handbook*. Watertown, MA, USA: Microsemi Corp., 1998.

[80] K. Kobayashi, A. Oki, D. Umemoto, S. Claxton, and D. Streit, "Monolithic GaAs HBT p-i-n diode variable gain amplifiers, attenuators, and switches," *IEEE Trans. on Microwave Theory and Techniques*, vol. 41, no. 12, pp. 2295–2302, Dec. 1993.

[81] K. Miyatbuji and D. Ueda, "A gaas high power RF single-pole dual throw switch IC for digital-mobile communication system," *IEEE Journal of Solid-State Circuits*, vol. 30, no. 9, pp. 979–983, Sept. 1995.

[82] Y. Ota, M. Sakakura, K. Fujimoro, S. Yamamoto, and H. Fujimoto, "High isolation and low insertion loss switch IC using GaAs MESFET's," *IEEE Trans. on Microwave Theory and Techniques*, vol. 43, no. 9, Sept. 1995.

[83] Z. Gu, D. Johnson, S. Belletete, and D. Fryklund, "A high power DPDT MMIC switch for broadband wireless applications," in *IEEE MTT-S Int. Microwave Symposium Digest 2003*, vol. 1, Philadelphia, PA, USA, June 8–13, 2003, pp. A173–A176.

[84] T. Campbell, "MEMS switch technology approaches the "ideal switch"," *Applied Microwave & Wireless*, May 2001.

[85] datasheets to the OMRON G6 high-frequency relay series.

[86] G. Moore, "No exponential is forever: but "Forever" can be delayed!" in *Proc. IEEE Int. Solid-State Circuits Conference ISSCC 2003*, San Franzisco, CA, USA, Feb. 9–13, 2003.

[87] "International technology roadmap for semiconductors itrs 2003," available at http://public.itrs.net/, Tech. Rep., 2003.

[88] G. M. Rebeiz, "RF MEMS for commercial and defense applications (invited talk)," in *Third Canadian Workshop on MEMS*, Ottawa, Canada, Aug. 22, 2003.

[89] H. F. Schlaak, "Potentials and limits of micro-electromechanical systems for relays and switches," in *Proc. Int. Conf. on Electrical Contacts*, Zurich, Switzerland, Sept. 9–12, 2002, pp. 19–30.

[90] R. Wood, R. Mahadevan, V. Dhuler, B. Dudley, A. Cowen, E. Hill, and K. Markus, "MEMS microrelays," *Mechatronics*, vol. 8, no. 5, pp. 535–547, Aug. 1998.

[91] S. Shen, D. Becher, Z. Fan, D. Caruth, and M. Feng, "Development of broadband low actuation voltage RF MEM switches," *Active and Passive Electronic Components*, vol. 25, no. 1, pp. 97–111, 2002.

[92] X. Rottenberg, H. Jansen, P. Fiorini, W. De Raedt, and H. A. C. Tilmans, "Novel RF-MEMS capacitive switching structures," in *Proc. European Microwave Conference 2002*, Milan, Italy, Sept. 24–26, 2002, pp. 809–812.

[93] M. Ulm, M. Reimann, T. Walter, R. Müller-Fiedler, and E. Kasper, "Capacitive RF MEMS switches for the W-band," in *Proc. European Microwave Conference 2001*, London, UK, Sept. 25–27, 2001, pp. 287–290.

[94] J. J. Yao and M. F. Chang, "A surface micromachined miniature switch for telecommunications applications with signal frequencies from DC up to 4 GHz," in *Proc. Transducers 1995*, Stockholm, Sweden, June 25–29, 1995, pp. 384–387.

[95] H. F. Schlaak, F. Arndt, and M. Hanke, "Switching characteristics of silicon-microrelay with electrostatic actuator," in *Proc. 19th Int. Conf. on Electric Contact Phenomena*, Nuremberg, Germany, Sept. 14-17, 1998, pp. 59–64.

[96] P. M. Zavracky, S. Majumder, and N. E. McGruer, "Micromechanical switches fabricated using nickel surface micromachining," *IEEE Journal of Microelectromechanical Systems*, vol. 6, no. 1, pp. 3–9, Mar. 1997.

[97] I. Schiele, J. Huber, C. Evers, B. Hillerich, and F. Kozlowski, "Micromechanical relay with electrostatic actuation," in *Proc. Transducers 1997*, Chicago, June 16–19, 1997, pp. 1165–1168.

[98] D. Hyman, A. Schmitz, B. Warneke, T. Y. Hsu, Y. Lam, J. Brown, J. Schaffner, A. Walston, R. Y. Loo, G. L. Tangonan, M. Mehregany, and J. Lee, "Surface micromachined RF MEMS switches on GaAs substrates," *Int. Journal of RF and Microwave Computer-Aided Engineering*, vol. 9, no. 4, pp. 348–361, July 1999.

[99] A. De Silva, C. Vaughan, D. Frear, L. Liu, S. Kuo, J. Foerstner, J. Drye, J. Abrokwah, H. Hughes, C. Amrine, C. Butler, S. Markgraf, H. Denton, and S. Springer, "Motorola MEMS switch technology for high frequency applications," in *Proc. IEEE Microelectromechanical Systems Conference 2001*, Berkeley, CA, USA, August 24–26, 2001, pp. 22–24.

[100] J. Ruan, M.; Shen and C. Wheeler, "Latching micro magnetic relays with multistrip permalloy cantilevers," in *Proc. IEEE Micro Electro Mechanical Systems 2001*, Interlaken, Switzerland, Jan. 21–25, 2001, pp. 224–227.

[101] M.-A. Grétillat, P. Thiebaud, N. de Rooij, and C. Linder, "Electrostatic polysilicon microrelays integrated with MOSFETs," in *Proc. IEEE Micro Electro Mechanical Systems 1994*, Oiso, Japan, Jan. 25–28, 1994, pp. 97–101.

[102] Press release by Texas Instruments, Plano, TX, USA, Apr. 26, 2004.

[103] C. Goldsmith, T.-H. Lin, B. Powers, W.-R. Wu, and B. Norvell, "Micromechanical membrane switches for microwave applications," in *IEEE MTT-S Int. Microwave Symposium Digest 1995*, vol. 1, Orlando, FL, USA, May 16–20, 1995, pp. 91–94.

[104] R. E. Mihailovich, M. Kim, J. B. Hacker, E. A. Sovero, J. Studer, J. A. Higgins, and J. F. DeNatale, "MEM relay for reconfigurable RF circuits," *IEEE Microwave and Wireless Components Letters*, vol. 11, no. 2, pp. 53–55, Feb. 2001.

[105] S. Duffy, C. Bozler, S. Rabe, J. Knecht, L. Travis, P. Wyatt, C. Keast, and M. Gouker, "MEMS microswitches for reconfigurable microwave circuitry," *IEEE Microwave and Wireless Components Letters*, vol. 11, no. 3, pp. 106–108, Mar. 2001.

[106] P. M. Zavracky, N. E. McGruer, R. H. Morrison, and D. Potter, "Microswitches and microrelays with a view toward microwave applications," *Int. Journal of RF and Microwave Computer-Aided Engineering*, vol. 9, no. 4, pp. 338–347, July 1999.

[107] S. Majumder, J. Lampen, R. Morrison, and J. Maciel, "An electrostatically actuated broadband MEMS switch," White Paper by Radant MEMS, Stow, MA, USA, 2003.

[108] C. O'Mahony, M. Hill, P. J. Hugher, and W. A. Lane, "Titanium as a micromechanical material," *Journal of Micromechanics and Microengineering*, vol. 12, no. 4, pp. 438–443, July 2002.

[109] Y. Komura, M. Sakata, T. Seki, K. Kobayashi, K. Sano, S. Horiike, and K. Ozawa, "Micro machined relay for high frequency application," in *Proc. 47th NARM Int. Relay Conference 1999*, Newport Beach, USA, Apr. 19–21, 1999.

[110] V. Milanovic, M. Maharbiz, A. Singh, B. Warneke, N. Zhou, H. K. Chan, and K. S. J. Pister, "Microrelays for batch transfer integration in RF systems," in *Proc. IEEE Micro Electro Mechanical Systems 2000*, Miyazaki, Japan, Jan. 23–27, 2000, pp. 787–792.

[111] D. Hah, E. Yoon, and S. Hong, "A low-voltage actuated micromachined microwave switch using torsion springs and leverage," *IEEE Trans. on Microwave Theory and Techniques*, vol. 48, no. 12, pp. 2540–2545, Dec. 2000.

[112] J.-C. Chiao, Y. Fu, L.-Y. Lin, and D. Choudhury, "MEMS millimeter-wave components," in *IEEE MTT-S Int. Microwave Symposium Digest 1999*, Anaheim, CA, USA, June 1999, pp. 1515–1518.

[113] F. Plötz, S. Michaelis, R. Aigner, H.-J. Timme, J. Binder, and R. Noé, "A low-voltage torsional actuator for application in RF-microswitches," *Sensors and Actuators A: Physical*, vol. 92, no. 1–3, pp. 312–317, Aug. 2001.

[114] J. J. Berenz, G. W. McIver, and A. E. Lee, TRW Inc., Redondo Reach, CA, USA, *Micro-electro system (MEMS) switch*, US patent no. 6069540, filed on Oct. 14, 1999, granted on May 30, 2000.

[115] D. Bechtle, G. C. Taylor, and A. Rosen, Georgia Tech Research Corporation, Atlanta, GA, USA, *Microelectronic mechanical systems (MEMS) switch and method of fabrication*, US patent no. 6535091, filed on Nov. 6, 2001, granted on Mar. 18, 2003.

[116] C. Bozler, R. Drangmeister, S. Duffy, M. Gouker, J. Knecht, L. Kushner, R. Parr, S. Rabe, and L. Travis, "MEMS microswitch arrays for reconfigurable distributed microwave components," in *IEEE MTT-S Int. Microwave Symposium Digest 2000*, vol. 1, Boston, MA, USA, June 11–16, 2000, pp. 153–156.

[117] J.-H. Park, K. Kang, N. Kang, C. Kim, C. Song, C.-Y. Cheon, Y. Kwon, and Y.-K. Kim, "A 3-voltage actuated micromachined RF switch for telecommunications applications," in *Proc. Transducers 2001*, Munich, Germany, June 10–14, 2001, pp. 1540–1543.

[118] Press release by ST Microelectronics, Geneva, France, July 21, 2003.

[119] S. Pacheco, C. T. Nguyen, and L. P. B. Katehi, "Micromechanical electrostatic k-band switches," in *IEEE MTT-S Int. Microwave Symposium Digest 1998*, vol. 1, Baltimore, MD, USA, June 1998, pp. 1569–1572.

[120] C. L. Goldsmith, Z. Yao, S. Eshelman, and D. Denniston, "Performance of low-loss RF MEMS capacitive switches," *IEEE Microwave and Guided Wave Letters*, vol. 8, no. 8, pp. 269–271, Aug. 1998.

[121] C. Goldsmith, J. Ehmke, A. Malczewski, B. Pillans, S. Eschelmann, Z. Yao, J. Brank, and M. Eberly, "Lifetime characterization of capacitive RF MEMS switches," in *Proc. IEEE MTT-S Int. Microwave Symposium*, Phoenix, AZ, USA, May 20–25, 2001, pp. 779–808.

[122] S.-C. Shen, D. Caruth, and M. Feng, "Broadband low actuation voltage rf mem switches," in *Proc. IEEE Gallium Arsenide Integrated Circuit Symposium 2000*, Seattle, WA, USA, Nov. 5–8 2000, pp. 161–164.

[123] J. B. Muldavin and M. R. Rebeiz, "High-isolation CPW MEMS shunt switches—Part 1: Design," *IEEE Trans. on Microwave Theory and Techniques*, vol. 48, no. 6, pp. 1053–1056, June 2000.

[124] J. Park, G. Kim, K. Chung, and J. Bu, "Electroplated RF MEMS capacitive switches," in *Proc. IEEE Micro Electro Mechanical Systems 2000*, Miyazaki, Japan, Jan. 23–27, 2000, pp. 639–644.

[125] X. Rottenberg, J. Geerlings, B. Nauwelaers, W. De Raedt, and H. A. C. Tilmans, "MEMS near-DC to RF capacitive series switches," in *Proc. European Microwave Conference 2002*, Munich, Germany, Oct. 6–10, 2003, pp. 975–978.

[126] G.-L. Tan and G. M. Rebeiz, "A DC-contact MEMS shunt switch," *IEEE Microwave and Wireless Components Letters*, vol. 12, no. 6, pp. 212–214, June 2002.

[127] R. Chan, R. Lesnick, D. Becher, and M. Feng, "Low-actuation voltage RF MEMS shunt switch with cold switching lifetime of seven billion cycles," *IEEE Journal of Microelectromechanical Systems*, vol. 12, no. 5, pp. 713–719, Oct. 2003.

[128] E. Fullin, J. Gobet, H. Tilmans, and J. Bergqvist, "A new basic technology for magnetic micro-actuators," in *Proc. IEEE Micro Electro Mechanical Systems 1998*, Heidelberg, Germany, Jan. 25–29, 1998, pp. 143–147.

[129] H. Tilmans, E. Fullin, H. Ziad, M. Van de Peer, J. Kesters, E. Van Geffen, J. Bergqvist, M. Pantus, E. Beyne, K. Baert, and F. Naso, "A fully-packaged electromagnetic microrelay," in *Proc. IEEE Micro Electro Mechanical Systems 1999*, Orlando, FL, USA, Jan. 17–21, 1999, pp. 25–30.

[130] Y. Liu, X. Li, T. Abe, Y. Haga, and M. Esashi, "A thermomechanical relay with microspring contact array," in *Proc. IEEE Micro Electro Mechanical Systems 2001*, Interlaken, Switzerland, Jan. 21–25, 2001, pp. 220–223.

[131] H.-S. Lee, C. H. Leung, J. Shi, S.-C. Chang, S. Lorincz, and I. Nedelescu, "Integrated microrelays: concept and initial results," *IEEE Journal of Microelectromechanical Systems*, vol. 11, no. 2, pp. 147–153, Apr. 2002.

[132] L. Que, J.-S. Park, and Y. B. Gianchandani, "Bent-beam electrothermal actuators — part I: single beam and cascaded devices," *IEEE Journal of Microelectromechanical Systems*, vol. 10, no. 2, pp. 247–254, June 2001.

[133] I. Schiele and B. Hillerich, "Comparison of lateral and vertical switches for application as microrelays," *Journal of Micromechanics and Microengineering*, vol. 9, no. 2, pp. 146–150, June 1999.

[134] T. Gromm, L. L. Howell, and R. H. Selfridge, "In-plane linear displacement bistable microrelay," *Journal of Micromechanics and Microengineering*, vol. 12, no. 3, pp. 257–264, May 2002.

[135] R. Streeter, C. Hall, R. Wood, and R. Mahadevan, "VHF high-power tunable RF bandpass filter using microelectromechanical (MEM) microrelays," *Int. Journal of RF and Microwave Computer-Aided Engineering*, vol. 11, no. 5, pp. 261–275, Sept. 2001.

[136] Y. Wang, Z. Li, D. T. McCormick, and N. C. Tien, "A micromachined RF microrelay with electrothermal actuation," *Sensors and Actuators A: Physical*, vol. 103, no. 1–2, pp. 231–236, Jan. 2003.

[137] J. Qiu, J. Lang, A. Slocum, and R. Strumpler, "A high-current electrothermal bistable MEMS relay," in *Proc. IEEE Micro Electro Mechanical Systems 2003*, Kyoto, Japan, Jan. 19–23, 2003, pp. 64–67.

[138] C.-L. Dai, K. Yen, and P.-Z. Chang, "Applied electrostatic parallelogram actuators for microwave switches using the standard cmos process," *Journal of Micromechanics and Microengineering*, vol. 11, no. 6, pp. 697–702, Nov. 2001.

[139] C. V. Jahnes, J. Cotte, J. L. Lund, H. Deligianni, A. Chinthakindi, L. P. Buchwalter, P. Fryer, J. A. Tornello, N. Hoivik, J. H. Magerlein, and D. Seeger, "Simultaneoous fabrication of RF MEMS and resonators using copper-based CMOS interconnect manufacturing methods," in *Proc. IEEE Micro Electro Mechanical Systems 2004*, Maastricht, The Netherlands, Jan. 25–29, 2004, pp. 789–792.

[140] H.-P. Chang, J. Qian, B. Cetiner, F. De Flaviis, M. Bachman, and G. Li, "RF MEMS switches fabricated on microwave-laminate printed circuit boards," *IEEE Electron Device Letters*, vol. 24, no. 4, pp. 227–229, Apr. 2003.

[141] C. Wang, R. Ramadoss, S. Lee, K. Gupta, V. Bright, and Y. Lee, "Flexible circuit-based RF MEMS switches," in *Proc. ASME Micro-Electro-Mechanical Systems 2001*, New York, NY, USA, Nov. 11–16, 2001, pp. 757–62.

[142] J. S. Go, Y.-H. Cho, B. M. Kwak, and K. Park, "Snapping microswitches with adjustable acceleration threshold," *Sensors and Actuators A: Physical*, vol. 54, no. 1–3, pp. 579–583, June 1996.

[143] M. Wycisk, T. Tönnesen, J. Binder, S. Michaelis, and H.-J. Timme, "Low-cost post-CMOS integration of electroplated microstructures for inertial sensing," *Sensors and Actuators A: Physical*, vol. 83, no. 1–3, pp. 93–100, May 2000.

[144] J. Noetzel, T. T., W. Benecke, J. Binder, and G. Mader, "Quasianalog accelerometer using microswitch array," *Sensors and Actuators A: Physical*, vol. 54, no. 1–3, pp. 574–578, June 1996.

[145] T. Matsuaga and M. Esashi, "Acceleration switch with extended holding time using squeeze film effect for side airbag systems," *Sensors and Actuators A: Physical*, vol. 100, no. 1, pp. 10–17, Aug. 2002.

[146] J. Simon, S. Saffer, F. Sherman, and C.-J. Kim, "Lateral polysilicon microrelays with a mercury microdrop contact," *IEEE Transactions on Industrial Electronics*, vol. 45, no. 6, pp. 854–860, Dec. 1998.

[147] L. Willks, "Advantages and uses of mercury wetted contact relays," *New Electronics*, vol. 12, no. 6, pp. 72, 74, Mar. 1979.

[148] J. Simon, S. Saffer, and C.-J. Kim, "A liquid-filled microrelay with a moving mercury microdrop," *IEEE Journal of Microelectromechanical Systems*, vol. 6, no. 3, pp. 208–216, Sept. 1997.

[149] X.-Q. Sun, K. R. Farmer, and W. N. Carr, "A bistable microrelay based on two-segment multimorph cantilever actuators," in *Proc. IEEE Micro Electro Mechanical Systems 1998*, Heidelberg, Germany, Jan. 25–29, 1998, pp. 154–159.

[150] J.-M. Huang, K. Liew, C. Wong, S. Rajendran, M. Tan, and A. Liu, "Mechanical design and optimization of capacitive micromachined switch," *Sensors and Actuators A: Physical*, vol. 93, no. 3, pp. 273–285, Oct. 2001.

[151] J. B. Muldavin and G. M. Rebeiz, "High-isolation CPW MEMS shunt switches—Part 2: Modeling," *IEEE Trans. on Microwave Theory and Techniques*, vol. 48, no. 6, pp. 1045–1052, June 2000.

[152] R. Sattler, F. Plötz, G. Fattinger, and G. Wachutka, "Modeling of an electrostatic torsional actuator: demonstrated with an RF MEMS switch," *Sensors and Actuators A: Physical*, vol. 97–98, pp. 337–346, Apr. 2002.

[153] L. L. Mercado, S.-M. Koo, T.-Y. T. Lee, and L. Liu, "A mechanical approach to overcome RF MEMS switch stiction problem," in *Proc. IEEE Electronic Components and Technology Conference 2003*, New Orleans, LA, USA, May 27–30, 2003, pp. 377–384.

[154] M. J. Madou, *Fundamentals of Microfabrication: the science of miniaturization*, 2nd ed. Boca Raton, London, New York, Washington D.C.: CRC Press, 2002.

[155] G. T. A. Kovacs, *Micromachined Transducers Sourcebook*, 1st ed. New York: McGraw-Hill, 1998.

[156] J. Schimkat, "Contact measurement providing basic design data for microrelay actuators," *Sensors and Actuators A: Physical*, vol. 73, no. 1–2, pp. 138–143, Mar. 1999.

[157] J. I. Seeger and B. E. Boser, "Charge control of parallel-plate, electrostatic actuators and the tip-in instability," *IEEE Journal of Microelectromechanical Systems*, vol. 12, no. 5, pp. 656–671, Oct. 2003.

[158] T. Seki, S. Sato, T. Masuda, I. Kimura, and K. Imanaka, "Low-loss RF MEMS metal-to-metal contact switch with CSP structure," in *Proc. Transducers 2003*, Boston, MA, USA, June 8–12, 2003, pp. 340–341.

[159] J. B. Muldavin and G. M. Rebeiz, "All-metal series and series/shunt MEMS switches," *IEEE Microwave and Wireless Components Letters*, vol. 11, no. 9, pp. 373–375, Sept. 2001.

[160] M. Sakata, Y. Komura, T. Seki, K. Kobayashi, K. Sano, and S. Horiike, "Micromachined relay which utilizes single crystal silicon electrostatic actuator," in *Proc. IEEE Micro Electro Mechanical Systems 1999*, Orland, FL, USA, Jan. 17–21, 1999, pp. 21–24.

[161] C. C. Cabuz, E. I. Cabuz, T. R. Ohnstein, J. Neus, and R. Maboudian, "Factors enhancing the reliability of touch-mode electrostatic actuators," *Sensors and Actuators A: Physical*, vol. 79, no. 3, pp. 245–250, Feb. 2000.

[162] Q. Ma, Intel Corporation, Santa Clara, CA, USA, *Microelectromechanical (MEMS) switch using stepped actuation electrodes*, US patent no. 6529093, filed on July 6, 2001, granted on Mar. 4, 2003.

[163] R. D. Nelson, Teravicin Technologies, Inc., Austin, TX, USA, *Device adapted to pull a cantilever away from a contact structure*, US patent no. 6646215, filed on June 29, 2001, granted on Nov. 11, 2003.

[164] N. Nishijima, J.-J. Hung, and G. M. Rebeiz, "Parallel-contact metal-contact RF-MEMS switches for high power applications," in *Proc. IEEE Micro Electro Mechanical Systems 2004*, Maastricht, The Netherlands, Jan. 25–29, 2004, pp. 781–784.

[165] J. D. Cobine, *Gaseous Conductors: Theory and Engineering Applications*, 1st ed. Dover: McGraw-Hill, 1941.

[166] L. H. Germer, "Electrical breakdown between close electrodes in air," *Journal of Applied Physics*, vol. 30, no. 1, pp. 41–47, 1959.

[167] T. Ono, D. Y. Sim, and M. Esashi, "Micro-discharge and electric breakdown in a micro-gap," *Journal of Micromechanics and Microengineering*, vol. 10, no. 3, pp. 445–451, Sept. 2000.

[168] Z.-K. Chen, "Wear and contamination of electroplated gold films in line contact," *IEEE Trans. on Components, Hybrids, and Manufacturing Technology*, vol. 15, no. 3, pp. 378–385, May 1992.

[169] M. Antler, "Gold plated contacts: effect of thermal aging on contact resistance," in *Proc. IEEE Holm Conf. on Electrical Contacts*, Philadelphia, PA, USA, Oct. 20–22 1997, pp. 121–131.

[170] M. D. Pashley, J. B. Pethica, and D. Tabor, "Adhesion and micromechanical properties of metal surfaces," *Wear*, vol. 100, no. 1–3, pp. 7–31, Dec. 1984.

[171] H. C. Angus, "Surface films on precious-metal contacts," *British Journal of Applied Physics*, vol. 13, pp. 58–63, 1962.

[172] R. Holm, *Electric Contacts Handbook*, 4th ed. Berlin, Germany: Springer Verlag, 1967.

[173] M. Antler, "Field studies of contact materials: Contact resistance behavior of some base and noble metals," *IEEE Trans. on Components, Hybrids, and Manufacturing Technology*, vol. 5, no. 3, pp. 301–307, Sept. 1982.

[174] M. Watanabe, M. Kishimoto, Y. Hiratsuka, S. Mitani, and T. Mori, "Study of contact failures caused by organic contamination on Ag-Si contacts," *IEEE Trans. on Components, Hybrids, and Manufacturing Technology*, vol. 5, no. 1, pp. 90–94, Mar. 1982.

[175] T. Tamai and K. Tsuchiya, "Direct observation for the effect of electric current on contact interface," *IEEE Trans. on Components, Hybrids, and Manufacturing Technology*, vol. 2, no. 1, pp. 76–80, 1979.

[176] J. Keller, D., "Electric contact phenomena in ultra clean and specifically contaminated systems," *IEEE Trans. on Parts, Hybrids, and Packaging*, vol. 8, no. 1, pp. 4–15, Mar. 1972.

[177] D. Hyman and M. Mehregany, "Contact physics of gold microcontacts for MEMS switches," *IEEE Trans. on Components and Packaging Technology*, vol. 22, no. 3, pp. 357–364, Sept. 1999.

[178] W. Scherer, B. Bader, and F. Gehrlach, "Untersuchung des elektrischen Kontaktverhaltens mikromechanischer Schaltelemente (FV-NR 11387N)," Hahn-Schickard-Gesellschaft, Institut für Feinwerk- und Zeitmeßtechnik, Tech. Rep., Jan. 31, 2001.

[179] J. Schimkat, "Contact materials for microrelays," in *Proc. IEEE Micro Electro Mechanical Systems 1998*, Heidelberg, Germany, Jan. 35–29, 1998, pp. 190–194.

[180] S. Majumder *et al.*, "Study of contacts in an electrostatically actuated microswitch," in *Proc. IEEE Electrical Contacts*, Arlington, VA, USA, Oct. 26–28, 1998, pp. 127–132.

[181] E. J. J. Kruglick and K. S. J. Pister, "Lateral MEMS microcontact considerations," *IEEE Journal of Microelectromechanical Systems*, vol. 8, no. 3, pp. 264–271, Sept. 1999.

[182] D. Peroulis and L. P. B. Katehi, "A novel device for *in situ* experimental characterization and reliability analysis of DC-contact RF MEMS switches," in *Proc. Transducers 2003*, Boston, MA, USA, June 8–12, 2003, pp. 867–870.

[183] J. DeNatale, R. Mihailovich, and J. Waldrop, "Techniques for reliability analysis of MEMS RF switches," in *Proc. IEEE Int. Reliability Physics Symposium*, Dallas, TX, USA, Apr. 7–11, 2002, pp. 116–117.

[184] G. Blaise and C. Le Gressus, "Charging phenomena, dielectric relaxation processes and breakdown of oxides," in *IEEE 1990 Annual Report., Conference on Electrical Insulation and Dielectric Phenomena*, Pocono Manor, PA, USA, Oct 28–31, 1990, pp. 231–236.

[185] N. Tas, T. Sonnenberg, H. Jansen, R. Legtenberg, and M. Elwenspoek, "Stiction in surface micromachining," *Journal of Micromechanics and Microengineering*, vol. 6, no. 4, pp. 385–397, Dec. 1996.

[186] R. Maboudian and R. T. Howe, "Critical review: Adhesion in surface micromechanical structures," *Journal of Vacuum Science and Technology B*, vol. 15, no. 1, pp. 1–20, Jan./Feb. 1997.

[187] S. M. Sze, *Physics of Semiconductor Devices*, 2nd ed. New York: John Wiley & Sons, Sept. 1981.

[188] M. Vogt and R. Hauptmann, "Plasma-deposited passivation layers for moisture and water protection," *Surface and Coatings Technology*, vol. 74–75, no. 2, pp. 676–681, Oct. 1995.

[189] T.-R. Hsu, *MEMS Packaging*, 1st ed., ser. EMIS Processing Series 3. London: Institution of Electrical Engineers INSPEC, 2004.

[190] R. R. Tummala, E. J. Rymaszewski, and A. G. Klopfenstein, *Microelectronics Packaging Handbook, part 2: Semiconductor Packaging*, 2nd ed. Boston, Dordrecht, London: Kluwer, 1999.

[191] Q.-Y. Tong and U. Gösele, *Semiconductor Wafer Bonding: Science and Technology*, 1st ed. New York: John Wiley & Sons, 1999.

[192] M. Alexe and U. Gösele, *Wafer Bonding: Applications and Technology*, 1st ed., ser. Materials Science. Berlin, Heidelberg, Germany: Springer, 2004.

[193] G. Li and A. Tseng, "Low stress packaging of a micromachined accelerometer," *IEEE Trans. on Electronics Packaging Manufacturing*, vol. 24, no. 1, pp. 18–25, Jan. 2001.

[194] Product brochures of the SAR10 gyro and the SP12 tire pressure sensors of SensoNor, Horten, Norway, Oct. 2002.

[195] E. Obermeier, "Anodic wafer bonding," in *Proc. Semiconductor Wafer Bonding: Science, Technology and Applications*, vol. 95-7, Reno, Nevada, May 1995, pp. 212–220.

[196] R. L. Smith and S. D. Collins, "Micromachined packaging for chemical microsensors," *IEEE Trans. on Electron Devices*, vol. 35, no. 6, pp. 787–792, June 1988.

[197] K. W. Oh, A. Han, S. Bhansali, and C. H. Ahn, "A low-temperature bonding technique using spin-on fluorocarbon polymers to assemble microsystems," *Journal of Micromechanics and Microengineering*, vol. 12, no. 2, pp. 187–191, Mar. 2002.

[198] T. T. Veenstra, J. W. Berenschot, J. G. E. Gardeniers, R. G. P. Sanders, M. Elwenspoek, and A. van den Berg, "Use of selective anodic bonding to create micropump chambers with virtually no dead volume," *Journal of the Electrochemical Society*, vol. 148, no. 2, pp. G68–G72, Feb. 2001.

[199] M. Kada and L. Smith, "Advancements in stacked chip scale packaging (S-CSP), provides system-in-a-package functionality for wireless and handheld applications," in *Proc. Pan Pacific Microelectronics Symposium 2000*, Maui, HI, USA, Jan. 25–27, 2000, pp. 246–251.

[200] F. Niklaus, P. Enoksson, P. Griss, E. Kälvesten, and G. Stemme, "Low-temperature wafer-level transfer bonding," *IEEE Journal of Microelectromechanical Systems*, vol. 10, no. 4, pp. 525–531, 2001.

[201] H. Kopola, J. Lenkkeri, K. Kautio, A. Torkkeli, O. Rusanen, and T. Jaakola, "MEMS sensor packaging using LTCC substrate technology," in *Proc. SPIE, The Int. Society for Optical Engineering*, vol. 4592, 2001, pp. 148–158.

[202] J. Wei, Z. Wang, H. Xie, and N. F. Lan, "Role of bonding temperature and voltage in silicon-to-glass anodic bonding," in *Proc. IEEE Electronics Packaging Technology Conference*, Singapore, Dec. 10–12, 2002, pp. 85–90.

[203] J. Wei, C. K. Wong, and L. C. Lee, "Improvement of anodic bond quality with the assistance of sputtered amorphous film," *Sensors and Actuators A: Physical*, vol. 113, no. 2, pp. 218–225, July 2004.

[204] B. Ziaie, J. A. V. Arx, M. R. Dokmeci, and K. Najafi, "A hermetic glass-silicon micropackage with high-density on-chip feedtroughs for sensors and actuators," *IEEE Journal of Microelectromechanical Systems*, vol. 5, no. 3, pp. 166–179, Sept. 1996.

[205] K. E. Petersen, "Method and apparatus for forming hermetically sealed electrical feedthrough conductors," Patent no WO 85/03381, 1985.

[206] K. M. Hiltmann, B. Schmidt, H. Sandmaier, and W. Lang, "Development of micromachined switches with increased reliability," in *Proc. Transducers 1997*, Chicago, USA, June 16–19, 1997, pp. 1157–1160.

[207] B. Lee, S. Seok, and K. Kukjin Chun, "A study on wafer level vacuum packaging for MEMS devices," *Journal of Micromechanics and Microengineering*, vol. 13, no. 5, pp. 663–669, Sept. 2003.

[208] A. Mehra, A. A. Ayón, I. A. Waitz, and M. A. Schmidt, "Microfabrication of high-temperature silicon devices using wafer bonding and deep reactive ion etching," *IEEE Journal of Microelectromechanical Systems*, vol. 8, no. 2, pp. 152–160, June 1999.

[209] B. Müller and A. Stoffel, "Tensile strength characterization of low-temperature fusion-bonded silicon wafers," *Journal of Micromechanics and Microengineering*, vol. 1, no. 3, pp. 161–166, Sept. 1991.

[210] S. S. Iyer and Auberton-Hervé, *Silicon Wafer Bonding Technology for VLSI and MEMS applications*, 1st ed., ser. EMIS Processing Series. London, UK: Institution of Electrical Engineers INSPEC, 2002.

[211] G. A. C. M. Spierings, J. Haisma, and F. J. H. M. van der Kruis, "Direct bonding of organic polymeric materials," *Philips Journal of Research*, vol. 49, no. 1–2, pp. 139–149, 1995.

[212] Q.-Y. Tong, G. Cha, R. Gafiteanu, and U. Gösele, "Low temperature wafer direct bonding," *IEEE Journal of Microelectromechanical Systems*, vol. 3, no. 1, pp. 29–35, Mar. 1994.

[213] T. Itoh, H. Okada, H. Takagi, R. Maeda, and T. Suga, "Room temperature vacuum sealing using surface activated bonding," in *Proc. Transducers 2003*, Munich, Germany, June 8–12, 2003, pp. 1828–1831.

[214] T. Suga, "Feasibility of surface activated bonding for ultra-fine pitch interconnection-a new concept of bump-less direct bonding for system level packaging," in *Proc. IEEE Electronic Components and Technology Conference*, Las Vegas, NV, USA, May 21–24, 2000, pp. 702–705.

[215] R. F. Wolffenbuttel and K. D. Wise, "Low-temperature silicon wafer-to-wafer bonding using gold at eutectic temperature," *Sensors and Actuators A: Physical*, vol. 43, no. 1–3, pp. 223–229, May 1994.

[216] M. B. Cohn, Y. Liang, R. T. Howe, and A. P. Pisano, "Wafer-to-wafer transfer of microstructures for vacuum packaging," in *Technical Digest Solid-State Sensor and Actuator Workshop*, Hilton Head Island, SC, USA, June 3–6, 1996, pp. 32–35.

[217] L. A. Field and R. S. Muller, "Fusing silicon wafers with low melting temperature glass," *Sensors and Actuators A: Physical*, vol. 23, no. 1–3, pp. 935–938, Apr. 1990.

[218] C. Lee, W. F. Huang, and J.-S. Shie, "Wafer bonding by low-temperature soldering," *Sensors and Actuators A: Physical*, vol. 85, no. 1–3, pp. 330–334, Aug. 2000.

[219] D. Sparks, G. Queen, R. Weston, G. Woodward, M. Putty, L. Jordan, S. Zarabadi, and K. Jayakar, "Wafer-to-wafer bonding of nonplanarized MEMS surfaces using solder," *Journal of Micromechanics and Microengineering*, vol. 11, pp. 630–634, Nov. 2001.

[220] L. Lin, "MEMS post-packaging by localized heating and bonding," *IEEE Trans. on Advanced Packaging*, vol. 23, no. 4, pp. 608–616, Nov. 2000.

[221] C. H. Tsau, S. M. Spearing, and M. A. Schmidt, "Fabrication of wafer-level thermocompression bonds," *IEEE Journal of Microelectromechanical Systems*, vol. 11, no. 6, pp. 641–647, Dec. 2002.

[222] F. Niklaus, "Adhesive wafer bonding for microelectronic and microelectromechanical systems," Ph.D. thesis, Royal Institute of Technology, Stockholm, Sweden, Oct. 2002.

[223] M. M. V. Taklo, P. Storås, K. Schjølberg-Henriksen, H. K. Hasting, and H. Jakobsen, "Strong, high-yield and low-temperature thermocompression silicon wafer-level bonding with gold," *Journal of Micromechanics and Microengineering*, vol. 14, no. 7, pp. 884–890, July 2004.

[224] J. Kim, M. Chiao, and L. Lin, "Ultrasonic bonding of in/au and al/al for hermetic sealing of MEMS packaging," in *Proc. IEEE Micro Electro Mechanical Systems 2002*, Las Vegas, NV, USA, Jan. 20–24, 2002, pp. 415–418.

[225] N. K. Budraa, H. W. Jackson, M. Barmatz, W. T. Pike, and J. D. Mai, "Low pressure and low temperature hermetic wafer bonding using microwave heating," in *IEEE Micro Electro Mechanical Systems 1999*, Orlando, FL, USA, Jan. 17–21, 1999, pp. 490–492.

[226] C.-T. Pan, H. Yang, S.-C. Shen, M.-C. Chou, and H.-P. Chou, "A low-temperature wafer bonding technique using patternable materials," *Journal of Micromechanics and Microengineering*, vol. 12, no. 5, pp. 611–615, Sept. 2002.

[227] B. Bilenberg, T. Nielsson, B. Claussen, and A. Kristensen, "PMMA to SU-8 bonding for polymer based lab-on-a-chip systems with integrated optics," in *Proc. Eurosensors 2003*, Guimarães, Portugal, Sept. 20–21, 2003, pp. 486–489.

[228] R. E. G. den Besten, C. van Hal, J. Munoz, and P. Bergveld, "Polymer bonding of micro-machined silicon structures," in *Proc. IEEE Micro Electro Mechanical Systems 1995*, Travemunde, Germany, Feb. 4–7, 1992, pp. 104–109.

[229] F. Niklaus, P. Enoksson, E. Kälvesten, and G. Stemme, "Low-temperature full wafer adhesive bonding," *Journal of Micromechanics and Microengineering*, vol. 11, no. 2, pp. 100–107, 2001.

[230] T.-K. A. Chou and K. Najafi, "3D MEMS fabrication using low-temperature wafer bonding with benzocyclobutene (BCB)," in *Proc. Transducers 2001*, Munich, Germany, June 10–14, 2001, pp. 1570–1573.

[231] S. K. Sampath, L. St. Clair, X. Wu, D. V. Ivanov, Q. Wang, C. Ghosh, and K. R. Farmer, "Rapid MEMS prototyping using SU-8, wafer bonding and deep reactive ion etching," in *Proc. Fourteenth Biennial University/Government/Industry Microelectronics Symposium*, Richmond, VA, USA, June 17–20, 2001, pp. 158–161.

[232] F. J. Blanco, M. Agirregabiria, J. Garcia, J. Berganzo, M. Tijero, M. T. Arroyo, J. M. Ruano, I. Aramburu, , and K. Mayora, "Novel three-dimensional embedded SU-8 microchannels fabricated using a low temperature full wafer adhesive bonding," *Journal of Micromechanics and Microengineering*, vol. 14, no. 7, pp. 1047–1056, July 2004.

[233] A. Frazier, "Low temperature IC-compatible wafer-to-wafer bonding with embedded micro channels for integrated sensing systems," in *Proc. IEEE Circuits and Systems 1995*, Rio de Janeiro, Brazil, Aug. 13–16, 1995, pp. 505–508.

[234] Y.-L. Park, H.-W. Park, D.-J. Lee, J.-H. Park, I.-S. Song, C.-W. Kim, C.-M. Song, Y.-H. Lee, C.-J. Kim, and B.-K. Ju, "A novel low-loss wafer-level packaging of the RF MEMS devices," in *Proc. IEEE Micro Electro Mechanical Systems 2002*, Las Vegas, NV, USA, Jan. 20-24, 2002, pp. 681–684.

[235] X. Wang, J. Engel, and C. Liu, "Liquid crystal polymer (LCP) for MEMS: processes and applications," *Journal of Micromechanics and Microengineering*, vol. 13, no. 5, pp. 628–633, Sept. 2003.

[236] E. C. Culbertson, "A new laminate material for high performance PCBs: liquid crystal polymer copper clad films," in *Proc. Electronic Components and Technology Conference*, Las Vegas, NV, USA, May 21–24, 1995, pp. 520–523.

[237] K. Jayaraj and B. Farrell, "liquid crystal polymers and their role in electronic packaging," *Advancing Microelectronics Magazine*, vol. 25, pp. 15–18, July/Aug. 1998.

[238] H. A. C. Tilmans, D. J. van de Peer, and E. Beyne, "The indent reflow sealing (IRS) technique-a method for the fabrication of sealed cavities for MEMS devices," *IEEE Journal of Microelectromechanical Systems*, vol. 9, no. 2, pp. 206–217, June 2000.

[239] K. Ikeda, H. Kuwayama, T. Kobayashi, T. Watanabe, T. Nishikawa, T. Yoshida, and K. Harada, "Three-dimensional micromachining of silicon pressure sensor integrating resonant strain gauge on diaphragm," *Sensors and Actuators A: Physical*, vol. 23, no. 1–3, pp. 1007–1010, Apr. 1990.

[240] W. Tang, T.-C. Nguyen, M. Judy, and R. Howe, "Electrostatic-comb drive of lateral polysilicon resonators," *Sensors and Actuators A: Physical*, vol. 21, no. 1–3, pp. 328–331, Feb. 1990.

[241] L. Lin, K. M. McNair, R. T. Howe, and A. P. Pisano, "Vacuum-encapsulated lateral microresonators," in *Proc. Transducers 1993*, Yokohama, Japan, June 7–10, 1993, pp. 270–273.

[242] K. S. K.S. Lebouitz, R. T. Howe, and A. P. Pisano, "Permeable polysilicon etch access windows for microshell fabrication," in *Proc. Transducers 1995*, Stockholm, Sweden, June 25–29, 1995, pp. 224–227.

[243] K. S. Lebouitz, R. T. Mazaheri, A. Howe, and A. P. Pisano, "Vacuum encapsulation of resonant devices using permeable polysilicon," in *IEEE Micro Electro Mechanical Systems 1999*, Orlando, FL, USA, Jan. 17–21, 1999, pp. 470 – 475.

[244] R. Aigner, K.-G. Oppermann, H. Kapels, and S. Kolb, "cavity-micromachining technology: Zero-package solution for inertial sensors," in *Proc. Transducers 2001*, Munich, Germany, June 10–14, 2001, pp. 186–189.

[245] M. Bartek, F. J. A., and R. F. Wolffenbuttel, "Vacuum sealing of microcavities using metal evaporation," *Sensors and Actuators A: Physical*, vol. 61, no. 1–3, pp. 364–368, June 1997.

[246] T. Hara, S. Kobayashi, and K. Ohwada, "A new fabrication method for low-pressure package with glass-silicon-glass structure and its stability," in *Proc. Transducers 1999*, vol. 2, Sendai, Japan, June 7–10, 1999, pp. 1316–1319.

[247] B. H. Stark and K. Najafi, "A low-temperature thin-film electroplated metal vacuum package," *IEEE Journal of Microelectromechanical Systems*, vol. 13, no. 2, pp. 147–157, Apr. 2004.

[248] E. Parton and H. A. C. Tilmans, "Wafer-level MEMS packaging: Hermeticity and cavity ambient control," *Advanced Packaging*, pp. 21–23, Apr. 2002.

[249] M. Previti and K. Gilleo, "Getters: micromolecular scavengers for packaging MEMS," in *Proc. IEEE Advanced Packaging Materials: Processes, Properties and Interfaces*, Braselton, GA, USA, Mar. 11–14, 2001, pp. 201–206.

[250] R. C. Kullberg, "Processes and materials for creating and maintaining reliable vacuum and other controlled atmospheres in hermetically sealed MEMS packages," *Proceedings of the SPIE*, vol. 3880, pp. 75–82, 1999.

[251] H. Henmi, S. Shoj, K. Yoshimi, and M. Esasshi, "Vacuum packaging for microsensors by glass-silicon anodic bonding," *Sensors and Actuators A: Physical*, vol. 43, no. 1–3, pp. 243–248, May 1994.

[252] T. Corman, "Vacuum-sealed and gas-filled micromachined devices," Ph.D. dissertation, Royal Institute of Technology, Stockholm, Sweden, 1999.

[253] R. Mohanty and K. Gilleo, "Preventing degradation of GaAs devices by the use of getter," in *Proc. GaAs Reliability Workshop 1999*, Monterey, CA, USA, Oct. 17, 1999.

[254] P. Wilkerson, M. Kranz, A. Przekwas, and T. Hudson, "Flip-chip hermetic packaging of RF MEMS," in *Proc. Microelectromechanical Systems Conference*, Berkeley, CA, USA, Aug. 24–26, 2001, pp. 91–94.

[255] A. Jourdain, P. De Moor, S. Pamidighantam, and H. A. C. Tilmans, "Investigation of the hermeticity of BCB-sealed cavities for housing (RF-)MEMS devices," in *Proc. IEEE Micro Electro Mechanical Systems 2002*, Las Vegas, NV, USA, Jan. 20–24, 2002, pp. 677–680.

[256] V. G. Kutchoukov, M. Shikida, J. R. Mollinger, and A. Bossche, "Through-wafer interconnect technology for silicon," *Journal of Micromechanics and Microengineering*, vol. 14, no. 7, pp. 1029–1036, July 2004.

[257] J. P. Becker and L. P. B. Katehi, "Multilevel finite ground coplanar line transitions for high-density packaging using silicon micromachining," in *IEEE MTT-S Int. Microwave Symposium Digest 2000*, vol. 1, Boston, MA, USA, June 11–16, 2000, pp. 303–306.

[258] T. Takizawa, S. Yamamoto, K. Itoi, and T. Suemasu, "Conductive interconnections through thick silicon substrates for 3D packaging," in *Proc. IEEE Micro Electro Mechanical Systems 2002*, Las Vegas, NV, USA, Jan. 20–24, 2002, pp. 388–391.

[259] C. H. Cheng, E. M. Chow, X. Jin, S. Ergun, and B. T. Khuri-Yakub, "An efficient electrical addressing method using through-wafer vias for two-dimensional ultrasonic arrays," in *Proc. IEEE Ultrasonics Symposium*, vol. 2, San Juan, Puerto Rico, Oct. 22–25, 2000, pp. 1179–1182.

[260] J. H. Wu, J. Scholvin, and J. A. del Alamo, "An insulator-lined silicon substrate-via technology with high aspect ratio," *IEEE Trans. on Electron Devices*, vol. 48, no. 9, pp. 2181–2183, Sept. 2001.

[261] J. H. Wu, J. A. Scholvin, J. del Alamo, and K. A. Jenkins, "A faraday cage isolation structure for substrate crosstalk suppression," *IEEE Microwave and Wireless Components Letters*, vol. 11, no. 10, pp. 410–412, Oct. 2001.

[262] N. D. Rotaru, C. S. Premachandran, and M. K. Iyer, "Design and electrical characterization of a novel wafer level package for RF MEMS applications," in *Proc. IEEE Electronic Components and Technology Conference*, May 27–30, 2003, pp. 1626–1630.

[263] H. T. Soh, C. P. Yue, A. McCarthy, C. Ryu, T. H. Lee, S. S. Wong, and C. F. Quate, "Ultra-low resistance, through-wafer via (TWV) technology and its applications in three dimensional structures on silicon," *Journal of Applied Physics*, vol. 38, pp. 2393–2396, Apr. 1999.

[264] Y.-K. Park, Y.-K. Kim, C.-J. Kim, B.-K. Ju, and J. O. Park, "Innovation ultra thin packaging for RF-MEMS devices," in *Proc. Transducers 2003*, vol. 1, Boston, MA, USA, June 8–12, 2003, pp. 903–906.

[265] C.-H. Chu, L.-S. Huang, J.-Y. Chen, I.-L. Lee, and P. Chang, "A new integration of device-scale micropackaging with bi-directional tunable capacitors," in *Proc. IEEE Micro Electro Mechanical Systems 2003*, Kyoto, Japan, Jan. 19–23, 2003, pp. 654–657.

[266] S. Majumder, J. Lampen, R. Morrison, and J. Maciel, "MEMS switches," *IEEE Instrumentation and Measurement Magazine*, pp. 12–15, Mar. 2003.

[267] M. Shikida, K. Sato, and T. Harada, "Fabrication of an s-shaped microactuator," *IEEE Journal of Microelectromechanical Systems*, vol. 6, no. 18, pp. 18–24, Mar. 1997.

[268] K. C. Chan, M. Teo, and Z. W. Zhong, "Characterization of low-k benzocyclobutene dielectric thin film," *Microelectronics International*, vol. 20, no. 3, pp. 11–22, 2003.

[269] M. E. Mills, P. Townsend, D. Casrillo, S. Martin, and A. Achen, "Benzocyclobutene (DVS-BCB) polymer as an interlayer dielectric (ILD) material," *Microelectronic Engineering*, vol. 33, no. 1–4, pp. 327–334, Jan. 1997.

[270] A. J. G. Strandjord, W. B. Rogers, Y. Ida, R. R. DeVeillis, S. Shiau, E. S. Moyer, D. M. Scheck, and P. E. Garron, "Photosensitive benzocyclobutene for stress-buffer and passivation applications (one mask manufacturing process)," in *Proc. Electronic Components and Technology Conference*, San Jose, CA, USA, May 18–21, 1997, pp. 1260–1268.

[271] P. Garrou, "Polymer dielectrics for multichip module packaging," *Proceedings of the IEEE*, vol. 80, no. 12, pp. 1942–1954, Dec. 1992.

[272] P. E. Garrou, R. H. Heistand, M. G. Dibbs, T. A. Manial, C. E. Mohler, T. M. Stokich, P. H. Townsend, G. M. Adema, M. J. Berry, and I. Turlik, "Rapid thermal curing of BCB dielectric," *IEEE Trans. on Components, Hybrids, and Manufacturing Technology*, vol. 16, no. 1, pp. 46–52, Feb. 1993.

[273] J. T. Beechinor, E. McGlynn, M. O'Reilly, and G. M. Crean, "Optical characterisation of thin film benzocyclobutene (BCB) based polymers," *Microelectronic Engineering*, vol. 33, no. 1–4, pp. 363–368, 1997.

[274] H. Pranjoto and D. D. Denton, "Moisture uptake of bisbenzocyclobutene (BCB) films for electronic packaging applications," in *Proc. Electronic Packaging Materials Science*, Boston, MA, USA, Nov. 26–29, 1990, pp. 295–302.

[275] J.-B. Lee, J. English, C.-H. Ahn, and M. Allen, "Planarization techniques for vertically integrated metallic MEMS on silicon foundry circuits," *Journal of Micromechanics and Microengineering*, vol. 7, no. 2, pp. 44–54, June 1997.

[276] G.-R. Yang, Y.-P. Zhao, J. M. Neirynck, S. P. Murarka, and R. J. Gutmann, "Chemical-mechanical polishing of polymer films: Comparison of benzocyclobutene (BCB) and parylene-N films by XPS and AFM," in *Proc. Low-Dielectric Constant Materials*, San Franzisco, CA, USA, Apr. 1–4, 1997, pp. 161–172.

[277] Y.-S. Choi, J.-S. Park, H.-D. Park, Y.-H. Song, J.-S. Jung, and S.-G. Kang, "Effects of temperatures on microstructures and bonding strengths of Si-Si bonding using bisbenzocyclobutene," *Sensors and Actuators A: Physical*, vol. 108, no. 1–3, pp. 201–205, Nov. 2003.

[278] D. Burdeaux, P. Townsend, J. Carr, and P. Garrou, "Benzocyclobutene (BCB) dielectrics for the fabrication of high density, thin film multichip modules," *Journal of Electronic Materials*, vol. 19, no. 12, pp. 1357–1366, Dec. 1990.

[279] P. B. Chinoy, "Reactive ion etching of benzocyclobutene polymer films," *IEEE Trans. on Components, Packaging, and Manufacturing Technology — Part C: Manufacturing*, vol. 20, no. 3, pp. 199–206, July 1997.

[280] S. A. Vitale, H. Chae, and H. H. Sawin, "Etching chemistry of benzocyclobutene (BCB) low-k dielectric films in $F_2$+$O_2$ and $Cl_2$+$O_2$ high density plasmas," *Journal of Vacuum Science and Technology A (Vacuum, Surfaces, and Films)*, vol. 18, no. 6, pp. 2770–2778, Nov. 2000.

[281] K. Ohba, "Overview of photo-definable benzocyclobutene polymer," *Journal of Photopolymer Science and Technology*, vol. 15, no. 2, pp. 177–182, 2002.

[282] F. Niklaus, H. Andersson, P. Enoksson, and G. Stemme, "Low temperature full wafer adhesive bonding of structured wafers," *Sensors and Actuators A: Physical*, vol. 92, no. 1–3, pp. 235–241, 2001.

[283] I. K. Glasgow, D. J. Beebe, and V. E. White, "Design rules for polyimide solvent bonding," *Sensors and Materials*, vol. 11, no. 5, pp. 269–278, 1999.

[284] J.-Y. Chen, L.-S. Huang, and P. C. Chu, Chia-Hua, "A new transferred ultra-thin silicon micropackaging," *Journal of Micromechanics and Microengineering*, vol. 12, no. 4, pp. 406–409, July 2002.

[285] S.-A. Kim, Y.-H. Seo, Y.-H. Cho, G. H. Kim, and U. B. Jong, "Fabrication and characterization of a low-temperature hermetic MEMS package bonded by a closed loop AuSn solder-line," in *Proc. IEEE Micro Electro Mechanical Systems 2003*, Kyoto, Japan, Jan. 19–23, 2003, pp. 614–617.

[286] M. Goetz and C. Jones, "Chip scale packaging for RF SAW devices," in *Proc. SEMICON West 2002*, 2002, pp. 63–66.

[287] X. Li, T. Abe, Y. Liu, and M. Esashi, "High density electrical feedthrough fabricated by deep reactive ion etching of pyrex glass," in *Proc. IEEE Micro Electro Mechanical Systems 2001*, Interlaken, Switzerland, Jan. 21–25, 2001, pp. 98–101.

[288] H. Seo, G. Lim, and M. Sashi, "Hybrid-type capacitive pressure sensor," *Sensors and Materials*, vol. 4, no. 5, pp. 277–289, 1993.

[289] P. J. Slikkerveer, P. C. P. Bouten, and F. C. M. de Haas, "High quality mechanical etching of brittle materials by powder blasting," *Sensors and Actuators A: Physical*, vol. 85, pp. 296–303, 2000.

[290] H. Wensink, J. W. Berenschot, H. V. Jansen, and M. C. Elwenspoek, "High resolution powder blast micromachining," in *Proc. IEEE Micro Electro Mechanical Systems 2000*, Miyazaki, Japan, Jan. 23–27, 2000, pp. 769–774.

[291] E. Belloy, A.-G. Pawlowski, A. Sayah, and M. A. M. Gijs, "Microfabrication of high-aspect ratio and complex monolithic structures in glass," *IEEE Journal of Microelectromechanical Systems*, vol. 11, no. 5, pp. 521–527, Oct. 2002.

[292] *MIL-STD-883E*, US department of defense, Dec. 31, 1996.

[293] S. S. He and V. L. Shannon, "Hydrogen diffusion and redistribution in PECVD Si-rich silicon nitride during rapid thermal annealing," in *Proc. Int. Conference on Solid-State and IC Technology*, Beijing, China, Oct. 24–28, 1995, pp. 269–271.

[294] R. K. Ulrich, W. D. Brown, S. S. Ang, S. Yi, J. Sweet, and D. Peterson, "PECVD silicon and nitride postbond films for protecting bondpads, bonds and bondwires from corrosion failure," in *Proc. Electronic Components and Technology Conference*, Atlanta, GA, USA, May 11–16, 1991, pp. 738–744.

[295] J. C. Whitaker, *The Electronics Handbook*. Boca Raton, FL, USA: CRC Press, 1996.

*Then the Lord said: If now, while they are one people, all speaking the same language, they have started to do this, nothing will later stop them from doing whatever they propose to do.*

*Genesis, XI, v.6,*
*New American Bible*

# Nomenclature

| | |
|---|---|
| AC | alternating current: electrical signal without any constant, i.e. DC component |
| ADC | analog to digital converter: converts an analog input signal related to reference voltages and quantization steps to a binary coded (digital) signal |
| AICC | autonomous intelligent cruise control: autopilot-like system for cars, based on automotive radar and a cruise control management unit |
| ATE | automated test equipment: full automated test equipment for the end-control and tests of products; requires signal switching with very wide bandwidth (DC to RF) and very high signal quality |
| AuCuCd | gold with an alloying addition of copper and cadmium, used as a hard contact material in relays |
| AuNi5 | gold with an alloying addition of 5% nickel, used as a hard contact material in relays |
| BCB | divinylsiloxane bis-benzocyclobutene, an epoxy-based polymer suitable for adhesive wafer bonding |
| BiCMOS | bipolar and →CMOS devices integrated on the same chip |
| C2W | 0-level packaging by cap to wafer bonding/encapsulation |
| CMOS | complementary metal oxide silicon: fabrication technology enabling NMOS and PMOS →FETs in push-pull configuration on the same chip, for linear as well as digital →ICs |
| CMP | chemical and mechanical polishing: chemically assisted lapping of a wafer to reduce its thickness |
| CPW | coplanar wave guide: microwave transmission line with ground-signal-ground lines in one plane; simple to fabricate and good mode-control over a large frequency range. Variations: finite ground coplanar waveguide (FGCPW) with limited lateral size of the ground lines; grounded CPW with a ground layer underneath the CPW. |

| | |
|---|---|
| CSP | chip scale package: package whose total area is not larger than 120% of the chip size |
| CTE | coefficient of thermal expansion: material property describing the relative elongation of a material with increasing temperature |
| CVD | chemical vapor deposition: deposition of silicon-containing layers in surface micromachining, based on convection, diffusion and absorption of reactants on the target surface followed by chemical reactions, desorption and transport of byproducts by diffusion and forced convection in the deposition tool. The most common deposition processes are APCVD (atmospheric pressure CVD), →LPCVD and →PECVD. |
| CW | continous wave |
| DC | direct current: electrical signal with constant, i.e. time invariant level |
| DIP | dual-in-line package: industry standard plastic or ceramic package for through-hole mounting |
| DLP | digital light processing device: a trademark of Texas Instruments for MEMS digital micromirror arrays used in projectors |
| DRIE | deep reactive ion etching: →ICP |
| EMI | electro-magnetic influence: externally or internally created electrical disturbances within or between devices, due to capacitive, inductive, ohmic or radiation coupling of electrical signals |
| EMR | electro-mechanical relay: conventional macro-world relay assembled with traditional mechanical engineering fabrication techniques |
| FBAR | (thin) film bulk acoustic resonators: passive electrical components similar to →SAW, based on propagating transversal bulk acoustic waves (BAW) in a thin freestanding film |
| FET | field effect transistor: semiconductor device operating as a voltage controllable resistor in a drain-gate-source configuration |
| FGCPW | →CPW |
| GaAs | gallium arsenide: III-V semiconductor material with very good RF properties compared to high resistivity silicon |
| HF | hydrofluoric acid |
| HRSS | high resistivity silicon substrate: in contrast to standard silicon substrate for MEMS fabrication (1–10 Ω·cm), substrate with a resistivity of over 1000 Ω·cm |
| IC | integrated circuit: highly integrated semiconductor device, nowadays consisting of up to a few hundred million individual components fabricated on one single chip |

| | |
|---|---|
| ICP | inductive coupled plasma process to etch deep structures with good control over the steepness of the side-walls |
| IP3 | intercept point of 3rd order: characterization of the nonlinear distortions of an electronic device by a two-tone intermodulation test. The IP3 is the fictive intersection of the linear portion of the output signal with the portion of the 3rd order intermodulation product |
| KOH | potassium (kalium) hydroxide, a crystal-orientation dependent etchant of silicon |
| LCP | liquid crystal polymer: thermoplastic polymer made of aligned molecule chains with crystal-like spatial regularity, exhibiting unique electrical, physical and chemical properties |
| LPCVD | low pressure chemical vapor deposition: a chemical deposition process (→CVD) in surface micromachining to deposit high-density silicon-containing layers at temperatures above 600 °C |
| LTCC | low temperature co-fired ceramic: material for multichip module (MCM) substrates and for ceramic packages with very good mechanical and electrical properties |
| LTO | low temperature oxide, deposited silicon dioxide with a combination of phosphorus and boron providing excellent low-temperature reflow properties |
| MEMS | microelectromechanical systems: traditionally, electromechanical devices fabricated in standard IC manufacturing facilities. MEMS is nowadays also used for a broader group of →microsystem devices. |
| MIMO | multiple input multiple output |
| MST | microsystem technology: a synonym for MEMS technology or for micromaching, especially often used in Europe |
| NiFe | nickel ferrum (typical permalloy composition of 81% Fe and 19% Ni): most common ferromagnetic material used in MEMS, providing the combination of relatively high saturation flux density, low hysteresis losses and near zero magnetostriction |
| OWR | obstacle warning radar: automotive radar for driving and parking aid (front and side collision control) |
| PCB | printed circuit board: multi-layer laminate with embedded metal lines and vertical vias used in electronics industries to mechanically mount and interconnect →ICs and passive components |
| PDMS | poly-dimethylsiloxane: biocompatible polymer material suitable for micromolding plastic replication with very simple processing since it is casted over the master structures and fully cured at 65 °C |

| | |
|---|---|
| PECVD | plasma enhanced chemical vapor deposition: a chemical deposition process (→CVD) in surface micromachining to deposit silicon-containing layers at low temperatures |
| PIN diode | semiconductor device operating as a variable resistor at RF and microwave frequencies, controlled by a bias current. The name stems from an intrinsic layer embedded between the p and the n-doped layers of a semiconductor diode. |
| PMMA | polymethyl methacrylate: thermoplastic material, usually structured by conventional or modified plastic replication techniques such as injection molding or hot embossing. |
| PZT | lead (Pb) zirconate titanate: along with lead titanate (PT) and lead metaniobate ($PbNb_2O_6$), one of today's most used ceramic piezoelectric materials |
| RF | radio frequency |
| RF MEMS | radio frequency microelectromechanical systems |
| RIE | reactive ion etching: plasma process to etch thin films |
| RT | room temperature |
| SAM (1) | scanning acoustic microscope: inspection tool detecting the change of acoustic impedance at material interfaces; especially to investigate failure mechanisms such as dilaminations and voids |
| SAM (2) | self assembled monolayer: in RF MEMS, mainly used for anti-stiction coating |
| SAW | surface acoustic wave filters: passive electrical component for signal processing (filtering, delaying) based on the interference/wave propagation of transversal or shear acoustic waves on the surface of a piezoelectric crystal substrate |
| SEM | scanning electron microscope: high resolution microscope based on an electron beam scanning the sample surface; in MEMS used to examinate micromachined structures |
| SiN | silicon nitride |
| $SiO_2$ | silicon dioxide |
| SMD | surface mounted devices: technology for surface mounting of devices in standard packages on printed circuit boards |
| SMR | solidly mounted resonator: thin film transversal-mode bulk acoustic wave (BAW) resonator similar to →FBAR, does not need a freestanding film, since it is based on reflecting films acoustically isolating from the substrate |

SOC system on a chip: microsystem components of different types (e.g. MEMS and CMOS circuits) are integrated on a chip, requires compatibility in the fabrication processes and a comparable yield, but leads to a more compact system and simpler first-level packaging than the →SiP approach.

SOI silicon on insulator: wafer consisting of a thick bulk silicon, a thin silicon dioxide isolation layer and a silicon device layer; used for RF CMOS and for MEMS fabrication

SOP (1) system on a package: microsystem components of different types (RF circuits, MEMS, CMOS logic) are fabricated on different wafers, diced and the chips integrated in a single package. This approach, in contrast to →SOC, is not restricted in terms of process compatibility and allows the optimum available technology for each sub-system, but involves interconnection problems and leads to a larger, more complicated package. The term SiP (system in package) is used synonymously and is more correct than the circumscription SOP, but the latter is more commonly used.

SOP (2) small outline package: industry standard package for surface mounted devices (SMD) on printed circuit boards (→PCB)

SPDT single pole double through: relay type characterized by its signal switching path: a single input is switched to one of the two outputs

SPST single pole single through: relay type characterized by its signal switching path: a single input is switched to a single output

SRF self resonance frequency, measured to characterize the high frequency behavior of passive components

SSR solid state relay: electronic relay for high current and high isolation voltage applications, based on →FET or bipolar transistors

TMAH tetramethyl ammonium hydroxide, a crystal-orientation dependent etchant of silicon typically allowing for smoother etch walls than →KOH

VCO voltage controlled oscillator

W2W 0-level packaging by wafer to wafer bonding/encapsulation

*S-parameters:* n-by-n matrix whose elements fully characterize a linear electrical network with n ports

*0-level packaging:* synonym to →wafer-level packaging

*all-metal switch:* electrostatic switch design without isolation layers between the electrodes; eliminates dielectric charge trapping causing failure due to electrostatic stiction; distance keeping bumps are used instead of a full covering isolation layer

*cold-switching:* term used in the lifetime (switching cycles) determination of MEMS metal-contact switches: the switching operation is carried out without electrical load; opposite: →hot-switching

*dry etching:* etching process based on a plasma with reactive chemical and/or ionic components, in contrast to chemical solutions used in wet etching.

*gyro:* rotational sensor based on an angular vibrating structure converting an external tilting force perpendicular to the rotation axis to a precession moment in the plane perpendicular to both the rotation plane and to the tilting force plane

*hot-switching:* term used in the lifetime (switching cycles) determination of MEMS metal-contact switches: the switching operation is carried out with applied electrical load; opposite: →cold-switching

*in-line switch:* cantilever based series switch with the signal line leading over the cantilever and also used as an electrode for the switch actuation; the electrical potentials of the actuation mechanism and the signal path are not isolated and the signal line is only interrupted by one gap in the off-state

*kapton:* flexible polyimide material with especially good performance in applications for very high (400 °C) and very low (-269 °C) temperature extremes. Kapton has been used for about 35 years in a wide variety of applications such as substrates for flexible printed circuits, transformer and capacitor insulation and bar code labels

*microsystem:* small scale, integrated system consisting of different components with data processing and interface functions, such as microelectronic circuits, electrical interfaces, transducers, MEMS actuators

*plasma etching:* →dry etching

*polysilicon:* silicon made up of regions, so-called grains, of crystalline material, with each grain being oriented differently from the neighboring grain. The interface between the regions is called a grain boundary. The main deposition process is →CVD

*pyrex:* glass type used as microsystem substrate with special etching properties and matched →CTE to silicon

*quasi-static modeling:* time-dependent description of a system by discrete time steps with the system being stable at each single step calculated by finding an equilibrium of the different kinds of potential energy in the system, not taking into account the dynamic behavior caused by the inertia of the involved energy stores

*step coverage:* many thin-film deposition techniques result in a very uniform layer on flat, horizontal surfaces. However, slopes or vertical walls are not

covered very well. The ratio between the thickness of the sidewall deposited layer to the thickness of the layer on the horizontal surface is called the step coverage factor.

*thermoplastic polymer:* polymer material which can be remelted many times when heated up above the melting temperature and returning to the rigid state, when cooled down below the melting temperature

*thermoset polymer:* polymer material which does not remelt, once fully cured

*wafer-level packaging:* packaging of the devices on the wafer before separation by dicing e.g.

*wafer-scale packaging:* packaging on wafer-level by full-wafer processes such as wafer bonding

# Appendix: Standardized frequency bands

**Table 16.** Standardized frequency bands [295].

| *From 30 Hz up to 300 GHz* | | | |
|---|---|---|---|
| Band designation | abbr. | Frequency | Wavelength |
| extremely low-frequency | ELF | 30 Hz...300 Hz | 10 Mm...1 Mm |
| voice-frequency | VF | 300 Hz...3 kHz | 1 Mm...100 km |
| very low frequency | VLF | 3 kHz...30 kHz | 100 km...10 km |
| low-frequency | LF | 30 kHz...300 kHz | 10 km...1 km |
| medium-frequency | MF | 300 kHz...3 MHz | 1 km...100 m |
| high-frequency | HF | 3 MHz...30 MHz | 100 m...10 m |
| very high-frequency | VHF | 30 MHz...300 MHz | 10 m...1 m |
| ultra high-frequency | UHF | 300 MHz...3 GHz | 1 m...10 cm |
| super high-frequency | SHF | 3 GHz...30 GHz | 10 cm...1 cm |
| extremely high-frequency | EHF | 30 GHz...300 GHz | 1 cm...1 mm |
| *At 1 GHz and above* | | | |
| Band designation | | Frequency | Wavelength |
| L band | | 1 GHz...2 GHz | 30 cm...15 cm |
| S band | | 2 GHz...4 GHz | 15 cm...7.5 cm |
| C band | | 4 GHz...8 GHz | 7.5 cm...3.75 cm |
| X band | | 8 GHz...12 GHz | 3.75 cm...2.5 cm |
| Ku band | | 12 GHz...18 GHz | 2.5 cm...1.67 cm |
| K band | | 18 GHz...26.5 GHz | 1.67 cm...1.13 cm |
| Ka band | | 26.5 GHz...40 GHz | 1.13 cm...7.5 mm |
| Q band | | 32 GHz...50 GHz | 9.38 mm...6 mm |
| U band | | 40 GHz...60 GHz | 7.5 mm...5 mm |
| V band | | 50 GHz...75 GHz | 6 mm...4 mm |
| W band | | 75 GHz...100 GHz | 4 mm...3.33 mm |

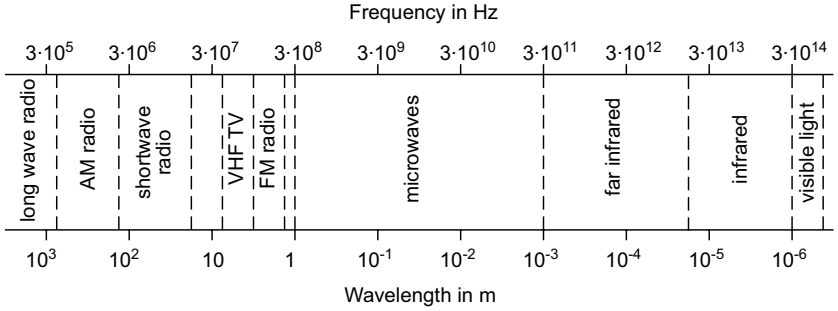


**Figure 49.** Typical frequency bands.

# Paper reprints

# Paper 1

**Selective Wafer-Level Adhesive Bonding with Benzocyclobutene for Fabrication of Cavities**

*Joachim Oberhammer*, Frank Niklaus, and Göran Stemme

Sensors and Actuators A: Physical, vol. 105, no. 3, pp. 297–304, July 2003.

Available online at www.sciencedirect.com
SCIENCE DIRECT®
Sensors and Actuators A 105 (2003) 297–304
SENSORS AND ACTUATORS A PHYSICAL
www.elsevier.com/locate/sna

# Selective wafer-level adhesive bonding with benzocyclobutene for fabrication of cavities

J. Oberhammer*, F. Niklaus, G. Stemme

*Microsystem Technology, Department of Signals, Sensors and Systems, Royal Institute of Technology (KTH), SE-10044 Stockholm, Sweden*

Received 15 July 2002; received in revised form 28 March 2003; accepted 24 April 2003

**Abstract**

In this work we describe an adhesive wafer-level bonding technique in which the adhesive material is structured prior to bonding. This technique can be used to create encapsulated cavities of different heights and sizes for surface micromachined devices directly in the bonding layer. Benzocyclobutene (BCB) was used as the adhesive bonding material. The structuring of the BCB was done either by dry etching or by using photosensitive BCB. The process parameters needed to achieve a high bond quality while retaining the shapes of the structures in the intermediate bonding layer have been investigated extensively. Both dry-etch and photosensitive BCB were found to be suitable for selective adhesive bonding. The dry-etch BCB must be soft-baked to a polymerisation degree of 50–60% to both withstand the patterning procedure and to be sticky enough for the following bonding. Soft-baking is not necessary for the photosensitive BCB. For both types of BCB, good bond results have been achieved with a bonding pressure of 2–3 bar and full curing of the BCB at 250 °C for 1 h. Furthermore, helium leak tests have been performed to investigate the suitability of selective adhesive bonding for applications with demands on quasi-hermetic seals. Cavities created with this bonding techniques showed a leak rate between $1.4 \times 10^{-8}$ and $4.8 \times 10^{-8}$ kg m$^2$ s$^{-3}$ ($1.4 \times 10^{-7}$ and $4.8 \times 10^{-7}$ mbar l s$^{-1}$), which is 3–10 times higher than the limit of MIL-STD 883E. Therefore, this encapsulation technique does not provide sufficient gas-tightness to fulfill the requirements of hermetic electronic encapsulations.


*Keywords:* Adhesive bonding; BCB; Selective bonding; Helium leak tests; Wafer-level encapsulation

## 1. Introduction

A variety of wafer-bonding methods exists in the fields of microsystem packaging, compound wafer fabrication and wafer transfer fabrication. Some common methods are anodic bonding [1], silicon fusion bonding [2], low-temperature direct bonding [3], surface activated bonding [4] and eutectic bonding [5]. The disadvantages of these techniques are the need for high temperature (silicon fusion bonding), high voltage (anodic bonding) or special surface conditions or preparation (surface activated bonding, low-temperature direct bonding). Eutectic bonding uses low bonding temperatures (370 °C for Au–Si bonds), which make this technique quite suitable for end-process applications. Metal compression bonding at room temperature or temperatures below 200 °C [6] requires high pressure and is therefore not yet suitable for wafer-level bonding. Adhesive wafer bonding [7,8] uses polymers or inorganic adhesives as intermediate bonding material. The advantages and disadvantages of adhesive bonding methods [9,10] are listed briefly in Table 1. The material used for the tests presented in this work is divinylsiloxane bisbenzocyclobutene (BCB), a silicon-containing, epoxy-based thermoset polymer which is widely used in electronics due to its superior electrical, mechanical and thermal properties. This includes properties such as a high level of planarization, low moisture uptake, rapid thermal curing, high thermal stability, high solvent resistance and a low dielectric constant over a wide spectrum [11–16]. Adhesive bonding with BCB has been used for void-free wafer bonding [9], to fabricate flow channels, for protective sealing of structures [17] and to transfer structures or films from one wafer to another [18]. In those applications, the BCB was unpatterned and completely uncured before the bonding procedure, which leads to a high bond strength. The fabrication of three-dimensional MEMS structures by bonding structures with photo-patterned BCB has recently been presented [20]. The bonding of patterned polyimide to unpatterned polyimide layers to create microfluidic channels has been published in [19]. As shown in [9], the outgasing of polyimide materials during the final hard-baking of the material which is done during the bonding process, leads to voids and therefore low bond quality.

* Corresponding author. Tel.: +46-8-790-6250; fax: +46-8-100-858.
*E-mail address:* joachim.oberhammer@s3.kth.se (J. Oberhammer).

0924-4247/$ – see front matter © 2003 Elsevier B.V. All rights reserved.
doi:10.1016/S0924-4247(03)00202-4

Table 1
Advantages and disadvantages of adhesive bonding

| Advantages | Disadvantages |
|---|---|
| Low bonding temperature (<200 °C possible) | No hermetic seals with organic materials |
| Applicable for various wafer materials, stress reduction due to the elastic properties of the adhesives | Limited long-term stability of most adhesives, especially in harsh environments |
| Compensation of surface nonuniformities by planarisation properties of the intermediate bonding film | Limited temperature stability of many adhesives |
| Simple, low-cost process steps | Lower bonding strengths than metal bonds |

BCB does not have any detectable outgasing during the curing, which could lead to voids in the bond interface [9]. The reason for this is that BCB curing is a purely thermal process which does not involve catalysts [12].

The suitability of dry-etch BCB for patterning and reactive ion etching (RIE) has already been investigated extensively [23]. Common etching gas mixtures are $CF_4/O_2$ and $SF_6/O_2$. Both a "hard mask" with deposited thin films such as silicon nitride [24] and a "soft mask" with photoresist [25] patterning can be used.

Photosensitive BCB is a negative acting photo-imageable polymer which requires a lower number of process steps to achieve a pattern compared to dry-etch BCB. However, the process control is much more difficult [11] and the storage conditions of the chemical are much more limited [22].

In the present paper, the suitability of patterned BCB-layers as intermediate bonding layers to achieve a localized, high-quality selective bond while retaining the structures of the shape in the intermediate bonding layer has been investigated. The main focus of this work is to investigate the process parameters for bonding of dry-etched BCB-layers as well as patterned layers of photosensitive BCB and their influence on the shapes of the structures in the intermediate bonding layer.

Organic polymers such as fluorocarbons, epoxies, and silicones are a few orders of magnitude more permeable to gases and moisture than glasses, ceramics or metals [26]. BCB is an epoxy-based polymer and therefore basically unsuitable for hermetic encapsulation. Hermeticity tests of cavities created by selective BCB-bonding have been carried out according to standardised helium leak test methods, to give a comparable characterisation of the hermeticity of this encapsulation technique.

## 2. Fabrication

CYCLOTENE of the 3022-series from The Dow Chemical Company was used as dry-etch BCB and, CYCLOTENE of the 4000-series as a photosensitive version of the material. The dry-etch BCB can be spun on to achieve thicknesses ranging from 1 to 26 μm, the photosensitive BCB from 2.5 to 40 μm. Both polymers need an additional adhesion promoter to achieve a higher bond strength. AP8000 was used as adhesion promoter for the dry-etch BCB and AP3000 for the photosensitive BCB [21,22].

Silicon wafers (100 mm diameter, 525 μm thickness, P type) were bonded to Pyrex 7740 glass wafers (100 mm diameter, 525 μm thickness) to allow easy visual inspection of the bond quality.

The process flow for both dry-etch and photosensitive BCB is shown in Fig. 1.

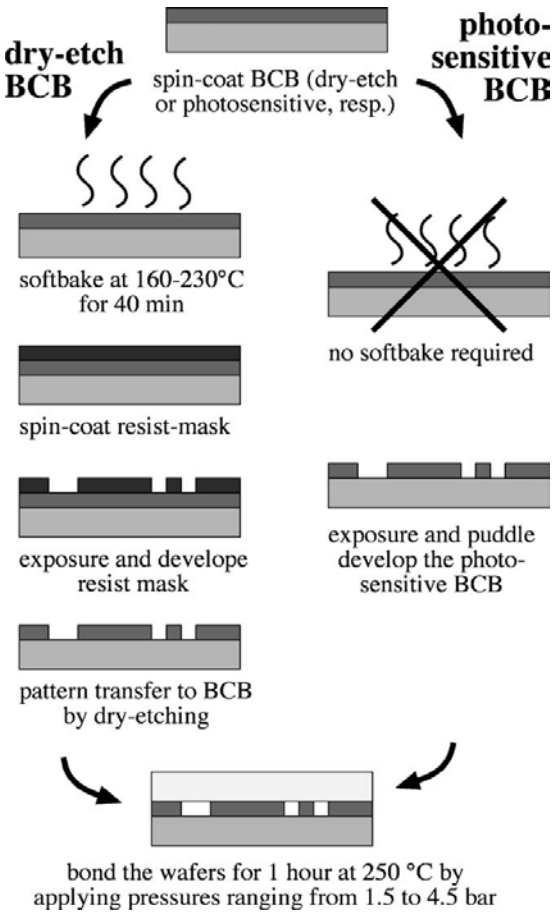


Fig. 1. A schematic view of the process flow.

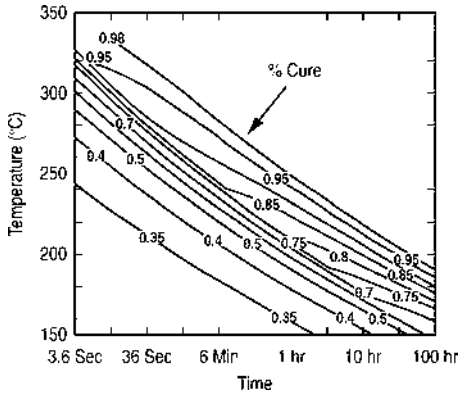


Fig. 2. Curing grade of CYCLOTENE as a function over time and temperature [22].

### 2.1. Selective bonding with dry-etch BCB

We used photoresist soft masks to pattern the dry-etch BCB. The dry-etch BCB was spun onto the silicon substrate after a surface preparation with the adhesion promoter AP8000. The investigated layer thicknesses ranged between 2 and 10 μm. The film must at least be soft-cured to ensure resistance to subsequent processes, in particular the plasma-etching and resist removing procedure. On the other hand, the degree of polymerisation (depending on curing temperature and curing time, see Fig. 2) should not be too high, since a hard-baked BCB film loses its adhesive properties and would not be suitable for bonding anymore. To find the optimum curing temperature, we cured the film at different temperatures ranging from 160 to 230 °C for 40 min (excluding ramping times). Since oxidation of the BCB has an impact on its properties [13] and oxidation occurs at temperatures higher than 150 °C, the soft-baking of the BCB was carried out in a nitrogen atmosphere. Afterwards, the BCB was spin-coated and a layer of resist spun on top (Shipley SPR 5740). The thickness of the resist must be chosen to be of the same order of magnitude as the thickness of the BCB (our etch process recipe has an etch selectivity of 1.3:1 of photoresist to BCB). After doing the resist lithography, reactive ion etching was used to transfer the pattern to the BCB coating. Our plasma etch process in a hexa-core cathode RIE-tool (AME 8111 from Applied Material) showed an etch rate of the BCB of 180 nm $min^{-1}$ (10% $CF_4$ in $O_2$, total flow 150 sccm, 600 W RF power, $1.33 \times 10^{-4}$ bar chamber pressure). Finally, the remaining resist was removed in acetone.

The glass wafers were bonded onto the silicon wafers covered with BCB-structures in a commercially available substrate bonder SB6 from Karl Suss. First, the wafers were joined in a vacuum atmosphere of $1.0 \times 10^{-4}$ mbar. Both top and bottom chucks of the bonder were heated up to 250 °C for 1 h to hard-bake the BCB while applying the chuck-tool pressure. The temperature, chuck pressure and chamber pressure profile over time are shown in Fig. 3.

### 2.2. Selective bonding with photosensitive BCB

The BCB was spun onto silicon wafers after surface preparation with the adhesion promoter AP3000. Then, the wafers were exposed with broadband UV-spectrum using a Karl Suss Mask Aligner MA6. The exposure rate was 110 mJ $cm^{-2}$ per micrometer of BCB thickness. After pre-development hotplate baking, the development of the photosensitive material was performed directly on the spinner by using the DS2001 developer from The Dow Chemical Company (see http://www.dow.com and http://www.cyclotene.com). This so-called "puddle-development

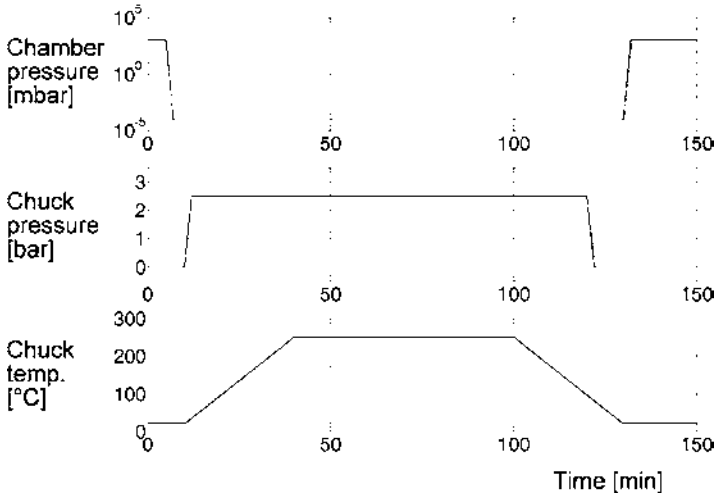


Fig. 3. Chamber pressure, chuck pressure and temperature during bonding as a function over time (for 2.5 bar chuck pressure).

technique" [22] consists of dispensing a puddle of developer onto the exposed substrate during slow rotation of the spinner and in a rinse and dry spin of the wafer afterwards. A brief descum in $O_2/CF_4$-plasma to remove polymer residues left behind in the development, completes the process. No soft-curing of the BCB layer was carried out after the lithography.

For bonding, the same procedure as with the dry-etch BCB was carried out.

## 3. Bonding results

We used two different methods characterising the bond interface. The first method consists of a visual characterisation. Here, the bond interface was directly observed through the covering glass wafer. Bonded areas can easily be distinguished from non-bonded areas, as illustrated in Fig. 4. Another advantage of using a glass wafer as a covering wafer is that the shape deformation of the structured intermediate bonding layers can also be observed through the glass wafer.

The second method to characterise the bond quality is to split the bonded wafer. That was done by inserting a razor blade in between the two wafers to push them apart. This method is very dependent on the subjective assessment of the operator and provides only a qualitative estimate of the bond strength [9]. Using this test on successfully bonded wafers with patterned BCB revealed that the bond interface could not be completely separated without cracking the glass wafer. This could be observed for both the dry-etch and the photo-sensitive material. It should be mentioned that only a few BCB residues were left on the pieces of the glass wafers after doing the test, implying that the bond interface is weaker than the strength of fully cured BCB of about 70–85 MPa [15,18].

Due to the consistency of the soft-cured BCB only a small volume deformation of the structures in the layer could be observed. The main reason for this is the shrinking of the polymer during the hard-curing during the bonding procedure, since the patterning was done in the soft-cured state of the material. The final bonding layer thickness corresponds to the thickness of the cured BCB, depending on the type of BCB and the spinning speed [21,22]. The shrinkage of BCB also changes the feature dimensions, e.g. structures with a width of 40 μm shrank to 35 μm, and feature gap

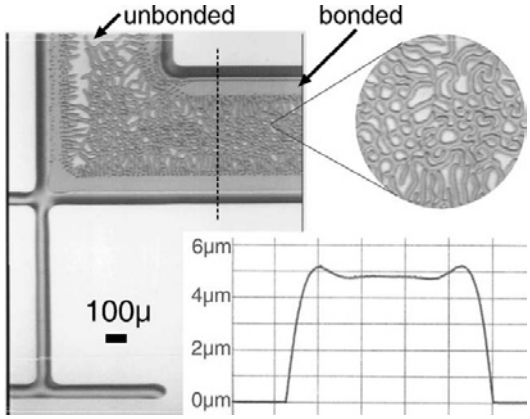


Fig. 4. Incomplete bond due to surface nonuniformity of the patterned intermediate bonding layer with the corresponding pre-bonding surface profile (soft-cure temperature 190 °C, bonding pressure 2.5 bar).

distances of 6 μm were stretched to 9 μm. The shapes of the structures in the polymer layer were retained very well throughout the whole process. This can be seen in Fig. 5(b) (thickness of the BCB-layer 4.7 μm, soft-cure temperature 200 °C, dry-etched, bonding pressure 2.5 bar).

The process parameters that were expected to have the highest influence on the bonding results, are (1) polymerisation degree of the dry-etch BCB before bonding; (2) the chuck pressure during bonding; (3) final hard curing parameters during bonding; and (4) the surface uniformity of the BCB layer before bonding.

The impact of these parameters on the bond quality of dry-etch BCB is discussed extensively in Section 3.1. The significant differences and similarities between photosensitive BCB and dry-etch BCB are discussed in Section 3.2. A compact overview of the influences of the process parameters on the bond quality is summarised for the dry-etch BCB and for the photo-patternable BCB in Tables 2 and 3, respectively.

### *3.1. Influence of process parameters on the bond interface with dry-etch BCB*

#### *3.1.1. Soft-curing parameters*

A standard soft-curing process, recommended by the supplier of the material [21], suitable for additional surface

Table 2
Influence of the process parameter on the bond quality of dry-etch BCB

| Parameter | Grade of influence | Suitable value |
|---|---|---|
| BCB soft-bake degree | Strong influence | 50–60% polymerisation ≈190–200 °C for 30 min |
| Surface uniformity | Strong influence | Standard spin-coating procedure onto flat surface is sufficient |
| Bonding pressure | Small influence | 2.5 bar |
| Hard-curing parameters | No influence | All tested time-temperature combinations leading to 99% polymerisation degree showed same bond quality. 250 °C for 1 h is recommended as standard curing procedure |

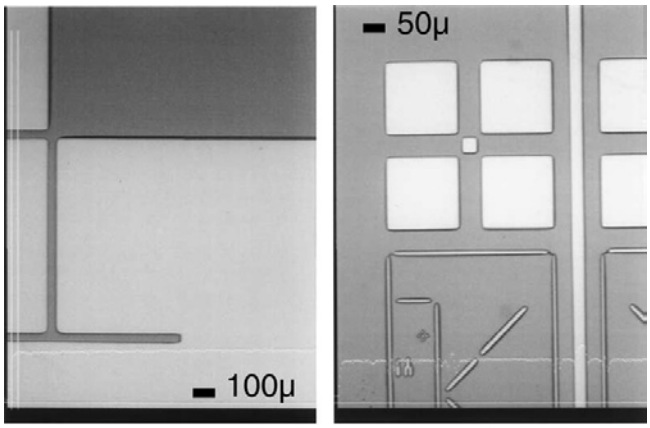


Fig. 5. Homogeneous bond of dry-etch BCB (dark areas): (a) same structures as in Fig. 4; (b) test structures and enclosed micro cavities (white squares). All structures show complete bonding to the top glass wafer (soft-cure temperature 200 °C, bonding pressure 2.5 bar).

Table 3
Influence of different process parameters on the bond quality of photosensitive BCB

| Parameter | Grade of influence | Suitable value |
|---|---|---|
| BCB soft-bake degree | NA | NA |
| Surface uniformity | Strong influence | Rough surface of the BCB after developing has to be smoothed by a brief descum-etch |
| Bonding pressure | Small influence | 2.0–2.5 bar |
| Hard-curing parameters | No influence | All tested time-temperature combinations leading to 99% polymerisation degree showed same bond quality. 250 °C for 1 h is recommended as standard curing procedure |

machining on top of the BCB layer, is 210 °C for 40 min (corresponding to a polymer conversion of about 75%). We have performed soft-curing at various temperatures ranging from 160 °C for 40 min (corresponding to a polymerisation degree of 35%) and 230 °C for 40 min (corresponding to 85% polymerisation). We found that soft-curing temperatures below 180 °C for 40 min (corresponding to less than 50% polymerisation) does not cure the polymer well enough for it to withstand the following processes. The structures in the intermediate bonding layer completely lose their shape during the bonding even though the bond attains a high-quality bond interface (see Fig. 6: (a) corresponds to the shape of the structures shown in Fig. 5(a)). Temperatures above 210 °C cure the BCB too much, so

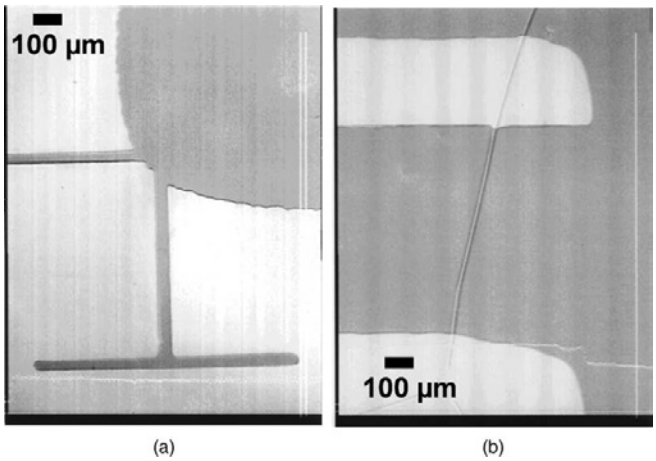


Fig. 6. Dry-etched BCB, soft-cured at temperatures below 180 °C, the shapes of the patterned structures are not retained due to insufficient consistency of the intermediate bonding layer (soft-cure temperature 160 °C, bonding pressure 2.5 bar).

that the material is not soft and sticky enough to achieve a strong bond, even though a pressure of up to 4.5 bar was applied between the two chucks of the bonding tool. The suitable soft-baking temperature range for our purpose was found to be between 190 °C to 210 °C for a time of 30 min, corresponding to a polymerisation degree of 50–60%.

#### 3.1.2. Chuck pressure

The influence of the chuck pressure in the bond tool was smaller than expected. We tested pressures ranging from 1.5 to 4.5 bar. Pressures above 2.5 bar significantly increased the risk for wafer cracks and did not lead to a higher bond quality. Lower pressure bonds (1.5 bar) had a slightly lower bond quality than bonds performed at 2.5 bar, in that the bond interface was not uniform over the entire wafer surface.

#### 3.1.3. Hard-curing parameters

The BCB was hard cured during the bonding and led to a polymerisation degree of 99% (1 h baking at 250 °C, compare Fig. 2). The different temperature–time combinations of the hard-baking which lead to the same polymerisation degree have impact on the internal stress of the material since different end temperatures of the curing cycle are used [14,15]. The hard-baking temperature cycle shown in Fig. 3 was used for most of the bonded structures in this work. Extending of the time, which allows a slightly lower vitrification temperature (compare Fig. 2), did not produce different bonding results. A rapid thermal curing (RTC, e.g. at 300 °C for a couple of seconds [15]) could not be carried out since our substrate bonding tool does not allow the fast heating and cooling ramps of both of the bond chucks.

#### 3.1.4. Surface uniformity

The surface uniformity of the BCB before the bonding procedure is a significant factor for the bond quality. Soft-cured BCB which retains the shapes of the structures is not soft enough to compensate for local surface nonuniformities in dimensions of 0.1–0.2 μm (BCB-layer thickness: 5 μm). Due to an error in the lithography (unintentional overetch of the BCB which transferred the pattern of shrunk thick resist to the BCB), we got some samples with a very nonuniform surface profile after patterning, which is shown in Fig. 4. However, these structures were used to investigate the sensitivity of the bonding procedure to surface nonuniformities. The bonding result shows an incomplete bond (Fig. 4, parameters: soft-cure temperature 190 °C for 30 min, bonding pressure 2.5 bar). Higher chuck pressures have also been used but did not result in a more homogeneous bond and therefore do not compensate for surface nonuniformities. Furthermore, the wafers crack at pressures above 4–5 bar.

A high quality surface flatness of the intermediate layer before the bonding results in good bonding of large areas. The results of such a bond are shown in Fig. 5 (the dark areas are the bonded structures). BCB spun onto a flat surface is planar enough to achieve a high bond quality. The planarisation ability of BCB is very good [12,16]. However, if the BCB layer is spun onto structured surfaces the resulting surface nonuniformity must be considered.

### 3.2. Evaluation of the photosensitive BCB bond interface

Photosensitive BCB retains the shape of its patterned structures equally well as the dry-etch BCB, even though soft-curing before the bonding is not necessary for this material. This is because the photosensitive BCB is already crosslinked to about 55% after the patterning with photolithography.[1] This polymerisation degree is high enough to retain the shapes of the polymer during the bonding and corresponds to the minimum soft-curing degree of the dry-etch BCB which we found to be necessary for bonding. The bond quality was comparable to the dry-etch BCB and good results could be achieved at bond pressures of 2–2.5 bar. The sensitivity of photosensitive BCB to surface nonuniformities was comparable to that of dry-etch BCB. The surface of the photosensitive material after developing is quite rough, and a brief etch in $O_2/CF_4$-plasma was used to create a smoother surface and produce better bonding results. This brief descum also removes the thin film of polymer residues left behind in the development process [22].

Prior research has shown that dry-etch BCB does not outgas during the curing process [12] and is therefore suitable for adhesive bonding processes where gases deriving from catalysts could create voids in the bonding interface [9]. The current literature does not provide information on whether photosensitive components of the photosensitive BCB outgas during the curing either. However, since no void formation in the bonding interface of photosensitive BCB could be observed in this work, it is either nonexistent or negligible.

## 4. Hermeticity tests

To measure the degree of hermeticity of cavities created by the selective BCB bonding method presented in this article, we performed helium leak tests based on test specifications of the MIL-STD-883E, method 1014.10: Seal, test conditions A1 [27]. This standard is widely accepted in quality control of electronics production. The sample cavity volume was 0.95 $mm^3$ (19 mm long, 10 mm wide, 5 μm high) and the surrounding BCB sealing ring was 5 μm high and 1.1 mm wide. The samples were exposed to helium at 5.2 bar for 2 h. After exposure, the helium flow out of the cavity through the polymer (the penetration through the silicon and the glass can be neglected) was measured with a ASM 142 Helium Leak Detector from ALCATEL, using the mass detection principle. The helium flow of the samples was measured 10 min and 60 min after the exposure and is illustrated

[1] Information from The Dow Chemical Company.

Table 4
Helium leak test results of cavities with size of 0.8 mm$^3$, encapsulated with a 110 μm wide and 5 μm high BCB ring by selective adhesive bonding

| Time after He exposure (min) | Helium leak rate (kg m$^2$ s$^{-3}$) |
|---|---|
| 10 | $4.2 \times 10^{-8}$ to $4.8 \times 10^{-8}$ |
| 60 | $1.4 \times 10^{-8}$ to $2.0 \times 10^{-8}$ |

The limit regarding MIL-STD-883E [27] is $5 \times 10^{-9}$ kg m$^2$ s$^{-3}$ ($5 \times 10^{-8}$ mbar l s$^{-1}$); the helium exposure was 5.2 bar for 2 h.

in Table 4. The limit to pass the leak test defined by the MIL-STD-883E is $5 \times 10^{-9}$ kg m$^2$ s$^{-3}$ ($5 \times 10^{-8}$ mbar l s$^{-1}$). The cavities encapsulated with this technique did not meet the requirements of the test standard, which is an expected result due to the high permeability of polymers. The test results correspond to a moisture penetration through the polymer which leads to an equilibrium of humidity in the encapsulation to the ambient after 5–20 days (ambient conditions: 25 °C, 70% RH; [26], p. II-887).

## 5. Conclusions

Wafer-level bonding with structured BCB as an intermediate bonding layer has been investigated. Both dry-etch BCB and photosensitive BCB were proven to be suitable for this purpose. Due to the high demands on the resistance of dry-etch BCB to subsequent patterning procedures (plasma etch), a certain degree of pre-baking of the material is necessary. This soft-baking treatment should not be too high, thereby avoiding any degradation of the polymer's adhesive abilities. For both types of the material the bonding quality depends on the surface flatness of the polymer film before bonding. Higher chuck pressures do not compensate for high surface nonuniformities in the range of tenths of micrometers. Patterned structures with a feature size in the same order of magnitude as the polymer thickness withstand the bonding process without losing their shapes. Possible applications for this technique are the fabrication of channels and structures for microfluidic systems, the creation of microcavities or wafer-level encapsulation. Helium leakage tests of cavities created by selective bonding have shown that BCB is not hermetic enough to provide sufficient gas tightness for MEMS applications with a strictly controlled atmosphere and does not sufficiently withstand moisture penetration for use in various MEMS and electronic applications.

## Acknowledgements

The cooperation with Ericsson Microelectronics AB, in whose facilities we could carry out the helium leak tests, is gratefully acknowledged. Special thanks are dedicated to Katarina Boustedt, Göran Palmskog and Björn Hygrell. The authors would also like to thank Albert Achen from The Dow Chemical Company, who provided us with information about the BCB during helpful discussions.

## References

[1] E. Obermeier, Anodic wafer bonding, Proc. Semicond. Wafer Bonding: Sci. Technol. Appl. 95–97 (1994) 212–220.
[2] J.B. Lasky, S.R. Stiffler, F.R. White, J.R. Abernathy, Silicon on insulator (SOI) by bonding and etch-back, in: Proceedings of the International Electron Devices Meeting, 1985, pp. 684–687.
[3] Qin-Yi Tong, Low temperature wafer direct bonding, J. Microelectromech. Syst. 3 (1) (1994) 29–35.
[4] H. Takagi, K. Kikuchi, R. Maeda, T.R. Chung, T. Suga, Surface activated bonding of silicon wafers at room temperature, Appl. Phys. Lett. 68 (16) (1996) 2222–2224.
[5] R.F. Wolffenbuttel, Low-temperature intermediate Au–Si wafer bonding: eutectic or silicide bond, Sens. Actuators A 62 (1997) 680–686.
[6] A. Singh, D. Bilic, R.T. Howe, Performance evaluation of batch-transferred surface micromachined resonators, Proc. Transducers 99 (1999) 1158–1161.
[7] D.E. Booth, C.E. Hunt, Low temperature adhesion bonding methods, in: Proceedings of the Symposium on Semiconductors Wafer Bonding, Phys. Appl. 3 (1995) 201–211.
[8] W.P. Eaton, S.H. Risbud, R.L. Smith, Silicon wafer-to-wafer bonding at $T < 200$ °C with polymethylmethacrylate, Appl. Phys. Lett. 65 (4) (1994) 439–441.
[9] F. Niklaus, P. Enoksson, E. Kälvesten, G. Stemme, Low-temperature full wafer adhesive bonding, J. Micromech. Microeng. 11 (2001) 1–8.
[10] W.M. Alvino, Plastics for Electronics: Materials, Properties and Design Applications, McGraw-Hill, New York, 1994.
[11] A.J.G. Strandjord, W.B. Rogers, Y. Ida, R.R. DeVeillis, S. Shiau, E.S. Moyer, D.M. Scheck, P.E. Garron, Photosensitive benzocyclobutene for stress-buffer and passivation applications, in: Proceedings of the Electronic Components and Technology Conference, vol. 47, 1997, pp. 1260–1268.
[12] P. Garrou, Polymer dielectrics for multichip module packaging, Proc. IEEE 80 (12) (1992) 1942–1954.
[13] D. Burdeaux, P. Townsend, J. Carr, P.E. Garrou, Benzocyclobutene (BCB) dielectrics for the fabrication of high density, thin film multichip modules, J. Electron. Mater. 19 (1990) 1357–1366.
[14] J. Strandberg, H. Thiede, A. Karlsson, P. Bodo, J. Haglund, S. Valizadeh, A. Weiland, Versatile multilayer MCM-D structure for high reliability applications, IEEE Trans. Comp. Packaging Manufacturing Technol. B 20 (3) (1997) 327–333.
[15] P.E. Garrou, R.H. Heistand, M. Dibbs, T.A. Manial, C. Mohler, T. Stokich, P.H. Townsend, G.M. Adema, M.J. Berry, L. Turlik, Rapid thermal curing of BCB dielectric, IEEE Trans. Comp. Packaging Manufacturing Technol. 16 (1) (1993) 46–52.
[16] P.B. Chinoy, Processing and microwave characterization of multilevel interconnects using benzocyclobutene dielectrics, Trans. Comp. Hybrids, Manufacturing Technol. 16 (7) (1993) 714–719.
[17] F. Niklaus, H. Andersson, P. Enoksson, G. Stemme, Low temperature full wafer adhesive bonding of structured wafers, Sens. Actuators A 92 (2001) 235–241.
[18] F. Niklaus, P. Enoksson, P. Griss, E. Kalvesten, G. Stemme, Low-temperature wafer-level transfer bonding, J. Microelectromech. Syst. 10 (4) (2001) 525–531.
[19] I.K. Glasgow, D.J. Beebe, V.E. White, Design rules for polyimide solvent bonding, Sens. Mater. 11 (5) (1999) 269–278.
[20] T.-K.A. Cou, K. Najafi, 3D MEMS fabrication using low-temperature wafer bonding with benzocyclobutene (BCB), Proc. Transducers 11 (2001) 1570–1573.

[21] The Dow Chemical Company, Processing Procedures for Dry-Etch CYCLOTENE Advanced Electronics Resins (Dry-Etch BCB), 1997, p. 3.
[22] The Dow Chemical Company, Processing Procedures for Cyclotene 4000 Series Photo BCB Resins, 1999, p. 8.
[23] P.B. Chinoy, Reactive ion etching of benzocyclobutene polymer films, Trans. Comp. Packaging Manufacturing Technol. C 20 (3) (1997) 199–207.
[24] M. Schier, Reactive ion etching of benzocyclobutene using a silicon nitride dielectric etch mask, J. Electrochem. Soc. 142 (9) (1995) 266.
[25] M.J. Berry, P. Garrou, B. Rogers, I. Turlik, Soft mask for via patterning in BCB dielectric, Int. J. Microcircuits Electron. Packaging 17 (1994) 210.
[26] R.R. Tummala, Microelectronics Packaging Handbook. Part 2. Semiconductor Packaging, second ed., Kluwer Academic Publishers, Boston, MA, 1999, pp. 873–930.
[27] MIL-STD-883E, Method 1014.10: Seal, US Department of Defense, 1996, pp. 72–83.

## Biographies

*Joachim Oberhammer* was born in Bruneck, Italy, on 13 April 1976, received his MSc degree in electrical engineering, specialisation in measurement technology, from the University of Technology Graz, Austria, in 2000. He has been working with automotive electronics and RF identification systems both at the University of Technology Graz and Vienna University of Technology, before he joined the Microsystem Technology group at KTH as PhD student in March 2001. Here, his research focus lies in RF MEMS and wafer-level packaging of MEMS components.

*Frank Niklaus* was born in Malsch, Germany, on 24 March 1971. He received his MSc degree in mechanical engineering in 1998 from the Technical University of Munich (TUM), Germany. Presently he is a graduate student in the Silicon Sensor Research Group at the Department of Signals, Sensors & Systems at the Royal Institute of Technology, Stockholm, Sweden. His research interest is in the field of silicon sensor and actuator technology, especially adhesive wafer bonding and infrared detectors.

*Göran Stemme* was born in Stockholm, Sweden, on 4 February 1958. He received his MSc degree in electrical engineering in 1981 and the PhD degree in solid state electronics in 1987, both from the Chalmers University of Technology, Gothenburg, Sweden. In 1981, he joined the Department of Solid State Electronics, Chalmers University of Technology, Gothenburg, Sweden. There, in 1990, he became an Associate Professor (Docent) heading the silicon sensor research group. In 1991, Dr Stemme was appointed Professor at the Royal Institute of Technology, Stockholm, Sweden. He heads the Instrumentation Laboratory at the department of Signals, Sensors & Systems. His research is devoted to sensors and actuators based on micromachining of silicon. Dr Stemme is a Subject Editor for the *IEEE/ASME Journal of Microelectromechnical Systems*.

# Paper 2

**Sealing of Adhesive Bonded Devices on Wafer Level**

*Joachim Oberhammer*, Frank Niklaus, and Göran Stemme

Sensors and Actuators A: Physical, vol. 110, no. 1–3, pp. 407–412, Feb. 2004.

Available online at www.sciencedirect.com
SCIENCE DIRECT®
Sensors and Actuators A 110 (2004) 407–412
SENSORS AND ACTUATORS A PHYSICAL
www.elsevier.com/locate/sna

# Sealing of adhesive bonded devices on wafer level

J. Oberhammer*, F. Niklaus, G. Stemme

*Department of Signals, Sensors and Systems, Microsystem Technology, Royal Institute of Technology (KTH), SE-10044 Stockholm, Sweden*

Received 20 September 2002; received in revised form 3 June 2003; accepted 10 June 2003

**Abstract**

In this paper, we present a low temperature wafer-level encapsulation technique to hermetically seal adhesive bonded microsystem structures by cladding the adhesive with an additional diffusion barrier. Two wafers containing cavities for MEMS devices were bonded together using benzocyclobutene (BCB). The devices were sealed by a combined dicing and self-aligning etching technique and by finally coating the structures with evaporated gold or PECVD silicon nitride. The sealing layer was inspected visually by SEM and helium leak tests were carried out. Devices sealed with silicon nitride and with known damage of the sealing layer showed a helium leak rate of about 7–14 times higher than the background level. Devices of the same size without damage in the sealing layer had a leak rate of only 1.5 times higher than the background level. Experiments with evaporated gold as cladding layer revealed leaking cracks in the film even up to a gold thickness of 5 μm. The sealing technique with silicon nitride shows a significant improvement of the hermeticity properties of adhesive bonded cavities, making this bonding technique suitable for applications with certain demands on gas-tightness.


*Keywords:* Hermetic sealing; Wafer-level encapsulation; Adhesive bonding; Benzocyclobutene

## 1. Introduction

MEMS devices need to be encapsulated in microcavities to either preserve their functionality in cases where they have certain demands on the atmosphere (accelerometers, resonators, absolute pressure reference), or to protect them from contamination or damage during the subsequent packaging process steps. Therefore, the encapsulation of such cavities containing the MEMS devices already on wafer level is an advantage since costs for the handling of the diced devices are reduced and the yield is improved.

Common wafer-bonding encapsulation techniques in MEMS are anodic bonding of both silicon to glass [1] and of glass to glass wafers [2], and direct silicon wafer bonding [3]. These bonding techniques provide a high and reliable gas-tightness and good control over the encapsulated atmosphere, which can be chosen with a high degree of independency in pressure and composition. All these techniques are mainly used to encapsulate bulk micromachined devices since special surface demands have to be fulfilled. Electrical interconnections to the device, by maintaining the hermeticity, are difficult to achieve and increase the cost and complexity [4]. Furthermore, in the case of anodic bonding, a high voltage is needed which is often not compatible with the devices to be sealed. Direct bonding techniques involve a special surface preparation and often not allowed high-temperature annealing steps (400–1200 °C) after the bonding. Glass to glass direct bonding provides efficient gas-tightness after an annealing step of 250 °C only [5], but glass technology is much more limited in terms of fabrication methods than micromachining in silicon substrates.

Another sealing technology uses chemical vapor deposition (CVD) methods with silicon dioxide or silicon nitride films which close the etch access channels after having removed the sacrificial layer [6,7]. The atmosphere inside the cavity cannot be chosen freely since it is determined by the processing gases during the deposition [8] and, unwanted very thin layers in the nanometer range are deposited inside the cavity [9]. It was shown that such films are avoided by using metal evaporation instead of CVD methods.

Eutectic bonding [10], forming an alloy of the involved materials at temperatures much lower than their melting temperatures, is a very promising sealing technique because an integrated low-permeability metal ring is formed, but the temperatures needed are still too high for some applications (e.g. Au–Si: 363 °C). Implemented microheaters in the sealing rings allow the temperature limits to be exceeded locally to form a strong eutectic or fusion bond [11,12]. Though, the fabrication of such heaters and their interconnections adds more process complexity.

* Corresponding author. Tel.: +46-8-790-6250; fax: +46-8-100-858.
*E-mail address:* joachim.oberhammer@s3.kth.se (J. Oberhammer).

0924-4247/$ – see front matter © 2003 Elsevier B.V. All rights reserved.
doi:10.1016/j.sna.2003.06.003

Adhesive wafer bonding [13] uses polymers or inorganic adhesives as intermediate bonding materials. This boding technique is very suitable for non-uniform surfaces, can be carried out at very low temperatures, and is simple to use. Divinylsiloxane bisbenzocyclobutene (BCB, Dow Chemical Company) has already been used as bonding material to fabricate flow channels and for protective sealing of structures [14]. By patterning this material before bonding, either by dry-etching or by using a photosensitive version of BCB, cavities and distance rings have been created successfully in the bonding interface [15,16]. Polymers are by far more permeable to gas and moisture than ceramics or metal sealants [17,18]. The hermeticity of BCB to seal cavities for MEMS devices, has also been investigated and was found not to be sufficient [15,16].

In this paper, we present a technique to seal adhesive bonded structures by cladding the permeable adhesive with an additional diffusion barrier after the bonding procedure. PECVD silicon nitride is a widely used passivation and protective diffusion barrier material in IC processing [19,20]. Furthermore, we investigate evaporated gold films as a diffusion barrier.

Hermeticity tests following the procedure described in MIL-STD-883E, Method 1014.9, are widely used in electronics device packaging. However, the standard test specifications have not been found to be very suitable for MEMS devices with small volume in the nanoliter range [16,21]. For the work presented in this paper, we used helium leak tests for comparative measurements between devices with known or artificially created defects in the cladding layer and successfully sealed devices. Also, gross leak tests specified in MIL-STD-883E and visual inspection of the sealing layer using a SEM have been carried out.

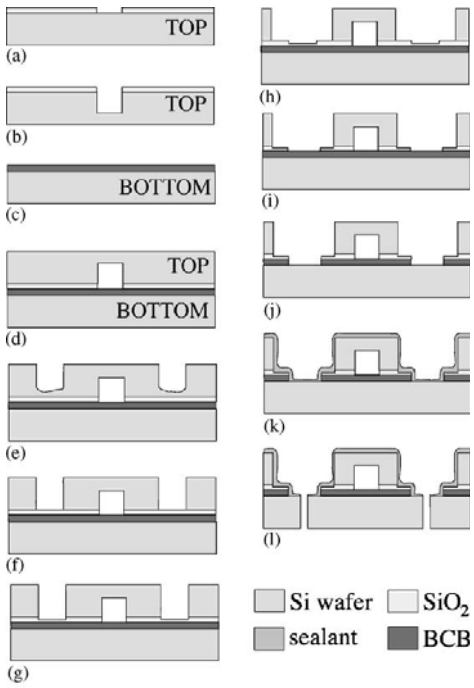


Fig. 1. Fabrication Procedure of the test structures: (a) patterning of thermal grown oxide of the top wafer; (b) DRIE of the cavities; (c) spinning of BCB onto the bottom wafer; (d) bonding of the wafers; (e) dicing of the trenches; (f) DRIE of the trenches; (g) removing of half of the oxide layer thickness in BHF; (h) isotropic DRIE; (i) etching of the oxide; (j) plasma etching of the BCB; (k) deposition of the sealant; (l) dicing of the samples.

## 2. Design and fabrication of the test samples

The fabrication procedure is shown in Fig. 1. A 100 mm diameter, 500 μm thick silicon wafer (top wafer) with previously grown oxide of a thickness of 2 μm was patterned and, cavities with a depth of 90 μm were etched using a deep reactive ion etching (DRIE) tool. BCB 3022-46 from the Dow Chemical Company was spun onto the bottom silicon wafer at a thickness of 2.5 μm. Then, the wafers were bonded together in a commercially available Karl Suss SB6 substrate bonder. During the bonding at a chamber pressure of $10^{-4}$ mbar, both bonding chucks were heated up to 280 °C for 30 min to hard-cure the BCB and a bonding pressure of 2.5 bar was applied. Then, the top wafer was sawed, creating 600 μm wide trenches reaching down to approximately 20–50 μm above the oxide layer of the top wafer. The rest of the trenches down to this oxide layer was etched anisotropically in a DRIE tool. Afterwards, about 1 μm of the 2 μm oxide layer of the top wafer was etched in BHF to create a step in the oxide layer which is necessary to guarantee a good coverage of the sealing layer later on. With an isotropic etch in the DRIE tool, the trenches in the silicon substrate were widened by about 30–50 μm, which uncovers the mentioned step in the oxide. Then, the oxide layer was etched in BHF again to uncover the BCB layer under the oxide layer step. The BCB layer was etched anisotropically in $CF_4/O_2$ plasma. Afterwards, the sealing layer was added by using PECVD $Si_3N_4$ at 300 °C of 0.5 and 1 μm thickness or by evaporating a titanium/gold layer of a thickness of 0.5 μm/4.2 μm. In the metal evaporation tool, the wafer was mounted at an angle of 45° to the direction of the evaporated material and was rotated during the evaporation, which guaranteed a very good step coverage. The process was completed by dicing of the samples. The whole process chain was carried out on wafer level and no process steps with temperature treatment above 300 °C were used. Furthermore, all of the etch steps are self-aligning to the diced grooves in order that no photolithography is necessary.

In Fig. 2, the fabrication technique with the created step in the BCB bonded base of the devices is compared to a straight-down etching technique. The coverage of PECVD silicon nitride in the corner directly underneath the 500 μm thick covering wafer (Fig. 2a) is not good enough for an

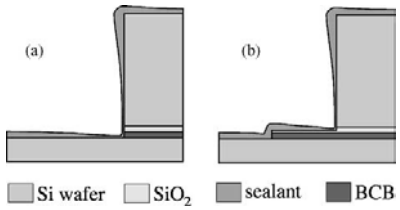


Fig. 2. Fabrication technique without (a) and with the step in the adhesive and oxide layer (b).

Table 1
Sample dimensions

| Sample size no. | Cavity length, width, depth (mm, mm, μm) | Samples | Cavity volume ($mm^3$) | BCB thickness (μm) | Width of BCB ring (mm) |
|---|---|---|---|---|---|
| 1 | 7.5, 7.5, 90 | A, ..., D | 5 | 2.5 | 2.5 |
| 2 | 2.5, 5, 90 | E, ..., L | 1.13 | 2.5 | 1.25 |

efficient sealing. The base step height of about 3 μm leads to a much better coverage by the deposition and thus to a completely closed silicon nitride layer (Fig. 2b).

The dimensions of the two major evaluated sample sizes are summarized in Table 1.

## 3. Hermeticity tests

In the MIL-STD 883E, Method 1014.9 (1995), hermeticity tests consist of a gross leak test and a fine leak test. Gross leaks down to a leak rate of $10^{-4}$ mbar l $s^{-1}$ [18] can be found by using a fluorocarbon bath. Fine leaks are detected by using a helium leak detector measuring the helium flow coming out of a sealed device which was previously exposed to 5.2 bar of helium for 2 h. We used an ALCATEL ASM 142 leak detector with a helium sensitivity of $10^{-11}$ mbar l $s^{-1}$. A single measurement with this device takes about 15 s, including the loading and unloading of the sample. We used the smallest suitable measurement chamber with a size of about 6 $cm^3$ to keep the background helium rate as low as possible and to allow the measured helium flow rate to be stabilized within a few seconds. It should be mentioned that the chamber to pressurize the samples with helium should not be situated in the same room where the measurements take place, to avoid a too high background helium rate.

Jourdain et al. [16] showed that the upper detection limit of such helium leak measurement depends on the sample cavity size and the dwell time between the helium exposure and the measurements. The helium could outgas completely and too fast through a larger leak and would therefore be undetectable after a certain dwell time. The pressure change per time inside the device can be estimated by [21]:

$$\frac{dp(t)}{dt} = \frac{Q(\Delta p)}{V} \quad (1)$$

Table 2
Estimated upper helium leak detection limits for the samples

| Sample size no. | Dwell time (min) | Pressure difference (bar) | Upper detection limit (mbar l $s^{-1}$) |
|---|---|---|---|
| 1 | 2 | 4 | $1.7 \times 10^{-4}$ |
| 1 | 5 | 4 | $6.7 \times 10^{-5}$ |
| 2 | 2 | 4 | $2.9 \times 10^{-5}$ |
| 2 | 5 | 4 | $1.5 \times 10^{-5}$ |

where $Q$ is the leak rate and $V$ is the volume of the device. For a rough estimation of the upper detection limit for a certain volume and dwell time, the leak rate can be assumed to be constant. With this assumption, the upper detection limit for reasonable dwell times of 2–5 min and a pressure difference, $\Delta p$, of 4 bar between the cavity and the environment was estimated and is shown in Table 2. The undefined leak rate regime between the gross and the fine leak test methods for small samples [16] is bridged for the larger type of our samples and very small for the smaller ones, since our sample volumes are 20–100 times larger than the cavities measured by Jourdain et al.

Furthermore, we used a SEM for visual inspection of the sealant on the adhesive layer, allowing us to detect larger cracks down to sub-micron size.

## 4. Test results and discussion

All of the 25 gold samples showed a helium leak rate of $(5–10) \times 10^{-8}$ mbar l $s^{-1}$, 3–5 min after the helium exposure, which even exceeds the limit specified in the MIL standard ($5 \times 10^{-8}$ mbar l $s^{-1}$). Some of these samples failed the gross leak test as well. A visual inspection of such samples in the SEM revealed that relatively large cracks in the adhesive layer were not covered completely by the gold film even though 5 μm of gold had been evaporated (Fig. 3).

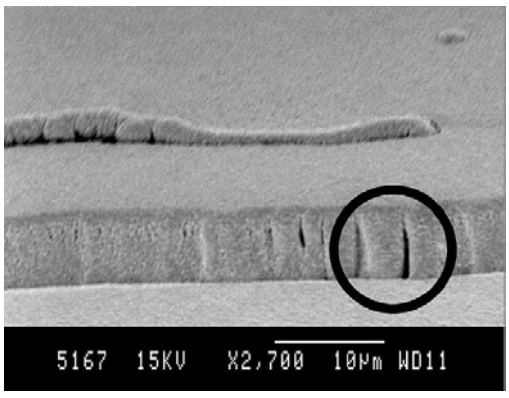


Fig. 3. SEM picture of the sidewall of the BCB layer (5 μm thick) covered with 0.5 μm Ti and 4.2 μm Au. Cracks in the metal seal leading to leakage are emphasized.

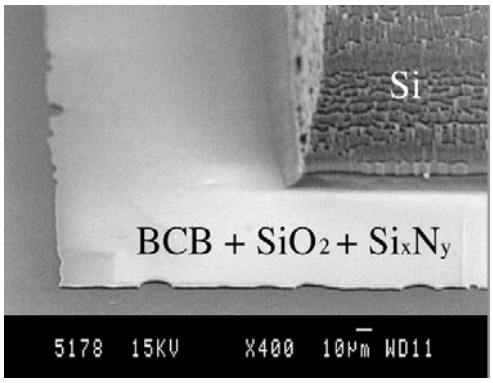


Fig. 4. SEM picture showing a corner of the silison structure on top of the base plateau of BCB (1 μm thick) covered by the remaining $SiO_2$ layer and sealed with 1.1 μm of PECVD silicon nitride.

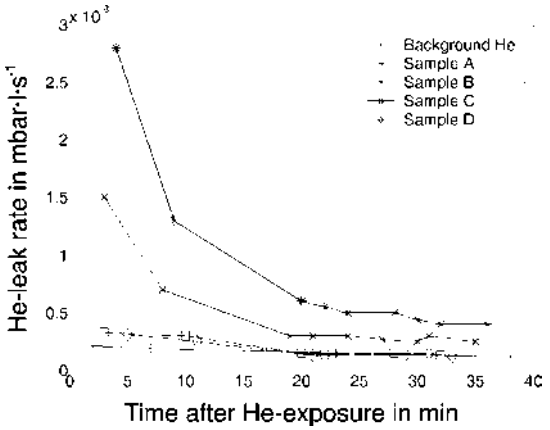


Fig. 5. Helium leak rates over time after the helium exposure, measured for two samples with known defects in the sealing layer (A and B) and two samples without defects (C and D). All samples are of size 1.

Twenty-seven samples of the two different cavity sizes shown in Table 1, covered with $Si_3N_4$ as a sealing layer, have been evaluated. All the measured samples passed the gross leak test in fluorocarbon liquid. Furthermore, visual inspection of the samples in the SEM did not reveal any detectable cracks or defects in the sealing layer (Fig. 4). No difference between a $Si_3N_4$ thickness of 0.5 and 1 μm could be observed.

Two of the samples of size 1, covered with 0.5 μm of $Si_3N_4$, have been cut too close to the sealed adhesion layer during the final dicing to create artificial defects in the sealing layer (samples A and B). The helium leak rate of these samples has been measured in time intervals between 2 and 36 min after the exposure and is compared with two samples without defects in Fig. 5. It can be seen that the helium leak rate of the damaged samples is still 7–14 times higher than the background helium rate after a dwell time of 2–4 min. The leak rate of the samples without defects (samples C and D) is only 1.5 times higher than the background helium rate. If the leak rate of the samples without defects were a reflection of the pressure change inside the cavity, the gas tightness of the sealant would not be high enough for most MEMS applications requiring a hermetic seal. Nese et al. [21] showed that a leak rate of only $5 \times 10^{-4}$ mbar l $s^{-1}$ out of a cavity volume of 3.6 $mm^3$ corresponds to an unacceptable increase of the pressure inside the cavity of 1–2 mbar per day. However, the measured helium flow of the samples without defects is insignificantly higher than the background level and could also come from helium trapped in the other surface of the samples.

Fig. 5 also shows that the leak rates are exponentially decreasing over time. That is due to the decreasing helium pressure inside the small cavity. Curve fitting of an exponential function to the measurement values of samples B and D is shown in Fig. 6. The time constants for the leak

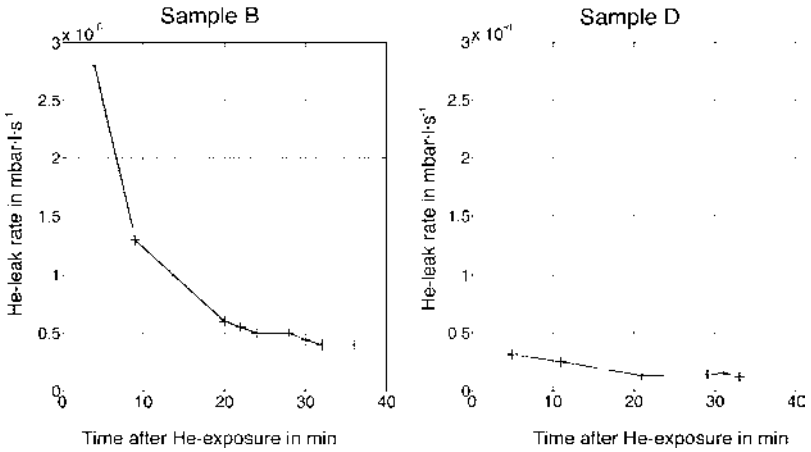


Fig. 6. Exponential curve fitting of the leak rates over time of samples B and D.

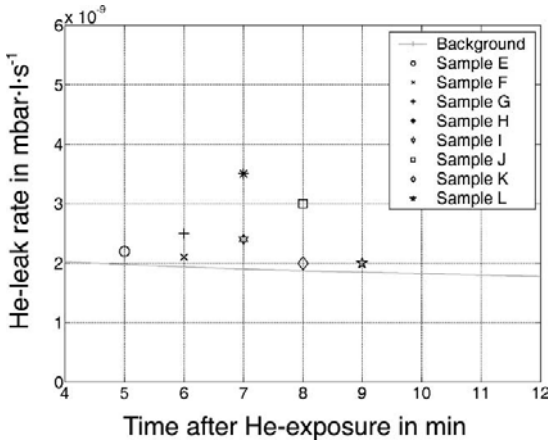


Fig. 7. Helium leak rates measured of samples of size 2. Samples H and J have artificial created defects. The sample size is too small for the helium leak test method to give significant results.

rates of sample B and D were calculated as 310 and 660 s, respectively. The leak rate for sample B dropped by a factor of 6.6 from $28 \times 10^{-9}$ mbar l s$^{-1}$ (4 min dwell time) to $4.2 \times 10^{-9}$ mbar l s$^{-1}$ (30 min dwell time). For the completely sealed sample D, the leak rate only dropped by a factor of 2 in the same time interval. Since the time constant of the decreasing helium leak rate is rather short, a very high helium leak rate immediately after the exposure to the helium can be assumed for the samples with the artificial damage.

The difference between samples with known damage to samples without damages is not clearly visible for the smaller samples of the size 2. The leak rate, measured for 8 samples after a dwell time of 5–9 min, is shown in Fig. 7. Sample H and J are two samples with known damage and show only an insignificantly higher value than the other samples. We assume that the dwell time after the helium exposure is too long for such small samples to show a clearer difference.

The efficiency of the step in the BCB bonded base of the devices, as shown in Fig. 2b, was verified by carrying out tests of devices sealed with silicon nitride after a straight-down etch as illustrated in Fig. 2a. All the samples created by the straight-down etching technique showed a leak rate in the range of $(5–10) \times 10^{-8}$ mbar l s$^{-1}$, which is in the same range as samples without any cladding layer at all. That indicates that the sealing layer coverage in the corners of the straight-down etched samples is not efficient, which was improved by the fabrication technique presented in this paper.

## 5. Conclusions

A low temperature wafer-level sealing method of BCB adhesive bonded cavities has been presented. The devices have been sealed by a combined sawing and self-aligning etching technique of the upper wafer and by final coating of the structures by deposition of a diffusion barrier onto the adhesive. The hermeticity of the cavities has been tested by carrying out helium leak tests, comparing devices with known defects in the sealing layer to devices without damages. The sealing with an evaporated gold layer was not successful and SEM pictures revealed unsealed cracks in the metal film even up to a gold layer thickness of 5 μm. Cladding with PECVD $Si_3N_4$ of 0.5–1 μm thickness improved the hermetic properties of the BCB bonded devices significantly. Possible applications of this packaging and sealing method are MEMS devices with a demand of near-hermetic packaging on wafer level such as MOEMS mirror arrays, RF MEMS switches and tunable capacitors.

## References

[1] A.V. Chavan, K.D. Wise, A monolithic fully-integrated vacuum-sealed CMOS pressure sensor, IEEE Trans. Electron devices 49 (1) (2002) 164–169.
[2] D.-J. Lee, B.-K. Ju, Y.-H. Lee, J. Jang, M.-H. Oh, Glass-to-glass anodic bonding for high vacuum packaging of microelectronics and its stability, Proc. Micro Electro Mechanical Systems (2000) 253–258.
[3] M.A. Huff, A.D. Nikolich, M.A. Schmidt, Design of sealed cavity microstructures formed by silicon wafer bonding, J. Microelectromech. Syst. 2 (2) (1993) 74–81.
[4] R. Ramesham, R. Ghaffarian, Challenges in interconnection and packaging of microelectromechanical systems (MEMS), in: Proceedings of the IEEE Electronic Components Technology Conference, 2000, pp. 666–675.
[5] D. Ando, K. Oishi, T. Nakamura, S. Umeda, Glass direct bonding technology for hermetic seal package, Proc. Micro Electro Mechanical Systems (1997) 186–190.
[6] Ch. Liu, Y.-Ch. Tai, Sealing of micromachinged cavities using chemical vapor deposition methods: characterization and optimization, J. Microelectromech. Syst. 8 (2) (1999) 135–145.
[7] K.S. Lebouitz, A. Mazaheri, R.T. Howe, A.P. Pisano, Vacuum encapsulation of resonant devices using permeable polysilicon, Proc. Micro Electro Mechanical Systems (1999) 470–475.
[8] R. Lengtenberg, H.A.C. Tilmans, Electrostatically driven vacuum-encapsulated polysilicon resonators. Part I. Design and fabrication, Sens. Actuators A 45 (1994) 57–66.
[9] M. Bartek, J.A. Foerster, R.F. Wolffenbuttel, Vacuum sealing of microcavities using metal evaporation, Sens. Actuators A 61 (1997) 364–368.
[10] R.F. Wolffenbuttel, Low-temperature intermediate Au–Si wafer bonding; eutectir or silicide bond, Sens. Actuators A 62 (1997) 680–686.
[11] Y.T. Cheng, L. Lin, K. Najafi, Localized silicon fusion and eutectic bonding for MEMS fabrication and packaging, J. Microelectromech. Syst. 9 (1) (2000) 3–8.
[12] Y.T. Cheng, L. Lin, K. Najafi, Fabrication and hermeticity testing of a glass–silicon package formed using localized aluminum/silicon-to-glass bonding, Proc. MEMS (2000) 757–762.
[13] D.E. Booth, C.E. Hunt, Low temperature adhesion bonding methods, in: Proceedings of the 3rd International Symposium on Semiconductor Wafer Bonding, 1995, pp. 201–211.
[14] F. Niklaus, et al., Low temperature full wafer adhesive bonding of structured wafers, Sens. Actuators A 92 (2001) 235–241.
[15] J. Oberhammer, F. Niklaus, G. Stemme, Selective wafer level adhesive bonding with Benzocyclobutene for fabrication of cavities, Sensors and Actuators A 105 (3) (2003) 297–304.

[16] A. Jourdain, P. De Moor, S. Pamidighantam, H.A.C. Tilmans, Investigation of the hermeticity of BCB-sealed cavities for housing (RF-) MEMS devices, Proc. Micro Electro Mechanical Systems (2002) 677–680.
[17] R.K. Traeger, Hermeticity of polymeric lid sealants, in: Proceedings of the 26th Electronic Components Conference, 1976, pp. 361–367.
[18] R.R. Tummala, Microelectronics Packaging Handbook. Part 2. Semiconductor Packaging, second ed., Kluwer Academic Publishers, Boston, 1999, pp. 873–930.
[19] S.S. He, V.L. Shannon, Hydrogen diffusion and redistribution, in: PECVD Si-rich silicon nitride during rapid thermal annealing, in: Proceedings of the Solid-State and Integrated Circuit Technology, 1995, pp. 269–271.
[20] R.K. Ulrich, et al., PECVD silicon nitride postbond films for protecting bondpads, bonds and bondwires from corrosion failure, in: Proceedings of the Electronic Components and Technology Conference, 1991, pp. 738–744.
[21] M. Nese, R.W. Bernstein, I. Johansen, R. Spooren, New method for testing hermeticity of silicon sensor structures, Proc. Transducers (1995) 260–262.

## Biographies

*Joachim Oberhammer*, born in Italy on 13 April 1976, received his MSc degree in electrical engineering, specialization in measurement technology, from the University of Technology Graz, Austria, in 2000. He has been working with automotive electronics and RF identification systems both at the University of Technology Graz and Vienna University of Technology, Austria, before he joined the Microsystem Technology Group at the Royal Institute of Technology, Stockholm, Sweden, as PhD student in March 2001. Here, his research focus lies in RF MEMS and wafer-level packaging of MEMS components.

*Frank Niklaus* was born in Malsch, Germany, on 24 March 1971. He received his MSc degree in mechanical engineering in 1998 from the University of Munich, Germany. Presently, he is a graduate student in the Silicon Sensor Research Group at the Department of Signals, Sensors and Systems at the Royal Institute of Technology, Stockholm, Sweden. His research interest is in the field of silicon sensor and actuator technology, especially adhesive wafer bonding and infrared detectors.

*Göran Stemme* received the MSc degree in electrical engineering in 1981 and the PhD degree in solid state electronics in 1987, both from the Chalmers University of Technology, Gothenburg, Sweden. In 1981, he joined the Department of Solid State Electronics, Chalmers University of Technology, Gothenburg, Sweden. There, in 1990, he became an associate professor (Docent) heading the silicon sensor research group. In 1991, Dr. Stemme was appointed a professor at the Royal Institute of Technology, Stockholm, Sweden, where he heads the Microsystem Technology group at the Department of Signals, Sensors and Systems. His research is devoted to microsystemtechnology based on micromachining of silicon. Between 1995 and 2001, he was a member of the International Steering Committee of the Conference series IEEE Microelectromechanical Systems (MEMS) and he was general co-chair of that conference in 1998. Dr. Stemme is a member of the Editorial Board of the IEEE/ASME "*Journal of Microelectromechnical Systems*" and of the Royal Society of Chemistry Journal "*Lab on a Chip*". 2001 he won, together with two colleagues, the final of the Swedish Innovation Cup. Dr. Stemme has published more than 100 research journal and conference papers and has been awarded eight patents.

# Paper 3

**Low-Voltage High-Isolation DC-to-RF MEMS Switch Based on an S-shaped Film Actuator**

*Joachim Oberhammer* and Göran Stemme

IEEE Transactions on Electron Devices, vol. 51, no. 1, pp. 149–155, Jan. 2004.

# Low-Voltage High-Isolation DC-to-RF MEMS Switch Based on an S-shaped Film Actuator

Joachim Oberhammer and Göran Stemme, *Senior Member, IEEE*

***Abstract*—This paper presents a new electrostatically actuated microelectromechanical series switch for switching dc to radio frequency (RF) signals. The device is based on a flexible S-shaped film moving between a top and a bottom electrode in touch-mode actuation. This concept, in contrast to most other microelectrochemical systems (MEMS) switches, allows a design with a low actuation voltage independent of the off-state gap height. This makes larger nominal switching contact areas for lower insertion loss possible, by obtaining high isolation in the off-state. The actuation voltages of the first prototype switches are 12 V to open, and 15.8 V to close the metal contact. The RF isolation with a gap distance of 14.2 $\mu$m is better than —45 dB up to 2 GHz and —30 dB at 15 GHz despite a large nominal switching contact area of 3500 $\mu$m$^2$.**

***Index Terms*—Broadband switches, microwave switches, millimeter wave switches, RF MEMS.**

## I. Introduction

MICROELECTROMECHANICAL SYSTEMS (MEMS) are mechanical devices fabricated with standardized integrated circuit technology, offering the advantages of high volume production with excellent uniformity in device properties over the whole wafer and over a whole batch of wafers. MEMS switches are devices mechanically opening or short-circuiting a transmission line. Such switches are of submillimeter size and offer superior performance such as high isolation, low insertion loss, excellent signal linearity, better impedance match, less frequency dependence and lower power consumption compared to conventional electronic switches based on p-i-n diodes or GaAs FETs [1], [2]. Therefore, such switches are very desirable for applications with demands on high signal purity, despite their slow switching time in the microsecond range and the higher costs for implementing mechanical parts into electronic devices. The first radio frequency (RF) MEMS switch was shown in 1991, consisting of an electrostatic actuated rotating transmission line piece [3]. However, that switch needed actuation voltages of 80 to 200 V.

The most promising RF MEMS switch designs, in terms of reliability and wafer-scale manufacturing techniques, are based on electrostatic actuation with almost zero power consumption in the on and off-states [1]. The two basic MEMS switch types from a function perspective are series switches and shunt switches [4], as illustrated in Fig. 1. The former are usually realized as metal-contact switches able to switch signals from dc to radio frequencies with high isolation. Also, series capacitive switches were presented in literature [5]. Most implementations of the shunt switch type are based on tunable capacitors short-circuiting the signal line in the on-state. The isolation of such capacitive shunt switches is very small for lower frequencies due to its capacitive short-circuiting principle but its performance is much better at higher frequencies in the millimeter wavelength range. Furthermore, such switches are usually smaller, easier to manufacture, show higher reliability compared to the stiction and degrading susceptible metal contacts, and have been investigated more thoroughly than the series switch type [6]. Typical applications for the different types of switches are e.g. in the fields of microwave radar and telecommunication systems for capacitive switches, and automated test equipment (ATE) for series shunt switches. However, metal-contact series switches have also been used successfully in the microwave domain, as in delay networks up to 40 GHz [7].

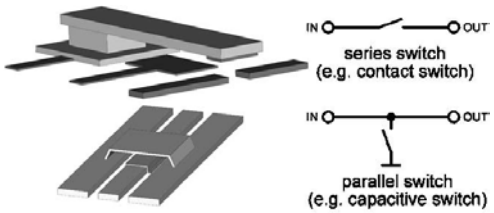


Fig. 1. Two basic switch types distinguished by how the signal line is switched.

The novel switch concept presented in this paper is basically suitable for both series and shunt switch implementation, but the prototypes where fabricated in metal-contact series switch configuration. Therefore, the focus of this paper is on this type of switch.

## II. S-Shaped Film Actuator Switch

The principle of the classical and so far widest used electrostatic series switch concept is shown in Fig. 2. To obtain a high RF isolation in the off-state, the gap height between the switching contacts should be sufficiently large. On the other hand, this leads to a high dc voltage needed to actuate the switch, since the electrostatic forces between two electrodes are proportional to $1/d^2$ where $d$ is the distance between the two electrodes. Actuation voltages are typically 20 to 50 V with a gap height of 3 to 4 $\mu$m [5], [8]. In order to maintain high RF isolation, the switching contact area is limited to sizes less than 500 $\mu$m$^2$, since the capacitive coupling over the small gap height

Manuscript received May 9, 2003; revised August 11, 2003. The review of this paper was arranged by Editor K. Najafi.

The authors are with the Microsystem Technology Group, Department of Signals, Sensors and Systems, the Royal Institute of Technology, SE-100 44 Stockholm, Sweden.

Digital Object Identifier 10.1109/TED.2003.820655

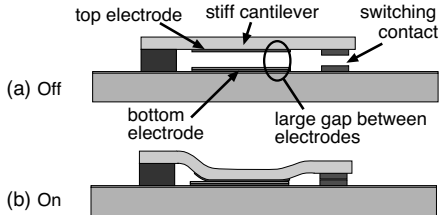


Fig. 2. Actuation principle and typical elements of conventional electrostatic series switch.

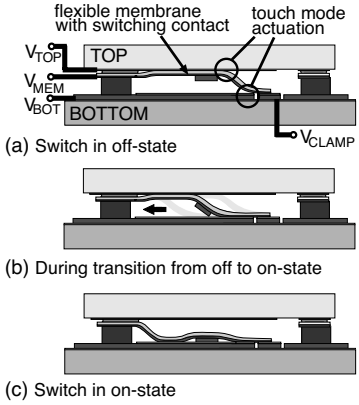


Fig. 3. Actuation principle and typical elements of the novel S-shaped film actuator switch, with the flexible membrane moving between the top and bottom electrodes.

is directly proportional to the switching contact areas. Furthermore, to be able to open the contact, the cantilever or membrane structure has to be relatively stiff to overcome the adhesion forces between the closed contacts, especially in the case of so-called "hot-switching," i.e., a signal current is present when opening the contacts. The stiffness of the structure additionally increases the actuation voltage. Improvements of this concept use a push-pull configuration [9] or a top counter electrode [10] ("double electrode principle").

Fig. 3 shows the operating principle of the novel S-shaped film actuator switch presented in this paper. At the basic level it consists of a thin and flexible membrane with electrodes and a metal switching contact moving between the top and bottom electrodes. Fig. 4 illustrates the two parts of the switch with their main elements before the assembly. To close the switch, a voltage has to be applied between the membrane electrodes and the bottom electrodes, and, to open it, between the membrane electrodes and the top electrodes, respectively ("double electrode principle"). For both cases, the electrodes are in so-called touch-mode actuation [11], i.e., the actuating parts of the electrodes are separated only by a very thin isolation layer or the thin membrane itself. Curled touch-mode actuators were already used for switch designs with actuation voltages lower than 30 V [5], [12]. Even at low actuation voltages, high attraction forces can be created between the electrodes, and the membrane rolls like a film over its counter actuation electrode. The S-shaped

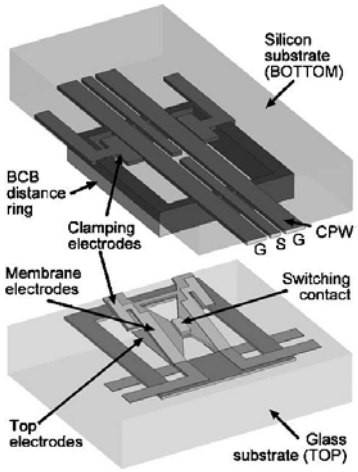


Fig. 4. Schematic illustration of the film actuator switch, with the switch shown upside-down. The bottom silicon substrate contains the coplanar waveguide, the clamping electrodes and the BCB distance ring. The top glass substrate contains the top electrodes, the silicon nitride film with the membrane electrodes and the switching contact. Details like isolation layers and etch holes are not shown.

film actuator principle, consisting of two of such touch-mode actuators, was shown in 1997 for a micromachined fluidic valve with dimensions in the order of millimeters [13]. For the presented switch, it allows the displacement of the switching contact bar to be defined independently of the effective electrode distance of the touch-mode actuators. Thus, the switch can be designed in a way having a high isolation in the off-state, determined by the large gap distance, but still requiring only low actuation voltages. In fact, the actuation voltage is independent of the choice of the gap distance, which is a highly desirable design criteria for electrostatically actuated RF MEMS switches. Since the presented switch provides with active-opening capability, no spring energy has to be stored in the mechanical moving structure to open the switch. Thus, the membrane is made very thin and flexible, which further lowers the actuation voltage.

Due to the possible large distance between the contacts in the off-state, the switching contact area may be designed substantially larger compared to other switch concepts without decreasing the RF isolation. This also implies lower insertion losses caused by the ohmic switching contacts and thus higher current handling capabilities, provided that the contact force is high enough.

Another advantage of having a top electrode design is that a higher force can be created to open the switch, which allows switching during applied signal currents ("hot-switching") with less risk of the switch sticking closed permanently due to contact microwelding occurring at a signal power greater than 20 dBm [1], [14]. Also, stiction of the mechanical moving parts beside the metal contacts is less problematic due to the active restoring force created by a voltage applied between the membrane electrodes and the top electrodes. Thus, the total reliability of the switch may be substantially increased.

In order to keep the membrane securely in touch-mode with the bottom electrodes during the off-state when the membrane is

TABLE I
DRIVING POTENTIALS OF THE ACTUATION ELECTRODES

| Switch State | $V_{TOP}$ | $V_{MEM}$ | $V_{BOT}$=GND | $V_{CLAMP}$ |
|---|---|---|---|---|
| On | + | + | 0 | + |
| Off | + | 0 | 0 | + |

pulled up toward the top electrodes, additional clamping electrodes are placed on the bottom wafer, as illustrated in Fig. 3 and Fig. 4. A potential applied between these electrodes and the membrane electrodes presses the ends of the membrane down to the bottom wafer, making it ready for touch-mode actuation between the membrane and the bottom electrodes for the next closing operation. This voltage is only needed for safe operation of the switch and not to make initial contact between the membrane and the bottom part, since the membrane is curling out-of-plane and already touches the bottom electrodes.

The switch thus needs a total of four electrodes for its actuation: the top electrodes and the membrane electrodes also forming the membrane clamping electrodes on the top part of the switch, and the bottom electrodes and clamping electrodes on the bottom part. However, for operating the switch after start-up only the driving potential of one electrode has to be altered and the other electrodes may be kept at a same potential, as shown in Table I.

The weakness of most MEMS components is the missing link to the packaging of the devices, which is especially important for devices with moving mechanical parts usually requiring an individual packaging and integration solution [15]. The packaging should already be taken into consideration during the design of the devices [1]. For successful commercialization, a cost effective housing and packaging is an important requirement. The switch concept presented in this paper addresses this problem since it consists of two parts, as shown in Fig. 4, fabricated on different substrates and finally assembled by adhesive wafer bonding, providing a fully packaged integrated switch. A further advantage of this concept is that the main switch elements are located on the top wafer and the bottom part consists only of a few nonmechanically moving elements, mainly the signal lines and electrodes. This allows a simple integration of the switch directly onto RF CMOS wafers, since the top part is fabricated on a different wafer and its devices can simply be picked-and-placed onto any RF circuit wafer. No special restrictions in process compatibility are put on the RF circuit wafer, as opposed to most other switch designs where the mechanical switching structure has to be processed directly onto the RF substrate. Thus, this technique also allows the use of different RF substrate materials.

Benzocyclobutene (BCB), the sealing material used to package the presented switch by bonding the two parts together, is a epoxy-based polymer and only provides with a so-called near-hermetic package. Therefore, it does not allow absolute control of the atmosphere inside the cavity [16]. Possible contamination of the metal switching contacts due to outgasing during the final bonding procedure is minimized since the BCB is pre-cured at temperatures above 200 °C before the bonding. However, BCB packaging for MEMS switches needs further investigation.

The prototype of the film actuator based switch presented in this paper is with a membrane length of 950 $\mu$m and a packaged cavity size of $1100 \times 1000 \times 182\ \mu m^3$, quite large compared to other MEMS switches published so far. However, this concept does not exclude reduction of the lateral switch dimensions while maintaining the large off-state gap height and its high performance.

OMRON Corporation has developed a fully packaged MEMS RF switch of similar dimensions as the prototype switch presented in this paper [17]. Table II compares some dimensions and performance parameters of the two switches.

## III. FABRICATION

### A. Bottom Wafer

The bottom part of the switch consists of the coplanar waveguide (CPW), the clamping electrodes, and the ring-shaped distance holder defining the cavity containing the switch. A scanning electron microscope (SEM) picture of the bottom part before the final assembly is shown in Fig. 5.

The substrate is a 100-mm diameter, 525-$\mu$m-thick, high resistivity silicon substrate (HRSS) wafer with a resistivity of 1500 $\Omega \cdot$ cm and an $\varepsilon_r$ of 11.9, covered with a 800-nm-thick silicon dioxide isolation layer. The 2-$\mu$m-thick finite ground coplanar waveguide (FG CPW) together with the clamping electrodes are created by electroplating gold. The length of the coplanar waveguide is 3300 $\mu$m, the signal line width 100 $\mu$m, the distance between the signal and each ground line 55 $\mu$m, and the ground line width is 200 $\mu$m, giving a nominal characteristic impedance of 50 $\Omega$ as estimated by empirical formulas [18]. A 200-nm-thick silicon nitride (SiN) layer, deposited by low temperature plasma-enhanced chemical vapor deposition (PECVD) and patterned by plasma etching, isolates the membrane electrodes from the CPW with the clamping electrodes. On top of the waveguide, BCB from the Dow Chemical Company is spun and hard-cured at 280 °C, resulting in a layer thickness of 18.2 $\mu$m. Taking into account the thickness of the metal switching bar and of the signal line, each 2 $\mu$m, BCB layer thickness of 18.2 $\mu$m results in a contact distance of 14.2 $\mu$m in the off-state. According to simulations, this gap height was found to be sufficient for decent RF isolation. The polymer is patterned in a $CF_4/O_2$ plasma in a reactive ion etching (RIE) tool using a thick photoresist mask [19], to create the wall outlining the cavity containing the switch and defining the distance between the bottom and the top parts.

### B. Top Wafer

The top part of the switch is fabricated on a 500-$\mu$m-thick, 100-mm diameter glass wafer. Fig. 6 shows a SEM picture of the structure after releasing of the membrane by etching the sacrificial layer.

The first layer on the substrate is a 150-nm-thick evaporated gold layer, patterned by wet etching. Then, a polyimide sacrificial layer follows with a thickness of 1.5 $\mu$m which has to be fully cured at 350 °C. The next layer is the 1-$\mu$m-thick low stress silicon nitride layer for the film membrane deposited by dual-frequency PECVD at 300 °C. Then, a 150-nm-thick gold

TABLE II
COMPARISON OF THE FILM ACTUATOR SWITCH PROTOTYPE WITH THE OMRON RF MEMS SWITCH [17]

| | OMRON switch | Prototype of film actuator switch |
|---|---|---|
| switch type | series metal contact | series metal contact |
| operation principle | vertically moving membrane | S-shaped rolling film actuator |
| actuation for closing | electrostatic forces | electrostatic forces |
| actuation for opening | spring forces | electrostatic forces (double electrode) |
| structural material | monocrystalline silicon | PECVD silicon nitride |
| signal line and contact | 1.0–1.6 $\mu$m sputtered gold [23] | 2.0 $\mu$m electroplated gold |
| packaged chip size | 3.0 x 2.0 x 1.0 mm$^3$ [a] | 1.7 x 1.4 x 1.0 mm$^3$ [b] |
| membrane size | 1400 x 1700 $\mu$m$^2$ | 950 x 900 $\mu$m$^2$ |
| membrane thickness | 18–24 $\mu$m [22] | 1 $\mu$m SiN + 0.190 $\mu$m Au/Cr |
| total electrode size | 2 x 1000000 $\mu$m$^2$ | 2 x 82500 $\mu$m$^2$ |
| switching contact area | unknown to the authors | 2 x 3500 $\mu$m$^2$ |
| open contact distance | 3 $\mu$m | 14.2 $\mu$m |
| actuation voltage | 19.2 V to close | 12 V to open, 15.8 V to close |
| contact force | 5 mN at 24 V, calculated | 102 $\mu$N at 15 V, simulated |
| contact resistance | <50 m$\Omega$ | 0.65 $\Omega$ |
| RF isolation | -40 dB (<2 GHz), -30 dB (10 GHz) | -45 dB (<2 GHz), -30 dB (15 GHz) |
| insertion loss | <0.5 dB | 2.5 dB at 10 GHz |
| open-state capacitance | 5 fF [22] | 4.2 fF |
| switch transfer by | anodic bonding (>350 °C) [c] | patterned adhesive bonding (BCB, 280 °C) [d] |
| packaging | CSP on WL by glass-frit bonding (450 °C) | together with switch transfer |
| sealing ring | 250 $\mu$m wide, 10 $\mu$m high, glass-frit | 200 $\mu$m wide, 18.2 $\mu$m high, BCB |
| package gas tightness | hermetic package | near-hermetic package |

[a] a smaller device with a CSP of 1.8 x 1.8 x 1.0 mm$^3$ was recently presented [24]
[b] size of the packaged prototype switch, excluding contact pad areas for manual probing
[c] thermo-compression bonding in [24]
[d] design target: to be done by patterned adhesive full-wafer bonding with BCB [16]

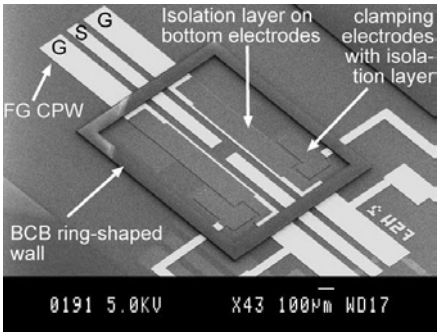


Fig. 5. SEM picture of the bottom part of the switch before the final assembly.

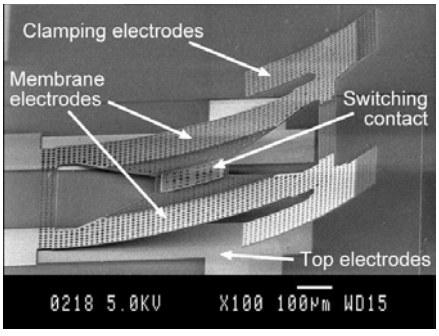


Fig. 6. SEM picture of the top part of the switch after etching the sacrificial layer and before the final assembly.

layer is evaporated on top of the membrane to create the membrane electrodes. The switching contact is formed afterwards by electroplating 2 $\mu$m thick gold. After patterning the membrane electrodes and the silicon nitride membrane, the structure is diced with a die saw and the membrane is released by etching the polyimide sacrificial layer in an $O_2$ plasma etcher.

Despite the use of low-stress silicon nitride for the membrane, the structure bends upward after the sacrificial layer etch due to a vertical stress gradient in the layer, as shown in the SEM picture in Fig. 6. By measuring the bending and by using equations given in [20], the stress gradient was estimated to be about

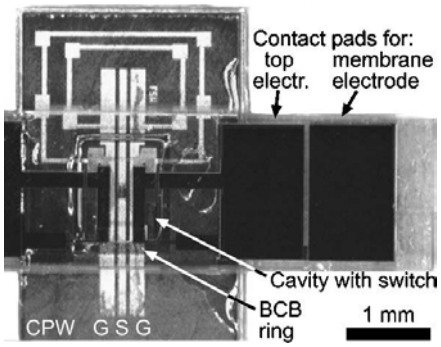


Fig. 7. Photograph of the assembled device.

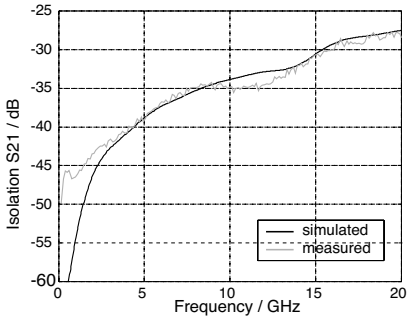


Fig. 8. Comparison of the simulated and measured switch isolation in the off-state up to 20 GHz. The open contact distance of the fabricated switch is 14.2 $\mu$m and the nominal switching contact area is 3500 $\mu$m$^2$.

39 MPa/$\mu$m. This bending prevents stiction during the sacrificial layer etching and puts the membrane in contact with the clamping electrodes on the bottom part of the switch after assembly.

### C. Assembly of the Prototypes

The switch is designed to be assembled on wafer level by using a commercially available substrate bonding tool. However, the first prototypes are assembled on device level in order to easily have access to the contact pads of the top part of the switch, which are facing the bottom substrate. The manually aligned devices are fixated by epoxy glue to ensure stability during the subsequent evaluation. This is not necessary for the assembly by full wafer-bonding, due to the sufficiently strong bond interface of patterned BCB [16]. A photograph of the assembled device is shown in Fig. 7.

## IV. DC Measurements

After the assembly of the switch, the membrane already touches the clamping electrodes of the bottom wafer due to its bending after removing the sacrificial layer. Therefore, a voltage of only 19.2 V is necessary to fully tie the clamping parts of the membrane to the bottom wafer clamping electrodes. This voltage should be kept above at least 13 V during operation of the switch to ensure that the membrane is always in touch-mode actuation with the bottom electrodes, even when the top electrodes are pulling it upward.

The switch closes when a voltage of 15.8 V is applied between the membrane electrodes and the bottom electrodes. The actuation voltage required between the membrane electrodes and the top electrodes to open the switch is 12 V at an applied clamping electrode voltage of 20 V. These are relatively low actuation voltages for an electrostatic actuated switch, especially considering the large displacement of the contacts, and are achieved by the small effective electrode distances of the touch-mode actuators (only 0.2 $\mu$m between the membrane and the bottom electrodes, and 1 $\mu$m between the membrane and the top electrodes, respectively).

All of these actuation voltages are very reproducible with standard deviations of in the range of 0.3 (clamp electrodes) to 0.7 V (bottom to membrane electrodes) during subsequent switching cycles of the same device.

The dc resistance of the closed switch is 0.65 $\Omega$, which is higher than expected considering the large contact area. This can be explained by the electroplated gold composition used for our prototypes, which was found not to be very suitable for contact switching. Also, the contact force of our first design, estimated by ANSYS simulations to be 102 $\mu$N per contact at an actuation voltage of 15 V, is not very high for switching gold contacts. This fact, in combination with possible organic residues on the surface of the contacts, might lead to the increased contact resistance [21]. However, the contact force of this switch concept can be improved without increasing the actuation voltage, by making the membrane around the switched metal bar thicker and thus stiffer.

## V. RF Simulations and Measurements

The switch design, including the 3300-$\mu$m-long coplanar waveguide, was simulated with the finite-difference/time-domain (FDTD) software CST Microwave Studio version 4. The RF model for the simulations consists of the whole switch structure, just excluding small details like the etch holes. The measurements of the fabricated devices were carried out with a Wiltron 360 vector network analyzer and a high-frequency probe-station with GGB Picoprobe 150 $\mu$m pitch GSG probes. To calibrate the setup, a through-load open-short calibration was done using a CS5 calibration substrate from the same company.

The actual characteristic impedance, $Z_0$, of the coplanar waveguide without switch was measured as 47.4 $\Omega$ and a value of 45.2 $\Omega$ was determined by the simulations, which is a relatively good match for a first design. The effective relative permittivity of the waveguide indicated by the measurements is $\varepsilon_r = 6.25$.

Fig. 8 compares the simulated with the measured isolation up to 20 GHz of the fabricated switches with a switching contact distance of 14.2 $\mu$m in the off-state. The measured isolation corresponds very well to the simulation over most of the frequency range. Due to the large contact distance in the off-state, the design has a high isolation of $-45$ dB up to 2 GHz and $-30$ dB at 15 GHz, despite the favored large nominal contact area of 3500 $\mu$m$^2$ of the 190 $\mu$m long and 100 $\mu$m wide metal contact bar. The fitted open-state series capacitance of the switch

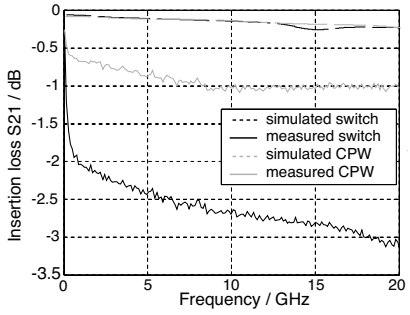


Fig. 9. Comparison of the simulated and measured insertion loss of the switch on the 3300-$\mu$m-long coplanar waveguide up to 20 GHz. The figure also shows the measured and simulated insertion loss of a through line coplanar waveguide without switch, fabricated on the same wafer as the switch.

was determined by simulations with FEMLAB to be 4.2 fF. This value is comparable to most other metal contact switch designs with similar isolation having an open-state capacitance of about 2–6 fF [22].

The simulated insertion loss of the switch on a 3300 $\mu$m long coplanar waveguide is compared to the measured insertion loss in Fig. 9. The measured insertion loss of the prototypes is far higher than expected and the authors assume it is mainly caused by:

1) The calibration was not carried out with a on-wafer calibration set, but with a calibration kit on a low-loss ceramic substrate.
2) The coplanar waveguide itself has quite high a loss. This can be concluded from the measurement data of the waveguide without switch, included in Fig. 9. The simulated insertion loss of the waveguide is also shown in the figure, and there is quite a large discrepancy between the simulation and the measurement data, as in the case of the waveguide with the switch.

However, even considering the high losses of the waveguide, the measurements show a remaining insertion loss of about 1.5 dB. The reason for this is not fully understood since the measured dc-contact resistance only creates an estimated insertion loss of about 0.06 dB.

## VI. Conclusion

An RF MEMS contact series switch based on a novel switch actuation concept has been designed, fabricated and evaluated. The S-shaped film actuator principle allows a high isolation and a low actuation voltage even with large switching contact areas. The RF properties of the switch design were simulated and the manufactured prototypes were characterized by dc and RF measurements. Already the first prototypes are actuated at voltages lower than 20 V and show high isolation of $-45$ dB at 2 GHz. The insertion loss of the prototypes with about $-2$ dB at 2 Ghz was found to be higher than expected. The feasibility of the novel switch concept was proved by successful fabrication and characterization of prototypes, but still needs some improvement, as shown by some of the not very good measurement data.

## Acknowledgment

The authors would like to thank to Björn Lindmark from the Antenna Systems Technology group at the Royal Institute of Technology, Stockholm, Sweden, for the assistance with the RF measurements.

## References

[1] G. M. Rebeiz and J. B. Muldavin, "RF MEMS switches and switch circuits," *IEEE Microwave Mag.*, vol. 2, pp. 59–71, Dec. 2001.
[2] E. R. Brown, "RF-MEMS switches for reconfigurable integrated circuits," *IEEE Trans. Microwave Theory Tech.*, vol. 46, pp. 1868–1880, Nov. 1998.
[3] L. E. Larson, R. H. Hackett, and R. F. Lohr, "Microactuators for GaAs-based microwave integrated circuits," in *Proc. Transducers 1991*, San Francisco, CA, June 24–27, 1991, pp. 743–746.
[4] J. Yao, "RF MEMS from a device perspective," *J. Micromech. Microeng.*, vol. 10, pp. R9–R38, 2000.
[5] S. Duffy, C. Bozler, S. Rabe, J. Knecht, L. Travis, P. Wyatt, C. Keast, and M. Gouker, "MEMS microswitches for reconfigurable microwave circuitry," *IEEE Microwave Wireless Comp. Lett.*, vol. 11, pp. 106–108, Mar. 2001.
[6] Z. Y. Yao, S. Chen, S. Eshelman, D. Denniston, and C. Goldsmith, "Micromachined low-loss microwave switches," *IEEE J. Microelectromech. Syst.*, vol. 8, no. 2, pp. 129–134, June 1999.
[7] M. Kim, J. B. Hacker, R. E. Mihailovich, and J. F. DeNatale, "A DC-to-40 GHz four-bit RF-MEMS true-time delay network," *IEEE Microwave Wireless Comp. Lett.*, vol. 11, no. 2, pp. 56–58, Feb. 2001.
[8] J. J. Yao and M. F. Chang, "A surface micromachined miniature switch for telecommunications applications with signal frequencies from dc up to 4 GHz," in *Proc. Transducers 1995*, June 25–29, 1995, pp. 384–387.
[9] D. Hah, E. Yoon, and S. Hong, "A low-voltage actuated micromachined microwave switch using torsion springs and leverage," *IEEE Trans. Microwave Theory Tech.*, vol. 48, pp. 2540–2545, Dec. 2000.
[10] S. Pacheco, C. T. Nguyen, and L. P. B. Katehi, "Micromechanical electrostatic k-band switches," in *IEEE MTT-S Int. Microwave Symp. Dig.*, June 1998, pp. 1569–1572.
[11] C. C. Cabuz, E. I. Cabuz, T. R. Ohnstein, J. Neus, and R. Maboudian, "Factors enhancing the reliability of touch-mode electrostatic actuators," *Sens. Actuators A, Phys.*, vol. 79, no. 3, pp. 250–254, Feb. 2000.
[12] H. F. Schlaak, F. Arndt, and M. Hanke, "Switching characteristics of silicon-microrelay with electrostatic actuator," in *Proc. Int. Conf. on Electric Contact Phenomena*, Nuremberg, Germany, Sep. 14–17, 1998, pp. 59–64.
[13] M. Shikida, K. Sato, and T. Harada, "Fabrication of an s-shaped microactuator," *IEEE J. Microelectromech. Syst.*, vol. 6, no. 18, pp. 18–24, Mar. 1997.
[14] D. Hyman and M. Mehregany, "Contact physics of gold microcontacts for MEMS switches," *IEEE Trans. Comp. Packag. Technol.*, vol. 22, no. 3, pp. 357–364, Sept. 1999.
[15] H. Reichl and V. Gosser, "Overview and development trends in the field of MEMS packaging," in *Proc. IEEE Micro Electro Mechanical Systems 2001*, Interlaken, Switzerland, Jan. 21–25, 2001, pp. 1–5.
[16] J. Oberhammer, F. Niklaus, and G. Stemme, "Selective wafer-level adhesive bonding with benzocyclobutene for fabrication of cavities," *Sens. Actuators A, Phys.*, vol. 105, no. 3, pp. 297–304, Aug. 2003.
[17] Y. Komura, M. Sakata, T. Seki, K. Kobayashi, K. Sano, S. Horiike, and K. Ozawa, "Micro machined relay for high frequency application," in *Proc. NARM Int. Relay Conf.*, Newport Beach, USA, Apr. 19–21, 1999.
[18] W. Heinrich, "Quasi-TEM description of MMIC coplanar lines including conductor-loss effects," *IEEE Trans. Microwave Theory Tech.*, vol. 41, pp. 45–52, Jan. 1993.
[19] P. B. Chinoy, "Reactive ion etching of benzocyclobutene polymer films," *IEEE Trans. Comp. Packag. Manufact. Technol. C*, vol. 20, no. 3, pp. 199–206, July 1997.
[20] W. Fang and J. A. Wickert, "Determining mean and gradient residual stresses in thin films using micromachined cantilevers," *J. Micromech. Microeng.*, vol. 6, no. 3, pp. 301–309, Sept. 1996.
[21] S. Majumder *et al.*, "Study of contacts in an electrostatically actuated microswitch," in *Proc. IEEE*, Arlington, VA, USA, Oct. 26–28, 1998, pp. 127–132.
[22] G. M. Rebeiz, *RF MEMS Theory, Design and Technology*, 1st ed. New York: Wiley, 2003, ch. 5.

[23] M. Sakata, Y. Komura, T. Seki, K. Kobayashi, K. Sano, and S. Horiike, "Micromachined relay which utilizes single crystal silicon electrostatic actuator," in *Proc. IEEE*, Orlando, FL, USA, Jan. 17–21, 1999, pp. 21–24.

[24] T. Seki, S. Sato, T. Masuda, I. Kimura, and K. Imanaka, "Low-loss RF MEMS metal-to-metal contact switch with CSP structure," in *Proc. Transducers 2003*, Boston, MA, June 8–12, 2003, pp. 340–341.

**Joachim Oberhammer** was born in Italy in 1976. He received the M.Sc. degree in electrical engineering from the University of Technology Graz, Austria, in 2000.

He was working with automotive electronics and RF identification systems at the University of Technology Graz, Austria, and Vienna University of Technology, Austria, before he joined the Microsystem Technology group at the Royal Institute of Technology, Stockholm, Sweden, as a Ph.D student in March 2001. His current research focus lies in RF MEMS and wafer-level packaging of MEMS components.

**Göran Stemme** (SM' 00) received the M.Sc. degree in electrical engineering, and the Ph. D. degree in solid state electronics, both from the Chalmers University of Technology, Gothenburg, Sweden, in 1981, and 1987, respectively.

In 1981, he joined the Department of Solid State Electronics, Chalmers University of Technology, Gothenburg, Sweden. In 1990, he became an Associate Professor (Docent) heading the silicon sensor research group. In 1991, he was appointed Professor, The Royal Institute of Technology, Stockholm, Sweden, where he heads the Microsystem Technology Group, Department of Signals, Sensors and Systems. His research is devoted to microsystemtechnology based on micromachining of silicon. He has published more than 100 research journal and conference papers and has been awarded 8 patents.

Dr. Stemme is a member of the Editorial Board of the IEEE/ASME JOURNAL OF MICROELECTROMECHNICAL SYSTEMS, and of the Royal Society of Chemistry journal, *Lab On A Chip*. From 1995 to 2001, he was a Member of the International Steering Committee of the Conference series IEEE Microelectromechanical Systems (MEMS), and he was General Co-Chair of that conference in 1998. In 2001 he won, together with two colleagues, the final of the Swedish Innovation Cup.

# Paper 4

**Design and Fabrication Aspects of an S-shaped Film Actuator Based DC to RF MEMS Switch**

*Joachim Oberhammer* and Göran Stemme

IEEE/ASME Journal of Microelectromechanical Systems, vol. 13, no. 3, pp. 421–428, June 2004.

# Design and Fabrication Aspects of an S-Shaped Film Actuator Based DC to RF MEMS Switch

Joachim Oberhammer and Göran Stemme, *Member, IEEE*

***Abstract*—This paper reports on design and fabrication aspects of a new microelectromechanical series switch for switching dc and RF signals. The switch consists of a flexible S-shaped film with the switching contact, rolling between a top and a bottom electrode in electrostatic touch-mode actuation. This design allows a low actuation voltage independent of the contact distance in the off-state. With a large contact distance, large overlapping switching contact areas are possible by obtaining a high off-state isolation. The RF transmission line and the MEMS part of the switch are fabricated on separate wafers, allowing an implementation of the switch with different RF substrates. The final assembly is done on device level for the first prototypes, even though the design provides the possibility of an assembly by full wafer bonding, leading to a near-hermetic package integrated switch. The measured prototype actuation voltages are 12 V to open and 15.8 V to close the contacts, with a resistance of 275 $\mathrm{m}\Omega$ of each contact at an estimated contact force of 102 $\mu$N. The measured RF isolation with a contact distance of 14.2 $\mu$m is better than $-45$ dB up to 2 GHz and $-30$ dB at 15 GHz, at a large nominal switching contact area of 3500 $\mu\mathrm{m}^2$. [1095]**

***Index Terms*—Film actuator, low-stress silicon nitride, MEMS switches, RF MEMS, touch-mode actuation.**

## I. Introduction

MICROELECTROMECHANICAL switches are devices mechanically opening or short-circuiting a transmission line. Such switches are of submillimeter size and are desirable for applications with demands on high signal purity in terms of isolation, insertion loss, signal linearity, impedance matching, frequency dependence and power consumption compared to conventional electronic switches based on p-i-n diodes or GaAs field-effect transistors (FETs) [1]–[3]. But their mechanical concept implies a slow switching time in the microsecond range and the higher costs for implementing mechanical parts into electronic circuits. The first micromachined switch was already shown in 1979 [4], and the first first RF MEMS switch in 1991 [5].

The most promising RF MEMS switch designs in terms of reliability and wafer-scale manufacturing techniques are based on electrostatic actuation with almost zero power consumption in the on and off-state [1]. The two most common MEMS switch types from a function perspective are series switches and shunt switches [6]. The former type opens and closes metal contacts and is therefore suitable for dc to RF applications such as automated test equipment (ATE). The latter type is usually based on a mechanically tunable capacitor short-circuiting an RF transmission line and is used for RF and microwave frequencies [7]. Other switch types like capacitive series switches [8] and ohmic shunt switches [9] have also been presented recently. An overview of different switch concepts is given in [10].

The switch concept presented in this paper was realized in series switch configuration with metal contacts suitable for switching both dc and RF signals. Therefore, the focus of this paper is on that type of switches.

The classical electrostatic metal contact series switch consists at the basic level of a beam or membrane structure with a switching contact closing the gap in a transmission line when a voltage is applied between the beam and an electrode on the substrate. A large distance between the beam and the substrate leads to a high RF isolation in the off-state, but also requires a relatively high actuation voltage. Typical actuation voltages are 20 to 50 V with a contact distance in the order of a few $\mu$m [11]–[14]. In order to maintain high RF isolation at such low contact distances, the overlapping switching contact area is limited to sizes less than 500 $\mu\mathrm{m}^2$ to minimize the capacitive coupling over the open contacts. Especially for metal contact switches, a substantial force has to be brought up to open the switch, since there is a risk of the switching contacts sticking closed permanently due to contact microwelding [15]. The restoring force to open the switch has to be brought up by the spring energy stored in the cantilever, which means that the structure needs a certain stiffness further increasing the actuation voltage. Improvements of this concept use an active force to open the switch by a push–pull configuration [16] or by a top counter electrode [17]. Also, curled "zipper-like" actuator designs with an initial low distance between the actuation electrodes but a larger distance between the contacts were found to improve the relation between isolation and the actuation voltage [8], [18], [19].

The actuator used for the switch in this paper consists of a membrane being attached at one end to a top and at the other end to a bottom electrode, allowing the membrane to move between the two electrodes. A micromachined fluidic valve with dimensions in the order of millimeters and an actuation voltage of 70 V, based on this actuator principle, was shown in 1997 [20].

A discussion of the novel switch concept and dc to RF measurement results of the fabricated prototypes are given in [21]. The present paper reports on design considerations of this switch concept and on fabrication aspects especially related to the thin and flexible membrane as the main part of

Manuscript received July 1, 2003; revised December 29, 2003. Subject Editor G. B. Hocker.

The authors are with the Microsystem Technology Group, Department of Signals, Sensors and Systems, the Royal Institute of Technology, Stockholm SE-100 44, Sweden.

Digital Object Identifier 10.1109/JMEMS.2004.828723

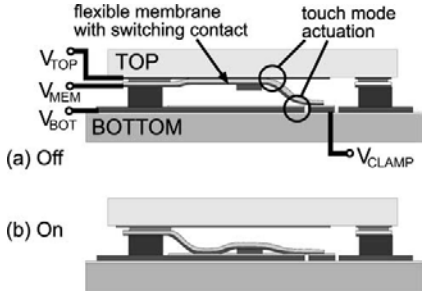


Fig. 1. Actuation principle with typical elements of the novel S-shaped film actuator switch.

the S-shaped film actuator. However, for the completeness of this paper, the particularities of the switch concept are briefly summarized in Section II, and some of the measurement results of the prototype characterization are given in Section V, beside new evaluation data on the actuator itself.

## II. S-Shaped Film Actuator Switch

The operating principle of the S-shaped film actuator switch presented in this paper is shown in Fig. 1. The core of the switch is a thin and flexible membrane with electrodes and a metal switching contact, moving between a top and a bottom electrode (double electrode principle). Both for opening and for closing the switch, the electrodes are in so-called touch-mode or "zipper-like" actuation [22]. That means that there where the initial actuation occurs, the electrodes are separated only by a very short distance. Thus, even at low actuation voltages, high electrostatic attraction forces are created, letting the membrane roll like a film over the actuating counterelectrode. Opposed to other curled actuator switch designs mentioned in the introduction, the touch-mode actuation principle is used both for opening and for closing the switch presented in this paper. Furthermore, the film actuator allows the displacement distance of the switching contact and thus the off-state isolation to be defined independently of the effective electrode actuation distance. The independence of the contact distance and the actuation voltage is a highly desirable feature for electrostatically actuated RF MEMS switches.

Since the switch is also opened actively by electrostatic forces between the top and the membrane electrodes, spring energy stored in the mechanical structure is not needed to open the switch. Therefore, the moving structure can be very thin and flexible, which is further lowering the actuation voltages.

Due to the large distance between the contacts in the off-state, the overlapping switching contact area may be designed substantially larger compared to other switches without decreasing the RF isolation. A large overlapping contact area does not necessarily reduce the contact resistance, which is determined by the applied force, the hardness and the surface roughness of the contact material, and possible surface contaminations of the contacts [15], [23], [24]. However, a large contact area is suitable for switching of signals with higher current, since the geometrical dimensions of the transmission line can be designed larger, which decreases the power dissipation in the switch and improves the distribution of the heat created by local high current densities in the contact interface. Larger contact areas of a soft material such as gold definitively increase the risk of contact stiction in the closed position, which is prevented by the active open capability of the presented switch concept.

TABLE I
Performance Criteria With Correlated Switch Features

| Performance criteria | Switch features |
|---|---|
| low actuation voltage | touch-mode actuation, thin and flexible structure |
| high isolation | large contact distance in off-state |
| current handling capability | wide signal lines with large nominal switching contact areas; active open capability |
| Packaging | two part assembly leading to encapsulated cavity with switch |
| integration with RF circuits | RF and MEMS part fabricated on different wafers → integration with any RF substrate possible |
| low switching speed | gas displacement around rolling membrane |

The actuation time of the film actuator is due to its nature determined by the displacement of the gas around the rolling film and not by its moving mass. The response time of a comparable film actuator was measured to be in the millisecond range for atmospheric pressure [25].

Table I is qualitatively summarizing the performance criteria correlated to the features of the film actuator switch concept.

## III. Prototype Design

The design of the switch is made in a way that the mechanical moving (MEMS) part of the switch is processed on a separate substrate than the RF transmission line. A schematic illustration of the switch with its elements is shown in Fig. 2. The RF target substrate to which the mechanical part of the switch is transferred, contains at the basic level only the signal transmission line, the bottom clamping electrodes, and the polymer ring-wall forming the cavity for the switch and defining the distance between the two parts of the switch after the final assembly.

A major advantage of this two-part fabrication concept is that the switch can easily be integrated with RF substrates of different materials without special restrictions in process compatibility of the MEMS part to the RF circuits. Having RF part and MEMS part processed on separate wafers is also a factor increasing the yield of the device fabrication as a whole. The transfer of the switch might be done either by pick-and-placing of single devices as done for our prototypes, or by full-wafer

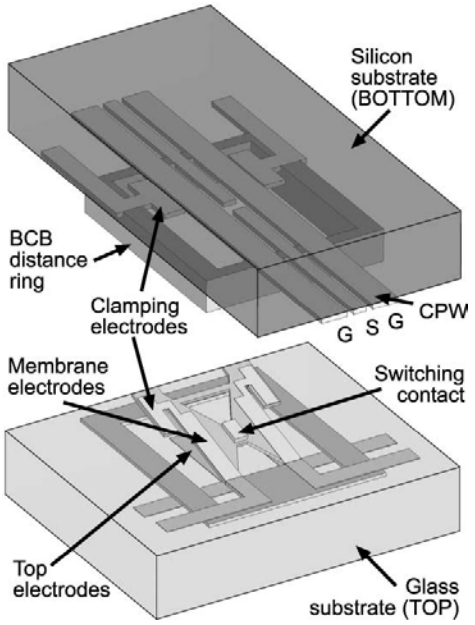


Fig. 2. Schematic illustration of the film actuator switch shown upside down. Details like isolation layers and etch holes are not shown.

bonding using a patterned adhesive layer, which is the target of our design. Furthermore, this concept leads to a near-hermetic package integrated switch, thus addressing one major problem of MEMS devices demanding an individual and complicated packaging solution [26].

The cavity finally containing all the parts of the switch is defined by the 100 $\mu$m wide ring-shaped polymer wall and has a size of 1100 $\mu$m$\times$ 1000 $\mu$m with a thickness of 18.2 $\mu$m. The prototype of the film actuator based switch presented in this paper is thus quite large compared to other MEMS switches published so far. However, this concept does not exclude reduction of the lateral switch dimensions while maintaining the large off-state contact distance and the relatively low actuation voltages of this switch concept.

### A. Actuator Design

The silicon nitride film actuator membrane is 960 $\mu$m long and 1 $\mu$m thick. Polyimide is used as a sacrificial layer to release the membrane. A dry-etchable sacrificial layer was chosen to avoid stiction of the very flexible membrane to the substrate. For the release-etch, sacrificial layer etch-holes with a size of 5 $\mu$m$\times$ 5 $\mu$m are placed all over the membrane with a distance of 10 $\mu$m between the holes.

The electroplated gold switching contact length is 190 $\mu$m, closing and opening a gap of 120 $\mu$m in the signal line of the coplanar waveguide. Thus, the switching metal bar has an overlap of 35 $\mu$m with each end of the signal line, forming two large nominal switching contact areas of 3500 $\mu$m$^2$ each. The switching contact force was estimated by simulations with ANSYS to 102 $\mu$N for each contact at an actuation voltage of 15 V between the membrane and the bottom electrodes.

The switch needs a total of four electrodes for its operation: the top electrodes, the membrane electrodes with their clamping electrodes part, the bottom electrodes and the bottom clamping

TABLE II
DRIVING POTENTIALS OF THE ACTUATION ELECTRODES

| Switch State | $V_{TOP}$ | $V_{MEM}$ | $V_{BOT}$=GND | $V_{CLAMP}$ |
|---|---|---|---|---|
| On | + | + | 0 | + |
| Off | + | 0 | 0 | + |

electrodes. However, to actuate the switch, only the driving potential of the membrane electrodes has to be altered, as shown in Table II. As bottom electrodes of the actuator, the two ground lines beside the signal line of the coplanar waveguide are used.

The function of the clamping electrodes is to keep the membrane securely in touch-mode with the bottom electrodes during the off-state when the membrane is pulled up toward the top electrodes. The area of the clamping electrodes is 54000 $\mu$m$^2$ each and they create, at a clamping voltage of 20 V, a nominal electrostatic force of 18 mN each to press the clamping part of the membrane down to the RF substrate. Without clamping electrodes, the switching membrane could completely be pulled up toward the top electrodes in the off-state, and the switch could not be closed again in case the membrane should stick to the top electrodes even after releasing the top electrode actuation voltage.

The touch mode actuation of both movements to open and to close the switch is achieved by a very small effective electrode distances, which are defined by a silicon nitride isolation layer of only 0.2 $\mu$m between the membrane electrodes and the bottom electrodes, and by the thickness of the membrane of 1 $\mu$m between the membrane electrodes and the top electrodes, respectively.

The contact pads of the top part of the switch are facing down toward the RF substrate after the assembly. Thus, they need to be connected to the RF substrate in a flip-chip like way or have to be accessed from the back side of the top substrate by through-wafer vias.

Dielectric charging of thin isolation layers causing "electrical stiction" of the actuator even after removing the actuation voltage, is one of the main reliability problems of electrostatic actuators [22]. If metal is used as the structural material of the moving part, dielectric charging can be avoided by replacing the complete covering isolation layer with small isolating bumps which keep the distance between the electrodes. For the present switch design, the moving membrane consists of silicon nitride which also acts as an isolation layer between the top and the membrane electrodes. A three-layer metal-nitride-metal structure could prevent dielectric charging problems, but would complicate the design much more. For a design with isolation layers, other methods like bipolar actuation voltage have shown to improve the switch reliability [27]. Also, a low actuation voltage design, as the presented one, substantially reduces the risk of failure due to dielectric charging, since an actuation voltage reduction of 6 V results in a 10-fold increase in the lifetime of MEMS switches [28].

### B. RF Design

A 2-$\mu$m-thick electroplated gold finite ground coplanar waveguide (FG CPW) is chosen as RF transmission line on the bottom part of the switch. The total length of the line is

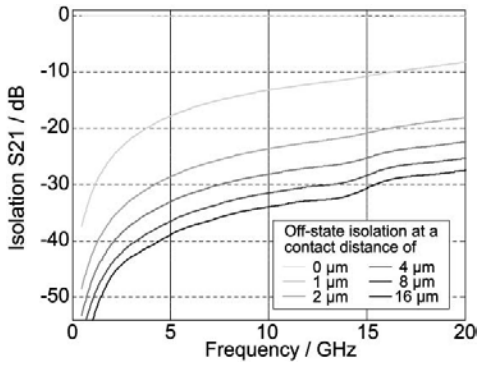


Fig. 3. FDTD simulation results of the off-state isolation of the prototype design with varying distance between the switching contacts, from 0.5 to 20 GHz.

3300 $\mu$m, the signal line width is 100 $\mu$m, the distance between the signal and each ground line is 55 $\mu$m, and the ground line width is 200 $\mu$m, to get a nominal characteristic impedance of 50 $\Omega$ estimated by empirical formulas [29].

RF simulations, carried out with the finite-difference-time-domain (FDTD) software CST Microwave Studio version 4, revealed that the prototype design has a relatively good isolation at gap-distances of 8 to 16 $\mu$m, as shown in Fig. 3. Thus, a thickness of the polymer distance keeping wall between the two parts of the switch of about 18 $\mu$m was chosen for the prototype switches, which results in a vertical traveling distance of about 14 $\mu$m of the switching contacts from the open to the close position, which is large enough for a decent off-state isolation even for the very large switching contact areas.

### C. Substrate Choices

A 100-mm diameter, 500-$\mu$m-thick high resistivity silicon substrate with a resistivity of 1500 $\Omega\cdot$cm is chosen as substrate material for the bottom part of the switch. The top part is fabricated on a Pyrex 7740 glass wafer with a diameter of 100 mm and a thickness of 500 $\mu$m. Pyrex glass, due to its high dielectric losses, is not a material of first choice for RF applications. However, since the top part of the switch is about 20 $\mu$m away from the coplanar waveguide, its material properties almost have no influence on the electrical field distribution of the waveguide, which was indicated by RF simulations. Thus, a cheap substrate may be chosen for the top part of the switch, which is a further advantage of this switch concept.

## IV. Fabrication

The design needs a total of seven photolithography masks. Three of them are used for the bottom part and the other four for the top part of the switch. All the processes involved in the fabrication of the two parts are standard clean-room surface-micromachining processes with a maximum temperature budget of 350 °C for the MEMS part of the switches. The fabrication procedure is schematically illustrated in Fig. 4 and explained in details in Sections IV-A–C.

### A. Bottom Wafer (Signal and Control Lines)

An 800-nm-thick silicon dioxide layer is deposited by LPCVD onto the high resistivity silicon wafer as an isolation layer. Then, a chromium/gold layer with a thickness of 40 nm/150 nm, acting as seed layer for the subsequent electroplating, is evaporated onto the wafer. The coplanar waveguide is created together with the clamping electrodes by electroplating of 2 $\mu$m of gold in an alkaline, noncyanide, thallium based gold bath [see Fig. 4(g)]. AZ 4562 photoresist from Clariant is used as a masking layer for the plating. The seed layer is etched away by a potassium iodide (KI) solution after removing the photoresist mask in acetone. A 200-nm-thin silicon nitride layer is deposited onto the wafer by low temperature PECVD. The adhesion of the silicon nitride layer to the plated gold was found to be very poor and the nitride layer just pealed off when the photoresist for patterning the layer was removed in acetone. An oxygen plasma treatment at 1000 W for 10 minutes immediately before the CVD improves the adhesion substantially. The silicon nitride layer is patterned by photolithography followed by reactive ion etching (RIE), using $CF_4$ plasma, and forms the isolation layer on top of the bottom electrodes [see Fig. 4(h)]. Afterward, the ring-shaped wall outlining the switch cavity is created using Benzocyclobutene (BCB) of the 3022-series from The Dow Chemical Company. This polymer is spun onto the wafer with a thickness of 18.2 $\mu$m [see Fig. 4(i)]. It is hard-cured at 280 °C and then patterned by photolithography using a thick photoresist mask and by etching in a RIE tool using $CF_4/O_2$ plasma [30], as shown in Fig. 4(j). Finally, the wafer is cut by a die saw [see Fig. 4(k)].

An SEM-picture of the bottom part before the final assembly is shown in Fig. 5. Fig. 6 shows the 18.2-$\mu$m-thick BCB ring-wall outlining the switch cavity with the transmission lines penetrating through it. The very good planarization properties of BCB lead to a very flat BCB surface, despite the interconnection lines penetrating through the polymer-wall with a thickness of 2 $\mu$m.

### B. Top Wafer (Switching Structure)

A 150-nm-thick gold layer with a 40-nm-thick chromium adhesion layer is evaporated onto the glass substrate to form the top electrodes. This layer is patterned subsequently by wet etching [see Fig. 4(a)]. Then, polyimide Pyralin PI 2555 from HD MicroSystems is spun with a thickness of 1.5 $\mu$m onto the wafer. The imidization of the polymer, which is used as sacrificial layer to release the membrane, occurs already at 180 °C. However, it has to be fully cured at 350 °C, since its curing temperature should be higher than any of the subsequent processing temperatures to avoid outgasing at a later fabrication step. Then, the 1-$\mu$m-thick silicon nitride membrane layer is deposited by low-stress PECVD at 300 °C, using dual-frequency RF power. Afterwards, a 40-nm/150-nm-thick chromium/gold layer is evaporated [see Fig. 4(b)]. This layer acts as seed layer for the following electroplating and is also used for the membrane electrodes with their membrane clamping electrode parts. The 2-$\mu$m-thick gold switching contact is electroplated using a Clariant AZ4562 photoresist mask [see Fig. 4(c)].

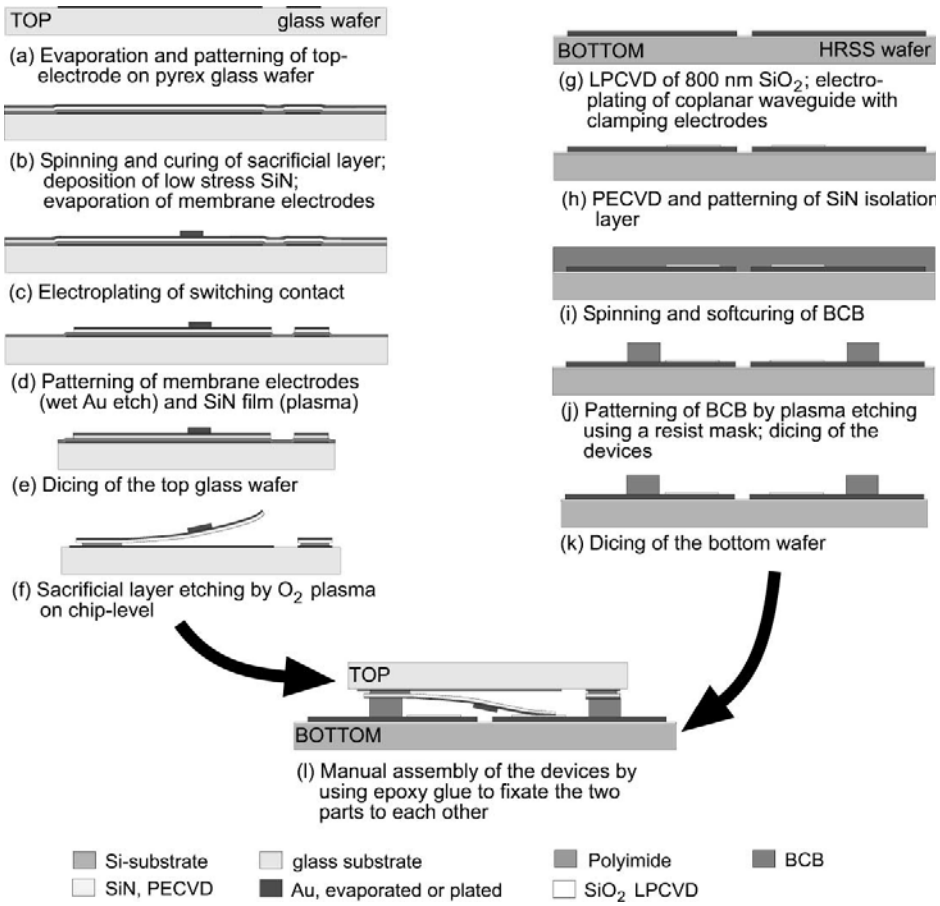


Fig. 4. Overview of the fabrication procedure.

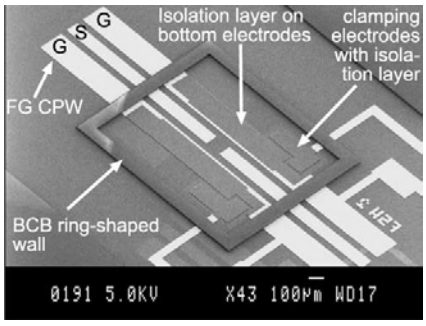


Fig. 5. SEM-picture of the bottom part of the switch before the final assembly.

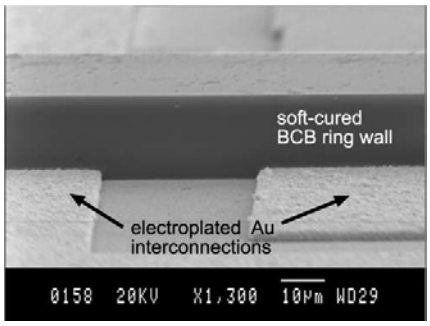


Fig. 6. SEM-picture of the 18.2-$\mu$m-thick BCB ring-shaped wall, surrounding the cavity containing the switch. The picture shows the very good planarization abilities of BCB resulting in a very flat surface despite the interconnection line thickness of 2 $\mu$m.

After removing this resist mask, the chromium/gold layer is patterned by wet chemistry. Then, the silicon nitride layer is etched down to the polyimide layer in a RIE tool using $CF_4$ plasma [see Fig. 4(d)]. The devices are cut by a die saw [see Fig. 4(e)] before etching the sacrificial layer, which is done in $O_2$ plasma at a power of 1000 W and a pressure of 100 mtorr [see Fig. 4(f)]. In Fig. 7, microscope pictures of a membrane detail after different sacrificial layer etching times are shown. The release-etch progress can be observed visually since the silicon nitride layer is highly transparent for visible light. The etching of the 1.5-$\mu$m-thick polyimide layer takes about 25 min due to the necessary lateral under-etching of the membrane of up to 7 $\mu$m.

Fig. 8 shows a SEM-picture of the whole top part of the switch after releasing the membrane, just before the final assembly. Because of the vertical stress gradient in the nitride layer of about 39 MPa/$\mu$m, estimated by measurements of the bending and by using equations given in [31], and due to stress in the nitride/gold multilayer-structure, the membrane bends upwards after its release. This bending puts the tips of the membrane in initial contact with the clamping electrodes on the bottom part of the switch after the assembly. The out-of-plane bending of the membranes is highly uniform all over the wafer and the release-etch was found to be successful for all of the 34 mem-

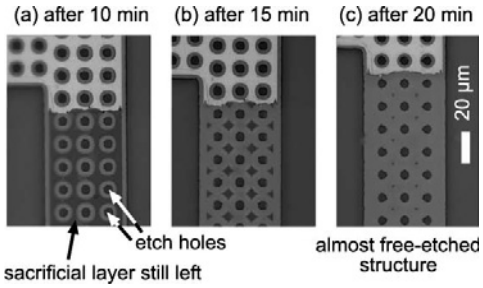


Fig. 7. Microscope pictures of a detail of the membrane after different sacrificial layer etching times. The stepwise etching of the polyimide sacrificial layer can be visually observed through the silicon nitride layer.

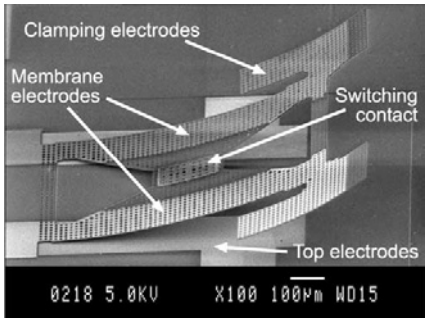


Fig. 8. SEM-picture of the top part of the switch after the sacrificial layer etch and before the final assembly, showing the out-of-plane bending of the membrane.

branes on each processed prototype wafer. Also, the silicon nitride-gold bilayer shows high reliability toward thermal induced stress. No single mechanical failure was observed when the structures were exposed to temperatures up to $280\,^{\circ}\mathrm{C}$ which are needed for the proposed wafer-level assembly of the devices.

### C. Assembly of the Prototypes

The switch is designed to be assembled on wafer level by using a commercial substrate bonder, fully curing the BCB distance ring during the bonding procedure. However, the first prototypes are assembled on device level in order to easily have access to the contact pads of the top part of the switch, which are facing the bottom substrate after assembly. The two parts are manually aligned with an accuracy of approximately $20\,\mu\mathrm{m}$. The alignment procedure is relatively simple since glass was chosen as substrate for the top part of the switch. Thus, the two toward each other facing structures are visible through the glass substrate. Despite the fact that the tips of the membranes are in contact with the bottom substrate during the alignment involving small lateral moments between the two parts, the membranes are not harmed by the procedure. Also, a full wafer alignment in a substrate alignment tool was found to be uncritical since the bending of the membrane does not exceed more than about $200\,\mu\mathrm{m}$ which is in the range of the programmable distance between the wafers in commercially available mask/substrate aligners during the loading and the initial approaching of the wafers in the tool.

After the manual and individually alignment of the prototypes, the parts are fixated to each other by epoxy glue to stabilize their handling during the measurements. Fig. 9 shows an overview photograph of the switch, with electrical wires glued by EPO-TEK H20E conducting epoxy to the prototype contact pads.

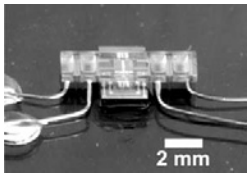


Fig. 9. Photograph of one of the prototype devices connected with electrical wires to access the different electrodes on the top part of the switch.

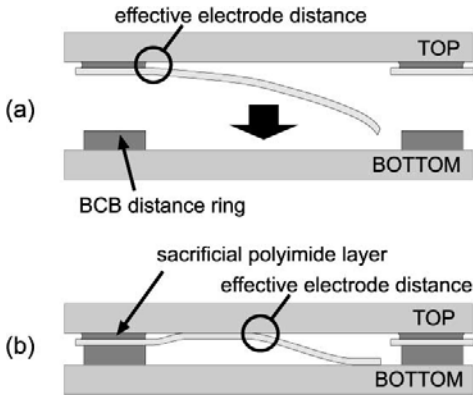


Fig. 10. Bending of the switch membrane before (a) and after (b) the assembly of the two parts of the switch. For the assembled switch (b), the membrane is pushed back to the top substrate, and the effective electrode distance is independent of the sacrificial layer thickness.

## V. Characterization and Performance

The actuation voltage between the membrane and the top electrode to open the switch is 12 V with an applied clamping electrode voltage of 20 V. The switch closes when a voltage of 15.8 V is applied between the membrane electrode and the bottom electrode. All of these actuation voltages are very well reproducible with a deviation of less than 0.7 V during subsequent cycles of the same device [21]. Reliability problems due to dielectric charging of the isolation layers were not observed during the basic characterization of the actuator, even though this problem was not explicitly investigated. Also, the relatively low actuation voltages of the presented design decrease the risk of dielectric charging.

Fig. 10 illustrates the shape of the membrane before and after the assembly, without any applied actuation voltage. Due to the bending and the contact of the membrane tips with the bottom substrate, the membrane is mechanically pushed up toward the top electrode, as shown in Fig. 10(b). Thus, the effective electrode distance of the top-to-membrane touch mode actuator is independent of the sacrificial layer thickness. This effect was confirmed by measurements revealing that there is no correlation between the actuation voltage and the sacrificial layer thickness. To further investigate this effect, the top actuator part only, as illustrated in Fig. 10(a), was evaluated. Here, the effective electrode distance has a total of $2.5\,\mu\mathrm{m}$, defined by the sacrificial layer thickness and the membrane thickness and results in an actuation voltage of 55 V to clutch the curling membrane

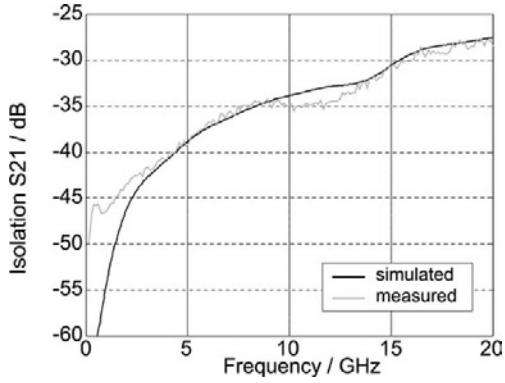


Fig. 11. Comparison of the simulated and the measured isolation of a prototype switch up to 20 GHz, with an open contact distance of $14.2\ \mu\mathrm{m}$ and a nominal switching contact area of $3500\ \mu\mathrm{m}^2$.

to its substrate. Furthermore, stiction between the membrane and the substrate could not be observed and is inhibited due to the vertical stress in the membrane and due to sufficient surface roughness. The membrane is curling up by itself when the actuation voltage drops below 8 V.

The dc resistance of the closed switch was determined by a 4-probe measurement, applying a 100-$\mu$A measurement current, to $0.650\ \Omega$. Subtracting the calculated resistance of the gold signal line, each contact has a resistance of $275\ \mathrm{m}\Omega$. For the simulated contact force of $102\ \mu\mathrm{N}$ per contact, literature reports different measured resistances of $10\ \mathrm{m}\Omega$ [24] and of $80$–$200\ \mathrm{m}\Omega$ [15] for clean gold contacts. The slightly higher contact resistance measured in the present investigation can be explained, beside uncertainties in the modeling and the simulations of the contact force, by organic residues on the metal contacts, which are known to increase the contact resistance at low contact forces, if the contacts are not undertaken to any special cleaning procedure [24]. Another study also observed an increased contact resistance of up to $1000\ \mathrm{m}\Omega$ for not clean gold surfaces at a contact pressure of $100\ \mu\mathrm{N}$ [23]. A possible source of the contact contamination, beside the fabrication procedure, is outgasing of the BCB during the final assembly. However, the authors assume that the contamination rather occurs during previous process steps, since the BCB is already soft-cured before the assembly and since the crosslinking of BCB does not involve catalysts and therefore does not cause detectable outgasing.[1]

The RF measurements, carried out with a Wiltron 360 vector network analyzer, revealed an off-state isolation of more than $-45$ dB up to 2 GHz and of $-30$ dB at 15 GHz, which is achieved due to the large contact distance of $14.2\ \mu\mathrm{m}$, despite the large overlapping switching contact area of $3500\ \mu\mathrm{m}^2$. Fig. 11 compares the simulated with the measured isolation at frequencies up to 20 GHz, showing a very good match of the measured to the expected performance of the prototype. Further information and more RF measurement results of the switch prototype can be found in [21].

## VI. Conclusion

Design and fabrication related aspects of a novel dc to RF MEMS metal contact switch based on an electrostatic touch-mode film actuator were presented. The S-shaped film actuator design allows a high isolation independent of a low-actuation voltage even at very large overlapping switching contact areas. Silicon nitride, deposited onto a polyimide sacrificial layer, is used as material for the flexible film membrane. The mechanical moving structure of the switch is fabricated on a different substrate and then transferred to a target RF substrate. Thus, the fabrication of the MEMS part is separated from the RF part which allows a simple integration with RF circuits with no special demands on process compatibility. Furthermore, the assembly of the two parts leads to a package integrated switch. The RF design was simulated with FDTD software and the manufactured prototypes were characterized by dc and RF measurements, showing low-actuation voltages and high isolation at very large nominal switching contact areas.

[1]information from the manufacturer

## Acknowledgment

The authors would like to thank to B. Lindmark from the Antenna Systems Technology group at the Royal Institute of Technology, Stockholm, Sweden, for the assistance with the RF measurements.

## References

[1] G. M. Rebeiz and J. B. Muldavin, "RF MEMS switches and switch circuits," *IEEE Microw. Mag.*, vol. 2, pp. 59–71, Dec. 2001.
[2] E. R. Brown, "RF-MEMS switches for reconfigurable integrated circuits," *IEEE Trans. Microw. Theory Techn.*, vol. 46, pp. 1868–1880, Nov. 1998.
[3] G. M. Rebeiz, *RF MEMS Theory, Design and Technology*, 1st ed. Hoboken, NJ: Wiley, 2003, ch. 1.
[4] K. E. Petersen, "Micromechanical membrane switches on silicon," *IBM J. Res. Dev.*, vol. 23, no. 4, pp. 376–385, July 1979.
[5] L. E. Larson, R. H. Hackett, and R. F. Lohr, "Microactuators for GaAs-based microwave integrated circuits," in *Proc. Transducers 1991*, San Franzisco, CA, June 24–27, 1991, pp. 743–746.
[6] J. Yao, "RF MEMS from a device perspective," *J. Micromech. Microeng.*, vol. 10, pp. R9–R38, 2000.
[7] Z. Y. Yao, S. Chen, S. Eshelman, D. Denniston, and C. Goldsmith, "Micromachined low-loss microwave switches," *J. Microelectromech. Syst.*, vol. 8, pp. 129–134, June 1999.
[8] S. Duffy, C. Bozler, S. Rabe, J. Knecht, L. Travis, P. Wyatt, C. Keast, and M. Gouker, "MEMS microswitches for reconfigurable microwave circuitry," *IEEE Microw. Wireless Compon. Lett.*, vol. 11, pp. 106–108, Mar. 2001.
[9] G.-L. Tan and G. M. Rebeiz, "A DC-contact MEMS shunt switch," *IEEE Microw. Wireless Compon. Lett.*, vol. 12, pp. 212–214, June 2002.
[10] H. A. C. Tilmans, "MEMS components for wireless communications (invited paper)," in *Proc. EUROSENSORS XVI*, Prague, Czech Republic, Sept. 15–18, 2002, pp. 1–34.
[11] J. J. Yao and M. F. Chang, "A surface micromachined miniature switch for telecommunications applications with signal frequencies from DC up to 4 GHz," in *Proc. Transducers 1995*, June 25–29, 1995, pp. 384–387.
[12] V. Milanovic, M. Maharbiz, A. Singh, B. Warneke, N. Zhou, H. K. Chan, and K. S. J. Pister, "Microrelays for batch transfer integration in RF systems," in *Proc. IEEE Micro Electro Mechanical Systems 2000*, Miyazaki, Japan, Jan. 23–27, 2000, pp. 787–792.
[13] S. Majumder, N. E. McGrues, and P. M. Zavracky, "Electrostatically actuated micromechanical switches," *J. Vacuum Sci. Technol. A*, vol. 15, no. 3, pp. 1246–1249, May/June 1997.
[14] M. -A. Gretillat, F. Gretillat, and N. F. de Rooij, "Micromechanical relay with electrostatic actuation and metallic contacts," *J. Micromech. Microeng.*, vol. 9, no. 4, pp. 324–331, Dec. 1999.
[15] D. Hyman and M. Mehregany, "Contact physics of gold microcontacts for MEMS switches," *IEEE Trans. Compon. Packag.Technol.*, vol. 22, pp. 357–364, Sept. 1999.
[16] D. Hah, E. Yoon, and S. Hong, "A low-voltage actuated micromachined microwave switch using torsion springs and leverage," *IEEE Trans. Microw. Theory Techn.*, vol. 48, pp. 2540–2545, Dec. 2000.

[17] S. Pacheco, C. T. Nguyen, and L. P. B. Katehi, "Micromechanical electrostatic k-band switches," in *Proc. IEEE MTT-S Int. Microwave Symposium Digest*, June 1998, pp. 1569–1572.
[18] H. F. Schlaak, F. Arndt, and M. Hanke, "Switching characteristics of silicon-microrelay with electrostatic actuator," in *Proc. 19th Int. Conf. on Electric Contact Phenomena*, Nuremberg, Germany, Sep. 14–17, 1998, pp. 59–64.
[19] I. Schiele, J. Huber, C. Evers, B. Hillerich, and F. Kozlowski, "Micromechanical relay with electrostatic actuation," in *Proc. Transducers 1997*, Chicago, IL, June 16–19, 1997, pp. 1165–1168.
[20] M. Shikida, K. Sato, and T. Harada, "Fabrication of an S-shaped microactuator," *J. Microelectromech. Syst.*, vol. 6, pp. 18–24, Mar. 1997.
[21] J. Oberhammer and G. Stemme, "Low-voltage high-isolation DC to RF MEMS switch based on a S-shaped film actuator," *IEEE Trans. Electron Devices*, vol. 51, Jan. 2004.
[22] C. C. Cabuz, E. I. Cabuz, T. R. Ohnstein, J. Neus, and R. Maboudian, "Factors enhancing the reliability of touch-mode electrostatic actuators," *Sens. Actuators A, Phys.*, vol. 79, no. 3, pp. 245–250, Feb. 2000.
[23] S. Majumder *et al.*, "Study of contacts in an electrostatically actuated microswitch," in *Proc. IEEE Electrical Contacts*, Arlington, VA, Oct. 26–28, 1998, pp. 127–132.
[24] J. Schimkat, "Contact materials for microrelays," in *Proc. IEEE Micro Electro Mechanical Systems 1998*, Heidelberg, Germany, Jan. 35–29, 1998, pp. 190–194.
[25] M. Shikida, K. Sato, K. Takeshita, and S. Suzuki, "Response time measurement of electrostatic S-shaped film actuator related to environmental gas pressure conditions," in *Proc. IEEE Micro Electro Mechanical Systems 1996*, San Diego, CA, Feb. 11–15, 1996, pp. 210–215.
[26] H. Reichl and V. Gosser, "Overview and development trends in the field of MEMS packaging," in *Proc. IEEE Micro Electro Mechanical Systems 2001*, Interlaken, Switzerland, Jan. 21–25, 2001, pp. 1–5.
[27] G. M. Rebeiz, *RF MEMS Theory, Design and Technology*, 1st ed. Hoboken, NJ: Wiley, 2003, ch. 7.2.
[28] C. Goldsmith, J. Ehmke, A. Malczewski, B. Pillans, S. Eschelmann, Z. Yao, J. Brank, and M. Eberly, "Lifetime characterization of capacitive RF MEMS switches," in *Proc. IEEE MTT-S Int. Microwave Symposium*, Phoenix, AZ, May 20–25, 2001, pp. 779–808.
[29] W. Heinrich, "Quasi-TEM description of MMIC coplanar lines including conductor-loss effects," *IEEE Trans. Microw. Theory Techn.*, vol. 41, pp. 45–52, Jan. 1993.
[30] P. B. Chinoy, "Reactive ion etching of benzocyclobutene polymer films," *IEEE Trans. Compon., Packag., Manufact. Technol.—Part C*, vol. 20, pp. 199–206, July 1997.
[31] W. Fang and J. A. Wickert, "Determining mean and gradient residual stresses in thin films using micromachined cantilevers," *J. Micromech. Microeng.*, vol. 6, no. 3, pp. 301–309, Sept. 1996.

**Joachim Oberhammer** born in Italy in 1976. He received the M.Sc. degree in electrical engineering from the University of Technology Graz, Austria, in 2000.

He was working with automotive electronics and RF identification systems both at the University of Technology Graz and Vienna University of Technology, Austria, before he joined the Microsystem Technology group at the Royal Institute of Technology, Stockholm, Sweden, as Ph.D. student in March 2001. Here, his research focus lies in RF MEMS and wafer-level packaging of MEMS components.

**Göran Stemme** (M'98) received the M.Sc. degree in electrical engineering and the Ph.D. degree in solid-state electronics, both from the Chalmers University of Technology, Gothenburg, Sweden, in 1981 and 1987, respectively.

In 1981, he joined the Department of Solid State Electronics, Chalmers University of Technology, Gothenburg, Sweden. There, in 1990, he became an Associate Professor (Docent) heading the silicon sensor research group. In 1991, he was appointed a Professor at The Royal Institute of Technology, Stockholm, Sweden, where he heads the Microsystem Technology group at the Department of Signals, Sensors, and Systems. His research is devoted to microsystemtechnology based on micromachining of silicon. Between 1995 and 2001, he was a Member of the International Steering Committee of the Conference series IEEE Microelectromechanical Systems (MEMS) and he was General Co-Chair of that conference in 1998. He has published more than 100 research journal and conference papers and has been awarded eight patents.

Dr. Stemme is a member of the Editorial Board of the IEEE/ASME JOURNAL OF MICROELECTROMECHNICAL SYSTEMS and of the Royal Society of Chemistry journal "*Lab On A Chip*". In 2001, he won, together with two colleagues, the final of the Swedish Innovation Cup.

# Paper 5

**Low-Cost Glass-Lid Packaging by Adhesive Full-Wafer Bonding with Two-Step Etched Electrical Feedthroughs**

*Joachim Oberhammer* and Göran Stemme

Submitted for journal publication.

# Low-Cost Glass-Lid Packaging by Adhesive Full-Wafer Bonding with Two-Step Etched Electrical Feedthroughs

Joachim Oberhammer and Göran Stemme

*Abstract*— **This paper reports on a low-cost fabrication technique to create glass-lid encapsulations for 0-level near-hermetic packaging of microsystem devices using adhesive full-wafer bonding with a previously patterned bonding layer of Benzocyclobutene (BCB). The glass lids are created by cutting the glass wafer with a die saw after bonding. The substrate wafer and thick electrical interconnections penetrating through the patterned BCB layer are not affected by this dicing process, since the outlines of the glass-lids are pre-cut on the side facing the substrate, allowing a lower vertical accuracy of the die saw. The bond interface of patterned BCB-bonds was investigated by scanning acoustic microscopy (SAM) and the bond strength was measured by carrying out tensile strength tests, resulting in a average bond strength of 5 MPa.**

**Furthermore, a new two-step technique to create low-density feedthroughs in glass substrates for electrical interconnections through the wafer is introduced. The vias are fabricated by combining a mechanical etch step by powder-blasting and a subsequent short hydrofluoric acid wet etch step. The advantage of this technique is that the major part of the via is etched without going completely through the wafer, allowing standard surface micromachining processes on the front-side of the glass wafer before the final opening of the via.**

**Both techniques were successfully combined to get glass-lid encapsulations by adhesive full-wafer bonding with thick electrical interconnections through the patterned adhesive layer to connect structures on the substrate, and with vertical feedthroughs through the glass wafer to electrically access structures on the glass-lids.**

*Index Terms*— **Adhesive bonding, glass lid encapsulation, powder blasting, through-wafer vias, wafer-level packaging.**

## I. Introduction

### A. Microcaps with in-plane interconnections

PACKAGING of microsystem devices is preferably done already on wafer-level to avoid contamination and harm of the structures during post-processing and the final assembly. Traditional MEMS encapsulation techniques by full-wafer bonding are fusion bonding [1] or anodic bonding [2], both having high demands on the roughness of the surfaces to be bonded [3]. Therefore, these techniques are very problematic if used to encapsulate surface-micromachined structures. Very thin electrical feedthroughs in the order of 50 to 100 nm can be manufactured with a special layout design without decreasing the hermeticity of the package [4]. A solution for interconnection lines with a thickness of 500 nm was proposed without characterizing the hermeticity [5]. Also, the relatively high temperatures of 1000 °C needed for fusion bonding and 300–500 °C for anodic bonding, respectively, and the high voltage in the latter technique limit the applications.

Wafer bonding with an adhesive intermediate bonding layer [6] has the main advantages of

- low-temperature
- simple processing (spin-on)
- high tolerance to surface non-uniformities in the order of several $\mu$m due to the good planarization properties of most adhesives, which allows thick electrical interconnection lines embedded in the adhesive layer
- no limitation to specific substrates or materials on the surfaces to be bonded
- the possibility to pattern the adhesive before the bonding to create 3D structures [7] and to get cavities for housing MEMS devices directly in the bonding layer [8]
- RF interconnection lines in or through the adhesive layer have very low losses and low reflections since adhesives with low loss tangent and low dielectric constants are available

A very suitable adhesive material showing the listed advantages is Benzocyclobutene (BCB) from The Dow Chemical Company, an epoxy-based polymer widely used in electronics manufacturing [9].

The main disadvantage of using polymers for packaging is that polymers are to a much higher degree permeable to gas as compared to metal seals [10]. However, polymers provide with a certain gas-tightness, and packages involving polymers are often classified as so-called "near-hermetic" packages. The properties of BCB as a gas diffusion barrier and its suitability for specific packaging applications is object of ongoing research [8], [11].

Encapsulation techniques by transferring sealing caps to a substrate wafer by using flip-chip-like pick-and-place techniques were shown with B-stage epoxy [12] and BCB [11]. Also, solder-bonding was used for flip-chip transfer of thin silicon microcaps [13]. Microcap packaging by full-wafer bonding, as shown in the present paper, is a significant further parallelization of the encapsulation process as compared to pick-and-place techniques. Such a technique, even with surface micromachined interconnection lines, was shown recently using AuSn eutectic bonding, but without solving the problem of how to access the interconnection lines, since the capping wafer and the substrate wafer were diced together [14]. Another technique uses microrivets for very low

J. Oberhammer and G. Stemme are with the Microsystem Technology Group, Department of Signals, Sensors and Systems, at the Royal Institute of Technology, SE-100 44 Stockholm, Sweden.

temperature joining of MEMS packages to a substrate wafer by electroplating the rivets through KOH-etched holes in the top wafer [15], where some of the KOH-etched holes were also used to access interconnection pads on the substrate wafer. A technique to create caps from a full-wafer by etching trenches in the top wafer after adhesive bonding, was proposed recently for electronics packaging of surface acoustic wave (SAW) filters [16].

The encapsulation approach in this paper uses full-wafer adhesive bonding of a top wafer to the substrate wafer, whereby the adhesive material is patterned before the bonding to form a distance keeping, closed wall surrounding the cavity to be encapsulated. Thick interconnection lines on the substrate wafer are penetrating through the adhesive wall. The top wafer is diced after the bonding to separate the glass-lids on wafer level.

Furthermore, this paper presents quantitative measurement values of the bond strength of patterned adhesive BCB-bonds. The bond strength was determined by carrying out tensile strength tests. So far, only qualitative investigations of the bond strength have been shown [8]. The present paper also reports on scanning acoustic microscopy (SAM) used to inspect the bond interface for delaminations and voids.

### *B. Vertical through-wafer interconnections in glass wafers*

Through-wafer vias are used in many kind of bonding applications, where structures on the two substrates facing each other have to be electrically connected and the interconnections can not be established within the bonding layer between the two wafers. The etching techniques for such vias in glass wafers presented so far are deep reactive ion etching (DRIE) of pyrex glass [17] and electrochemical discharge drilling [18].

The new through-wafer vias fabrication technique presented in this paper consists of two etch steps, where the first etch step is carried out ”almost-through” the wafer before any other process step and the second etch step to finally complete the holes is done after all other fabrication steps on the wafer.

## II. The packaging concept

The encapsulation technique presented in this paper creates near-hermetic glass-lid packages by adhesive full-wafer bonding. The BCB adhesive layer is patterned before the bonding by reactive ion etching (RIE) to form a closed wall-structure surrounding the device to be encapsulated. This wall also defines the distance between the wafers and thus the height of the device cavity. Surface micromachined interconnection lines with a thickness of up to a few $\mu$m can be fabricated on the substrate wafer, since three-dimensional structures are very smoothly covered by the spun-on BCB. The glass-lids are defined after the wafer bonding by dicing with a die saw, where unbonded glass parts just fall off. The substrate wafer and the interconnection lines are not affected by the dicing, since grooves are cut about 50 $\mu$m deep into the front-side of the glass wafer following the outlines of the later microcaps. These grooves allow a low vertical accuracy of the final dicing of the glass-lids without endangering structures on the surface of the substrate wafer. For a BCB layer thicker than the vertical accuracy of the die saw, the pre-cutting of the groves might be omitted.

The fabrication technique for through-wafer vias consists of two etch steps. The first etch step is carried out before any other processing on the wafer and etches the major part of the holes, resulting in recesses or ”almost-through holes” in the back-side of the wafer. Since the front-side of the wafer is not affected by this main etch step, any kind of standard surface-micromachining compatible to the substrate can be done on the front-side despite the almost completed holes on the back-side, including the processing of metal contact pads opposing the recesses and possible wafer-level packaging. Finally, the vias are completed by an unproblematic, since short and maskless etch step from the back-side. This procedure, illustrated in Fig. 1 might be applied with suitable etching-techniques for any kind of substrate. In the present paper, this technique is applied to glass wafers, where the first etch step is a mechanical etch by powder-blasting [19], and the second etch step is a wet-etch step with hydrofluoric acid (HF). This gives the following advantages in particular for glass wafer vias:

- the main etch step (here accomplished by powder-blasting) is carried out before any other process step on the glass wafer and can therefore be done outside clean-room facilities which lowers the costs
- powder-blasting is a rather inexpensive process for controlled deep etching in glass
- the metal contact pad to be accessed from the back-side through the wafer, acts also as etch-stop layer for the HF etch step
- both etch processes are applicable on different kind of glass wafers, even though Pyrex 7740 or Hoya SD-2 glass is the preferred substrate due to their high etch-rates in HF

Basically, also the first etch step could consist of a HF wet-etch step in the glass substrate. However, the presented technique using powder-blasting is superior due to higher etch integrity of the mask and allows smaller feature size as in the case of HF wet-etching.

## III. Fabrication

### *A. Glass wafer before the bonding*

The first fabrication step is the powder-blasting of the ”almost-through holes” in the back-side of the wafer (Figure 2a), about 400 to 450 $\mu$m deep into a 500 $\mu$m thick pyrex glass wafer. This process step is inexpensive and done outside clean-room facilities by powder-blasting equipment available for commercial production. Since the sidewalls of the etched recesses have a slope of about 70° to the surface of the wafer, an aspect ratio of up to 1.4:1 can be achieved. The wafer, after powder-blasting of recesses with a side length ranging from 400 $\mu$m up to 2 mm, is shown in Figure 3. Figure 4 shows a SEM picture of a cross-sectional cut of a single powder-blasted recess. After cleaning the wafer in an isopropanol bath and rinsing it with deionized water, any kind of microsystem structures compatible to the substrate can be processed on the front side of the glass wafer (Figure 2b), including the metal

layer used both for interconnection pads and as etch-stop layer for the later HF etch step. In this work, 150 nm evaporated gold onto a 40 nm thick chromium adhesion layer is used as an etch-stop layer. Afterwards, the grooves ooutlining the glass-lids are cut about 50 $\mu$m deep into the front-side of the glass wafer (Figure 2c), to allow a low vertical accuracy of the final dicing of the microcaps after the bonding (Figure 2i) without destroying structures on the substrate wafer.

### *B. Substrate wafer before the bonding*

The substrate wafer may house any kind of microsystem structures or interconnections lines processed by standard surface and/or bulk micromachining techniques which are compatible to the BCB processing (Figure 2d). Dry-etch BCB of the series Cyclotene 3022 from The Dow Chemical Company is spun onto the wafer and soft-cured at 210 °C for 30 minutes in a polymer oven with inert nitrogen atmosphere (Figure 2e). During the soft-curing, the polymer film is crosslinked to only about 50% of polymerization to ensure resistance to subsequent processes, in particular the plasma-etching for patterning the adhesive. However, if the film is cured too much, the BCB loses its adhesive properties and would no longer be suitable for bonding [8]. The patterning of the BCB to form the ring-wall surrounding the cavity to be encapsulated is done by $CF_4/O_2$ plasma etching using a thick photoresist mask [20], which is afterwards removed in Acetone (Figure 2f). The BCB film thickness also determines the cavity height between the two wafers. For the work presented in this paper, film thicknesses up to 18.2 $\mu$m were used. Due to the good planarization ability of the polymer, thick surface interconnection lines penetrating through the ring-wall are very smoothly covered by the polymer without disturbing the bond interface. Figure 5 shows such interconnection lines created by electroplating of 2 $\mu$m thick gold, covered by a 18.2 $\mu$m thick patterned BCB layer.

The contact pads of the glass wafer, acting as an etch-stop layer, are also supported by BCB on the substrate wafer to make the contact area mechanically strong enough for possible wire-bonding. The mask layout to pattern the BCB layer is shown in Figure 6 for a typical sample device as used in this investigation, with the BCB ring-wall and two of such supporting BCB areas.

### *C. Bonding and microcap formation*

The bond alignment is done in a bond alignment tool MA6/BA6 from Karl Suss and is rather uncritical for the feedthroughs, since they are quite large and require only an alignment accuracy in the order of 50 $\mu$m. Since a glass wafer is used as the top wafer, the alignment is done by looking through the glass wafer at both structures of the top and the bottom wafer, not requiring any back-side alignment marks on the bottom wafer. The two wafers are bonded in a commercially available substrate bonding tool SB6 from Karl Suss, applying 2.5 bar pressure between the bonding chucks which are heated to 250 °C for 1 hour to fully cure the polymer. To avoid gas being trapped in the bond interface and oxidation of the BCB during the bonding, the process is carried out in a vacuum of $10{\cdot}10^{-6}$ bar (Figure 2g).

After the bonding, the through-wafer vias are completed by a wet-etch step in 50% concentrated HF down to the gold pad acting as etch-stop layer (Figure 2h). Then, the glass-lids are cut out by dicing along their outlines with a die saw (Figure 2i). Due to the previous cutting of groves in the front side of the glass wafer (Figure 2c), the vertical accuracy requirements of the dicing are very low and can be achieved with any standard die saw equipment, independent on the BCB layer thickness. Unbonded glass parts just fall off without destroying the interconnection lines on the substrate wafer. Finally, the contact pads on the glass wafers can be electrically connected, e.g. by wire bonding, as shown in Figure 2j. Figure 7 shows a SEM picture of one of the final devices, where one end of the bonding wire is glued to the connection pad of the glass-lid by using the conducting epoxy TDS CW2400 from Chemtronics. The total resistance of such a connection from a glass-lid contact pad over a 30 $\mu$m thick gold bonding wire to a pad on the bottom wafer was measured to be 1.6 $\Omega$.

## IV. Investigation of the bonding interface

A total of 11 samples, with a dry-etch BCB pattern as shown in Figure 6, were subject of the bond interface investigation. Figure 8 shows a photograph of such a sample. The bond interface of all of these samples was evaluated by visual inspection through the transparent glass wafer. Eight of the 11 samples achieved a bond area which was larger than 70% of the total BCB pattern, and were therefore regarded as successfully bonded samples (hereafter classified as group A). The remaining 3 samples were classified to be unsuccessfully bonded samples (group B). Tensile strength tests were carried out on all samples. Table I shows the tensile strength test results with the corresponding bond strength of the samples of group A, and Table II summarizes the measurement results of the samples of group B. The samples of group A have an average bond strength of 5.01 MPa, which is about one tenth of the tensile strength of BCB itself. The average bond strength of the samples of group B was with 1.18 MPa much weaker than the bond strength of group A, which is in accordance to the visual inspection.

Furthermore, the bond interface was investigated by scanning acoustic microscopy (SAM), which is a nondestructive failure analysis or inspection technique to produce high resolution images of a sample's interior structure. Delaminations, voids or cracks in the interface of two materials or within a material are detectable using the change of acoustic impedance between different medias. The samples were placed into a water bath and scanned with an acoustic transducer using a carrier frequency of 50 MHz. In Figure 9, the SAM-picture of a sample with a successfully bonded interface is compared to an unsuccessfully bonded sample. Delaminations in the bond interface of the latter sample are clearly visible. SAM is a very suitable method to find such delaminations in the bond interface. However, if the bond interface is visible because a transparent wafer is used as in the present investigation, SAM

does not provide more information about the bond quality than visual inspection by a microscope, especially since the SAM pictures are often more difficult to interpret.

## V. Conclusions

A low-cost glass-lid encapsulation technique for MEMS devices using adhesive full-wafer bonding with patterned BCB as intermediate bonding layer was presented. The glass-lids are bonded as a whole wafer to the substrate with the BCB pattern, and diced after the bonding with a die saw. The dicing without destroying the bottom wafer is possible since the outlines of the glass-lids are pre-cut in the glass wafer. This technique also allows thick planar interconnection lines since they are very well covered by BCB due to its good planarization property.

Furthermore, a new technique of creating low density electrical through-wafer vias in glass wafers was shown using a novel two-step etching technique with a mechanical etch step (powder-blasting) and a subsequent wet-etch step in hydrofluoric acid. This technique gives the possibility to fabricate the main part of the hole outside clean-room environment, but still allowing standard surface-micromachining processes on the front-side of the glass wafer before the final opening of the vias by etching in HF.

The bond interface of patterned adhesive bonds with dry-etch BCB was characterized quantitatively by carrying out tensile strength tests. Also, scanning acoustic microscopy (SAM) was used to investigate possible delaminations in the bond interface.

## Acknowledgment

The authors would like to thank to the Little Things Factory, Ilmenau, Germany, especially to Mr. Bucke and Mr. Frank for the support and and the discussion about the powder-blasting.

Furthermore, the authors are very grateful to Mo Zhimin and Johan Liu, Division of Electronics Production at Chalmers University of Technology, Gothenburg, Sweden, for carrying out the tensile strength tests.

Also, the friendly and extensive help of Leena Korhonen, Ericsson Mobile Communications AB, Kumla, Sweden, with the SAM is highly appreciated.

## References

[1] A. Mehra, A. A. Ayón, I. A. Waitz, and M. A. Schmidt, "Microfabrication of high-temperature silicon devices using wafer bonding and deep reactive ion etching," *IEEE Journal of Microelectromechanical Systems*, vol. 8, no. 2, pp. 152–160, June 1999.

[2] E. Obermeier, "Anodic wafer bonding," in *Proc. Semiconductor Wafer Bonding: Science, Technology and Applications*, E. Society, Ed., vol. 95-7, Reno, Nevada, May 1995, pp. 212–220.

[3] B. Ziaie, J. A. V. Arx, M. R. Dokmeci, and K. Najafi, "A hermetic glass-silicon micropackage with high-density on-chip feedtroughs for sensors and actuators," *IEEE Journal of Microelectromechanical Systems*, vol. 5, no. 3, pp. 166–179, Sep. 1996.

[4] K. E. Petersen, "Method and apparatus for forming hermetically sealed electrical feedthrough conductors," Patent no WO 85/03381, 1985.

[5] K. M. Hiltmann, B. Schmidt, H. Sandmaier, and W. Lang, "Development of micromachined switches with increased reliability," in *Proc. Transducers 1997*, Chicago, USA, June 16–19, 1997, pp. 1157–1160.

[6] F. Niklaus, P. Enoksson, E. Kälvesten, and G. Stemme, "Low-temperature full wafer adhesive bonding," *Journal of Micromechanics and Microengineering*, vol. 11, no. 2, pp. 100–107, 2001.

[7] T.-K. A. Chou and K. Najafi, "3D MEMS fabrication using low-temperature wafer bonding with benzocyclobutene (BCB)," in *Proc. Transducers 2001*, Munich, Germany, June 10–14, 2001, pp. 1570–1573.

[8] J. Oberhammer, F. Niklaus, and G. Stemme, "Selective wafer-level adhesive bonding with benzocyclobutene for fabrication of cavities," *Sensors and Actuators A: Physical*, vol. 105, no. 3, pp. 297–304, Aug. 2003.

[9] P. B. Chinoy, "Processing and microwave characterization of multilevel interconnects using benzocyclobutene dielectrics," *Transactions on Components, Hybrids, and Manufacturing Technology*, vol. 16, no. 7, pp. 714–719, Nov. 1993.

[10] R. R. Tummala, E. J. Rymaszewski, and A. G. Klopfenstein, *Microelectronics Packaging Handbook, part 2: Semiconductor Packaging*, 2nd ed. Boston, Dordrecht, London: Kluwer, 1999, ch. 14.

[11] A. Jourdain, P. De Moor, S. Pamidighantam, and H. A. C. Tilmans, "Investigation of the hermeticity of BCB-sealed cavities for housing (RF-)MEMS devices," in *Proc. IEEE Micro Electro Mechanical Systems 2002*, Las Vegas, Nevada, Jan. 20–24, 2002, pp. 677–680.

[12] Y.-L. Park, H.-W. Park, D.-J. Lee, J.-H. Park, I.-S. Song, C.-W. Kim, C.-M. Song, Y.-H. Lee, C.-J. Kim, and B.-K. Ju, "A novel low-loss wafer-level packaging of the RF MEMS devices," in *Proc. IEEE Micro Electro Mechanical Systems 2002*, Las Vegas, Nevada, Jan. 20-24, 2002, pp. 681–684.

[13] J.-Y. Chen, L.-S. Huang, and P. C. Chu, Chia-Hua, "A new transferred ultra-thin silicon micropackaging," *Journal of Micromechanics and Microengineering*, vol. 12, no. 4, pp. 406–409, July 2002.

[14] S.-A. Kim, Y.-H. Seo, Y.-H. Cho, G. H. Kim, and U. B. Jong, "Fabrication and characterization of a low-temperature hermetic MEMS package bonded by a closed loop AuSn solder-line," in *Proc. IEEE Micro Electro Mechanical Systems 2003*, Kyoto, Japan, Jan. 19–23, 2003, pp. 614–617.

[15] B. Shivkumar and C.-J. Kim, "Microrivets for MEMS packaging: Concept, fabrication, and strength testing," *IEEE Journal of Microelectromechanical Systems*, vol. 6, no. 3, pp. 217–225, Sep. 1997.

[16] M. Goetz and C. Jones, "Chip scale packaging for RF SAW devices," in *Proc. SEMICON West 2002*, 2002, pp. 63–66.

[17] X. Li, T. Abe, Y. Liu, and M. Esashi, "High density electrical feedthrough fabricated by deep reactive ion etching of pyrex glass," in *Proc. IEEE Micro Electro Mechanical Systems 2001*, Interlaken, Switzerland, Jan. 21–25, 2001, pp. 98–101.

[18] H. Seo, G. Lim, and M. Sashi, "Hybrid-type capacitive pressure sensor," *Sensors and Materials*, vol. 4, no. 5, pp. 277–289, 1993.

[19] P. J. Slikkerveer, P. C. P. Bouten, and F. C. M. de Haas, "High quality mechanical etching of brittle materials by powder blasting," *Sensors and Actuators A: Physical*, vol. 85, pp. 296–303, 2000.

[20] P. B. Chinoy, "Reactive ion etching of benzocyclobutene polymer films," *IEEE Trans. On Components, Packaging, and Manufacturing Technology - Part C*, vol. 20, no. 3, pp. 199–206, July 1997.

**Joachim Oberhammer** , born in Italy in 1976, received his M.Sc. degree in electrical engineering from the University of Technology Graz, Austria, in 2000. He was working with automotive electronics and RF identification systems both at the University of Technology Graz and Vienna University of Technology, Austria, before he joined the Microsystem Technology group at the Royal Institute of Technology, Stockholm, Sweden, as Ph.D-student in March 2001. Here, his research focus lies in RF MEMS and wafer-level packaging of MEMS components.

**Göran Stemme** received the M.Sc. degree in electrical engineering in 1981 and the Ph. D. degree in solid state electronics in 1987, both from the Chalmers University of Technology, Gothenburg, Sweden. In 1981, he joined the Department of Solid State Electronics, Chalmers University of Technology, Gothenburg, Sweden. There, in 1990, he became an associate professor (Docent) heading the silicon sensor research group. In 1991, Dr. Stemme was appointed a professor at The Royal Institute of Technology, Stockholm, Sweden, where he heads the Microsystem Technology group at the department of Signals, Sensors and Systems. His research is devoted to microsystemtechnology based on micromachining of silicon.

Between 1995 and 2001 he was a member of the International Steering Committee of the Conference series IEEE Microelectromechanical Systems (MEMS) and he was General Co-Chair of that conference in 1998. Dr. Stemme is a member of the Editorial Board of the IEEE/ASME "Journal of Microelectromechnical Systems" and of the Royal Society of Chemistry journal "Lab On A Chip". 2001 he won, together with two colleagues, the final of the Swedish Innovation Cup. Dr. Stemme has published more than 100 research journal and conference papers and has been awarded 8 patents.

TABLE I

BOND STRENGTH MEASUREMENTS OF THE SAMPLES WITH A WELL-BONDED AREA LARGER THAN 70% (GROUP A)

| Sample no. | tensile strength N | bond strength MPa |
|---|---|---|
| 2 | 29.68 | 3.65 |
| 5 | 30.00 | 3.69 |
| 6 | 62.78 | 7.71 |
| 7 | 34.42 | 4.23 |
| 8 | 60.99 | 7.49 |
| 9 | 55.00 | 6.76 |
| 10 | 20.10 | 2.47 |
| 11 | 33.21 | 4.08 |
| average | 40.70 | 5.01 |
| std. dev. | 16.28 | 2.00 |

TABLE II

BOND STRENGTH MEASUREMENTS OF THE SAMPLES WITH DELAMINATIONS LARGER THAN 30% OF THE BCB AREA (GROUP B)

| Sample no. | tensile strength N | bond strength MPa |
|---|---|---|
| 1 | 9.65 | 1.19 |
| 3 | 14.56 | 1.79 |
| 4 | 4.65 | 0.57 |
| average | 9.61 | 1.18 |

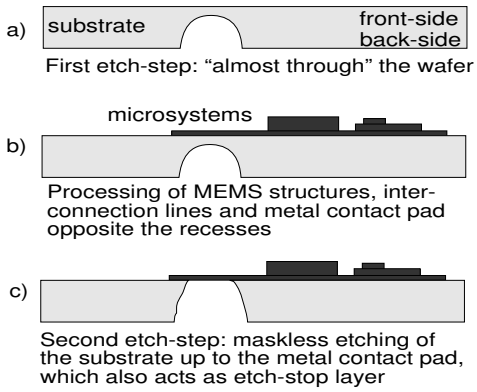


Fig. 1. Two-etch-step technique for through-wafer vias.

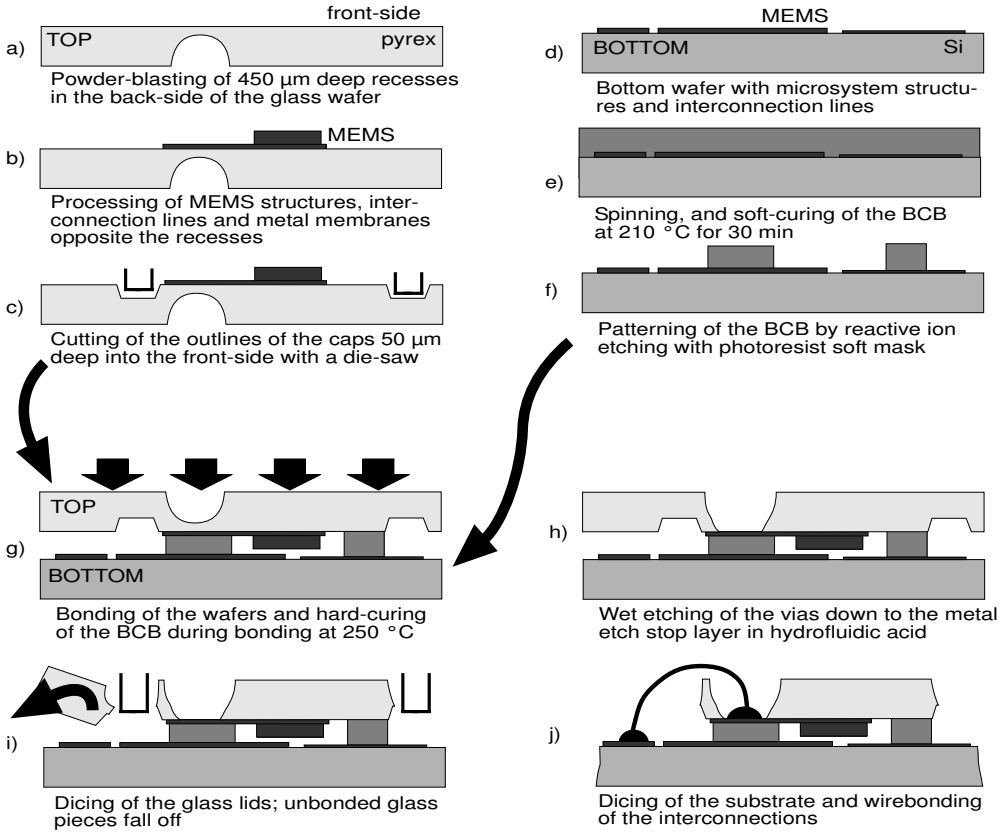


Fig. 2. Schematic process flow.

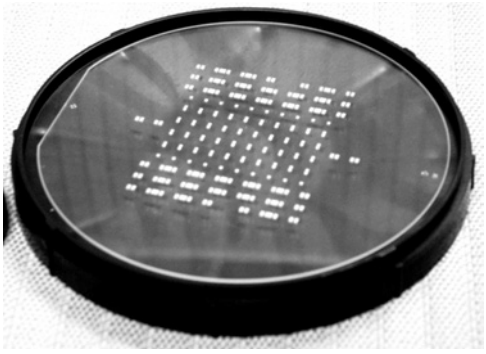

Fig. 3. Powder-blasted recesses in a 100 mm pyrex glass wafer.

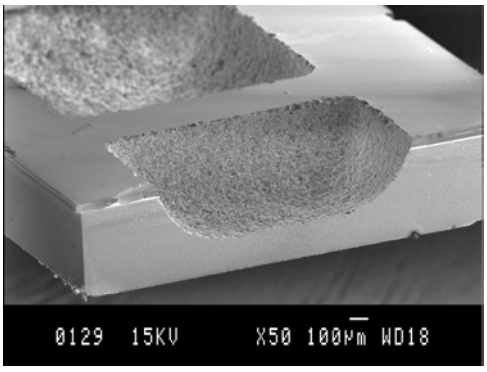


Fig. 4. SEM-picture of an about 450 $\mu$m deep powder-blasted recesses in a 500 $\mu$m thick pyrex glass wafer.

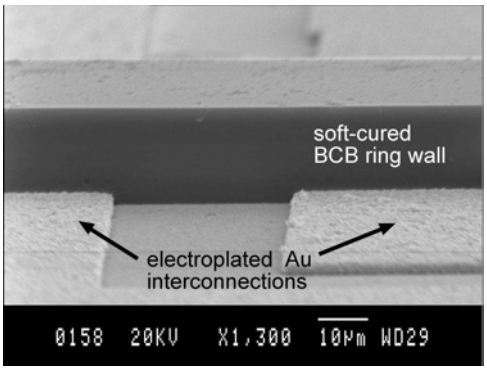


Fig. 5. SEM-picture showing the planarization ablilities of 18.2 $\mu$m thick BCB spun onto 2 $\mu$m thick electroplated interconnection lines after soft-curing and patterning the BCB by reactive ion etching.

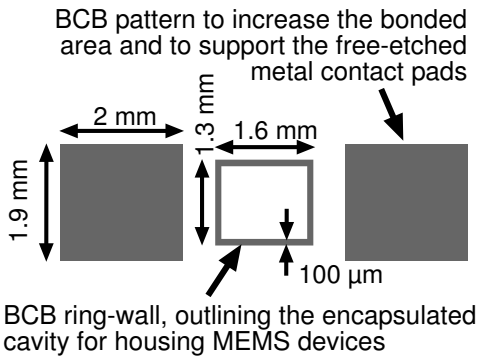


Fig. 6. Mask layout of the BCB pattern of the samples.

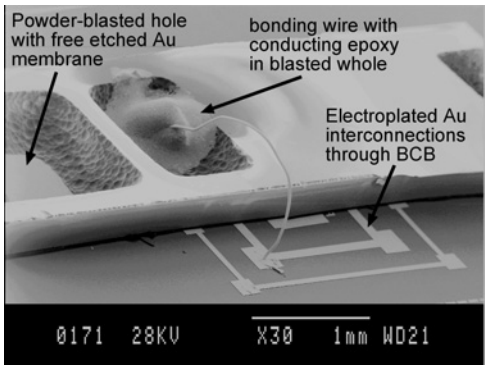


Fig. 7. SEM-picture of the glass-lid package with interconnection through-wafer vias and bonding wire. Also, planar interconnection lines penetrating through the BCB ring-wall on the substrate wafer are visible.

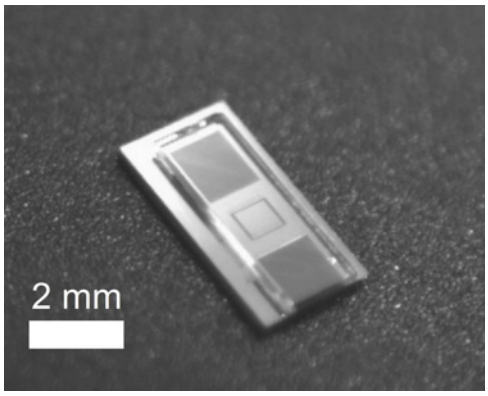


Fig. 8. Single sample before the tensile strength tests.

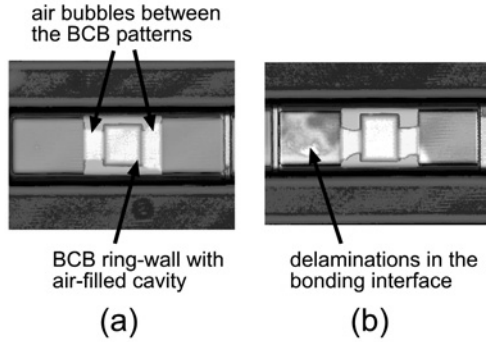


Fig. 9. Scanning acoustic microscope pictures of a well bonded sample (a) and of a sample with dilaminations in the bonding interface (b).

# Paper 6

**BCB Contact Printing for Patterned Adhesive Full-Wafer Bonded 0-Level Packages**

*Joachim Oberhammer* and Göran Stemme

IEEE/ASME Journal of Microelectromechanical Systems, accepted for publication, tentative print issue December 2004.

# BCB Contact Printing for Patterned Adhesive Full-Wafer Bonded 0-Level Packages

Joachim Oberhammer and Göran Stemme

*Abstract*— **Adhesive wafer bonding with a patterned polymer layer is increasingly attracting attention as cheap and simple 0-level packaging technology for microstructures, because the patterned polymer both fulfills the bonding function and determines the volumes between the two wafers housing the devices to be packaged. To be able to pattern a polymer, it has to be cross-linked to a certain degree which makes the material rigid and less adhesive for the bonding afterward. In this paper, a simple method is presented which combines the advantages of a patterned adhesive layer with the advantages of a liquid polymer phase before the bonding. The pattern in the adhesive layer is "inked" with viscous polymer by pressing the substrate toward an auxiliary wafer with a thin liquid polymer layer. Then, the substrate with the inked pattern is finally bonded to the top wafer.**

**Benzocyclobuene (BCB) was used both for the patterned structures and as the "ink". Tensile bond strength tests were carried out on patterned adhesive bonded samples fabricated with and without this contact printing method. The bonding yield is significantly improved with the contact printing method, the fabrication procedure is more robust and the test results show that the bond strength is at least 2 times higher. An investigation of the samples' failure mechanisms revealed that the bond strength even exceeds the adhesion forces of the BCB to the substrate.**

**Furthermore, the BCB contact printing method was successfully applied for 0-level glass-lid packaging done by full-wafer bonding with a patterned adhesive layer. Here, the encapsulating lids are separated after the bonding by dicing the top wafer independently of the bottom wafer.**

## I. Introduction

### A. Patterned Adhesive Bonding

Adhesive full-wafer bonding is a technique using a polymer as intermediate layer between the two wafers to be bonded [1]–[3]. The polymer is applied, usually by spin coating, on one of the two wafers, and the bonding is carried out involving pressure and a temperature high enough to fully cross-link the polymer in order to achieve a strong adhesion between the wafers and the polymer, and to get a strong bulk of the polymer itself. Some polymers can also be cross-linked at room temperature by photo-curing or by the hardening of two components epoxy.

The main advantages of adhesive bonding are:

- integrated circuit (IC) compatibility due to low temperature processing and since no voltages are involved as compared to anodic bonding
- insensitivity to particles and surface non-uniformities up to a few micrometers
- the thickness of the adhesive intermediate bonding layer can be chosen within a wide range
- simple and robust processing
- polymers show relatively good adhesion to most materials used in microsystems and microelectronics production
- the process is independent of the substrate materials and different substrates can be bonded to each other
- polymers do not contain ions which might diffuse into silicon and change its electrical characteristics
- the adhesive can be patterned before the bonding to create defined cavities in the bonding layer
- due to their elastic properties, polymer bonding layers act as a stress buffer between the bonded structures

A variety of polymer materials used in electronics production are suitable for adhesive bonding. Materials for a specific bonding application should be selected considering process compatibility, thermal stability, mechanical stability, creep strength, chemical resistance, handling, etc. The main restriction in the polymer choice is that the material is not allowed do evolve volatile substances during the cross-linking, which create delaminations and cracks due to trapped gases in the bonding interface.

Benzocyclobutene (BCB) [4]–[7] from the Dow Chemical Company was found to be suitable for adhesive bonding [8], since its curing process does not involve catalysts and thus no detectable outgasing of the polymer occurs after evaporating the solvents. It is also possible to pattern this material in a soft-cured, i.e. not fully cross-linked state, which makes it suitable for wafer bonding with patterns in the adhesive layer. The patterning can be done either by dry-etching [9], [10] or by using a photosensitive version of the material [11]. Successful bonding with such a patterned BCB layer was already reported, both by using photosensitive BCB [12] and by using dry-etch BCB [13]. Dry-etch BCB is available in different viscosities resulting in a single-layer thickness ranging from 1 to 26 $\mu$m, and the photosensitive version is available for single-layers up to 40 $\mu$m.

The bond strength of a patterned adhesive layer is lower than the bond strength of an unpatterned layer, since the polymer has to be cross-linked to a certain degree before the bonding, in order to be chemically and physically resistant enough for the patterning processes. Also, the soft-cured BCB is much less elastic than an uncured and basically liquid BCB layer, which decreases the bonding yield in case of surface non-uniformities on both of the wafers to be bonded [13].

In this paper, a simple method is presented which combines the advantages of a patterned adhesive layer with the advantages of a viscous polymer phase before the bonding. The pattern in the adhesive layer is "inked" by pressing the

J. Oberhammer and G. Stemme are with the Microsystem Technology Group, Department of Signals, Sensors and Systems, at the Royal Institute of Technology, SE-100 44 Stockholm, Sweden.

substrate with the patern toward an auxiliary wafer with a thin and almost-liquid polymer layer. Then, the substrate with the inked pattern is finally bonded to the second wafer.

### *B. Wafer-Level Packaging by Adhesive Bonding*

In electronics manufacturing, wafer-level packaging (WLP) is a trend in flip-chip mounting of integrated circuits (IC) directly to the printed circuit board (PCB) or multichip-module (MCM), without a separate carrier for redistribution of the pads [14]. Thus, the sawing of the wafer is the last process step. In MEMS, the term wafer-level packaging is used if the cavity containing the mechanical device is sealed and tested on wafer level, then diced and finally integrated into the high-level system or the final electronic package. The key-advantages of this wafer-level approach for both electronics and MEMS are substantially lower cost and higher volume throughput and a higher degree of system miniaturization [15], [16].

Glass-lid encapsulation on wafer-level with flip-chip-like techniques, where each encapsulating lid is individually placed and bonded to the corresponding device on the still complete substrate wafer, was shown with b-stage epoxy [17] and with photosensitive BCB [18]. The disadvantages of this wafer-level capping technique are that the caps have to be separated by a die saw before the bonding and thus introduce a source of particles to the process chain, and that the packaging process of the whole wafer takes a very long time due to the individual chip alignment and bonding. Wafer-level packaging by full wafer bonding significantly parallelizes the packaging process which is reduced to one single bonding step. Anodic bonding follows this approach and became a key packaging technology which enabled high volume fabrication of MEMS microactuators and mircosensors like accelerometers [19].

The authors of the present paper recently demonstrated an encapsulation technique by full-wafer bonding using a patterned BCB layer. Here, a full wafer is bonded to the substrate wafer containing the devices to be packaged and BCB patterns in the shape of rings surrounding the devices. The encapsulating lids are diced after the bonding without harming the substrate wafer [20]. In the present paper, the BCB contact printing technique is applied to improve the yield and reliability of this 0-level packaging method.

Packaging by polymer bonding does not provide with hermeticity in terms of gas-tightness [21, Section 14.4.1], even for an epoxy-based polymer such as BCB. The authors of the present paper already published a method to improve the hermeticity of BCB bonded packages by adding an additional silicon nitride diffusion barrier in form of a passivation layer [22].

## II. FABRICATION

Figure 1 shows the fabrication sequence of the 0-level glass-lid encapsulation technique by using the BCB contact printing method. The 100 mm diameter, 500 $\mu$m thick silicon substrate wafer contains the BCB pattern in the shape of a wall surrounding the device to be packaged (Figure 1a). The contact printing method can also be applied with any other patternable organic or non-organic material to achieve a local adhesive bond by printing and curing a viscous polymer. In this paper, dry-etch BCB CYCLOTENE 3022-56 is used as patternable material with a resulting layer thickness of 18 $\mu$m. On some wafers, adhesion promoter AP8000 was applied before spinning the BCB to investigate a possible bond strength improvement. The BCB is spun onto the substrate and soft-cured at 210 °C for 30 minutes before patterning it in $CF_4/O_2$ plasma with a Shipley SPR 5740 photoresist mask with a thickness of 20 $\mu$m. The "ink" for the contact printing, also BCB of the same kind, is spun onto an auxiliary silicon wafer with a resulting thickness of 1 $\mu$m. This layer is not cured and the wafer is not even put onto a hotplate, to keep the BCB as viscous as possible. The top surface of the BCB pattern on the substrate is then "inked" by pressing the auxiliary wafer to the substrate wafer (Figure 1c). This process is carried out in a commercially available substrate bonder Karl Suss SB6, involving a bonding pressure of 350 to 500 mbar for 10 min. Afterward, the wafers are separated by inserting a razor blade in between the two wafers. Since no bonding and no curing of the BCB film occured, the auxiliary wafer can be easily removed, leaving a thin liquid BCB layer on top of the BCB pattern of the substrate (Figure 1d). The top glass wafer, 100 mm diameter and 500 $\mu$m thick, is then bonded to the substrate, applying a pressure of 2.5 bar and a temperature of 250 °C for 1 hour, to fully cross-link both of the polymer films (Figure 1f). For the glass-lid packaging, the outlines of the final glass-lids might be cut into the front-side of the glass wafer before the bonding (Figure 1e). Such groves allow a lower vertical accuracy of the die saw when finally dicing the top wafer after the bonding to separate the glass-lids (Figure 1g). This process step may be omitted if the thickness of the polymer layer is larger than the vertical accuracy of the die saw. After the bonding, only the top wafer is cut along the outlines of the glass-lids without harming structures on the bottom wafer, and unbonded glass parts just fall off. Finally, also the bottom wafer is diced (Figure 1h).

To fabricate the samples required for the bond interface investigation, it would be sufficient to cut the bonded wafers with one single cut into test samples. As a more general glass-lid encapsulation technique, the presented method cutting the top wafer independently of the bottom wafer has the advantage that structures on the front-side of the bottom wafer, such as electrical contact pads for wire-bonding, can easily be accessed. Figure 2 shows an array of glass-lid packages still on the substrate wafer after dicing the glass wafer only. Figure 3 shows a photograph of one of the samples after the whole fabrication procedure.

It should be mentioned that a similar improvement of the bonding technique could also be achieved by simply spinning a thin polymer layer directly on the top wafer. However, the local transfer of the thin polymer layer has the advantage that the top wafer can also contain microsystem structures which might not allow to be covered by a polymer film. Another modification of the fabrication is the spinning and patterning of the BCB pattern on the top wafer instead of the bottom wafer, if the bottom wafer contains free-etched mechanical structures which can not be covered by the spin-on polymer. If both wafers contain sensitive mechanical structures, the BCB

could also be printed on the wafer.

For the samples fabricated with the "conventional" patterned BCB bonding technique, the soft-cured BCB was directly bonded to the top glass wafer after patterning the polymer. This is possible since the material is cross-linked to only about 50% during the soft-curing, making it robust enough for the patterning but still leaving it sufficiently adhesive for the bonding. During the bonding process, the material is fully cured and creates a bond with the surface of the glass wafer. The degree of soft-curing and thus the soft-curing parameters are very important for a successful patterning and bonding [13], whereas it is very uncritical for the BCB contact printing method which also works using a fully cured BCB pattern.

The fabrication with both methods uses the same photomask for the patterning of the BCB, the same procedure for its soft-curing and its patterning, and the same final bonding procedure. The only difference is the transfer of the "BCB-ink" to the BCB pattern for the contact printing method.

## III. Bonding results

### A. BCB-ink Transfer

The BCB-ink is still viscous even though most of the solvents of the thin film are expected to be evaporated quickly. Therefore, the patterned ink is flowing slightly out of shape during the bonding procedure, as shown in the microscope photograph of Figure 4, taken through the glass wafer after bonding. Especially in concave corners, the BCB is also flowing into the cavity. However, this effect can be predicted and the volume deformation of the viscous BCB film can be considered in the design by knowing the width of the BCB wall and the ratio of the thickness of the BCB-ink layer to the thickness of the BCB wall. For the fabricated samples with a 18 $\mu$m thick and 100 $\mu$m wide BCB wall and a 1 $\mu$m thick BCB-ink layer, the BCB flow into the encapsulated cavity is calculated to be less than 3 $\mu$m, assuming a uniform displacement of the material and a complete transfer of the ink from the auxiliary wafer. Measurements on the samples confirmed a flow in this order of magnitude and also a very uniform displacement, except in concave corners where the flow length for a pattern width of 100 $\mu$m was measured to be between 5 and 10 $\mu$m, in some cases even up to 30 $\mu$m, as shown in Figure 4. Smaller pattern areas however also cause less volume deformation of the BCB-ink, thus small features with a width of 10 $\mu$m are distorted by less than 2 $\mu$m and even concave corners are very sharp after the bonding process, as shown in Figure 5a.

Figure 6 shows the negative imprint of the BCB-stamp of Figure 4 in the BCB layer on the auxiliary wafer after separating the auxiliary wafer from the substrate wafer. The BCB is transferred very uniformly to the BCB stamp which leads to a very homogeneous bond. That means that 1) the adhesion of the viscous BCB film to the BCB pattern is higher than the adhesion of the film to the auxiliary silicon wafer substrate, and 2) that the cohesive forces within the viscous BCB film are smaller than both the adhesion to the BCB pattern and the adhesion to the auxiliary wafer. When investigating the auxiliary wafer, a pattern shift in the range of 100 $\mu$m was observed. The authors assume that the displacement between the auxiliary wafer and the substrate wafer occurs during the manual separation of the two wafers, and not during the film transfer in the bonder. This assumption is also supported by the observation that during the final bonding of the glass wafer to the substrate wafer, the wafers move not more than a few micrometers, because a "smeared" BCB pattern would be visible on the glass wafer after the bonding if the movement between the wafers would have been larger than the volume deformation of the ink. As demonstrated in Figure 5, even inked patterns with a feature size of 10 $\mu$m do not show any such "smearing effect" at all, and thus the wafer movement during the bonding is assumed to be less than 2 $\mu$m. That is much less than was found during previous research work, done at our institute with the same bonding machine, which revealed that the post bonding alignment accuracy for adhesive bonding using viscous (not pre-cured) epoxy-based resins such as BCB with a thickness of 2 to 3 $\mu$m is in the range of up to 15 $\mu$m [23][1]. For the present investigation however, the not pre-cured transferred BCB film is assumed to be much thinner than the actual layer thickness on the auxiliary wafer due to some displacement of the BCB underneath the pattern caused by the involved pressure during the "inking" process, and thus results in a larger mechanical resistance against lateral movements during the final bonding.

The whole process of transferring the BCB ink and the bonding with the soft-cured/viscous BCB layers was found to be very robust, since already the first process parameter set was very successful and all the pictures of the bonded structures and the auxiliary wafer are taken from the very first bonding experiment (Figures 4, 5, 6).

### B. Bond Interface Investigation

The test samples fabricated with the "conventional" patterned BCB bonding technique are classified in the following text as group A, as group B1 and B2 if fabricated with the BCB contact printing method, whereas group B1 was fabricated without using adhesion promoter between the silicon substrate and the BCB pattern, and group B2 with applying the adhesion promoter AP8000.

The bond quality of the samples was investigated by carrying out tensile strength measurements, by visual inspection through the glass wafer, and by scanning acoustic microscopy (SAM). Since the top wafer was a glass wafer in all bonding experiments, delaminations in the bond interface can easily be found by visual inspection with a microscope. Also, scanning acoustic microscopy has proved to be a very suitable inspection tool since it can be used also for non transparent materials, even though the lateral resolution is not as good as with visual inspection. The tensile strentgh was measured with a pull-tester with a capability of up to 1 kN, and the samples were glued to the sample holders by epoxy. The strength of

[1]The wafer movement in adhesive bonding with not pre-cured adhesives is larger than typically observed in other wafer bonding techniques such as anodic bonding, because a viscous adhesive layer is mechanically less resistant to the shear stress created by the two bonding chucks being not leveled absolutely parallel to each other, which results in a lateral movement.

the epoxy for the set-up is similar to the bond strength of the BCB, but the glued area is much larger than the bonded area.

Due to the fact that the soft-cured BCB of the samples of group A is not as flexible as the viscous BCB, some of the samples of group A had delaminations in the bond interface. Figure 7 shows SAM pictures of samples of group A. The sample in Figure 7a is very well bonded, whereas the sample in Figure 7b clearly has delaminations over a large area. SAM is done in a heated water bath and all of the pictures taken have trapped air bubbles inside the encapsulated cavity and between BCB structures. The well bonded area was for 78% of the samples of group A lower than 70% of the BCB pattern, whereas all of the samples of the groups B1 and B2 had an almost 100% successfully bonded area.

Tensile strength measurements were carried out on 11 samples of group A, on 5 samples of group B1 and on 11 samples of group B2. The average bond strength of the samples of group B1 (BCB contact printed without adhesion promoter) was with 11.34 MPa almost 3 times higher than the average bond strength of the samples of group A ("conventional" patterned soft-cured BCB bonding technique) with 3.97 MPa. The average bond strength of the samples of group B2 (BCB contact printed with adhesion promoter) was unexpectedly slightly lower than the average bond strength of the samples of group B1, but still significantly higher than the average bond strength of those of group A. A summary of the measurements is given in Table I, and the measurement results of all tested samples are shown in Figure 8. Table II gives an overview of the bond strength of different bonding methods to be compared with the technique proposed in the present paper.

After the tensile strength tests, some samples of group A and all 11 samples of group B2 were further inspected to investigate the failure mode. The samples of group A broke at the interface of the BCB-pattern to the glass wafer which is the actual bonding interface. Thus, the bond strength of the already soft-cured BCB is lower than the adhesion force between spun-on BCB and the silicon substrate. The failure mode of all of the samples of group B2 is of adhesive nature. Seven samples broke at the interface between the BCB-pattern and the silicon wafer (Figure 9b), and the remaining 4 samples broke partly at the BCB to the glass wafer interface and partly at the BCB-pattern to the silicon wafer interface (Figure 9c). Thus, no cohesive fracture was observed between the two BCB phases and the tensile strength of the samples of group B was merely limited by the adhesion forces of the BCB to the substrates.

It is interesting to observe that most of the adhesive failures of the samples of group B2 happened at the surface of the silicon wafer. That means that the adhesion of BCB to the polished silicon surface is despite the use of the adhesion promoter less strong than the adhesion of BCB to the glass surface. Also, the tensile strength tests of the samples of the groups B1 and B2 show that the use of the adhesion promoter seems not to improve the adhesion of the spun-on dry-etch BCB to the silicon wafer.

In table II, the bond strengths of various wafer bonding methods are compared with the bond strength of the BCB contact printing method.

## IV. Conclusions

This paper described a contact printing method with viscous BCB as "ink" and using a soft-cured BCB pattern as stamp to improve the bond strength of full-wafer adhesive bonding with patterned BCB as intermediate bonding layer. The technology was successfully demonstrated for glass-lid encapsulations created by full-wafer bonding. The bond strength of samples fabricated with the new method was measured by tensile strength tests and compared with samples fabricated with the "conventional" patterned BCB bonding technique. The BCB contact printing method leads to an increased bond strength by a factor of at least 2, which even exceeds the adhesive strength of spun-on BCB to the substrate wafers.

## Acknowlegments

The authors would like to thank to Mo Zhimin and Prof. Johan Liu, Division of Electronics Production at Chalmers University of Technology, Gothenburg, Sweden, for carrying out the tensile strength tests.

Also, the friendly and extensive help of Leena Korhonen, Ericsson Mobile Communiacations AB, Kumla, Sweden, with the scanning acoustic microscope is highly appreciated.

## References

[1] D. E. Booth, C. E. Hunt, W. E. Brown, and R. J. Stover, "Low temperature adhesion bonding methods," in *Proc. 3rd Int. Symp. on Semiconductor Wafer Bonding: Physics and Applications*, Reno, NV, USA, May 21–26, 1995, pp. 201–211.

[2] W. Eaton, S. Risbud, and R. Smith, "Silicon wafer-to-wafer bonding at T<200 degrees C with polymethylmethacrylate," *Applied Physics Letters*, vol. 65, no. 4, pp. 439–441, July 1994.

[3] C. den Besten, R. E. G. van Hal, J. Munoz, and P. Bergveld, "Polymer bonding of micro-machined silicon structures," in *Proc. IEEE Micro Electro Mechanical Systems 1992*, Travemunde, Germany, Feb. 4–7, 1992, pp. 104–109.

[4] K. C. Chan, M. Teo, and Z. W. Zhong, "Characterization of low-k benzocyclobutene dielectric thin film," *Microelectronics International*, vol. 20, no. 3, pp. 11–22, 2003.

[5] P. Garrou, "Polymer dielectrics for multichip module packaging," *Proceedings of the IEEE*, vol. 80, no. 12, pp. 1942–1954, Dec. 1992.

[6] P. E. Garrou, R. H. Heistand, M. G. Dibbs, T. A. Manial, C. E. Mohler, T. M. Stokich, P. H. Townsend, G. M. Adema, M. J. Berry, and I. Turlik, "Rapid thermal curing of BCB dielectric," *IEEE Trans. on Components, Hybrids, and Manufacturing Technology*, vol. 16, no. 1, pp. 46–52, Feb. 1993.

[7] Y.-S. Choi, J.-S. Park, H.-D. Park, Y.-H. Song, J.-S. Jung, and S.-G. Kang, "Effects of temperatures on microstructures and bonding strengths of Si-Si bonding using bisbenzocyclobutene," *Sensors and Actuators A: Physical*, vol. 108, pp. 201–205, 2003.

[8] F. Niklaus, P. Enoksson, E. Kälvesten, and G. Stemme, "Low-temperature full wafer adhesive bonding," *Journal of Micromechanics and Microengineering*, vol. 11, no. 2, pp. 100–107, 2001.

[9] P. B. Chinoy, "Reactive ion etching of benzocyclobutene polymer films," *IEEE Trans. On Components, Packaging, and Manufacturing Technology - Part C*, vol. 20, no. 3, pp. 199–206, July 1997.

[10] S. A. Vitale, H. Chae, and H. H. Sawin, "Etching chemistry of benzocyclobutene (BCB) low-k dielectric films in $F_2$+$O_2$ and $Cl_2$+$O_2$ high density plasmas," *Journal of Vacuum Science and Technology A (Vacuum, Surfaces, and Films)*, vol. 18, no. 6, pp. 2770–2778, Nov. 2000.

[11] A. J. G. Strandjord, W. B. Rogers, Y. Ida, S. Shiau, E. S. Moyer, D. M. Scheck, R. R. DeVellis, and P. E. Garrou, "One mask process for stress-buffer and passivation applications using photosensitive benzocyclobutene," in *Proc. Int. Electronic Manufacturing Symp. and Int. Microelectronics Conf.*, Apr. 16–18, 1997, pp. 261–266.

[12] T.-K. A. Chou and K. Najafi, "3D MEMS fabrication using low-temperature wafer bonding with benzocyclobutene (BCB)," in *Proc. Transducers 2001*, Munich, Germany, June 10–14, 2001, pp. 1570–1573.

[13] J. Oberhammer, F. Niklaus, and G. Stemme, "Selective wafer-level adhesive bonding with benzocyclobutene for fabrication of cavities," *Sensors and Actuators A: Physical*, vol. 105, no. 3, pp. 297–304, Aug. 2003.
[14] W.-C. Lo, L.-C. Shen, S.-M. Chang, Y.-C. Chen, H.-T. Hu, J.-R. Lin, K.-C. Chen, and Y.-J. Hwang, "The development of enhanced wafer level packaging," in *Proc. IEEE Electronics Packaging Technology Conference*, Singapore, Dec. 10–12, 2002, pp. 218–222.
[15] H. Reichl and V. Gosser, "Overview and development trends in the field of MEMS packaging," in *Proc. IEEE Micro Electro Mechanical Systems 2001*, Interlaken, Switzerland, Jan. 21–25, 2001, pp. 1–5.
[16] R. Goch, T. Schimert, W. McCardel, and B. Ritchey, "wafer-level vacuum packaging for MEMS," *Journal of Vacuum Science Technology A*, vol. 17, no. 4, pp. 2295–2299, Jul./Aug. 1999.
[17] Y.-L. Park, H.-W. Park, D.-J. Lee, J.-H. Park, I.-S. Song, C.-W. Kim, C.-M. Song, Y.-H. Lee, C.-J. Kim, and B.-K. Ju, "A novel low-loss wafer-level packaging of the RF MEMS devices," in *Proc. IEEE Micro Electro Mechanical Systems 2002*, Las Vegas, Nevada, Jan. 20-24, 2002, pp. 681–684.
[18] A. Jourdain, X. Rottenberg, G. Carchon, and H. A. C. Tilmans, "Optimization of 0-level packaging for RF-MEMS devices," in *Proc. Transducers 2003*, Boston, MA, USA, June 8–12, 2003, pp. 1915–1918.
[19] E. Obermeier, "Anodic wafer bonding," in *Proc. Semiconductor Wafer Bonding: Science, Technology and Applications*, E. Society, Ed., vol. 95-7, Reno, Nevada, May 1995, pp. 212–220.
[20] J. Oberhammer and G. Stemme, "Incrementally etched electrical feedthroughs for wafer-level transfer of glass lid packages," in *Proc. Transducers 2003*, Boston, MA, USA, June 8–12, 2003, pp. 1832–1835.
[21] R. R. Tummala, E. J. Rymaszewski, and A. G. Klopfenstein, *Microelectronics Packaging Handbook, part 2: Semiconductor Packaging*, 2nd ed. Boston, Dordrecht, London: Kluwer, 1999.
[22] J. Oberhammer, F. Niklaus, and G. Stemme, "Sealing of adhesive bonded devices on wafer level," *Sensors and Actuators A: Physical*, vol. 110, no. 1–3, pp. 407–412, Feb. 2004.
[23] F. Niklaus, P. Enoksson, E. Kälvesten, and G. Stemme, "A method to maintain wafer alignment precision during adhesive wafer bonding," *Sensors and Actuators A: Physical*, accepted for publication.
[24] J. Wei, Z. Wang, H. Xie, and N. F. Lan, "Role of bonding temperature and voltage in silicon-to-glass anodic bonding," in *Proc. IEEE Electronics Packaging Technology Conference*, Singapore, Dec. 10–12, 2002, pp. 85–90.
[25] H. J. Quenzer, A. V. Schulz, T. Kinkopf, and T. Helm, "Anodic-bonding on glass layers prepared by a spin-on glass process: preparation process and experimental results," in *Proc. TRANSDUCERS 2001*, Munich, Germany, June 10–14, 2001, pp. 230–233.
[26] M. M. Visser, D. T. Wang, and A. B. Hanneborg, "Fast silicon to silicon wafer bonding with an intermediate glass film," in *Proc. Semiconductor Wafer Boding Science: Technology and Applications*, San Franzisco, CA, USA, Fall 2001, pp. 74–84.
[27] B. Müller and A. Stoffel, "Tensile strength characterization of low-temperature fusion-bonded silicon wafers," *Journal of Micromechanics and Microengineering*, vol. 1, no. 3, pp. 161–166, Sep. 1991.
[28] D. Sayah, A. Solignac, T. Cueni, and M. A. M. Gijs, "Development of novel low temperature bonding technologies for microchip chemical analysis applications," *Sensors and Actuators A: Physical*, vol. 84, no. 1–3, pp. 103–108, Aug. 2000.
[29] R. F. Wolffenbuttel and K. D. Wise, "Low-temperature silicon wafer-to-wafer bonding using gold at eutectic temperature," *Sensors and Actuators A: Physical*, vol. 43, no. 1–3, pp. 223–229, May 1994.
[30] B. Bilenberg, T. Nielsson, B. Claussen, and A. Kristensen, "PMMA to SU-8 bonding for polymer based lab-on-a-chip systems with integrated optics," in *Proc. Eurosensors 2003*, Guimarães, Portugal, Sep. 20–21, 2003, pp. 486–489.
[31] C.-T. Pan, H. Yang, S.-C. Shen, M.-C. Chou, and H.-P. Chou, "A low-temperature wafer bonding technique using patternable materials."

**Joachim Oberhammer** , born in Italy in 1976, received his M.Sc. degree in electrical engineering from the University of Technology Graz, Austria, in 2000. He was working with automotive electronics and RF identification systems both at the University of Technology Graz and Vienna University of Technology, Austria, before he joined the Microsystem Technology group at the Royal Institute of Technology, Stockholm, Sweden, as Ph.D-student in March 2001. Here, his research focus lies in RF MEMS and wafer-level packaging of MEMS components.

**Göran Stemme** received the M.Sc. degree in electrical engineering in 1981 and the Ph. D. degree in solid state electronics in 1987, both from the Chalmers University of Technology, Gothenburg, Sweden. In 1981, he joined the Department of Solid State Electronics, Chalmers University of Technology, Gothenburg, Sweden. There, in 1990, he became an associate professor (Docent) heading the silicon sensor research group. In 1991, Dr. Stemme was appointed a professor at The Royal Institute of Technology, Stockholm, Sweden, where he heads the Microsystem Technology group at the department of Signals, Sensors and Systems. His research is devoted to microsystemtechnology based on micromachining of silicon.

Between 1995 and 2001 he was a member of the International Steering Committee of the Conference series IEEE Microelectromechanical Systems (MEMS) and he was General Co-Chair of that conference in 1998. Dr. Stemme is a member of the Editorial Board of the IEEE/ASME "Journal of Microelectromechnical Systems" and of the Royal Society of Chemistry journal "Lab On A Chip". 2001 he won, together with two colleagues, the final of the Swedish Innovation Cup. Dr. Stemme has published more than 100 research journal and conference papers and has been awarded 8 patents.

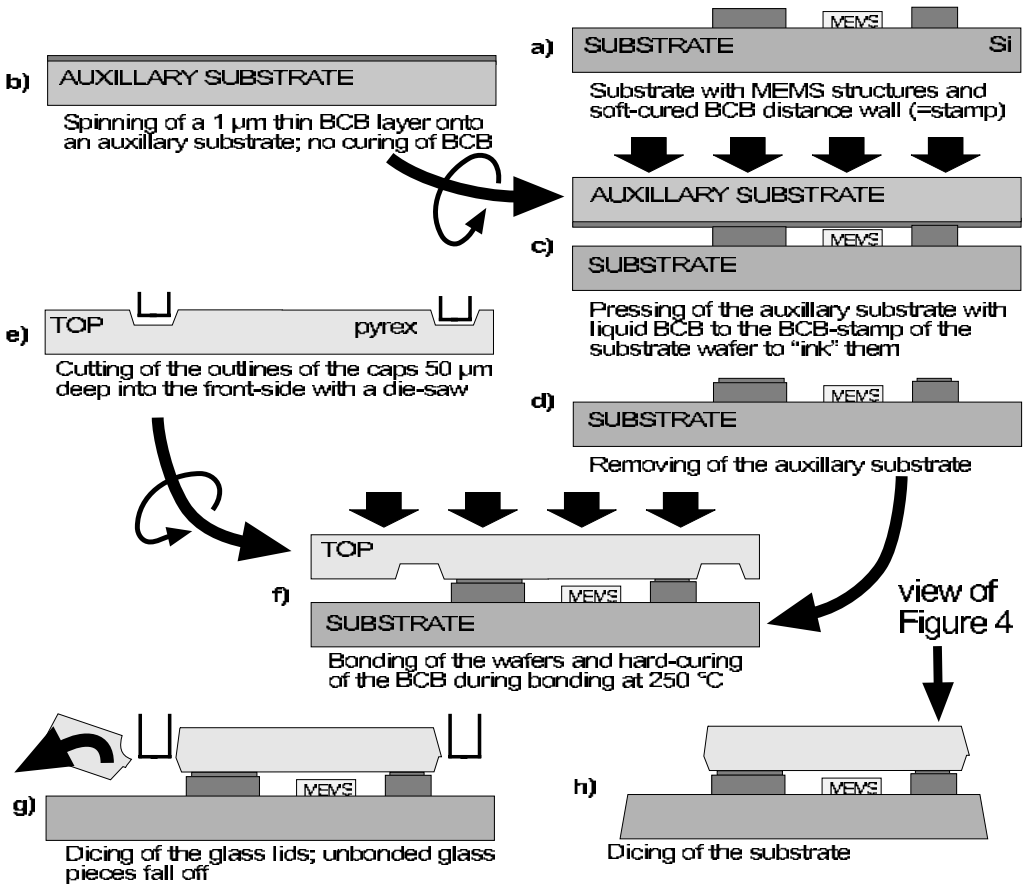


Fig. 1. Process flow of the glass lid encapsulation technique by BCB contact printing.

TABLE I

RESULTS OF TENSILE STRENGTH MEASUREMENT OF THE BCB-BONDED SAMPLES.

| | Unit | soft-cured BCB (group A) | BCB contact printing without AP (group B1) | BCB contact printing with AP (group B2) |
|---|---|---|---|---|
| avg. bond strength | MPa | 3.97 | 11.34 | 8.68 |
| max. bond strength | MPa | 7.71 | 21.32 | 14.64 |
| number of samples | - | 11 | 5 | 11 |

TABLE II

BOND STRENGTH OF DIFFERENT FULL-WAFER BONDING TECHNIQUES.

| bonding technique | bond strength with reference |
|---|---|
| anodic bond. glass-silicon | 30–40 MPa [19], >10 MPa [24] |
| anodic bond. silicon-glass-silicon | >30 MPa [25], 9.2–10.0 MPa [26] |
| anodic bond. glass-aluminum | >12 MPa [25] |
| fusion bond. silicon-silicon | 23.5 MPa [27] |
| direct bond. glass-glass | 10 MPa [28] |
| eutectic bond. silicon-gold | 18 MPa [29] |
| patterned adh. bond. SU-8 to SU-8 | 16 MPa [30], 20.6 MPa [31] |
| patterned adh. bond. BCB | 9–11 MPa [the present paper] |

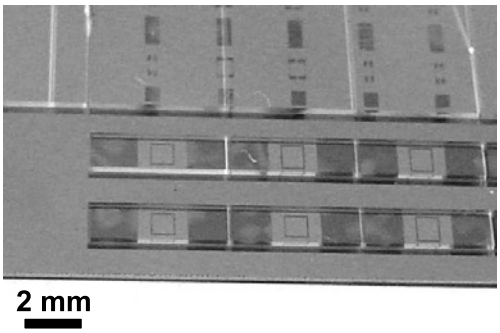


Fig. 2. Array of glass-lid packages on the substrate wafer after dicing the glass wafer.

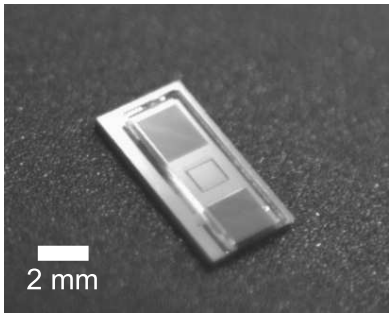


Fig. 3. Single sample after dicing, before carrying out the tensile strengh test.

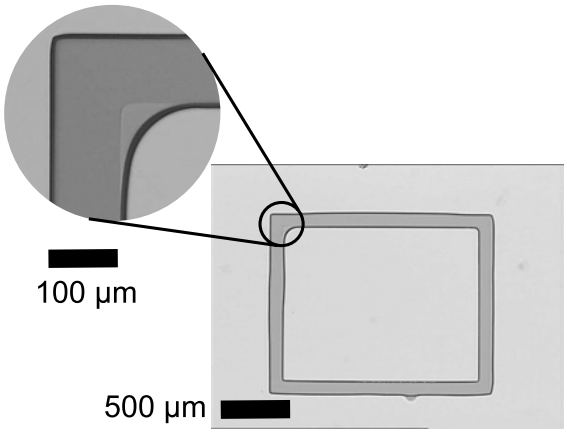


Fig. 4. Microscope picture through the covering glass wafer after bonding with the BCB printing technique, showing the 'BCB-ink' slightly flowing out of the shapes of the BCB stamp, which occurs especially in concave corners.

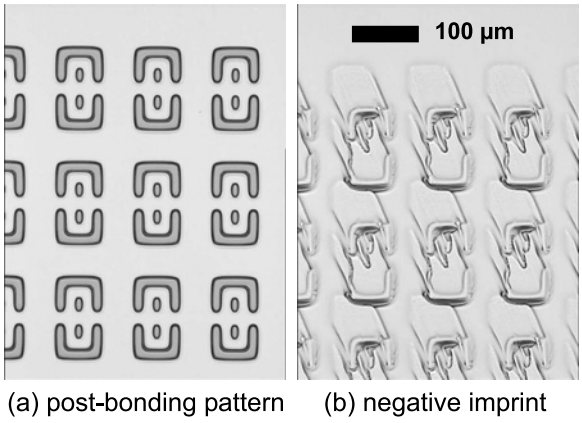


Fig. 5. Also small patterns, here with a line width of 10 $\mu$m, keep their shapes during printing quite well (a), even though the negative imprint is distorted when removing the auxiliary wafer (b).

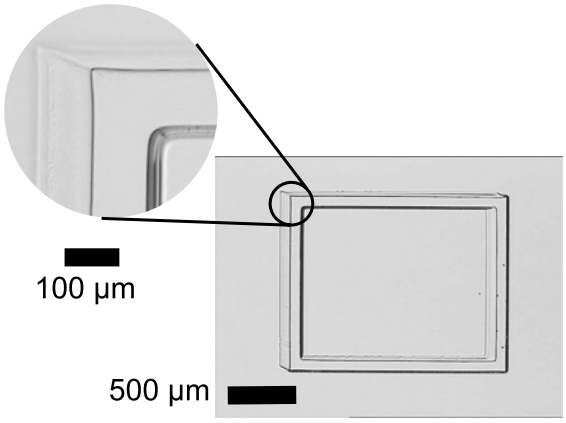


Fig. 6. Microscope picture of the 'negative imprint' of the BCB stamp in the liquid BCB layer of the auxiliary wafer.

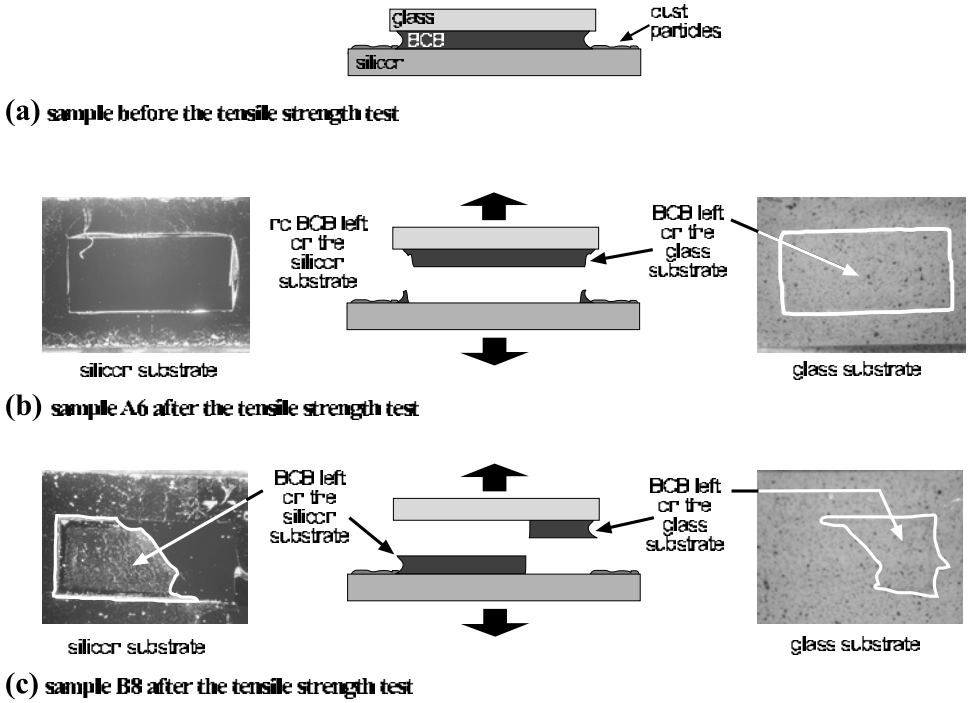


Fig. 9. Failure mode analysis of two samples of group B2 after the tensile strength tests.

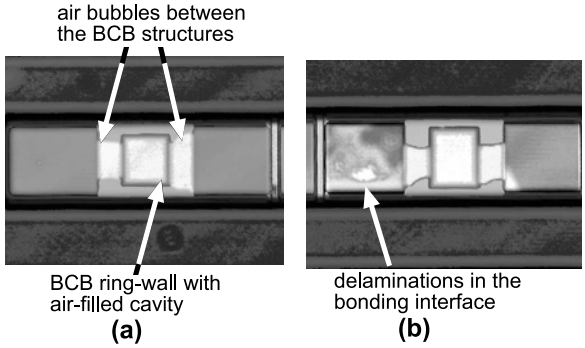


Fig. 7. Scanning acoustic microscope pictures of the bond interface of soft-cured BCB (group A); (a) well bonded sample; (b) voids in the interface.

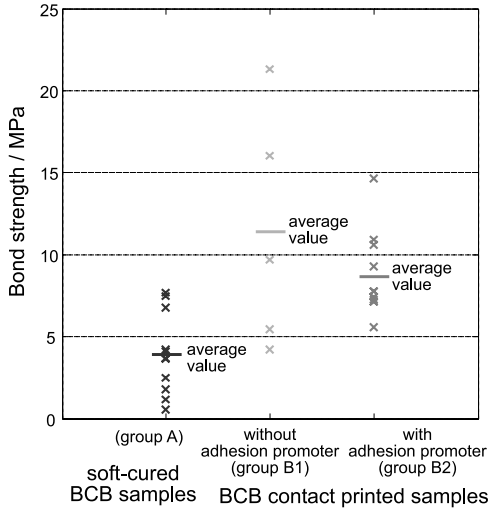


Fig. 8. Tensile strength measurement results of soft-cured BCB bonded samples and BCB contact-printed samples with and without adhesion promoter, corresponding to Table I.

# Paper 7

**A 2-bit Reconfigurable Meander Slot Antenna with High-Displacement Low-Voltage RF MEMS Switches**

Marc Mowler, *Joachim Oberhammer*, Björn Lindmark, and Göran Stemme

Manuscript for journal publication.

# A 2-bit Reconfigurable Meander Slot Antenna with High-displacement Low-voltage RF-MEMS Switches

M. Mowler, J. Oberhammer, B. Lindmark, and G. Stemme
Department of Signals, Sensors and Systems, KTH, Stockholm, Sweden, Email: marcm@s3.kth.se

***Abstract*— A novel slot antenna with RF-MEMS switches is proposed with two switches placed symmetrically on an asymmetrical meander-shaped slot yielding four different operating frequencies. A microstrip-fed meander slot antenna with copper tape acting as switches was manufactured as a prototype to test the concept. The measured results were satisfying for all four frequencies with a return loss well under -10 dB. Further use of additional switches on the same antenna is discussed in the paper.**

## I. Introduction

Antennas used in handheld devices have to be small, and at the same time they should operate at different frequency bands. For this purpose, slot antennas are well-suited since they have advantages such as being low profile, light weight, low cost, conformable, and easy to fabricate. They can be combined with RF-MEMS[1] switches to form reconfigurable antennas.

Recent years have seen an increased interest in RF-MEMS switches [1]. Also, great interest has been shown for the use of such switches for reconfigurable antennas. These include frequency reconfigurable patch [2], [3], spiral microstrip [4], and slot [5] antennas, reconfigurable apertures [6], and polarization switching antennas [7], [8].

In this paper a novel reconfigurable antenna with MEMS shunt switches is presented. The antenna is a microstrip-fed meander slot antenna based on a similar stripline-fed meander slot antenna [9]. As shown in [9] a meandered slot can provide a very low resonant frequency for a given antenna area.

We have two RF-MEMS switches acting as logical switches resulting in a 2-bit reconfigurable antenna. Due to the meander slot configuration, it also seams possible to extend the design to include an arbitrary number of switches. An additional inherent advantage is the combination of shunt switches with a slot antenna, since the ability of a shunt switch to short-circuit a slot is greatest at high frequencies. This matches the requirement for short slot length at hight frequency.

The development of the antenna comprises four steps: Validation of the switches [11], design of the meander slot, testing of a copper prototype, and finally fabrication of the antenna including the gold layer and the switches. At the time of writing, the switches are being mounted on the antenna. The measured results of the final antenna with switches will be presented in future papers. Instead, measured results with conducting copper tape on a copper antenna are presented in this paper. A picture of the final antenna in a stripline-fed configuration before mounting on the switches is provided by figure 1. A picture of the prototype microstrip-fed antenna before placing copper tape on it is seen in figure 2

[1]Radio Frequency Microelectromechanical Systems

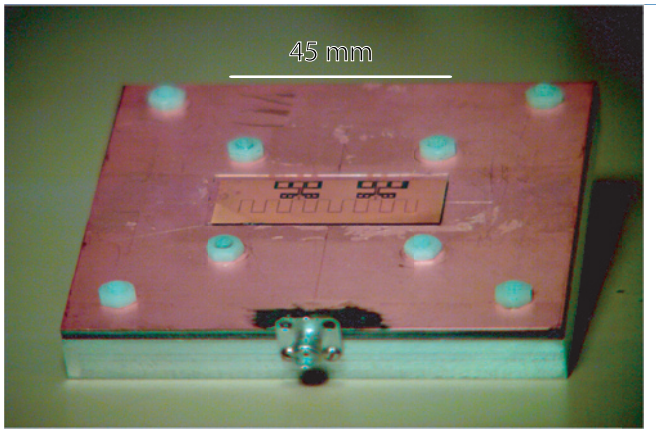


Fig. 1. Picture of the final antenna with gold layer in a stripline-fed configuration before switches are mounted. The gold layer is on top of a glass substrate which is lowered inside a whole in the copper layer.

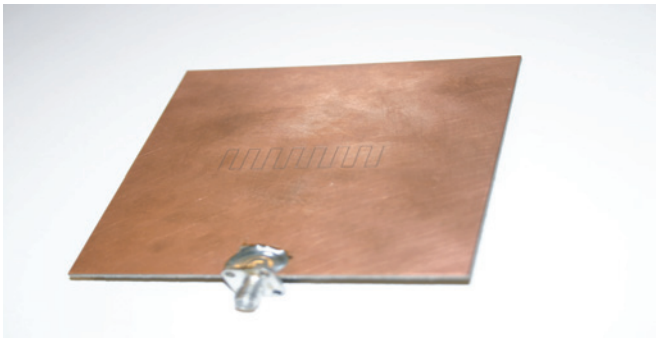

Fig. 2. Picture of the microstrip-fed meander slot antenna with a teflon substrate and a ground plane in copper. The overall size is 100x100 mm. Measurements have been done on this antenna and presented in this paper.

## II. Design overview

### A. Concept

Preferably we would like to use a monolithic integration of the switches with the antenna as in [10]. Due to

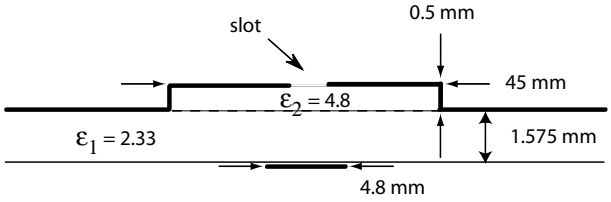


Fig. 3. Side-view of the microstrip-fed meander slot antenna with a gold layer.

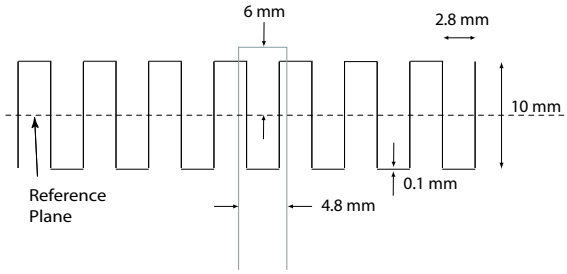


Fig. 4. Birds-eye view of the microstrip-fed meander slot antenna in copper.

restrictions in our manufacturing process, the copper could not be used entirely. For the parts where the meander slot is place as well as the parts where the switches are to be mounted, a gold layer was used instead. Placing the switches on the antenna is the next step. A side-view drawing the final antenna with gold layer is visible in figure 3. Presented in this paper are the results of the corresponding antenna with only copper. To switch the antenna copper tape was used. This was a prototype used to verify the design of the final antenna.

### B. *Antenna configuration*

As a prototype a copper antenna was used. An overview of the microstrip-fed meander slot antenna design is presented in figure 4. The overall setup structure including the ground plane is 100x100 mm. The feed is in the middle relative to the ground plane and the upper conducting plane. This design shows to be a suitable configuration for the four different frequencies to be excited.

We are using switches in a capacitive shunt configuration [11]. The area where the switch is mounted on the antenna is shown in figure 5.

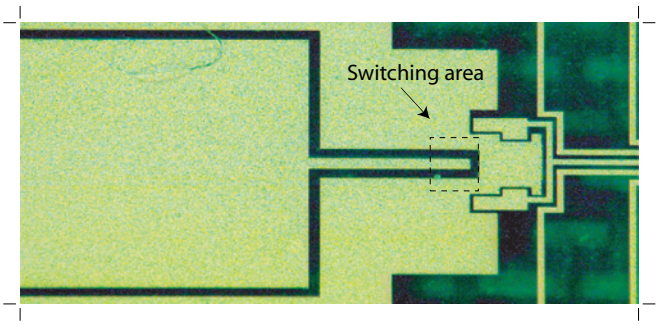


Fig. 5. Part of the meander where the switch is mounted

The switches are placed on the edge of each meander section. Since the meander is slightly asymmetric with reference to the strip line, the two different switch positions will yield different frequencies when switched down one at a time.

When the right switch is down, the right side of the meander is deactivated, and when the left switch is down the opposite is true. Both switches could be down simultaneously as well as being up simultaneously. Consequently four different frequencies of operation are possible.

The particular combination of the slot antenna and the capacitive switches helps the antenna to behave correctly at given frequencies. At low frequencies when both switches are in up mode, the capacitance is small. This means that the blockage at low frequencies is minimized. The opposite is true for high frequencies. With both switches down, a well-defined slot with minimized leakage is seen.

### C. *Switch technology*

The switch design, based on a S-shaped film actuator, provides with a large vertical traveling distance of the switching membrane by maintaining low actuation voltages [11]. The large gap distance in the off-state (membrane up) of 14.2 $\mu$m of the switch prototypes allows having very large overlapping areas of 10000 $\mu m^2$ for the capacitive short-circuiting of the meander-shaped antenna slot in the on-state (membrane down) , without significantly disturbing the signal propagation in the off-state.

Furthermore, this switch is designed in a way that its mechanically switching part (upper part) is fabricated independently of the substrate with the RF lines to be switched. Thus, the switching part can be placed directly onto the antenna circuit by flip-chip like bonding, as shown in Figure 6. Figure 7 shows a SEM-picture of the switching part with the mechanically mowing membrane before the final assembly to the bottom RF circuits. The photograph in Figure 8 is taken of the switching part on a coplanar waveguide fabricated on a high-resistivity silicon substrate, which was used to evaluate the switching performance

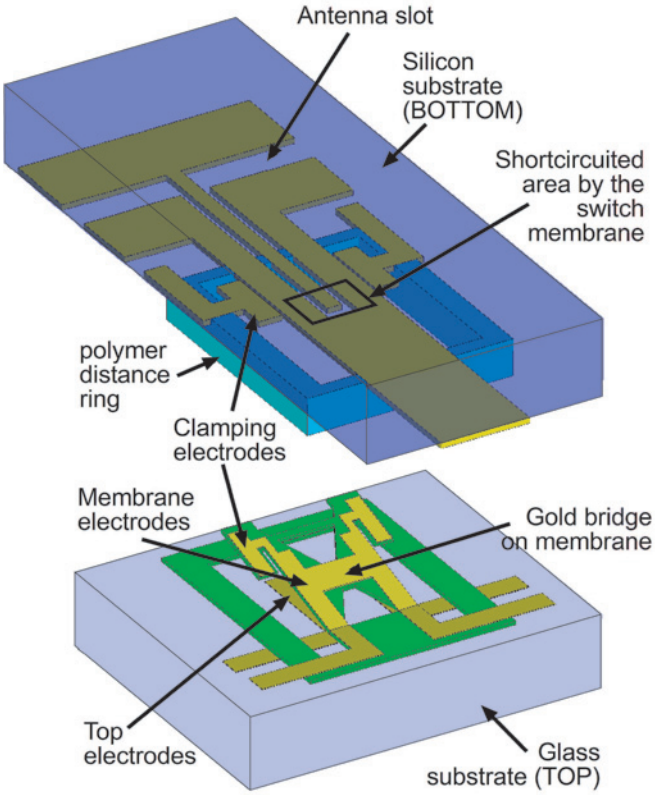


Fig. 6. Schematic drawing of the switch and how it is mounted to the antenna substrate. The top part containing the moving MEMS structures, is shown below the antenna part with the meander-shaped slot.

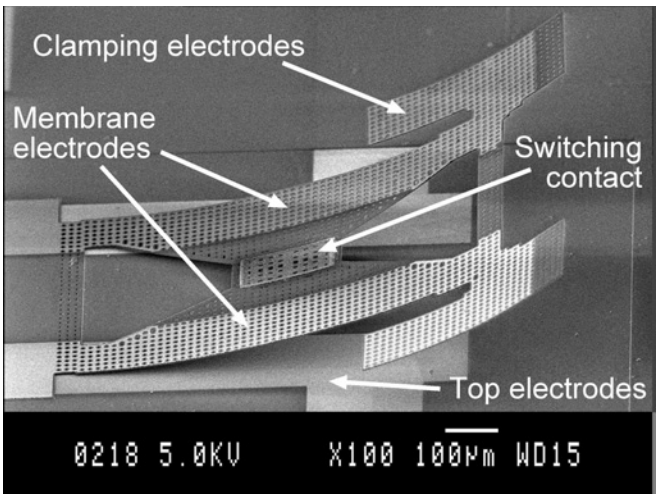


Fig. 7. SEM picture of the top part of the switch, showing the free-etched switching membrane.

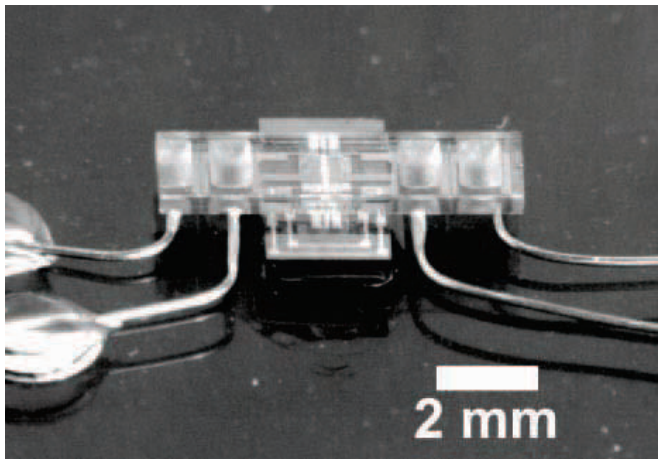


Fig. 8. Photograph of a assembled switch to a substrate wafer part with a coplanar waveguide, to evaluate the RF performance of the switch.

## III. Results

We have four different configurations. The measurements were made on the copper antenna, which has a ground plane made in copper only and switched with copper tape. The return loss resulting from simulations as well as from measurements for the prototype antenna without copper tape is presented in figure 9 The measured return loss versus frequency for all four slot lengths of the copper antenna is provided by figure 10. The length of the feed had to be changed slightly in order to find a good match for all four configurations. Pos 1 in the figure refers to the configuration with the lowest operating frequency. Pos 4 refers to the configuration with the highest operating frequency.

With the two switches simultaneously in the up-mode, the operating frequency occurs at 900 MHz with a good return loss. This is the situation when all of the meandered slot is free to radiate and represents a switch-free antenna. The other extreme occurs when both switches are pulled down and the meandered slot is minimized by the switches. The working frequency then occurs at 1.8 GHz. When this is the case, the antenna has its minimum length corresponding to the highest achievable frequency. Instead of moving both switches up and down, only one switch position can be changed giving a resulting frequency in between the previously mentioned frequencies. For the left switch the active slot area is the right side of the meander. In this case, the antenna operates at a frequency of 1.2 GHz. When, instead, the right switch is pulled down (and the left switch is open), the left side is radiating leaving the right side closed. The frequency of operation is now 1.1 GHz.

An interesting outcome from analyzing the antenna is that the impedance is close to 50 ohm for all four different antenna configurations. This fact indicates that there is a

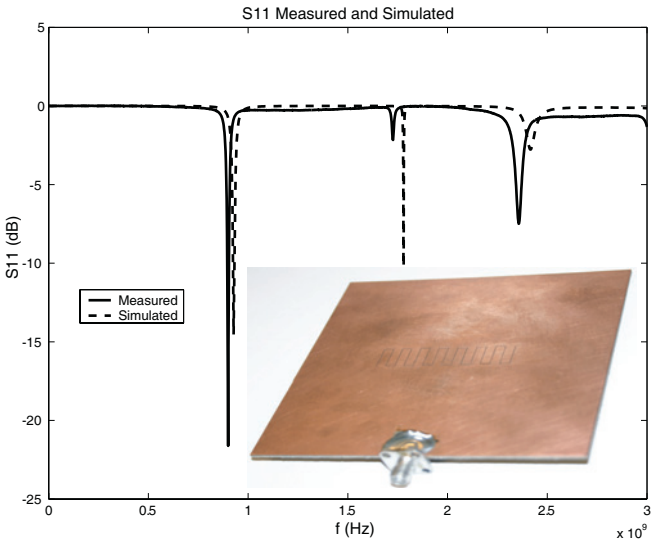


Fig. 9. Measured and simulated return loss for the fabricated copper antenna.

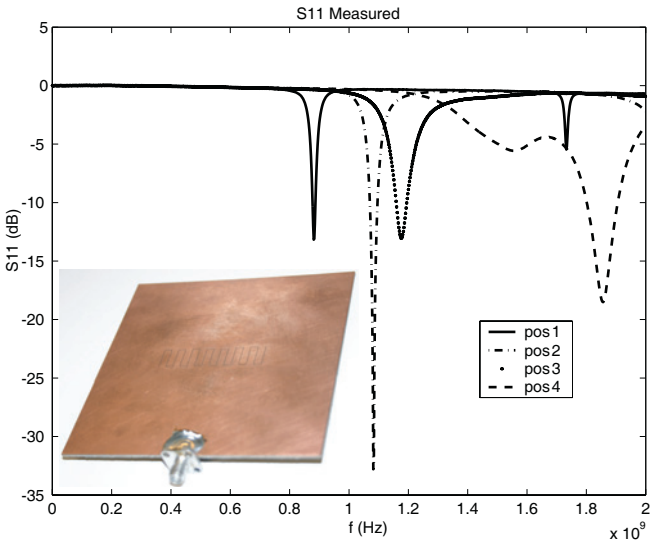


Fig. 10. Measured return loss for the four different slot lengths corresponding to the four different switching positions of the antenna. The four peaks represent the four different combinations of the switches being up or down. Copper tape has been used to change the length of the slot.

potential in placing more switches next to the two already presented in this paper. Since the meander is made with equally sized meander sections, we could place switches on all the meander sections in order to create an overall antenna with numerous switches. This type of antenna would then adapt to the particular frequency band required by the current application of the antenna.

## IV. Conclusion

A reconfigurable antenna has been proposed in order to show the synergism between proper antenna design and RF-MEMS switches. The results were satisfactory and provide a starting point for future advancements in the field of multi-purpose antennas.

## References


[1] E. R. Brown, "RF-MEMS switches for reconfigurable integrated circuits," in *IEEE Transactions on Microwave Theory and Techniques*, vol. 46, 1998, pp. 1868–1880.

[2] R. N. Simons, D. Chun, and L. P.B. Katehi, "Reconfigurable array antenna using microelectromechanical systems (MEMS) actuators," in *IEEE Antennas and Propagation Society International Symposium*, vol. 3, 2001, pp. 674–677.

[3] S. Xiao, B.-Z. Wang, and X.-S. Yang, "A novel frequency-reconfigurable patch antenna," in *Microwave and Optical Technology Letters*, vol. 1, 2003, pp. 295–297.

[4] G. Huff, J. Feng, S. Zhang, and J. Bernhard, "A novel radiation pattern and frequency reconfigurable single turn square spiral microstrip antenna," in *IEEE Microwave and Wireless Components Letters*, vol. 13, 2003, pp. 57–59.

[5] J. H. Shaffner,"RF-MEMS for antenna applications," in *Workshop SC-5, IEEE International Antennas and Propagation Symposium and USNC/CNC/URSI North American Radio Science Meeting*, 2003.

[6] W.H. Weedon, W.J. Payne, and G. M. Rebeiz, "MEMS-switched reconfigurable antennas," in *IEEE Antennas and Propagation Society International Symposium*, 2001, pp. 654–657.

[7] F. Yang and Y. Rahmat-Samii, "A reconfigurable patch antenna using switchable slots for circular polarization diversity," in *IEEE Microwave and Wireless Components Letters*, vol. 12, 2002, pp. 96–98.

[8] R. N. Simons, D. Chun, and L. P.B. Katehi, "Polarization reconfigurable patch antenna using microelectromechanical systems (mems) actuators," in *IEEE Antennas and Propagation Society International Symposium*, vol. 2, 2002, pp. 6–9.

[9] H. Y. Wang, J. Simkin, C. Emson, and M. J. Lancaster,"Compact meander slot antennas," in *Microwave and Optical Technology Letters*, vol. 24, 2000, pp. 377–380.

[10] B. A. Cetiner, J. Y. Qian, H. P. Chang, M. Bachman, G. P. Li, and F. D. Flaviis, "Monolithic integration of rf mems switches with a diversity antenna on pcb substrate,"in *IEEE Transactions on Microwave Theory and Techniques*, vol. 51, 2003, pp. 332–335.

[11] J. Oberhammer, B. Lindmark, and G. Stemme, "RF characterization of low-voltage high-isolation mems series switch based on a s-shaped film actuator," in *Proc. SBMO/IEEE MTT-S Int. Microwave and Optoelectronics Conference, Foz de Iguacu, Brazil*, 2003.